Assessment of the protective efficiency of nonphotochemical quenching in higher plants

Maxwell A. Ware

A thesis submitted for the degree of Doctor of Philosophy at Queen Mary, University of London

Supervisor Professor A. Ruban

School of Biological and Chemical Sciences

Queen Mary, University of London

February 2017

Declaration

I, Maxwell Ware, confirm that the research included within this thesis is my own work or that where it has been carried out in collaboration with, or supported by others, that this is duly acknowledged below and my contribution indicated. Previously published material is also acknowledged below.

I attest that I have exercised reasonable care to ensure that the work is original, and does not to the best of my knowledge break any UK law, infringe any third party's copyright or other Intellectual Property Right, or contain any confidential material.

I accept that the College has the right to use plagiarism detection software to check the electronic version of the thesis.

I confirm that this thesis has not been previously submitted for the award of a degree by this or any other university.

Maxwell A. Ware (130217893)

Prior Presentation of Work - Publications

Ware MA., Dall'Osto L., Ruban, AV. (2016) An *in vivo* quantitative comparison of photoprotection in *Arabidopsis* xanthophyll mutants. *Front Plant Sci,* 7: 841.

Benson S., Maheswaran P., Ware MA., Hunter CN., Horton P., Jansson S., Ruban AV., Johnson MP. (2015) An intact photosystem I light harvesting antenna system is required for complete state transitions in *Arabidopsis*. *Nature Plants*, 1: 15176.

Ware MA., Giovagnetti V., Belgio E., Ruban AV. (2015) PsbS protein modulates non-photochemical chlorophyll fluorescence quenching in membranes depleted from photosystems. *J Photochem Photobiol B*, 152: 301-307.

Carvalho FEL., Ware MA., Ruban AV. (2015) Quantifying the dynamics of light tolerance in *Arabidopsis* plants during ontogenesis. *Plant Cell Env*, 38: 2603-2617.

Ware MA., Belgio E., Ruban AV. (2015) Photoprotective capacity of non-photochemical quenching in plants acclimated to different light intensities. *Photosynth Res*, 126: 261-274.

Giovagnetti V., Ware MA., Ruban AV. (2015) Assessment of the impact of Photosystem I chlorophyll fluorescence on the pulse-amplitude modulated quenching analysis in leaves of *Arabidopsis thaliana*. *Photosynth Res*, 125: 179-189.

Ware MA., Belgio E., Ruban AV. (2014) Comparison of the protective effectiveness of NPQ in *Arabidopsis* plants deficient in PsbS protein and zeaxanthin. *J Exp Bot*, 66: 1259-1270.

Prior Presentation of Work - Conferences

Bioenergetics Christmas Meeting, Imperial College London, London, UK, 18/12/2015.

Gordon Research Conference, Waltham, MA, USA, 28/06-03/07/2015.

Vienna International Science Conferences & Events Association, Vienna, Austria, 25-26/06/2015.

Light Harvesting Processes, Banz Monastery, Germany, 08-12/03/2015.

International Conference on the Regulation of Photosynthetic Function, Guilin, China, 16-19/08/2014.

Abstract

Photosystem II (PSII) is the primary generator of electrons required for photosynthesis. The reaction center protein of PSII (RCII) is the most susceptible component of the photosynthetic machinery to damage. Photodamage can lead to long-term downregulation of photosynthesis. This occurs because plants are exposed to rapid light fluctuations and high light conditions, leading to the over accumulation of excess energy around PSII. Plants have developed a mechanism to dissipate this excess energy called nonphotochemical quenching (NPQ). In order to quantify the protectiveness of NPQ (pNPQ), a novel methodology was developed and employed. During methodology development, development, it is shown that a variable PSI fluorescence should be taken into account, and how it can be calculated. Application of the procedure assessed the contribution of xanthophylls lutein, violaxanthin, zeaxanthin, and the PsbS protein to pNPQ. Results show that the most important factors governing photoprotection are the PsbS protein and the correct xanthophyll composition in their natural binding sites. The more xanthophyll variation, the greater the photodamage at the end of the pNPQ assessment procedure. PsbS is essential to achieve the maximum pNPQ. PsbS increases the aggregation of LHCII. *Arabidopsis* with excess PsbS has three-times more aggregated LHCII than wild type levels of PsbS. The phototolerance and pNPQ required for *Arabidopsis* grown under different conditions and for leaves of different ages was also calculated. Plants grown under low light conditions accumulate disconnect antenna (LHCII), which is inefficient at protecting RCII, despite the high NPQ levels. Investigating plants of different ages, it was found that eight-week old *Arabidopsis* are the optimum age for pNPQ effectiveness. Younger and older leaves suffer photodamage at lower light intensities and form less pNPQ. This thesis demonstrates the novelty and adaptability of the pNPQ assessment procedure, and offers a sound case for its use in acclimation and photoinhibition experiments.

Acknowledgements

I acknowledge the Queen Mary Principal's Research Studentship for the funding of my PhD studentship. I acknowledge the funding that I have received from the Society for Experimental Biology (COB), Biochemical Society General Travel Grant, The Royal Society International Exchanges Scheme and Queen Mary Postgraduate Research Fund for financial support to attend the conferences listed on page 3.

I would like to thank Dr/Prof Ruban, Duffy, Johnson, Murchie, Nixon, Belgio, Kuang and Shen for their ideas, time and use of facilities during my PhD studies. The diverse range of environments and discussions have been stimulating and helped to shape my ideas and evolution as a scientist. I would like to say a special thank you to my supervisor Sasha. These three years have been more stimulating and exciting than I could ever have imagined. I am extremely grateful for the opportunities I have been granted, and I have thoroughly enjoyed my time in the lab. I have become a much better researcher for this opportunity and I hope that we will continue to collaborate in the future.

I would like to thank my colleagues and friends of 4.36 during my studies, particularly Yonglan, Petra, Joanna and Fabricio whose company I have enjoyed immensely. I am extremely grateful for the friendships I have developed with Chris and Vasco during this time, it has been a pleasure.

I am grateful for the support of my parents and family during my thesis and education before this. The friendship from my sister Laura has been unwavering in both the good and bad times, I will always be indebted. I hope that this is testament to the encouragement that you have all given me over the last 20 years, thank you.

Last but not least, to Tímea. You have brought so much happiness into my life. Your support and understanding has meant the world to me and I am short of words. For this and more, you have my deepest love and thanks.

Abbreviations

77K	low temperature (77K) fluorescence
aba4npq1lut2 or *viol*	*Arabidopsis* where violaxanthin replaces all xanthophylls
AL	actinic light
Arabidopsis	*Arabidopsis thaliana* (Col-0)
ATP	adenosine triphosphate
BSA	bovine serum albumin
CEF	cyclic electron flow
ch1	*Arabidopsis* knock-outs of Chl *b*
Chl	chlorophyll
Chl *a*	chlorophyll *a*
Chl *b*	chlorophyll *b*
chy1chy2lut5 or *lute*	*Arabidopsis* where lutein replaces all xanthophylls
CP24	24 kDa apoprotein of the PSII antenna complex
CP26	26 kDa apoprotein of the PSII antenna complex
CP29	29 kDa apoprotein of the PSII antenna complex
CP43	43 kDa apoprotein of the PSII core complex
CP47	47 kDa apoprotein of the PSII core complex
Cyt b_6/f	cytochrome b_6/f complex protein
D1 protein	PSII core component D1 protein
D2	PSII core component D2
Da	Dalton
DAS	days after sowing

DCMU	3-(3,4-dichlorophenyl)-1,1-dimethylurea
DTT	1,4-dithiothreitol
EDTA	ethylendiamine tetraacetic acid
ETC	electron transport chain
ETR	electron transport rate
Fd	ferredoxin
FFEM	freeze fracture electron microscopy
Fm	fluorescence maximum
fML	fluorescence measuring light
FNR	ferredoxin:NADP+ oxidoreductase
Fo	fluorescence minimum
FR	far red light
Fs	steady state fluorescence
Fv/Fm	maximum photochemical quantum yield of photosystem II
g	centrifugal force
h	hour
h	hours
HEPES	N-2-hydroxyethypiperazin-N'-2-ethansulfonate
HL	high light growth environment acclimated (~450 µmol m^{-2} s^{-1})
HPLC	high pressure liquid chromatography
K	kelvin
kDa	kilodalton
L	litre

L17	*Arabidopsis* with PsbS overexpressor
LED	light emitting diode
LHC	light harvesting complex
lhca	gene of light harvesting complex protein of photosystem I
lhcb	gene of light harvesting complex protein of photosystem II
LHCII	major, trimeric light harvesting protein complex of PSII
LL	low light growth environment acclimated (~40 µmol m^{-2} s^{-1})
lut2	no α-carotene or lutein
lut2npq2 or *zea*	*Arabidopsis* where zeaxanthin replaces all xanthophylls
min	minute
ml	millilitre
ML	medium light growth environment acclimated (~200 µmol m^{-2} s^{-1})
Mya	million years ago
NADP+	oxidised nicotinamide adenine dinucleotide phosphate
NADPH	reduced nicotinamide adenine dinucleotide phosphate
nm	nanometre
NoM	*Arabidopsis* with lhcb4, lhcb5 and lhcb6 knock-outs
NPQ	non-photochemical quenching of chlorophyll *a* fluorescence
npq1	zeaxanthin-deficient *Arabidopsis*
npq2	*Arabidopsis* lacking violaxanthin and neoxanthin
npq4	PsbS protein-deficient *Arabidopsis*
ns	nanosecond
^{o}C	degree Celsius

OEC	oxygen evolving complex
PAM	pulse amplitude modulation
pH	potential of hydrogen
pNPQ	protective NPQ
PSI	photosystem I
PSII	photosystem II
QA	primary quinine acceptor molecule
QB	secondary quinine acceptor molecule
qE	energy dependent quenching
qI	photoinhibition-dependent quenching
qM	chloroplast movement-dependent quenching
qN	non-photochemical quenching coefficient
qP	photochemical quenching coefficient
qP_d	photochemical quenching coefficient in the dark
qT	state transition-dependent quenching
qZ	zeaxanthin-dependent quenching
RCII	reaction centre of photosystem II
ROS	reactive oxygen species
rpm	rotations per minute
RuBisCo	Ribulose-1,5-bisphosphate carboxylase/oxygenase
s	second
SD	standard deviation
SDS-PAGE	sodium dodecyl sulfate polyacrylamide gel electrophoresis

SEM	standard error of the mean
SP	saturating pulse
TCSCP	time-correlated single photon counting
TEM	transmission electron microscopy
Var2	*Arabidopsis* with FtsH homologue knock-out
WT	wild-type *Arabidopsis*
α-Carotene	alpha-Carotene
α-DM	a-dodecyl maltoside (detergent)
β-Carotene	beta-Carotene
ΔpH	trans-membrane pH
µ	micro
µmol m^{-2} s^{-1}	photosynthetic photon flux
Φ	quantum yield

Table of Contents

List of Tables

List of Figures

Chapter I –

Introduction

1.1 Solar Energy

The Sun is the source of the majority of energy on our planet. The Sun emits 3.8×10^{26} Joules of energy every second, and after reflection and filtration of solar radiation in the Earth's atmosphere, approximately 1,000 J/(m^2·s) of sunlight strikes the Earth's surface (Qiang, 2003; Ruban, 2012). The Earth's terrestrial and aquatic environments have been shaped by the organisms that convert this sunlight into oxygen and carbohydrates:

$$CO_2 + H_2O + \textit{solar energy} = C_m(H2O)_n + O_2 \quad \text{(Equation 1.01)}$$

Where CO_2 represents carbon dioxide, H_2O water, $C_m(H2O)_n$ carbohydrates and O_2 oxygen. Solar energy can also be expressed according to Planck's equation:

$$E = hv \quad \text{(Equation 1.02)}$$

Here, energy (E) in Joules is equal to Planck's constant (h, $6.626\text{x}10^{-34}$ J.s) multiplied by frequency (v, Hz or 1 s^{-1}). Using sunlight, photosynthetic organisms are able to convert the energetically-poor but abundant chemical compounds of carbon dioxide (CO_2) and water (H_2O) into complex and high-energy carbohydrates ($C_m(H2O)_n$).

1.2 Theory of Photosynthesis

Even conceptually, the process by which photosynthetic organisms must capture and utilise sunlight is a difficult one. It has to catch this bullet of light (photon) travelling at approximately 3×10^8 m/s, it must then slow the bullet down, but it cannot stop the photon or it will cease to exist, then once slowed, it must convert the energy carried into a safe and readily accessible form of storage. The latter point is vitally important as the energy can be dangerous and give rise to free radicals. These singlet oxygens can damage the proteins and accessory pigments used by photosynthetic organisms to trap and store it sunlight (Ohad *et al.*, 1984; Vass *et al.*, 1992; Aro *et al.*, 1993). Over ~2.7 billion years, chlorophyll containing

organisms have managed to overcome these obstacles and have evolved maximum quantum efficiencies of ~80%, displaying a remarkable light absorbing efficiency. What is more is that they are able to survive its damage and produce vegetation and offspring. Photosynthetic organisms do this by photon-exciton-electron-proton transformations (Fig 1.01). When a photon strikes a light harvesting pigment, electrons change excited state within $1x10^{-15}$s. Upon achieving this excited state, energy can be transferred within groups of pigments via electromagnetic resonance. When the pigment connected to the electron transport chain becomes excited, an electron is donated. The subsequent coupling of electron and proton transfer leads to the creation of ATP and NADPH energy storage molecules, which can be used to drive carbohydrate formation. Over the last 409-439 million years, vascular land plants have utilised this technique to change the Earth's atmosphere and climate (Edwards and Feehan, 1980; Edwards *et al*., 1992), with aquatic organisms and non-vascular plants affecting the planet long before then (Dalrymple, 2001; Heckman *et al.*, 2001; Sanderson *et al.*, 2003). With over 290,000 identified species of terrestrial angiosperms, they have also changed the landscape too (Fig 1.02; Berner, 1997). With this tightly regulated and complex biochemical process, photosynthetic organisms have created the prerequisite for life on Earth as we know it (Barber, 2002; Barber, 2009).

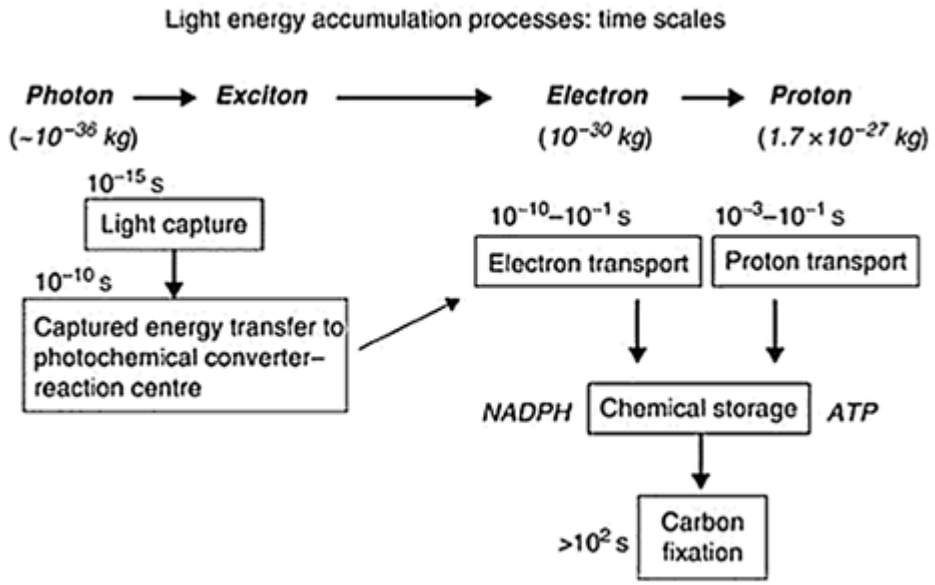

Figure 1.01 Time scales of the photon-exciton-electron-proton energy transfer pathway (Ruban, 2012). Order of magnitude differences in speed of each subsequent stage of the pathway minimises donor-side energy limitations, but can increase the chance of harmful energy accumulation in the membrane.

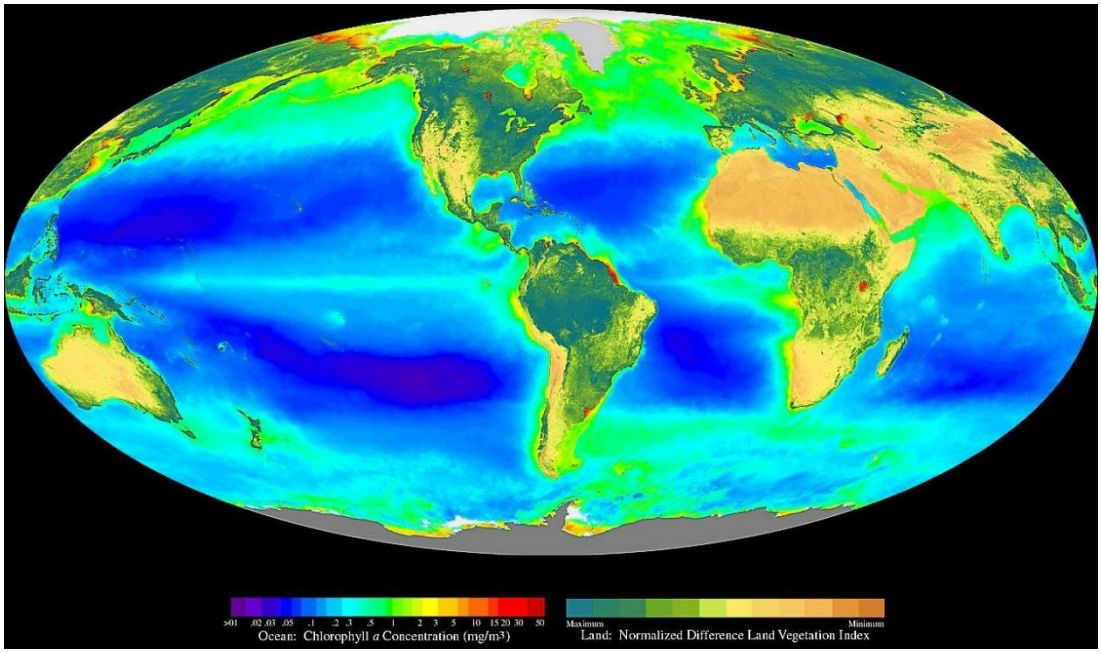

Figure 1.02 A composite satellite image of the Earth's chlorophyll concentration between 2007 and 2010 (NASA Seawifs, 2017). Chlorophyll was measured as mgm^3 chlorophyll *a*. This image displays the vast range of habitats occupied by chlorophyll containing organisms.

1.3 Machinery of Photosynthesis

It is a wonder to think that photosynthesis is responsible for absorbing ~2,000 terawatts of energy annually (Pisciotta *et al.*, 2010). To put this in some perspective, that amount of energy could power all 7.4 billion people on Earth around the world on a bicycle at a speed of 20 mph, and still have some energy to spare. Or for those not into cycling, the energy use of all the humans on Earth could be satisfied seven times over (Nealson and Conrad, 1999). What is more is that this is the collective result of countless chlorophyll containing chloroplasts that are only 10 microns long by 0.5-2 microns deep (Lodish *et al.*, 1995; Ruban, 2012). Chlorophylls are found in a wide variety of organisms from cyanobacteria to algae, and occupy almost every ecosystem on the planet. It would be fascinating to explore the variations of photosynthetic machinery, and adaptations of some of the world's flora in greater detail. However, for the remainder of this work, photosynthesis in higher plants will be discussed unless referred to otherwise. In higher plants, the photosynthetic organelles called chloroplasts, are located in specialised mesophyll cells contained in the leaf. In the model organism *Arabidopsis thaliana*, each mesophyll cell contains approximately 100 chloroplasts (Königer *et al.*, 2008). Inside chloroplasts, in an area called the stroma, there is a system of vesicles called thylakoids (Fig 1.03). Thylakoids are double membrane structures, which contain in the membrane the four essential complexes for photosynthesis: photosystem II (PSII), cytochrome *b6/f* (Cyt *b6/f*), photosystem I (PSI) and adenosine tri-phosphate (ATP) synthase (Fig 1.04). Thylakoids can exist as 'stacks' or as single 'lamellae' (Fig 1.03). The difference between these two forms is the binding of magnesium or potassium cations, which bind to the negatively charged protein complexes exposed on the surface of the thylakoid membrane, and thus cancels out the electrostatic repulsion between individual thylakoids allowing them to bind together (Lu *et al.*, 1995; Kaftan *et al.*, 2002). The thylakoid membranes envelop an aqueous interior called the thylakoid lumen. This space is vitally important for the generation of a transmembrane ΔpH, which is created during the pumping of electrons through the electron transport chain (ETC) in the light-dependent phase of photosynthesis. Outside of the thylakoid membranes, but

inside the stroma, is where the light independent reactions occur, both will be explained in greater detail below.

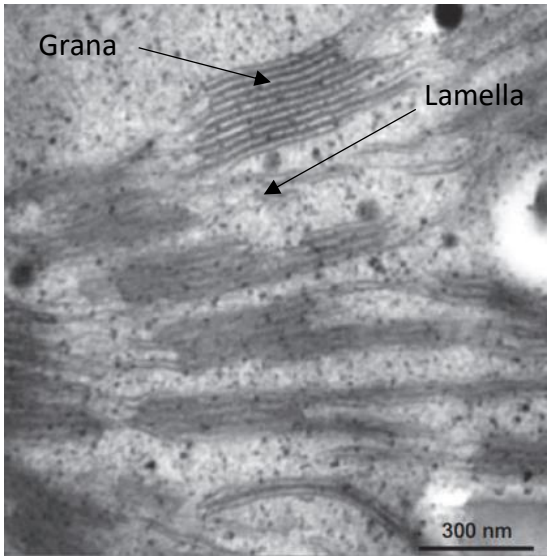

Figure 1.03 Arrangement of thylakoids in chloroplasts taken by transmission electron microscopy of ultrathin sections. Thylakoids are found in stacked 'grana' or single layer 'stroma lamella' formations, indicated by labels in the figure (adapted from Belgio *et al.*, 2015).

1.4 Light-Dependent Reactions

The light-dependent phase of photosynthesis involves the generation of ATP and NADPH from an absorbed photon. In order to do this, plants have evolved two separate structures to first catch the photon, then to generate an electron and produce the stable energy carrier molecules. The light harvesting antenna (LHC) and reaction center (RC) are the two respective components evolved to do this. LHC is composed of a variety of chlorophyll and carotenoid containing proteins (Caffarri *et al.* 2001; Ruban 2012). This cocktail of interconnected pigments collectively absorbs a large proportion of the visible light spectra, thus making them great light harvesters (Peter and Thornber, 1991). RC is comprised of two specialised chlorophyll *a* (Chl *a*) molecules. In PSII, the RC is referred to as RCII, or by the name for the specialised chlorophyll *a* P680, owing to the wavelength at which charge separation of Chl *a* occurs, and P being an abbreviation of primary donor. Concordantly, the RC of PSI is called P700 or RCI (Croce and van Amerongen, 2014). The primary charge separation event occurs at PSII. In PSII, LHC (LHCII) and RCII

form supercomplexes, where two RCII bound to 2-6 LHCII proteins ($C_2S_2M_2L_2$), depending on the plants acclimation history (Bassi *et al.*, 1987; Boekema *et al.*, 1995; Boekema *et al.*, 1998; Yakushevska *et al.*, 2003). High-light acclimated plants have less LHCII bound to each RCII, typically ~2, compared to low-light acclimated, which contain 4-6 LHCII. How the photon is guided to the RC is an interesting discussion. It has been proposed that the LHC proteins are arranged in a formation that 'funnels' the photon towards RCII (Melis and Anderson, 1983; Ruban *et al.*, 2011; Ruban, 2015). This is achieved by the LHC nearest RCII having electrons occupying energy states slightly lower than its' neighbour on the periphery of the supercomplex. Thus, when electrons in outer pigments are raised from the ground state to a singlet excited state, after relaxation, the S1 state of an acceptor occupies a region suitable for the virtual transfer of the exciton. With successive transfers like this, the exciton is guided towards RCII and an electron is generated for the electron transport chain (ETC) to use. It has also been suggested that there is no funnelling technique involved and that the result of an exciton reaching RCII arises by chance. Owing to the inefficiency of this model, whereby too much energy would likely be lost as heat, it has been proposed that plants obey the uncertainty principle. In short, this means that you cannot be reasonably certain that the exciton exists in any one place. Thus, due to the wave and particle-like properties of photons, when a photon strikes a leaf, the exciton created simultaneously spreads itself out over the cell and is therefore able to find the quickest way to RCII. This means that there is no funnelling technique involved, but the almost instant ability to find the direct route to RCII (Al-Khalili, 2014; O'Reilly and Olaya-Castro, 2014). Regardless of the mode of exciton transfer to P680, once RCII becomes oxidised, a regulated chain of events is started that produces ATP and NADPH.

Once energy has been successfully transferred to P680, charge separation occurs and an electron is excited (Barber, 2002; Umena *et al.*, 2011). Theoretically, this electron could return to the ground state by emitting the energy as light (fluorescence), heat, resonance or the electron could be donated itself. The latter process is encouraged by the position of the primary electron acceptor, pheophytin, being $< 10^{-10}$ m away from P680. Pheophytin then donates the electrons to a carrier

molecule plastoquinone. Plastoquinone is reduced to plastoquinol, whereby it transports the accepted electrons to Cyt *b6/f* (Fig 1.04). A subsequent series of redox reactions leads to the acceptance of electrons by plastocyanin, which transports the electrons to PSI. Upon reaching PSI, the electrons can be utilised in a cyclic or non-cyclic flow. The transport of electrons through the ETC, is coupled with the transfer of protons across the thylakoid membrane into the thylakoid lumen. Therefore, in order to generate more ATP, PSI can donate the electrons to plastoquinol, whereby they are used in the ETC again, thus generating a greater ΔpH. The accumulated protons in the thylakoid lumen are then released into the chloroplast stroma via ATP synthase (ATPase) and result in the generation of ATP. This process is referred to as cyclic electron flow. In non-cyclic electron flow, electrons are transferred from PSI to ferredoxin, located in the stroma. This carrier donates the electrons to Ferredoxin—NADP($^{+}$) reductase (FNR), which reduces NADP+ to NADPH. Photons absorbed of a longer wavelength, ~700nm, directly excite P700. It is therefore extremely important that P700 can use electrons in cyclical or non-cyclical electron flows. The final products of the light dependent reactions, NADPH and ATP, are then used to drive the formation of carbohydrates from CO_2.

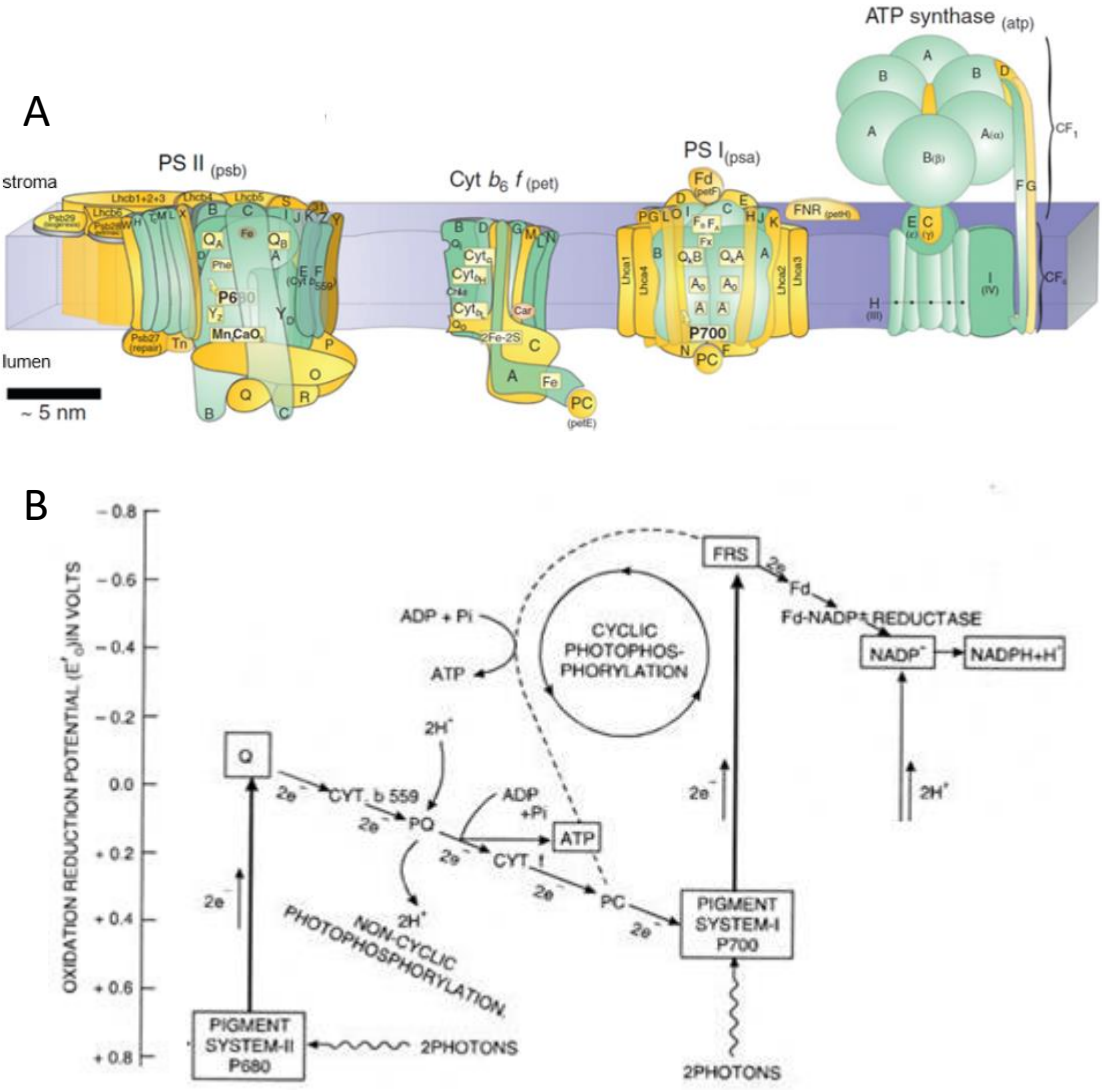

Figure 1.04 A Schematic image representing the arrangement of the four major complexes of the photosynthetic membrane: PSII (photosystem II), Cyt b6/f (cytochrome *b6/f*), PSI (photosystem I) and ATP synthase. Letters represent polypeptides that make up the protein complexes. Green images are chloroplast-encoded and yellow images nucleus-encoded polypeptides and proteins (Allen *et al.*, 2011). B Adaptation of the Z-scheme first proposed by Hill and Bendall (1960) and depicted by Berg *et al.,* (2002). Wavy lines illustrate photon excitement of primary charge complexes, straight arrows show non-cyclic electron transfer flow and dashed lines illustrate cyclic electron flow. Abbreviations represent electron transport carrier molecules and energy storage molecules.

1.5 Light-Independent Reactions

This second stage of photosynthesis occurs in the stroma. During this phase, the products of the light-dependent reactions, ATP and NADPH, are used in the Calvin-Benson-Bassam cycle (C3 cycle) to convert CO_2 into carbohydrates (Fig 1.05). Although this stage is called light-independent, it occurs during daylight, as the reactions performed in the C3 cycle are coupled to NADPH which is directly reduced from $NADP^+$ at PSI. The C3 cycle has three distinct components: carbon fixation, reduction and regeneration of ribulose. In the first stage of the cycle, using the enzyme RuBisCo, a CO_2 molecule is bound to ribulose 1,5-biphosphate (RuBP). The six carbon enediol-enzyme is unstable and is immediately split into two 3-phosphoglycerates (3-PGA). In this subsequent phase, ATP is used to phosphorylate 3-PGA to 1,3-bisphosphoglycerate (1,3BPGA), and as there are two, this requires two ATP molecules. NADPH is then used to reduce 1,3BPGA to glyceraldehyde 3-phosphate (G3P), with the oxidised $NADP^+$ available for electron acceptance at PSI. In the final stage of the C3 cycle, RuBP is regenerated from the G3P produced. One G3P molecule is used to make carbohydrates, most commonly hexose ($C_6H_{12}O_6$). The other five via a series of redox reactions and three ATPs are converted into three five carbon RuBP molecules, thus completing the cycle. The whole process can be summarised as:

$$3\ CO_2 + 6\ NADPH + 5\ H_2O + 9\ ATP \rightarrow G3P + 2\ H^+ + 6\ NADP^+ + 9\ ADP + 8\ P_i$$

Where Pi represents inorganic phosphate, this concludes the second phase of photosynthesis. The focus of my research was however on the excess energy dissipation mechanism that occurs in the light-dependent phase of photosynthesis, and this will therefore be explained in greater detail.

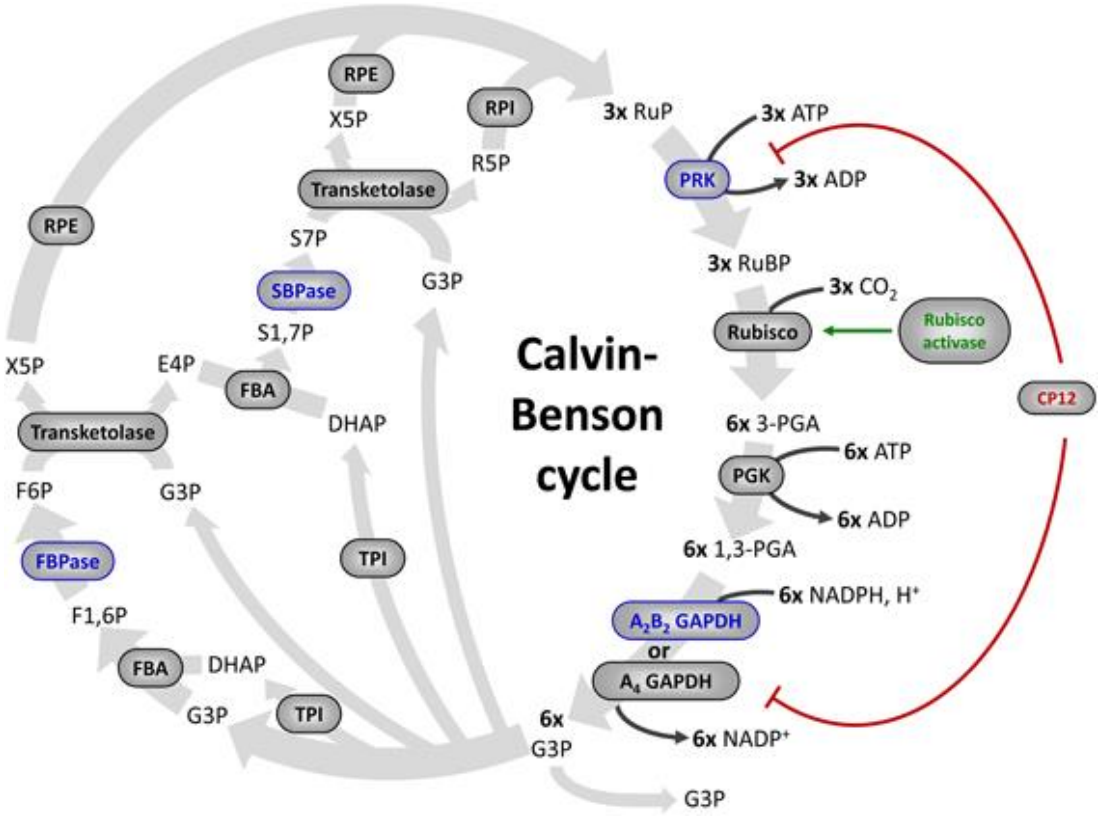

Figure 1.05 Light independent phase of photosynthesis illustrating the C3 carbon fixation process in the Calvin cycle. The eleven enzymes of the cycle are indicated in grey ellipses. Four enzymes (in blue) are activated directly by TRXs. Some proteins that control the activity of Calvin–Benson cycle enzymes are also regulated by TRXs: Rubisco activase (in green), and CP12 (in red), which forms a complex with PRK and A4-GAPDH and inhibits both enzymes. Enzymes: Rubisco, ribulose-1,5-bisphosphate Carboxylase/Oxygenase; PGK, phosphoglycerate kinase; GAPDH, glyceraldehyde-3-phosphate dehydrogenase; TPI, triose phosphate isomerase; FBA, fructose-1,6-bisphosphate aldolase; FBPase, fructose-1,6-bisphosphatase; TK, transketolase; SBPase, sedoheptulose-1,7-bisphosphatase; RPE, ribulose-5-phosphate 3-epimerase; RPI, ribose-5-phosphate isomerase; PRK, phosphoribulokinase. Metabolites, RuBP, ribulose-1,5-bisphosphate; 3-PGA, 3-phosphoglycerate; 1,3-PGA, 1,3-bisphosphoglycerate; G3P, glyceraldehyde-3-phosphate; DHAP, dihydroxyacetone phosphate; F1,6P, fructose-1,6-bisphosphate; F6P, fructose-6-phosphate; X5P, xylulose-5-phosphate; E4P, erythrose-4-phosphate; S1,7P, sedoheptulose-1,7-bisphosphate; S7P, sedoheptulose-7-phosphate; R5P, ribulose-5-phosphate; RuP, ribulose-5-phosphate. Taken from Michelet *et al.*, (2013).

1.6 Pigments of the Photosynthetic Membrane

The photosynthetic membrane can be used as the encompassing term for the complexes located in the thylakoid membrane which are responsible for photosynthesis. Of the four essential complexes involved in photosynthesis (PSII, Cyt *b6/f*, PSI and ATPase), two of these are responsible for light capture: PSII and PSI. Light harvesting would not be possible in these two complexes without the chlorophyll and carotenoid pigments.

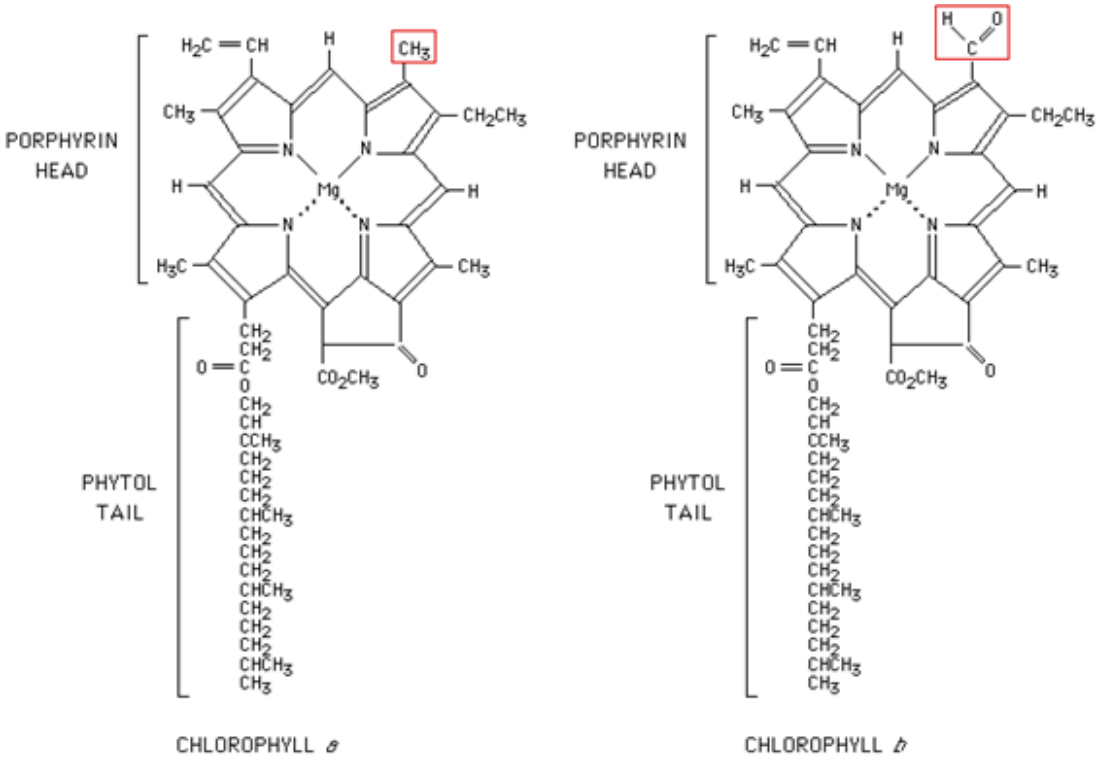

Figure 1.06 Structure of chlorophyll *a* (left) and *b* (right). Molecules consist of a magnesium bound chlorin head and a long alcohol tail (Raven and Johnson, 1989). The chlorophylls are identical except for the methyl (-CH_3) group in chlorophyll *a* and the aldehyde group (-CHO) in chlorophyll *b*.

1.6.1 Chlorophyll

Chlorophyll has many excellent properties that fulfil the function of an ideal light harvesting pigment. During photosynthesis, the photon – exciton – electron energy transfer pathway takes approximately 10^{-15}, 10^{-10} and 10^{-10}-10^{-1} s for each step respectively (Fig 1.01; Briantais *et al.*, 1979; Ruban, 2012). Chlorophyll serves as an excellent energy storage molecule by having an excited state and radiative lifetime of ~5 ns and 15^{-9} s correspondingly. Chlorophyll has a large molar attenuation coefficient of at least 10^5 M^{-1} cm^{-1}, coupled with a large absorption spectrum in the 400-700 nm visible light range (Porra, 1989). Absorption of light at 680 nm is enough for electrons to achieve their lowest S1 energy state. Light absorption by chlorophyll in the red end of the light spectrum is often referred to as the Qy band. This excited state contains enough energy, 1.8 eV, to drive photosynthesis. Furthermore, S2 energy states can be reached at the blue end of the visible light spectrum, generating ~3.0 eV. This is commonly called the Soret band or region. These energy harvesting capacities make chlorophylls ideal harvesting pigments.

Responsible for the absorption of sunlight in chlorophyll molecules is a chlorin ring (Fig 1.06). Chlorin is part of a family of heterocyclic aromatic rings called porphyrins. Porphyrins are composed of rings of four carbons and one nitrogen, pyrroles. Chlorin differs from a porphyrin as one of the pyrroles is oxidised to a pyrroline (FIGS). Located in the centre of the ring is a bound magnesium, which is responsible for donating electrons used in photosynthesis. A feature of the chlorin ring is that there are 24 delocalised π-electrons that have two orbitals. Upon the absorption of light, the π-electrons can be readily promoted to the higher energy state, giving them their light absorbing function. This chlorin structure can also be referred to as the chromophore, as it is the light harvesting part of the structure. Chlorophylls also have a tail bound to the chromophore, which is the hydrophobic part of the structure.

The biophysical properties of chlorophyll can be utilised to great effect when coupled with the physical size of the molecule. As amphipathic molecules, they can be readily incorporated into a lipid bilayer. The area of a typical chlorophyll *a*

molecule when incorporated in the thylakoid membrane is < 1 nm^2. This allows thylakoid membranes to be packed with chlorophyll molecules. As chloroplasts contain over 100 thylakoids in grana or lamellae structures, a 1 cm^2 leaf area contains a total grana membrane of approximately 40 cm^2 (Ruban, 2012). These properties make for huge light harvesting capacities of chlorophylls.

There are two types of chlorophylls in higher plants, chlorophyll *a* and chlorophyll *b* (Willstätter and Stoll, 1913).

1.6.1.1 Chlorophyll *a*

Chlorophyll *a* is the most abundant of the chlorophylls found in photosynthetic organisms. This molecule contains a chlorin ring and phytol tail, but differs structurally from other chlorophylls as it has a methylated C7 atom ($-CH_3$). It is a coordination complex, and at the centre of the molecule is a Mg^{2+} ion, which is fundamental for photosynthesis. Chlorophyll *a* has two absorption peaks at 430 nm in the Soret region and 662 nm in the Qy band. P680 and P700 are specialised chlorophyll *a* molecules, that exist as dimers, but behave as a single molecule in the centres of PSII and PSI respectively. These specialised molecules have absorption maximums at 680 and 700 nm. The other bound chlorophyll *a* molecules in the photosynthetic membrane are preferentially accumulated in the core of PSII.

1.6.1.2 Chlorophyll *b*

Chlorophyll *b* is similar to chlorophyll *a*, but it contains a formyl (-CHO) group on the C7 atom instead of a $-CH_3$ structure. This simple transformation results in different absorption peaks in this chlorophyll, with 642 and 460 nm peaks in the red and blue light absorption regions. Chlorophyll *b* is not found in RCII, but accumulated in the LHC complexes. The preferential absorption of shorter wavelengths in the Qy region fulfils this role. Energy transfer from the higher S1 states occurs more readily from chlorophyll *b* to chlorophyll *a* than the uphill transfer in reverse. Due to the spatial separation of the chlorophylls, Chl *a*/*b* ratios

are a common tool to assess the acclimation histories of plants. This is due to the upregulation of LHC proteins in shade/low light adapted plants.

Having a variety of chlorophylls in the photosynthetic membrane results in greater spectral absorption properties. Varying the proteins bound to each chlorophyll also broadens their spectral properties. This can be seen by the wide absorption peaks in a typical *Arabidopsis* absorption spectrum. Other photosynthetic organisms have varied chlorophyll cocktails, depending on the environments they inhabit. For instance, algae and diatoms have chlorophyll *c* molecules, which contain double porphyrin structures, and cyanobacteria contain *d* and *f* chlorophylls, which have formyl groups attached to different carbon atoms. The absorption spectra of higher plants are further increased by the inclusion of yellow light absorbing pigments called carotenoids.

1.6.2 Carotenoids

Carotenoids are one of the most abundant pigments found in the natural world. ~600 million tonnes of just one carotenoid called isoprene, the precursor for the most important xanthophylls in higher plants, is produced annually (Guenther *et al.*, 2006). Over 600 types of carotenoids have already been discovered and they are highly versatile. They are responsible for the autumnal orange colour of leaves, the redness of a cooked lobster and the yellow tinge of the human eye. With the exceptions of two animals, spider mites and aphids, the rest are produced by algae, bacteria, fungi and plants. Carotenoids are often yellow, orange or red in colour, and this is due to the absorption peaks in the purple to green end of the visible light spectrum (400-550 nm). Although the strength of the light harvesting capacity can be debated due to the very short lifetimes in the excited state (~3 s^{-13}), they have much wider absorption spectra than chlorophylls. Indeed, in the xanthophylls of higher plants, there are 0-0 electronic transitions, but also 0-1 and 0-2 vibrational transitions. This gives xanthophylls a three-peak broad absorbance spectra. This range of peak absorptions between ~410 and ~480 nm complements the 430-462 nm Soret band region of chlorophylls. Varying the number of conjugated double

bonds results in different absorption peaks between the xanthophylls. Whereby, if xanthophylls are not increasing the absorption spectra of the photosynthetic membrane, they can act as effective excess energy dissipaters. In higher plants there are two main groups of carotenoids: α-carotenes and β-carotenes (Fig 1.07). These two classes arise from the same precursor lycopene. Lycopene is arranged from eight isoprene subunits, which forms an all trans structure with 11 conjugated double bonds along its backbone. Conversion to α-carotene and β-carotene involves cyclisation of the hydrocarbons by lycopene cyclase. Cyclisation produces two types of complexes: β- and ε-cyclases. α-carotene is an asymmetrical molecule, consisting of one β- and ε- terminal cyclase. β-carotene is a homodimer with two β-cyclases at either end of the hydrocarbon backbone. The two rings differ due to the positions of the double bonds in the cyclase complex. Oxygenation of the cyclase in these carotenes gives rise to the four essential xanthophylls: lutein, violaxanthin, zeaxanthin and neoxanthin. Variations in the numbers of double bonds in the hydrocarbon tail, and oxygenation of the rings gives rise to different slightly different properties for all the xanthophylls. These variations affect the three vital functions of the xanthophylls: structure, photoprotection and light harvesting. The structures of each xanthophyll and their roles will be discussed in further detail below.

1.6.2.1 Lutein

Lutein is the most common xanthophyll in the natural world (Pogson et al., 1996; Zia, 2010). Of the four major xanthophylls in higher plants, it is the only one in the α -carotene biosynthesis pathway. It is converted from α -carotene via the single oxygenated zeinoxanthin intermediary, to have two oxygenated rings. Lutein has 10 conjugated double bonds in its backbone, with β- and ε-rings located at opposing ends of the molecule. Its structure creates a broad absorption spectrum with three peaks around 424, 445 and 472 nm in ethanol (N'soukpoé-Kossi, 1988). The S1 energy states of lutein are just below those of chlorophyll *a* and *b*, making them good acceptor molecules. There are two luteins bound to each LHCII trimer, with sites called L1 and L2, and are located in the centre of the LHCII complex. The

lutein in the L1 position is called Lut 620 and in the L2 position Lut 621. The lutein molecules located in the hydrophobic centre of the LHCII trimer are responsible for binding central helices A and B. lut2 knock-outs are inhibited in the lutein biosynthesis pathway. These mutants have been shown to lack LHCII structures, but the plants still accumulate individual polypeptides. This illustrates the importance of the 'scaffold-like' function that lutein plays. Evidence for the energy dissipation role of lutein was first demonstrated by Ruban and co-workers (Ruban *et al.*, 2007). Using Resonance Raman spectroscopy, it was demonstrated that upon excitation of chloroplasts, Lut 620 undergoes conformational changes. Lut 620 is also located next to the three chlorophyll *a* molecules, Chl *a*610, *a*611 and *a*612, that are most likely to be delocalised when the membrane is excited by light, as they are the lowest energy chlorophylls in the antenna (van Grondelle and Novoderezhkin, 2006). Furthermore, the contortions of Lut 620 have been suggested to bring it closer to Chl *a* 612, thus increasing its ability to act as a quencher for this excited chlorophyll (Wentworth *et al.*, 2003). This was supported by theoretical calculations of Duffy *et al.*, (2013), which showed that the chlorophyll to Lut 620 energy transfer pathway could be a major quencher in the qE process. More recently Fox and co-workers have shown that the coupling between Lut 620 and neighbouring chlorophylls is affected by the distortion of the lutein molecule (Fox *et al.*, 2015). Lutein is undoubtedly vital for the correct structural arrangement of the major light harvesting antenna of PSII, and increasing evidence also suggests that it plays a major role in the NPQ process.

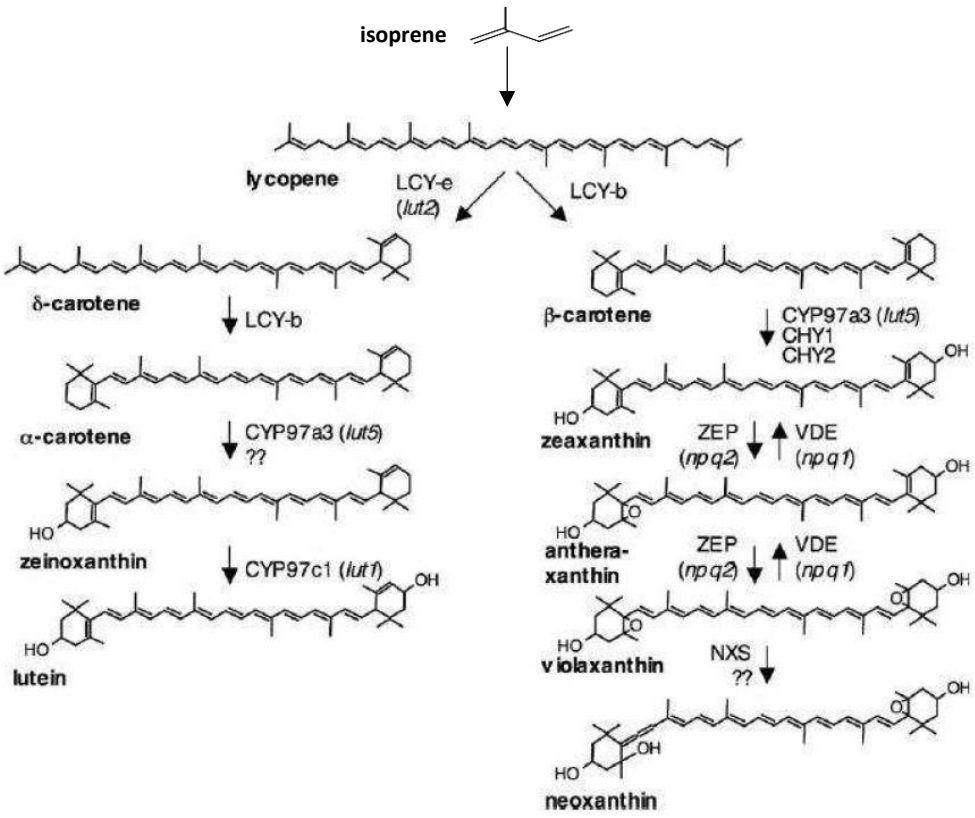

Figure 1.07 The carotenoid and xanthophyll biosynthesis pathway in *Arabidopsis thaliana*. Question marks depict mutants that are currently undefined (Raven and Johnson, 1989). Mutations of xanthophyll conversion enzymes has been used to limit the accumulation of certain xanthophylls in the light harvesting membrane. Inhibition of violaxanthin de-epoxidase (VDE) stops the conversion of violaxanthin back to antheraxanthin, therefore leading to a build-up of only violaxanthin.

1.6.2.2 Zeaxanthin

Zeaxanthin is the first xanthophyll in the β-carotene biosynthesis pathway, however it is not present in the membrane in notable amounts during dark or low light harvesting conditions. This is due to its role in photoprotection. The zeaxanthin structure is an alternating single/double bonded hydrocarbon with terminal oxygenated β-cyclases. It has a total of 11 double bonds which contribute to the typical carotenoid broad visible light absorption spectrum. It has peaks at 426, 451 and 478 nm in ethanol (N'soukpoé-Kossi, 1988). Also, the S1 energy state occupied is just below chlorophyll, so it can act as an energy receiving molecule. Zeaxanthin was first recognised as playing a prominent role in the NPQ process by Barbara Demmig (1987). She discovered that the conversion of violaxanthin to zeaxanthin was associated with increased NPQ levels. Since then it has been proposed to be the major quencher in NPQ by a number of groups (Demmig-Adams, 1990; Dreuw *et al*., 2003). Zeaxanthin promotes NPQ by increasing the hydrophobicity of the complexes it is bound to, which, increases the aggregation of the complexes, primarily LHCII. It has subsequently been shown to not be essential but still important to generate maximum NPQ (Rees et al., 1989; Niyogi et al., 1997). A role for zeaxanthin has recently been proposed by Sacharz *et al.* (2017) whom suggest that zeaxanthin is responsible for the binding of the antenna PsbS protein, particularly by the minor antenna. This will be discussed in greater detail in section 1.7.1.6 - PsbS Protein. Zeaxanthin clearly plays a role in photoprotection, but is not as structurally integral to LHCII as neoxanthin and lutein molecules. The V1/Z1 binding site is located on the periphery of LHCII. This allows the violaxanthin, antheraxanthin and zeaxanthin interconversion cycle (VAZ cycle) to be more easily activated in the lumen, but in exchange for this, it cannot act as a scaffold like lutein.

1.6.2.3 Violaxanthin

The third xanthophyll in β-carotene biosynthesis pathway is violaxanthin. It is converted to and from zeaxanthin via the violaxanthin de-epoxidase/zeaxanthin

epoxidase cycle (Fig 1.07). Antheraxanthin is the intermediate of the violaxanthin/zeaxanthin conversion. Violaxanthin has two epoxides, with antheraxanthin containing one, with it being absent in zeaxanthin. These cyclic ethers are positioned on the β-cyclase carbons which bind the cyclases to the hydrocarbon backbones. At pH > 6.5, epoxidation is more common, with violaxanthin being found throughout the thylakoid and lumen (Hager, 1969; Hager and Holocher, 1994). Violaxanthin de-epoxidase (VDE) is the enzyme responsible for the accumulation of violaxanthin in these conditions, after first being identified and purified in 1970 (Hager and Perz, 1970; Muller-Moule *et al.*, 2002). As is the case with zeaxanthin, due to its occupation of the peripheral V1 site, it is not as vital as a structural xanthophyll as lutein or neoxanthin. It is also unlikely to play a significant role in photoprotection. It has 9 double bonds, all in the hydrocarbon chain, and thus has a different absorption spectrum to lutein and zeaxanthin. It had been proposed that the S1 state of violaxanthin occupies a higher excited state orbital than chlorophyll. Consequently, due to the energetically unfavourable transfer pathway required, it is deemed to not act as a good excess energy dissipater. However, this will be discussed in more detail in section 1.8.3. Furthermore, the mere fact that during the NPQ process it is converted to zeaxanthin, would support the notion that it is not an effective energy acceptor molecule from excited chlorophylls. Due to the polar nature of violaxanthin, it is vital for maintaining the light harvesting state of PSII (Horton *et al.*, 1991; Ruban and Horton, 1999).

1.6.2.4 Neoxanthin

The most polar of the xanthophylls is neoxanthin. Synthesised from violaxanthin, it is the most structurally different from β-carotene in this biosynthesis pathway. One of the epoxide rings has a highly reactive allene bond connecting it to the hydrocarbon chain. Two notable recent papers have ascribed this conversion to neoxanthin synthase (Bouvier *et al.*, 2000; Dall'Osto *et al.*, 2007). In nature it can adopt both trans and cis formations, but in higher plants light

harvesting antenna, it only adopts the 9-cis conformation. There is one neoxanthin bound to helix c in the chlorophyll *b*-rich LCHII trimer (Domonkos *et al.*, 2013). The structural importance of neoxanthin was documented by the Bassi laboratory, who reported that it was not possible to incorporate more than two xanthophylls into recombinant LHCII without the presence of neoxanthin (Croce *et al.*, 1999a, 1999b). Besides the structural role of this xanthophyll, neoxanthin is not widely ascribed a major role in photoprotection, but it does exhibit several characteristics of energy acceptor molecules. In NPQ conditions the absorption peaks of chlorophylls in the blue region are quenched, neoxanthin changes conformational shape in the aggregated LHCII. Indeed, the greater the aggregation of LHCII, the greater the degree of distortion (Ruban *et al.*, 2005). This has been demonstrated *in vivo* and *in vitro* (Pascal *et al.*, 2005; Ruban *et al.*, 2005; Ruban *et al.*, 2007). The movement of this molecule to a non-linear plane has been proposed to allow the adoption of an S1 state when excited. This state encourages the energetically favourable transfer of energy from chlorophyll *b* to neoxanthin. With neoxanthin found almost exclusively in LHCII, and with a particular affinity for interactions with Chl *b* (Croce et al., 1999a; Croce et al., 1999b), it has been proposed to be a key component in the Chl *a*-Lutein 620 energy dissipation pathway. However, knockouts of neoxanthin, which accumulate violaxanthin instead, do not have a markedly reduced NPQ capacity.

1.7 The photosynthetic membrane

The photosynthetic membrane is composed of four major complexes: PSII, Cyt *b6/f*, PSI and ATPase. These complexes are arranged in the thylakoid membrane for efficient linear electron flow, which starts with the primary generator of electrons, PSII.

1.7.1 Photosystem II

PSII is a multi-subunit complex (Fig 1.08), and is the primary generator of oxygen on planet Earth. It is a water-plastoquinone oxireductase and contains the most powerful natural oxidising agent, P680. The PSII supercomplex is approximately 1100 kDa and is composed of 40 protein subunits (Dekker and Boekema, 2005; Shi *et al.*, 2012a; 2012b). PSII is highly conserved amongst photosynthetic organisms. For instance, the three subunits which make up the OEC: PsbO, PsbP and PsbQ, which are sometimes called OEC33, 24 and 17 respectively, are found in plants and algae. PsbO is also found in cyanobacteria, with homologues of the other two subunits (PsbU and PsbV) fulfilling similar functions (Bricker and Frankel, 2011; Bricker *et al.*, 2012; Shi *et al.*, 2012a). There are also 10 LHC proteins in vascular plants, and despite over 350 million years of evolution of the tracheophytes, none of the LHC proteins have been lost (Andersson *et al.*, 2001). The conserved PSII can be broken down into three major groups: RCII, OEC and LHCII.

1.7.1.1 Reaction Center and Oxygen Evolving Complex

At the core of the reaction center of PSII is a chloroplast-encoded heterodimer of D1 and D2 proteins (Loll *et al.*, 2005; Umena at al., 2011). The D1 protein is encoded by the psbA1, A2 and A3 genes, with D2 by psbD1 and D2 genes (Golden *et al.*, 1986; 1988). Each of these homologous proteins are anchored in the membrane via five transmembrane helices. They also bind six Chl *a*, and two modified Chl *a* (pheophytin *a*) molecules, which contain two centrally bound H+ atoms instead of Mg^{2+}. The proteins, particularly D1 protein, serve as a scaffold for all of the vital redox co-factors associated with PSII, which includes: P680, Mn_4CaO_3 cluster, pheophytin *a*, and plastoquinone molecules Q_A and Q_B. D1 protein is the most susceptible protein to photodamage and it is has the highest turnover of the RCII associated proteins (Ohad *et al.*, 1984). Indeed, the Ruban lab have recently used the treatment of plats with the chloroplast-inhibitor antibiotic lincomycin to

create ‘RCII-less’ plants, thus demonstrating the importance and high turnover rate of the D1 protein (Belgio *et al.*, 2012; 2014). The D1 repair cycle is therefore of vital importance for restoring PSII function, and will be discussed in section 1.8.2.

Also associated with the core are two proteins called CP43 (PsbC) and CP47 (PsbB). Each of these subunits are fixed in the thylakoid membrane via six transmembrane helices (Rhee *et al.*, 1998, Ferreira *et al.*, 2004). These proteins serve two major roles: excitation energy transfer to RCII and light harvesting. These roles are fulfilled by the binding of 29-30 Chl *a* molecules, with 13-14 and 16 being attributed to the individual subunits respectively, with the transfer being proposed to happen via the RCII associated ChlZD1 and ZD2 chlorophyll *a* molecules (Ferreira *et al.*, 2004; Umena *et al.*, 2011). Xanthophylls are not associated with these subunits (Kamiya and Shen, 2003), therefore they are unlikely to play a role in energy dissipation, despite this having been previously proposed (Bassi, 1996).

The three highly conserved PsbO, PsbP and PsbQ subunits make up the OEC. These subunits are found at the lumenal side of the thylakoid membrane and are involved in the binding, stabilising and isolation of the OEC (Zouni *et al.*, 2001; De Las Rivas *et al.*, 2004; Boekema *et al.*, 2000). At the heart of the OEC is the Mn_4CaO_3 cluster which is essential for the splitting of water. The process occurs via the sequential oxidation of Mn atoms from S0 to S4 states, via the absorption of four photons driving the four charge separations (Kok *et al.*, 1970). Electrons are replaced in the cluster via the deprotonation of two water molecules. PsbO is vital for binding the OEC to CP43 and CP47 subunits and stabilises the catalytic cluster. The PsbP and PsbQ polypeptides enclose the catalytic site of the Mn_4CaO_3 cluster.

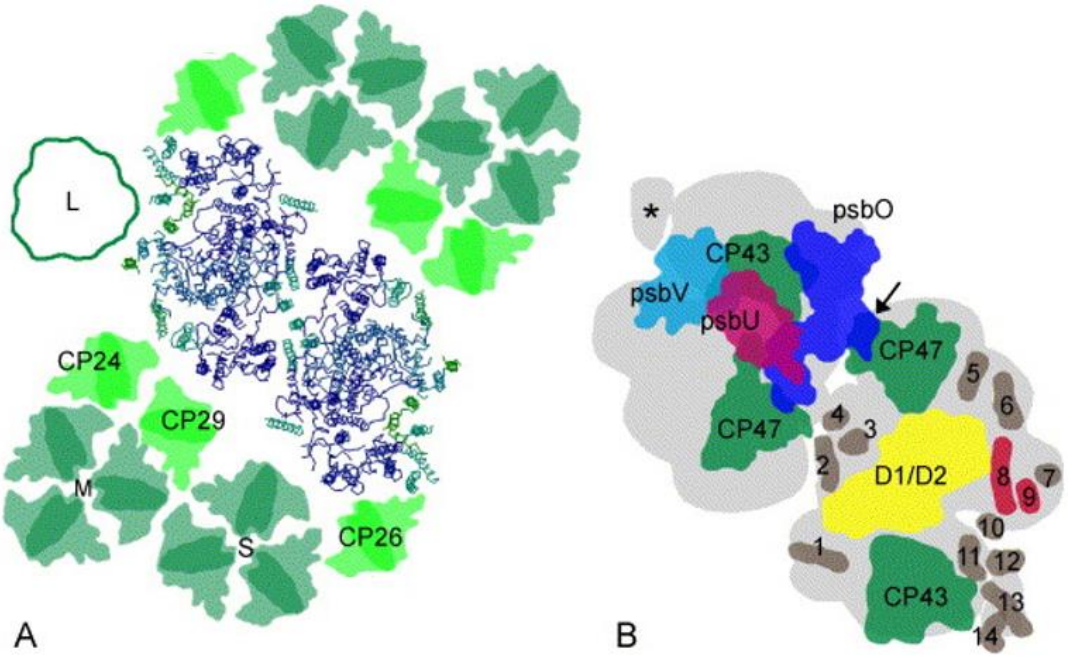

Figure 1.08 A Depiction of PSII supercomplex structure adapted from transmission electron microscopy images taken by Boekema *et al.*, (1999) at 3.7-Å. Strength of antenna bond is represented by S, M and L for strong, medium and loose. CP24, CP26 and CP29 indicated the positions of the minor antenna. B Enlarged representation of RCII, from electron microscopy experiments by Ferreira *et al.*, (2004). Abbreviations indicate: D1/D2, reaction center heterodimer; CP43 and CP47, reaction center bound transmembrane proteins; psbO, psbU, psbV, PSII stabilising subunits bound to the OEC. Images taken from Dekker and Boekema (2005).

1.7.1.2 The Major Antenna - Lhcb1-3 (LHCIIb)

The three polypeptides, lhcb1, lhcb2 and lhcb3, exist as a trimeric complex in the photosynthetic membrane (Fig 1.09). Owing to this, collectively, lhcb1, lhcb2 and lhcb3 are called LHCII, LHCIIb or the major antenna complex. The individual polypeptides in ascending order are 28, 27 and 25 kDa (Peter and Thornber, 1991). The average ratio of the polypeptides lhcb1, lhcb2 and lhcb3 in the trimeric complex is correspondingly 8:3:1, although in different mutants and under different conditions, the polypeptide concentrations and ratios can change (Jansson, 1994; Jansson, 1999; Jackowski *et al.*, 2001; Ruban *et al.*, 2003). Four-six trimers are

bound to each RCII, leading to the supercomplex often being referred to as the C2S2M2 or C2S2M2L2 supercomplex, depending on the acclimation history of the plants (Boekema *et al.*, 1995; Caffarri *et al.*, 2009). The complex contains the majority of the supercomplex bound chlorophyll and pigments, with approximately 60% of chlorophyll and 80% of pigments in PSII bound to the trimer (Peter and Thornber, 1991; Caffarri *et al.* 2001; Ruban 2012). It is also the most abundant membrane-bound protein on earth (Ogawa *et al.*, 1966; Thornber, 1969). Each monomer in the complex contains 14 chlorophyll molecules, of which, eight are Chl *a* and six Chl *b* (Peter and Thornber 1991; Bassi and Dainese 1992; Liu *et al.*, 2004). The chlorophylls are unevenly distributed with specific binding sites. Chl *b* is found at the monomer-monomer interfaces and Chl *a* more centrally located (Liu *et al.*, 2004). There are four xanthophylls associated with each monomer, two luteins, one neoxanthin and one violaxanthin/zeaxanthin (see 1.6.2 for more details). Each of these xanthophylls is bound at a site L1, L2, N1 and V1, with each letter indicating the xanthophyll that is bound there: lutein 1 and 2, neoxanthin and violaxanthin/zeaxanthin. The interchangeability of violaxanthin to zeaxanthin encourages the aggregation of LHCII upon exposure to light, and is one of the key features of the NPQ mechanism (see 1.8.4 for further details). Although not bound permanently to LHCII, it has been demonstrated that the PsbS protein affects the rigidity of the membrane (Kereiche *et al.*, 2010; Goral *et al.*, 2012). It has recently been demonstrated that it does this by binding directly to LHCII, particularly lhcb1 and lhcb3 of the moderately bound LHCII, and lhcb2 of the loosely bound LHCII as part of the process (Sacharz *et al.*, 2017). This might be one of the reasons that LHCII mutants, demonstrated by lhcb2 antisense knockdowns (aslhcb2), only have a 60% NPQ capacity compared to WT, despite the upregulation of lhcb5 in response to reduced LHCII (Yakushevka *et al.* 2003; Ruban *et al.*, 2003). *ch1* mutants have no Chl *b* proteins, which preferentially affects the major antenna causing a loss of LHCII, and it is more prone to photoinhibition than WT plants (Havaux *et al.*, 2004). LHCII is also involved in the redistribution of excitation energy between PSI and PSII in low light conditions, referred to as state transitions or qT (Nilsson *et al.*, 1997; Benson *et al.*, 2015). PsbS protein and state transitions are discussed further in sections 1.7.1.4 and 1.8.3.2 respectively.

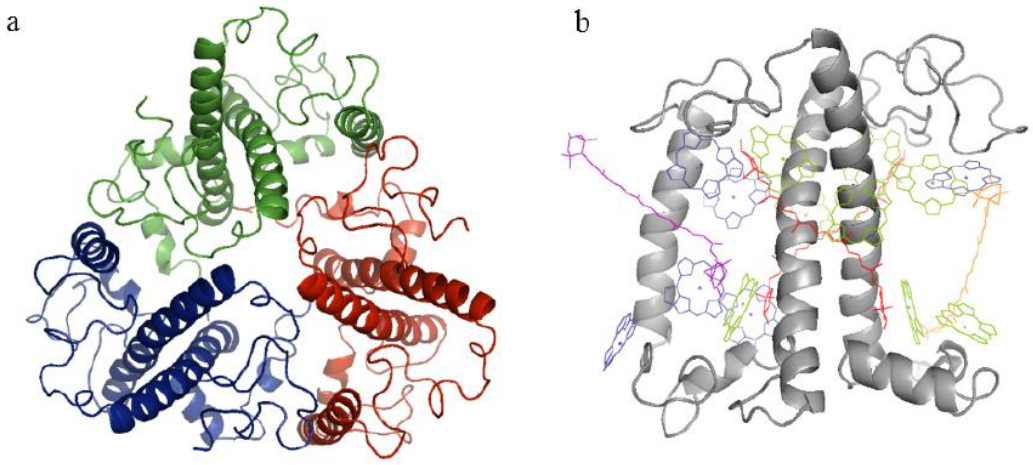

Figure 1.09 A Trimeric LHCII as visualised from the stroma. Monomers are shown in different colours (Standfuss *et al.*, 2005). B A monomer of the complex displayed perpendicular to the thylakoid membrane. The monomeric polypeptide structure is in grey with bound pigments illustrated in different colours: lutein – red, neoxanthin purple, violaxanthin – orange, chlorophyll *a* – green and chlorophyll *b* – blue (Liu *et al.*, 2004). Chlorophylls have phytol tails removed for image clarity.

1.7.1.3 The minor antenna - lhcb4, lhcb5 and lhcb6

The minor antenna complexes refer to the complexes encoded by the lhcb4, lhcb5 and lhcb6 genes. Lhcb4, lhcb5 and lhcb6 are also referred to by the molecular weight in kDa of the complexes: CP29, CP26 and CP24 weighing 29, 26 and 24 kDa respectively (Peter and Thornber, 1991; Croce *et al.*, 2002). The minor antenna complexes bind xanthophylls and chlorophylls in different quantities (Peter and Thornber, 1991; Sandona *et al.*, 1998; Bassi *et al.*, 1999). CP29 binds six Chl *a* and two Chl *b* molecules, three xanthophylls, lutein, neoxanthin and violaxanthin in a 10:8:15 ratio. CP26 binds six Chl *a* and three Chl *b* molecules, three xanthophylls, lutein, neoxanthin and violaxanthin, in a 2:4:1 ratio. Finally, CP24 binds five Chl *a* and five Chl *b* molecules, but only two xanthophylls, one lutein and one violaxanthin (Peter and Thornber, 1991; Bassi, 1996; Croce *et al.*, 2002; Wehner *et al.*, 2006). The roles of the minor antenna have been studied using a combination of

biochemical techniques, antisense and knock-out mutants, and more recently reconstituted liposomes. However, despite the vast research into the form and function of the minor antenna, the results are often conflicting and leave the exact roles of the minor antenna still to be elucidated.

Although the Bassi laboratory champion the notion that the minor antenna is the site of NPQ, it was actually the Horton laboratory who first utilised N,N'-Dicyclohexylcarbodiimide (DCCD). The binding of DCCD is used to test whether proteins can be protonated. The inhibition of qE by DCCD was discovered by Ruban et al., (1993). CP29 binds DCCD, and was thus proposed to be heavily involved in photoprotection (Pesaresi et al., 1997). Recent independent work by Fan et al., (2015) suggested that DCCD disrupts the intermolecular bonds on proteins that it binds to, and can thus alter the shape and properties of the proteins. This adds some doubt to the validity of the conclusions drawn from the Pesaresi work.

A number of different groups have researched the effects of antisense and knock-outs of minor antenna genes. De Bianchi *et al.*, (2011) showed that, all three isoforms of the lhcb4 genes, lhcb4.1, lhcb4.2 and lhcb4.3, are required to be knocked-out for marginal effects to be observed. Knock-outs of one or two isoforms did not reduce ETR or NPQ, as knock-outs of all isoforms did. Miloslavina *et al.* (2011) produced single knock-outs of CP26 and CP29, and a double knock-out of CP24/26. NPQ measurements show that the koCP26 and koCP24/26 do not have markedly reduced NPQ levels, or altered fluorescence decays in the Fm state, compared to WT plants. The koCP29 has significantly reduced NPQ compared to WT plants, but not less than the other mutants. The koCP26 also has the same fluorescence decay as the WT in the NPQ state, although the double KO and koCP29 have markedly slower fluorescence decays in the NPQ state. Knock-downs were shown to have less severe side-effects (Andersson *et al.*, 2001). KoCP26 had one less LHCII per supercomplex compared to WT, but besides this, koCP29 and koCP26 had no physical alterations of the supercomplexes. Furthermore, fluorescence measurements of quantum yields and separate CO2 consumption rates were not markedly altered compared to WT plants (Andersson *et al.*, 2001). Again, KOs had extreme side-effects, and reduced the ability to investigate the minor antenna

effectively. Both Yakushevka *et al.* (2003) and Kovacs *et al.* (2006) were unable to extract intact PSII supercomplexes from koCP29 and koCP24 thylakoid membranes, suggesting that the minor antenna is essential for maintaining the supercomplex structure. The conclusions are echoed by Dall'Osto *et al.*, (2014). Luca Dall'Osto has recently created a triple knock-out of all three minor antenna complexes, aptly called 'No Minor Antenna' or NoM for short. Time resolved fluorescence experiments performed on dark adapted koCP29/24, koCP26/24 and NoM thylakoids, are progressively slower than the WT thylakoids suggesting that exciton transfer from LHCII to RCII is impaired in the plants lacking minor antenna. In contrast to this, work on proteoliposomes lacking minor antenna did not have altered 77 K spectra or fluorescence induction experiments, compared to proteoliposomes with minor antenna (Sun *et al.*, 2015). These recent results therefore indicate the temperamentality of light harvesting without the minor antenna, indicating structural and functional importance in the membrane, and would be an interesting avenue of future research.

The various research investigating the minor antenna leads to an unclear picture of the exact roles of the minor antenna during NPQ, and that perhaps some of the conclusions drawn from experiments might be premature. A very recent publication by the Ruban lab has inadvertently elucidated an important role of the minor antenna in NPQ. The recent work of Sacharz *et al.* (2017) suggests that the minor antenna does play an important role, being the site of PsbS protein and zeaxanthin interaction. Indeed, pull-down assays show that all minor antenna complexes interact with the PsbS protein, a vitally important component of the NPQ process. Reproducing this work with different antenna proteins, rather than focussing on the PsbS protein, could provide the crucial missing link in elucidating the role of these complexes.

1.7.1.4 PsbS Protein

Although the location of the PsbS protein has not been formally identified, it is related to the Lhc family of proteins. Like the Lhc family it is highly conserved amongst green organisms and has homologues in moss and algae (Anwaruzzman *et al.*, 2004; Peers *et al.*, 2009). However, unlike the Lhc proteins, it does not bind any xanthophylls or chlorophylls (Fan *et al.*, 2015). Indeed, it was suggested that it did not play a significant role in PSII, and was one of the reasons that it took so long to investigate the function of PsbS (Li *et al.*, 2000), after its discovery by Funk et al., (1994). PsbS protein is smaller than other antenna proteins at only 22 kDa (Funk *et al.*, 1994), but much of the protein form and function remains a mystery. Fan and co-workers have suggested that whilst LHCII requires lutein to fold into its trimeric structure, the transmembrane 2 and 4 (TM2, 4) regions of PsbS fulfil this function (Fig 1.10). PsbS protein exists as a dimer as hydrogen bonds and salt bridges form between the TM 2 and TM 3 domains. It has previously been reported that PsbS protein exists as a dimer when the PSII membrane is in the light harvesting state, but upon acidification of the thylakoid lumen, PsbS monomerises (Bergantino. *et al.*, 2003; Teardo *et al.*, 2007; Wilk *et al.*, 2013; Gerotto *et al.*, 2015). This has been recently questioned as Fan *et al.* (2015) who mutated the 'pH sensing' glutamate residues of PsbS, in order to make it maintain its light harvesting state. The group found that it exists as dimers in both light harvesting and light dissipating states. It was acknowledged that PsbS protein does elute at different speeds when it is found in neutral and acidic conditions. The group suggested that at ~pH 7, there is a larger distance between the two PsbS monomers, due to the weakening of intermolecular forces, which causes the 'acidified' dimer to elute more slowly. Sacharz *et al.*, (2017) attribute the differences between the activated monomer versus constituent dimer debate as differences between the *in vivo* and *in vitro* nature of the studies respectively. As well as the difficulties in defining the structure of PsbS, the mode of action upon activating the dissipation of excess energy is controversial. Firstly, the Niyogi laboratory found that knock-outs of the PsbS gene (*npq4*) resulted in plants that were unable to form NPQ (Li *et al.*, 2000). This lead the group to propose that PsbS protein was the site of NPQ (Niyogi et al, 2004.). Then the Ruban laboratory demonstrated that *npq4* plants are able to form NPQ. Firstly, it

was shown that WT NPQ levels could be achieved in these plants if an enhanced artificial ΔpH was applied to chloroplasts (Johnson and Ruban, 2011), and subsequently that NPQ is formed over a slower timescale in the absence of PsbS (Ruban and Belgio, 2014). It therefore appears that PsbS protein is not the site of NPQ, but acts as an enhancer of NPQ. Indeed, this was suggested by Kereiche *et al.*, (2010) and Goral *et al.*, (2012) who independently demonstrated that the absence of PsbS protein increases the rigidity of the membrane. The most recent and detailed proposal for the involvement of PsbS protein in NPQ comes from the Ruban lab. Sacharz *et al.*, (2017) ascertained through pull-down assays that PsbS interacts with lhcb's 1, 2 and 3 of the major antenna, and also lhcb's 4, 5 and 6 of the minor antenna, with a particular preference for binding lhcb4. This lends support to the notion that PsbS protein acts as an enhancer of NPQ by increasing aggregation of antenna proteins.

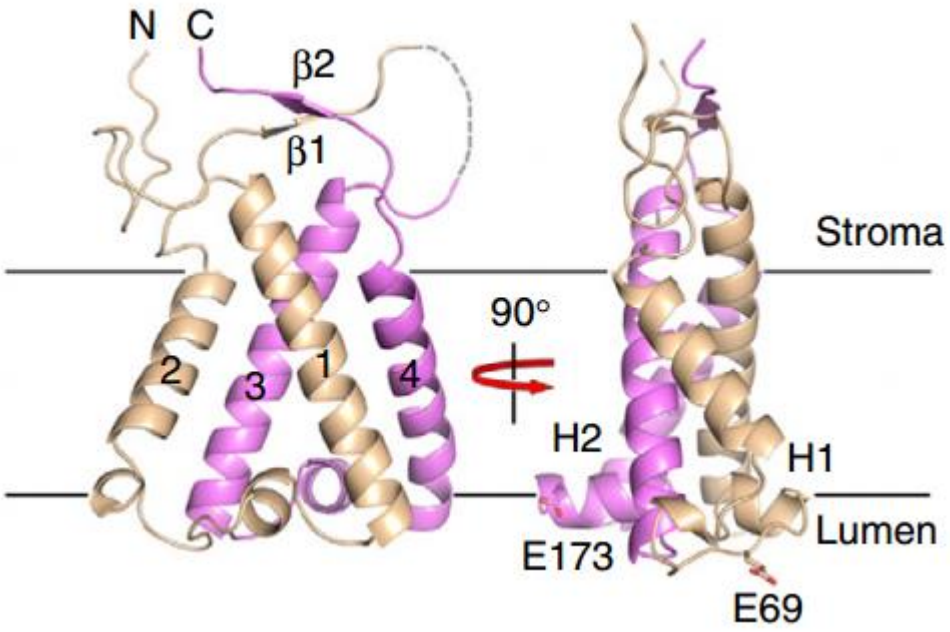

Figure 1.10 PsbS protein representation as it is positioned in the thylakoid membrane. Calculated from 2.35-Å crystallised spinach proteins. 1, 2, 3 and 4 represent the transmembrane polypeptides of the protein. N and C indicate the terminal domains of the proteins. E173 and E69 show the glutamate exposed residues of PsbS. Taken from Fan *et al.*, (2015).

1.7.2 Cytochrome b_6/f Complex

The Cyt b_6/f complex is a dimeric transmembrane complex. It has four small and four major subunits: cytochrome b_6 complex (Cyt b_6/f), cytochrome *f* complex (Cyt *f*), Rieske iron-sulphur protein and subunit IV (Fig 1.11). The Cyt b_6/f complex also binds one Chl *a* molecule and one β-carotene, the role of these pigments has not yet been determined (Baniulis *et al.*, 2008, Yeates, 2015). The Cyt b_6/f complex occupies the second position of major complexes in the transport of electrons in the photosynthetic transport system. It serves as the transitional carrier of energy between PSI and PSII. Indeed, that is why it is located in the periphery of grana stacks, regions in between the PSII and PSI-rich grana stacks and lamellae respectively (Allen and Forsberg, 2001; Dekker and Boekema, 2005). During the process of electron transfer, two protons are accepted by plastoquinone, which is immediately reduced by two electrons from a Q_B carrier. It then diffuses to the lumen side of the membrane to donate the electrons to Cyt b_6/f, and two protons pass into the lumen. The two electrons are separated at the Q side of the membrane. The first electron is transferred, via the Rieske iron-sulphur protein, to plastocyanin. This is then used to reduce NADP to NADPH at ferredoxin NADP reductase on the stromal side of the membrane, through the Cyt *f* complex. When plastocyanin is in the reduced state, the electron returned to an oxidised plastoquinone near the stromal edge of the thylakoid by the Cyt b_6 complex, and it is used to transfer protons back across the membrane. Out of the two electrons that are transported to the Q-site of the Cyt b_6/f complex, one is used for further photochemical reactions, and one is reused to increase the ΔpH. This two-fate electron cycle is referred to as the Q cycle. Many of the electron carrier molecules have other roles within chloroplasts. For instance, ferredoxin is not only essential for the transfer of electrons to ferredoxin NADP(+) reductase, but it is involved in nitrogen and sulphur fixation, CO2 assimilation, and is a key regulator in the function of many enzymes (Fukuyama, 2004).

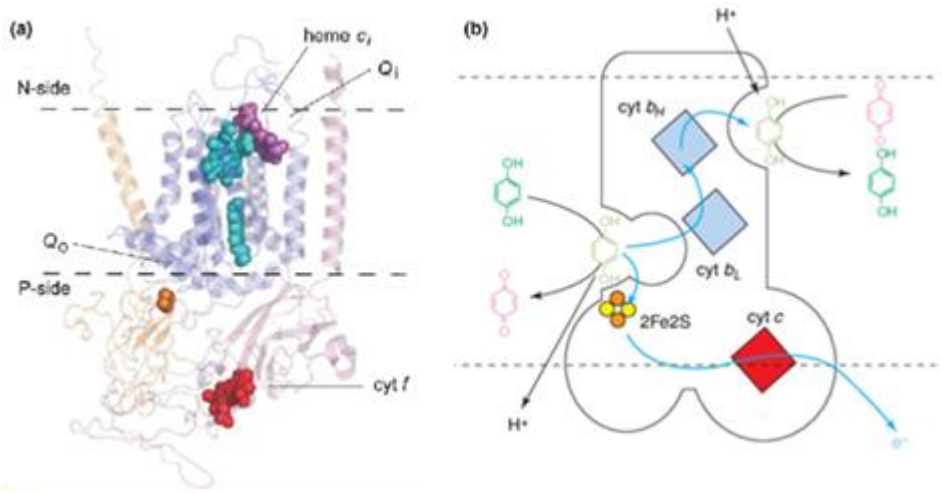

Figure 1.11 A The cytochrome *b6/f* complex of *Chlamydomonas reinhardtii*. B The Q cycle of electron flow through the cytochrome *b6/f* complex. Colours represent different protein subunits and cofactors: orange, Rieske cluster; slate, cyt *b*; red, cyt *f* and cyt *c* 1; cyan, cyt *b* L and cyt *b* H; purple, heme *c* i; green, stigmatellin; yellow, antimycin-A. Dashed lines represent the thylakoid membrane, with the N-side representing the chloroplast stroma, and the P-side the thylakoid lumen (Cape *et al.*, 2006).

1.7.3 Photosystem I

PSI, like PSII, consists of a reaction center (RCI) and a light harvesting antenna (lhca; Fig 1.12). Besides this, there are many differences between the two photosystems. RCI exists as a monomer, it contains 13 subunits, 19 carotenoids and 174 Chl *a* molecules. There are four lhca antenna complexes bound to each core protein, which exist as lhca2-lhca3 and lhca1-lhca4 heterodimers. The Chl *a*/*b* ratio of the lhca proteins is much higher than the Chl *a*/*b* ratio of PSII, with 143 Chl *a* and 12 Chl *b* molecules bound to the light harvesting antenna. There are also 35 carotenoids bound to the lhca antenna complex, only five of which are lutein and four violaxanthin (Amunts *et al.*, 2007; Amunts *et al.*, 2010; Qin *et al.*, 2015). A recent role for the lhca antenna proteins has been discovered. Lhca, particularly lhca4 is responsible for the binding of LHCII during state transitions (Benson *et al.*,

2015). The structure of the PSI-LHCI supercomplex is key to its ~100% photochemical efficiency, which in turn reduces the need for NPQ in PSI (Nelson 2009; Qin *et al.*, 2015).

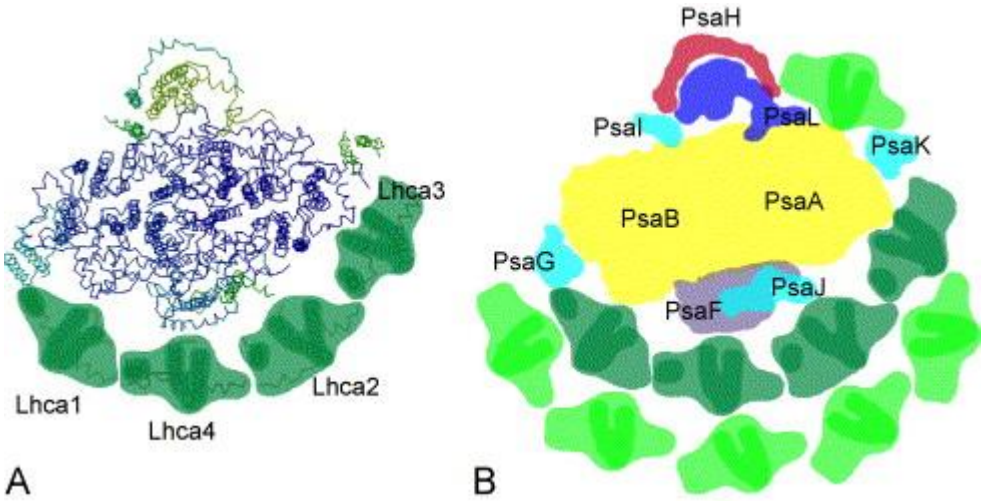

Figure 1.12 A Depiction of PSI supercomplex structure adapted 4.4-Å images taken by Ben-Shem *et al.*, (2003). Lhca stands for the light harvesting complex of PSI. B Enlarged representation of PSI including RCI, from electron microscopy experiments by Germano *et al.*, (2003). Images taken from Dekker and Boekema (2005). The Psa abbreviation is for protein subunit A-L in PSI.

1.7.4 ATP synthase

The ΔpH that has been accumulating during the course of photosynthesis is used to drive the formation of ATP by the catalyst, ATP synthase complex (ATPase). ATPase is a transmembrane complex, and like Cyt b_6/f is composed of eight subunits. It is located in the stroma lamellae, and the edges of the stacked thylakoid regions. ATPase is sometimes referred to as CF_1F_o-ATP synthase, as it is composed of two main subunits. The hydrophobic CF_o subunit is located in the membrane. Using the electrochemical gradient and proton motive force, it rotates the stromally exposed CF_1 to drive the phosphorylation of ADP.

1.8 The Need for Avoidance, Repair and Photoprotection

Plants have colonised most of the planet, and show remarkable adaptations to changing environments, as they utilise sunlight to form carbohydrates. Indeed, the competitive and colonisation traits of plants in the quest for sunlight was something Darwin reported on (Darwin, 1865; Darwin, 1881). Higher plants require sunlight for photosynthesis, yet capturing sunlight is not without consequences. Under fluctuating or high light environments, they can become inefficient and photodamaged. Terrestrial plants evolved from sea dwelling organisms which are typically adapted to lower light intensities, more stable light conditions and a red-shifted spectrum compared to terrestrial counterparts. Therefore, plants have had to evolve new properties to deal with the change in light conditions, and clearly judging by their colonisation of almost every ecosystem on Earth, they have managed to overcome/minimise the drawbacks of light harvesting. These can generally be referred to as light avoidance responses, excess energy dissipation and photodamage repair (Fig 1.13).

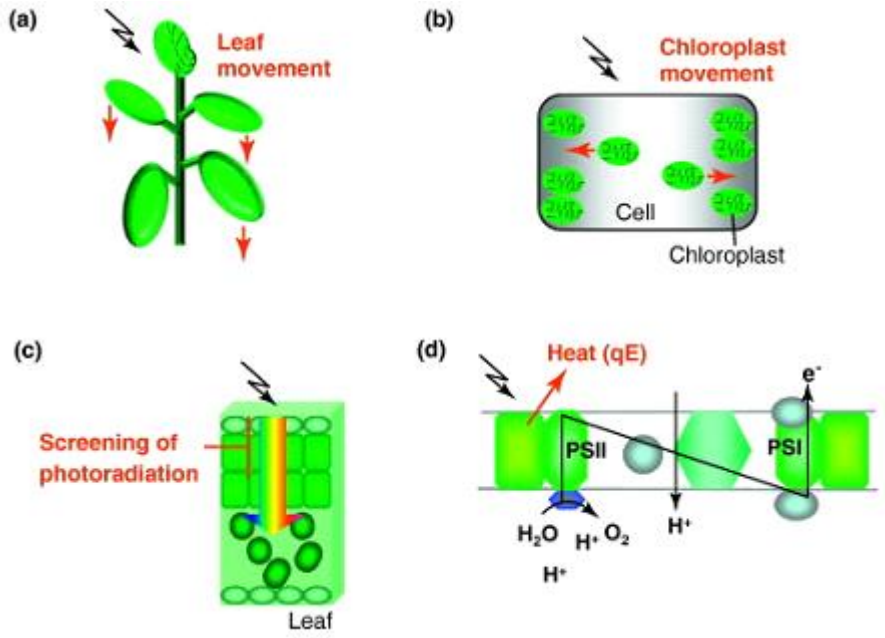

Figure 1.13 Depiction of A) leaf and B) chloroplast movements, C) physical leaf adaptations D) and NPQ, light avoidance and excess energy dissipation mechanisms of higher plants. The black lightning-shaped arrow displays the direction of irradiation, with the red arrows representing the directional mechanisms of avoidance.

1.8.1 Light Avoidance

Plants have both avoidance and energy dissipation mechanisms. Avoidance techniques vary depending on the timescale of photon avoidance. Over the longest timescales, plants can alter the expression of genes. This includes the amount and proportions of light-harvesting proteins, altered PSII/PSI ratios, the accumulation of anthocyanins or photosynthetic pigments, variations in leaf thickness, photosynthetic capacities, RuBisCo content (Lichtenthaler *et al.*, 1981; Leong and Anderson, 1984; Seeman *et al.*, 1987; Anderson *et al.*, 1988; Chow *et al.*, 1990; Bailey *et al.*, 2001; Bailey *et al.*, 2004; Hogewoning *et al.*, 2012; Kouřil *et al.*, 2012; Wientjes *et al.*, 2013). Short-term responses, that occurs over minutes to hours, includes leaf and chloroplast movements. Chloroplasts movements are controlled by the *phot1* and *phot2* genes. *Phot1* is responsible for chloroplast accumulation in low light conditions, with *phot2* being the dominant gene 'overriding' *phot1*, causing chloroplasts to migrate to the periphery of cells. It appears that only in double *phot1phot2* mutants are chloroplasts unresponsive to blue light (Jarillo *et al.*, 2001; Kagawa *et al.*, 2001; Sakai *et al.*, 2001; Tsuboi and Wada, 2011; Dall'Osto et al, 2014). There are two types of leaf movement, that which increases light absorption (diaheliotropism) and the other decreasing light absorption (paraheliotropism). Inhibition of paraheliotropism has been shown to increase the amount of photoinhibition of plants (Kao and Forseth, 1992; Pastenes *et al.*, 2004). Abiotic stress can also affect the ability of leaf movement, with water, mineral and temperature stress affecting plant mobility (Shackel and Hall, 1979; Fu and Ehleringer, 1989; Kao and Forseth, 1991). Furthermore, pteridophytes with extreme paraheliotropism can curl up on themselves. This mechanism contributes to their being some of the most desiccation-tolerant plants on Earth. When higher plants absorb too much sunlight, they can also remove the energy via a number of ways, collectively called non-photochemical quenching (NPQ, see section 1.8.3). Plants also have a means of repairing the component of the photosynthetic membrane that is most susceptible to photodamage, the D1 protein.

1.8.2 D1 protein repair cycle

Structure of PSII, D1 and D2 key. Photoinhibition of photosystem II (PSII) can occur under prolonged periods of high light or in fluctuating light environments. Accessory pigments and light harvesting antenna (LHCII) are highly efficient at absorbing light, yet the slower redox reactions of specialised reaction center (RCII) chlorophyll *a* (P680) and primary electron acceptors Pheophytin, Q_A and Q_B, are comparatively slower. This disparity creates a bottleneck leading to the formation of reactive oxygen species in the membrane.

In normal conditions, the primary charge separation intermediates 1[P680+ Pheo−] are restored by redox reactions of the electron transport chain. When electron donation cannot keep pace with P680+ oxidation, the P680+ radical lifetime becomes extended. This powerful oxidising agent, as well as degrading neighbouring reaction center proteins, can also inhibit the Tyr/Z electron transfer pathway. When Q_A is fully reduced and unable to accept electrons from a reduced Pheophytin, 3[P680+ Pheo−] is formed. This leads to the formation of ^{3}P680 and $^1O_2$. These reactive oxygen species directly oxidise neighbouring proteins, which can lead to the degradation of the D1 protein.

The reaction center D1 protein is vital for photosynthesis as it is the binding site, through a lumenally exposed tyrosine residue, to the oxygen evolving complex and Mn_4CaO_3 cluster. However, the D1 protein is the main site of damage during photoinhibitory conditions. D1 repair can take hours, which undermines the yield of PSII (ΦPSII) in the long-term. As the D1 protein is at the centre of PSII and is connected to many other complexes, it is unsurprising that the process takes as long as it does. Although the timeframe of hours is extremely long, compared to the microsecond heat emission of NPQ, the 60-minute turnover of the D1 protein is one of the quickest in the natural world (Tyystjarvi *et al.*, 1994, Sacharz, 2015). It is currently under debate as to whether the D1 repair mechanism is solely dependent on the functionally redundant FtsH protease family, or whether it also requires the Deg family of proteases (Spetea *et al.*, 1999; Haussuhl *et al.*, 2001; Bailey *et al.*, 2002; Silva *et al.*, 2003; Zaltsman *et al.*, 2005; Barker *et al.*, 2006; Nixon *et al.*, 2010; Zhang *et al.*, 2010). The ‘two-protease’ mechanism is started by the cleavage of the

stromal-exposed D1 protein loop, which attaches the D1 protein to CP43, by the Deg2 protease. The FtsH2/FtsH3 hexamer facilitates the removal of the N-terminal domain. The N-terminal domain is 23 kDa, and it is this fragment which is often used in Western blots to test for photoinhibition and D1 protein degradation (Spetea *et al.*, 1999; Haussuhl *et al.*, 2001). The 'FtsH-only' model predicts the physical changes in the PSII core, including the disassembly of the RC47-D1-CP43 domain, during photoinhibition. The FtsH2/FtsH3 complex then cleaves the damaged D1 protein in synchrony with the insertion of a newly synthesised D1 protein (Silva *et al.*, 2003; Barker *et al.*, 2006; Nixon *et al.*, 2010).

1.8.3 Non-photochemical quenching - NPQ

Non-photochemical quenching of chlorophyll fluorescence has been a recognised phenomenon since *1957*. Using a fluorometer it was observed that the Φfluorescence decreased upon exposure to light. Yet it was not until *1987* when Demig-Adams (nee Demig) showed that the violaxanthin de-epoxidase cycle was activated upon exposure to light. Since then, there has been a lot of research in the field that has elucidated many changes in the photosynthetic membrane, and these has collectively been attributed to components of NPQ. Proclaimed mechanisms of NPQ include: ΔpH energy dependent quenching (qE), state transitions (qT), photoinhibition (qI), chloroplast movement/relocation (qM) and zeaxanthin dependent quenching (qZ). These will be explained in greater detail below.

1.8.3.1 qE – Energy Dependent Quenching

Energy dependent quenching, or qE, is the ΔpH-dependent component of NPQ (Wraight and Crofts, 1970; Briantais *et al*., 1979; Krause and Behrend, 1988). It is also the quickest and most significant mechanism of excess energy dissipation. The emission of heat can be observed within 1.4 μs, and relaxation occurs within

second to minutes after the removal of light (Krause and Weis, 1991; Mullineaux *et al*., 1994). Linked to photosynthetic electron transfer, in high light conditions, it is triggered by the over accumulation of protons in the thylakoid lumen, with qE triggered at pKa 6.0. The decreased pH conditions trigger the two other major events of qE: the de-epoxidation of violaxanthin (Sapozhnikov *et al*., 1957; Demmig *et al*., 1987), and the protonation/activation of the PsbS protein (Funk *et al*., 1995; Li *et al*., 2000). Each of these characteristics have been inhibited using chemical or natural inhibitors. Using uncouplers, such as nigericin, blocks the formation of qE and all subsequent events. Arabidopsis with knock-outs of the VDE enzyme (npq1), or infiltrated with dithiothreitol (DTT) have significantly reduced qE (Bilger *et al*., 1989; Rees *et al*., 1989; Niyogi *et al*., 1997). PsbS protein knockouts also show reduced qE, with a reduced maximum NPQ capacity (Li *et al*., 2002b; Johnson and Ruban, 2011). It is important to note that that qE does not compete with photosynthesis for excitons, but aids the removal of excess energy from the PSII membrane. Indeed, the rates of photosynthesis are unaffected by qE activation (Weis and Berry, 1987; Genty *et al*., 1989). It has been recently proposed that this is achieved by increasing the effective cross section of PSII in the qE state compared to the light harvesting state adopted in the dark (Belgio *et al*., 2014). There is still some debate regarding the mechanism of qE. Indeed, there is still not a common consensus on whether there is a change in the whole photosynthetic membrane which increases the efficiency of thermal dissipation, or whether a particular component, most likely PsbS or zeaxanthin, is the cause of excess energy dissipation. The currently proposed mechanisms of excess energy dissipation will be discussed in greater detail below (see 1.8.4). It is apparent however that a trans-thylakoidal ΔpH, zeaxanthin and PsbS protein are vital to maximal excess energy dissipation.

1.8.3.2 qT - State Transitions

The state transition, or qT, mechanism is somewhat different in nature from the excess energy dependent mechanisms qE, qI, qZ and qM. It is not a response to high light conditions. In fact, state transitions do not occur during strong illumination (Aro *et al.*, 1993). qT serves to balance the excitation of PSII and PSI in sub-saturating light conditions. In such environments, typically under shaded canopies or sunsets, the light harvesting systems of PSII are phosphorylated and become attached to PSI. This process is controlled by the redox state of plastoquinone. When the electron carrier molecules are in a reduced state, the serine-threonine kinases STN7 and STN8 are activated. STN7 phosphorylates the LHCII subunits Lhcb1 and Lhcb2 of the loosely bound LHCII trimer (Bellafiore *et al.*, 2005; Benson *et al.*, 2015). The cleaved trimers migrate from the PSII rich stacked grana regions of the chloroplast, to the lamella PSI enriched regions. The attachment of LHCII to PSI is recognised as State II. The PSI-LHCI-LHCII supercomplexes which arise have recently been shown to depend on a complete array of Lhca subunits, with Lhca2 and Lhca4 the most important, for the energetic coupling of LHCII to PSI (Benson *et al.*, 2015). Formation of the supercomplexes is also dependent on PsaH and L as the binding site for LHCII. In red-shifted light conditions, when plastoquinone becomes oxidised, STN7 is no longer activated. Here, TAP38/PPH1 phosphatase dephosphorylates the LHCII bound to PSI, and the antenna migrates back to PSII. The state when LHCII is bound to PSII is referred to as State I. Also activated, but with a less prominent role is STN8. This is involved in the phosphorylation of RCII proteins (Vainonen *et al.*, 2005). Altogether, this qT quenching can contribute to ~15% of the total quenching of PSII.

1.8.3.2 qI - Photoinhibition

Although it has been termed: photoinhibitory quenching, photoinhibition, irreversible quenching or qI, closed RCII are believed to be photoprotective for other open RCII. The names for this type of quenching arises from the mechanisms

slowly reversible or irreversible nature (Krause, 1988; Jahns and Holzwarth, 2012). Photoinhibition can range from taking between minutes to days to recover. There are several methods to determine the proportion of closed RCII. Oxygen evolution, Western blots for D1 protein degradation and fluorescence (rises in Fo') can all be used. The problem with all of these methods, excluding the latter, is that they require invasive biochemical techniques that can reduce chloroplast viability. Research using a combination of these techniques has suggested that indications of qI include: the direct damage and degradation of D1 protein (Greenberg *et al.*, 1987; Aro *et al.*, 1993a; Tyystjärvi and Aro), it is due to the continued quenching of the antenna due to conformational changes of the membrane after illumination is stopped (Gilmore and Björkman, 1994; Ruban and Horton, 1995; Horton *et al.*, 1996), it is independent of ΔpH (Neubauer and Yamamoto, 1992; Neubauer, 1993; Ruban and Murchie, 2012) or that it is reversible after the application of uncouplers (Ruban and Horton, 1995), or that zeaxanthin binding to minor antenna complexes causes photoinhibition (Dall'Osto *et al.*, 2005). It is therefore difficult to agree on a common consensus for qI. For the remainder of this thesis, qI will be used as the term for the slowest reversible sustained quenching component of NPQ, that is the result of RCII damage, and is ΔpH independent.

1.8.3.4 qM - Chloroplast Movement-Dependent Quenching

qM or chloroplast movement dependent quenching, is a recent addition to the excess energy dissipation mechanisms (Dall'Osto et al, 2014). The group proposed that chloroplast movements to the periphery of cells is an excess energy dissipation defence mechanism that occurs during the same timeframes as qE and qZ (Dall'Osto *et al.*, 2014). For further information on chloroplast relocation, further details are included in chloroplast movements as a light avoidance mechanism (see 1.8.1).

1.8.3.5 qZ - Zeaxanthin-dependent quenching

Zeaxanthin-dependent quenching (qZ) has historically been encompassed in the qE and qI components of NPQ (Leitsch *et al.*, 1994; Jahns *et al.*, 1996; Thiele *et al*., 1996; Thiele *et al*., 1998; Jahns and Holzwarth, 2011). However, with the creation of a constitutive zeaxanthin expressing *Arabidopsis* plant, *npq2*, it has come to be interpreted as an independent element of the NPQ process. The first documentation of a zeaxanthin state was proposed by Horton *et al.*, 1991. The group recognised that in the dark, long after exposure to light and after the collapse of the ΔpH, LHCII was still more aggregated than in the dark. With the advent of the npq2 mutant, it was shown that in the dark, Fv/Fm was decreased compared to WT plants, a sign that NPQ was already employed (Niyogi *et al.*, 1992). qZ has now broadly defined as forming over 10-30 minutes after illumination and being reversed over 10-60 minutes after light is removed (Nilkens *et al.*, 2010; Jahns and Holzwarth, 2012). Like qE it is activated by a ΔpH formation, in order to start violaxanthin de-epoxidation, but unlike qE it remains after the collapse of the ΔpH.

1.8.4 Mechanism of NPQ

There are a number of different models that have been put forward to describe the NPQ process in action, and the major site of its activity. One of the universal agreements between the models is that NPQ occurs in the light harvesting proteins of the supercomplex, rather than the RCII core. This is based upon the observation that NPQ is dependent on zeaxanthin, lutein and the PsbS protein. These three factors are located only in the antenna proteins. Furthermore, the use of lincomycin has supported this conclusion. Lincomycin is an antibiotic that inhibits the synthesis of the chloroplast genome. As RCII is encoded by chloroplast genes, this results in the reduction of RCII compared to LHCII, which is encoded by the nucleus. In this almost LHCII-only model, NPQ is actually higher than in the WT

control plants. Besides commonality, the debate continues, with minor vs major LHCs being the site, zeaxanthin vs lutein the quencher, and chlorophyll-chlorophyll vs chlorophyll-carotenoid dissipation pathways proposed.

1.8.4.1 Molecular Gearshift Model

The molecular gearshift model predicts zeaxanthin as the quencher of excess energy. Some of the qualities that make zeaxanthin a quencher are discussed in section 1.6.2. The model was based on the correlation between increased zeaxanthin levels and greater NPQ levels (Sapozhnikov *et al.*, 1957; Demmig *et al.*, 1987). Frank *et al.* (1994) predicted the S1 energy states for violaxanthin and zeaxanthin to occur above and below the Q_Y state of chlorophyll respectively. This work fitted the hypothesis of zeaxanthin as the quencher, and was supported and depicted in Fig 1.14A by Owens (1994). This model is not as popular anymore owing to the numerous studies on zeaxanthin-less mutants (npq1) which also form NPQ, and the dependency of NPQ on the PsbS protein (Rees et al., 1989; Niyogi et al., 1997; Johnson and Ruban, 2011). Furthermore, PSI exhibits NPQ, but there is no zeaxanthin bound to this complex (Qin *et al.*, 2015). Replacing zeaxanthin with another carotenoid, auroxanthin, increased the quenching capacity of isolated LHCII complexes (Ruban *et al.*, 1998). Furthermore, independent experiments have demonstrated that the S1 state of violaxanthin is also below the Q_X and Q_Y bands of chlorophyll (Fig 1.14B), somewhat undermining the zeaxanthin only dissipation state (Polivka *et al.*, 1999; Frank *et al.*, 2000).

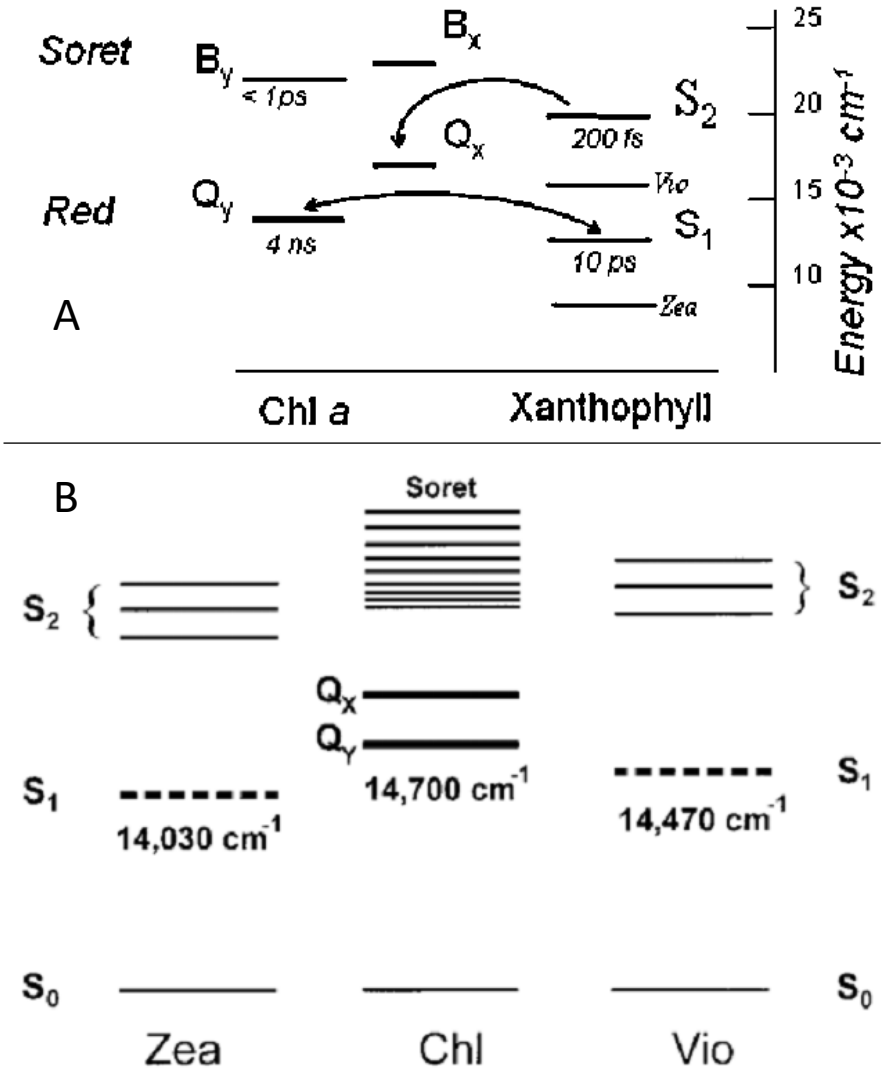

Figure 1.14A Proposed model of change in S_1 state of violaxanthin (Vio) and zeaxanthin (Zea), whereby zeaxanthin can act as an acceptor molecule for excited chlorophyll (Q_Y). In this model, the excitation of Zea has a lower energy maxima than Vio, with Zea the only xanthophyll able to accept energy from chlorophyll. B The calculated S1 and S2 energy states of zeaxanthin and violaxanthin by Polivka *et al.*, (1999). In this model, the S_1 states of both Vio and Zea sit below the Q_Y state of chlorophyll, meaning both xanthophylls can be acceptor molecules of chlorophyll.

1.8.4.2 Radical Cation Model

Energy transfer from chlorophyll-zeaxanthin also underpins the radical cation model, however the state of zeaxanthin is different. Unlike chlorophylls, carotenoids do not form reactive oxygen species when they form cations. The temporary formation of carotenoid radicals have been proposed as an energy dissipation pathway. PsbS-zeaxanthin and chlorophyll-zeaxanthin heterodimers are formed in high light conditions, with energy being transferred to the zeaxanthin molecules. The charge separation of the heterodimer, with zeaxanthin donating an electron to the excited state chlorophyll. The radicals can then return to the ground state via charge recombination. Carotenoid radicals have been observed in a number of experiments, typically recognised by increased absorption spectra at wavelengths longer than 800 nm (Fig 1.15). As however is the case with the molecular gearshift model, the limitation of zeaxanthin as the quencher limits this model to the role of a minor contributor in the NPQ process (Holt *et al.*, 2005).

1.8.4.3 Chlorophyll-chlorophyll

Chlorophyll-chlorophyll interactions have been proposed as the major quencher in PSII by the Holzwarth laboratory. Based on the phenomena that chlorophylls form dimers and oligomers in the NPQ state, the overlap of pigments and chlorophylls increases (Miloslavina *et al.*, 2008). In zeaxanthin-less (*npq1*) and constitutive zeaxanthin expressing (*npq2*) *Arabidopsis* oligomeric LHCII, carotenoids were found not to affect the femtosecond transient absorption experiments on LHCII. Furthermore, the group reported that the molar absorption coefficient of S1 state carotenoids was absent from the fluorescence kinetic experiments, and thus, the excess energy dissipation only occurred via chlorophyll-chlorophyll interactions (Muller *et al.*, 2010). These Chl-Chl charge transfer states probably contribute to excess energy dissipation, however, the absence of zeaxanthin and PsbS protein from *Arabidopsis* plants does undermine the conclusion that it is the major dissipative pathway, especially considering the limited mobility but key

contributions of minor antenna to NPQ (Rees et al., 1989; Niyogi et al., 1997; Johnson and Ruban, 2011; Dall'Osto et al., 2014).

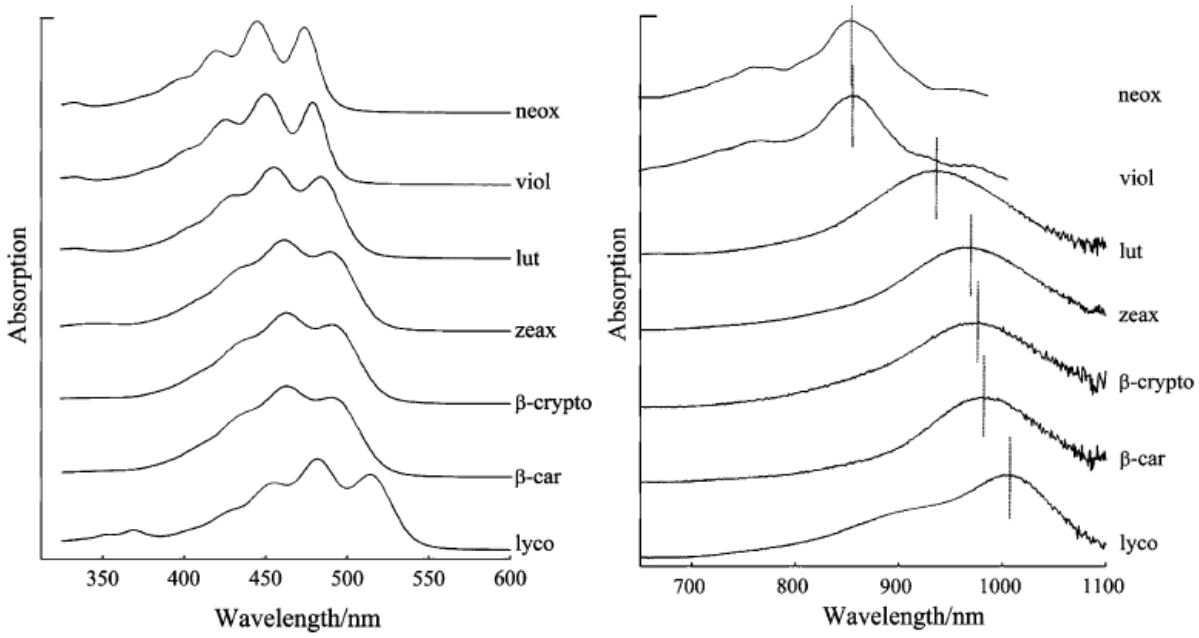

Figure 1.15A Absorption spectra of neoxanthin (neox), violaxanthin (viol), lutein (lut), zeaxanthin (zeax), β-cryptoxanthin (β-crypto), β-carotene (β-car) and lycopene (lyco) between 300-600 nm. Spectra are vertically offset for greater clarity. B Absorption spectra of neoxanthin, violaxanthin, lutein, zeaxanthin, β-cryptoxanthin, β-carotene and lycopene cation radicals between 650-1100 nm. Vertical lines depict absorption maxima. Spectra are vertically offset for greater clarity (Galinato *et al.*, 2007).

1.8.4.4 Allosteric Model

The model championed by the Horton laboratory is the 'allosteric model' or 'LHCII aggregation model' (Horton *et al.*, 1991). This model proposes four states of aggregation, depending on the degree of quenching in the photosynthetic membrane (Fig 1.16A). Aggregation of the membrane depends on the deepoxidation/epoxidation state of the xanthophyll at the peripheral V1 binding site of LHCII (Rees *et al.*, 1989; Horton *et al.*, 1996). The presence of zeaxanthin is not the sole determinant of the aggregation state. Zeaxanthin acts as a promoter of the LHCII aggregation state at higher pKa values 6.0, with violaxanthin acting as an inhibitor, with the pKa required to reach 4.0 to cause aggregation (Ruban et al., 2012). The violaxanthin/zeaxanthin state also helps to 'prepare' the light harvesting membrane for subsequent saturation, by the slower rates of epoxidation than collapsing ΔpH. State 1, which is representative of the dark-adapted state of the membrane, has violaxanthin bound to LHCII, pH close to neutral conditions (pH ~6.5) and LHCII in its most hydrophilic state, with as great a distance between complexes as possible (Fig 1.16B). State 4 is the heavily quenched state, where the lumen pH is ~4.5, antennae proteins are protonated, including PsbS protein, and violaxanthin is deepoxidated to zeaxanthin. These conditions and changes in the membrane induce LHCII aggregation and excess energy dissipation. State 2 and state 3 represent the partially quenched states of the membrane. In state 2, zeaxanthin is still bound to LHCII, after the ΔpH has collapsed, conditions similar to those proposed in qZ quenching. With zeaxanthin present, the membrane is in a 'stand-by' mode, NPQ can be activated more readily, so ΔpH does not need to become as low for heat emission to occur. State 3, the membrane is protonated by low lumen pH, but violaxanthin is still present. This state can occur in the very early stages of NPQ activation, before violaxanthin has been deepoxidated to zeaxanthin, or, the maximum NPQ state in VDE mutants (*npq1*). Although the greatest structural changes have been suggested to occur in the major antenna complex, the aggregation model is not restricted to LHCII. This view, that not one particular antenna protein is not the sole site of NPQ, is supported by the presence of carotenoids in the minor and major antenna, the presence of NPQ in NoM and ch1

mutants, as well as the many other single and double lhcb knock-outs. Furthermore, this model incorporates and allows the three major chlorophyll-carotenoid dissipative pathways: 'neoxanthin site' - neoxanthin, lutein 621 and chls *b*606/*b*607; 'V1 domain' – violaxanthin and chls *a*601/*a*611; chlorophyll terminal emitter – lutein 620 and chls *a*611/*a*612, *b*608 (Pascal *et al.*, 2005; Yan *et al.*, 2007). Conformational changes in the antenna increase the efficiency of energy transfer via these routes. Indeed, Belgio and co-workers have found an increase in functional PSII cross section during NPQ, a conclusion that would support the rearrangement of the membrane to increase excess energy dissipation (Belgio *et al.*, 2014).

From the above explanations and diagrams, it is clear that there is some considerable overlap of mechanisms, components and timing of activation and relaxation. It is therefore worth noting that the above mechanisms are meant to relieve the over-excitation of PSII before photodamage impairs photosynthesis. Therefore, rather than continue to add to the increasingly muddled field, an overall encompassing view of NPQ approach was taken by Ruban and Murchie (2012). Here it was proposed to investigate the protective capacities of NPQ, regardless of the underlying mechanism. They proposed to break it down into pNPQ and photoinhibition, using a fluorescence based approach.

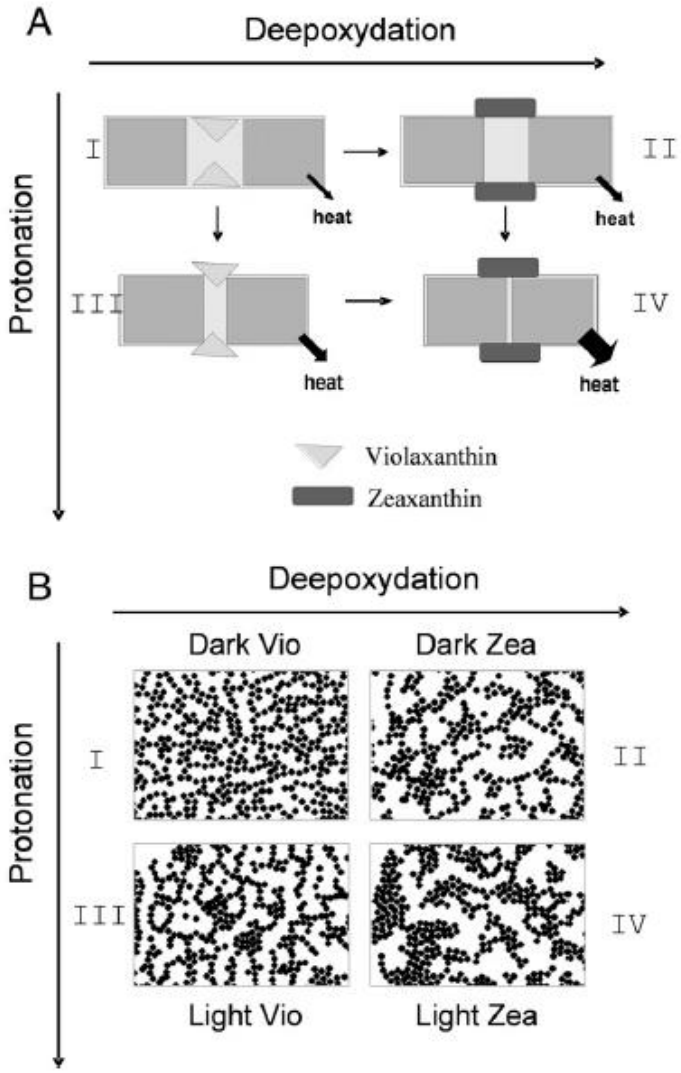

Figure 1.16A The LHCII aggregation model of Horton and Ruban, (1992) depicting the four states of NPQ. Dark-grey squares depict LHCII trimers, with light grey rectangles indicating the space in between trimers. B Freeze-fracture electron microscopy experiments illustrating the aggregation of LHCII in the dark and various light adapted states of spinach chloroplasts. Closed circles illustrate LHCII trimers. Images taken from Ruban *et al.*, (2012).

1.8.4.5 Two mechanisms for excess energy dissipation

The most recent proposal for the activation and dissipation of excess energy is a collective proposal of the Bassi and Niyogi lab (Dall'Osto *et al*., 2017). The group of Roberto Bassi had previously proposed that the minor antenna, particularly the binding of zeaxanthin to the L1 site at CP29, is the site of qE. The group successfully generated mutant Arabidopsis with no minor antenna (NoM), and have characterised the excess energy dissipation mechanism in this mutant. The work demonstrated that NPQ is formed at close to WT levels in the first minute of light illumination, however there is a decrease in NPQ from 2-4 mins, before the NoM has WT levels of NPQ from 5 min onwards. The NoM mutant showed no additional impairment with the KO of lutein, but was unable to form NPQ with additional zeaxanthin and PsbS protein KOs. The researchers therefore propose that the minor antenna is responsible for the earliest part of the quenching process, with LCHII being vital for the latter part of quenching. PsbS and zeaxanthin are proposed to cause the separation of LHCII and CP24 from a C2S2 complex which contains CP29 and CP26 (Fig 1.14 below). The LHCII component is dependent only upon zeaxanthin and PsbS, but the monomeric supercomplex requires lutein, zeaxanthin and PsbS. This newest mechanism therefore appears to be a contradiction to the recent work of Belgio *et al.* (2014) which suggested that the PSII cross section increases during the NPQ process, and also the work of Sacharz *et al.* (2017) and Ilioaia *et al.* (2013), who suggest that CP29 is the site of PsbS interaction when zeaxanthin is not present, and that CP29 becomes simultaneously disconnected to RCII and energetically coupled to emitters in LHCII.

1.9 Fluorescence and Pulse Amplitude Modulated Fluorometers

When the photosynthetic membrane absorbs a photon, an exciton is generated. Upon this achieving this excitation, there are three pathways that the energy can be channelled through (Fig 1.17). The first mechanism utilises the energy and is called photosynthesis. The other three modes are fluorescence,

radiationless decay and heat, which are all dissipaters. Each individual exciton can return to the ground state via any one of these mechanisms, but also only by one. Chlorophyll *a* fluorescence measuring devices, fluorometers, take advantage of this phenomenon, and are thus able to use changes in fluorescence levels to quantify the amount of photochemistry (K_p), fluorescence (K_f), radiationless decay (K_d) and heat dissipation (K_{NPQ}).

$$\Phi f = \frac{Kf}{(Kf+Kd+Kp+KNPQ)} \qquad \text{(Equation 1.03)}$$

Heat dissipation is a reversible mechanism and is only activated in light exposed leaves. Therefore, prior to starting fluorescence measurement experiments, plants are dark adapted. This removes the heat dissipation from the competing pathway of excitation energy utilisation/dissipation. Using a measuring light intensity of ~1 µmol m^{-2} s^{-1}, photosynthesis can occur at the maximum rate without any light induced damage, or the heat dissipation mechanism being activated. The only competing mechanism to photosynthesis is fluorescence, as radiationless decay is a background constant that does not change. This physiological state is referred to as the minimum fluorescence level or Fo.

$$\Phi fo = \frac{Kf}{(Kf+Kd+Kp)} \qquad \text{(Equation 1.04)}$$

Once this value has been established, a saturating pulse is applied. This is often in the range of 6,000-10,000 µmol m^{-2} s^{-1} and temporarily 'saturates' all of the RC, thus inhibiting photosynthesis. In this moment, the only method available for energy removal is fluorescence. This phase is called the fluorescence maximum or Fm state.

$$\Phi fm = \frac{Kf}{(Kf+Kd)} \qquad \text{(Equation 1.05)}$$

Thus, with two simple parameters, the minimum and maximum fluorescence levels have been measured. Fo and Fm are also used to measure the maximum quantum yield of photosynthesis:

$$\frac{Fv}{Fm} = \frac{(Fm-Fo)}{Fm}$$ (Equation 1.06)

Thus the maximum rate of photosynthesis can also be readily calculated from Fo and Fm. It should be noted though that all values obtained using fluorescence are relative and quantum coefficients based on the initial Fo and Fm states. As leaves are subsequently exposed to light, the changes in Fo and Fm states, which are Fo' and Fm' when illuminated, will be due to changes in the heat dissipation mechanism.

When an electron is raised to a higher energy level, it relaxes within picoseconds and thus loses some of its energy to the environments. Fluorometers take advantage of this by exciting leaves at a low wavelength, and detecting light emission at a longer wavelength. A JUNIOR-PAM excites leaves at 450 nm, and detects signals at 645 nm. This, combined with filters, minimises the chances of the light source being directly absorbed and measured by the detector. Pulse amplitude modulation (PAM) fluorometers have revolutionised the field of fluorescence. PAM devices are useful tools as they allow external light sources to be applied to leaves, without affecting the fluorescence measurements. PAM means a measuring light beam is only applied intermittently, and the detector measures only the signal that arises from fluorescence corresponding to the regime. This effectively means that the fluorometer responds to only the fluorescence yield, rather than the light intensity. A leaf could therefore be exposed to direct sunlight or a bedside lamp, and the fluorescence trace would have the same peak, despite the vast differences in external light intensity. This offers a more accurate alternative to the previous fluorometers, where the fluorescence traces would be difficult to compare, due to the potentially vast differences in trace peaks.

1.10 Principle of pNPQ Methodology

ΦPSII is affected by NPQ and RCII photodamage. It was therefore essential to disseminate the ΦPSII reduction attributed to each factor. This can be achieved by adapting the equations 1.03 to 1.06 and expressing ΦPSII in the dark as:

$$\Phi PSII = \frac{qPd*Kp}{[Kf+Kd+Kp]} \qquad \text{(Equation 1.07)}$$

Or with NPQ included, such as in the dark after exposure to light:

$$\Phi PSII = \frac{qPd*Kp}{[Kf+Kd+Kp+KNPQ]} \qquad \text{(Equation 1.08)}$$

Transforming the rate constants into fluorescence yields, Fo, Fm and Fv, ΦPSII looks like:

$$\Phi PSII = \frac{qPd*\frac{Fv}{Fo}}{[1+\frac{Fv}{Fo}+NPQ]} \qquad \text{(Equation 1.09)}$$

Fv/Fo can be expressed as:

$$\frac{Fv}{Fo} = \frac{1}{(\frac{Fm}{Fv}-1)} \qquad \text{(Equation 1.10)}$$

Considering the conversion of rate constants to yields (Equation 1.09), and expressing Fv/Fo as in Equation (1.10), the following formula thus relates ΦPSII to NPQ, qP_d, and Fv/Fm:

$$\Phi PSII = \frac{qPd*\frac{Fv}{Fm}}{[1+(1-\frac{Fv}{Fm})*NPQ]} \qquad \text{(Equation 1.11)}$$

Expressing the relationship of ΦPSII in this form shows its downregulation is a hyperbolic of NPQ. Furthermore, qP_d manifests as a direct reduction in ΦPSII. In the absence of photoinhibition, $qP_d = 1$, and this can be used to estimate the theoretical ΦPSII without any photodamage to compare to photodamaged plants:

$$Theoretical\ \Phi PSII = \frac{1*\frac{Fv}{Fm}}{[1+(1-\frac{Fv}{Fm})*NPQ]} \qquad \text{(Equation 1.12)}$$

The proportion of open RCII was calculated as:

$$qPd = \frac{(Fm - Fo'act.)}{(Fm - Fo'calc.)} \qquad \text{(Equation 1.13)}$$

where Fm' is the maximum fluorescence after actinic light illumination; $Fo'_{act.}$ is the measured dark level of fluorescence after illumination, and $Fo'_{calc.}$ is the calculated dark fluorescence level. The latter was calculated using the formula proposed by Oxborough and Baker (1997):

$$Fo'calc. = \frac{1}{(\frac{1}{Fo} - \frac{1}{Fm} + \frac{1}{Fm'})} \qquad \text{(Equation 1.14)}$$

For a detailed guide including the text batch file used to encode the pNPQ assessment procedure, computer programming to extract the data files and the formatting used to present the results, see Appendix Items 1 and 4.

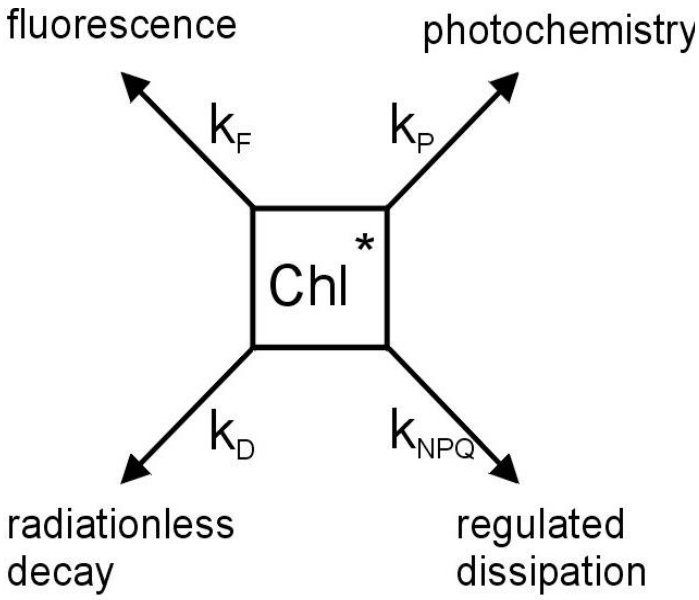

Figure 1.17 The four fates of excited state chlorophylls in higher plants and their abbreviations (Klughammer and Schreiber, 1994).

1.11 Project Outline

Whilst there has been a lot of progress made towards establishment of a molecular mechanism of NPQ, little is known about the efficiency with which it protects the delicate molecular machinery of PSII. Indeed, such knowledge would offer an invaluable insight into the factors that determine the fast and efficient

tracking of the light environment by plants that avoids compromise of the PSII quantum efficiency. The key objective of this program is to develop a novel methodology to accurately assess the effectiveness and limitations of the major photoprotective process of plants, NPQ.

NPQ and photoinhibition both diminish the quantum yield of PSII (ΦPSII). In order to separate these effects the yield needs to be expressed in terms of the amplitude of NPQ (Equation 1.11). Monitoring the dependence of ΦPSII upon NPQ during the progressive increase in the illuminating light intensity could produce unique experimental data that would be fitted to the analytical expression above. The point of deviation of experiment from theory would indicate an onset of photodamage. In addition, a parallel measurement of the fraction of damaged reaction centers using pulse modulated chlorophyll fluorescence technique, PAM, will independently track the onset of photoinhibition. As a result of the use of these two very promptly performed approaches a number of new physiological quantitative parameters reflecting the functional state of PSII will be obtained:

a) the maximum tolerable light intensity:
b) the light intensity which would damage 100% of reaction centers; and
c) the minimum amount of NPQ required to protect plants from photodamage at a given light intensity.

The role of different PSII components, like the minor LHCII antenna, PsbS protein and various types of carotenoids in effective protection of RCII will be studied on a number of readily available *Arabidopsis* mutant plants. The effectiveness of the fast tracking of environmental light intensity by NPQ will also be studied on these plants. Interactions between slow, acclamatory changes in the structure and functions of PSII and adjustments in the effectiveness of photoprotection will be investigated.

Chapter II –
Materials and Methods

2.1 *General laboratory chemicals*

All chemicals used in experiments and listed in this chapter were obtained from Sigma-Aldrich (St. Louis, Missouri, United States) unless otherwise stated.

2.2 *Plant Material*

All *Arabidopsis thaliana* plants investigated are from the Columbia (Col-0) ecotype. Arabidopsis plants used were:

Mutation	**Abbreviation**	**Description**	**Reference**
aba4npq1lut2	*viol*	violaxanthin replaces all xanthophylls	Fuciman *et al.*, (2012)
ch1	*ch1*	Chl *b* and LHC knock-out	Havaux *et al.*, (2001)
chy1chy2lut5	*lute*	lutein replaces all xanthophylls	Dall'Osto *et al.*, (2007)
L17	L17	PsbS protein overexpressor	Li *et al.*, (2002)
lhcb4.1lhcb4.2lhcb5	NoM	lhcb4, lhcb5 and lhcb6 knock-outs	Dall'Osto *et al.*, (2014)
lut2	*lut2*	no α-carotene or lutein	Pogson *et al.*, (1998)
lut2npq2	*zea*	zeaxanthin replaces all xanthophylls	Niyogi *et al.*, (2001)

npq1	*npq1*	zeaxanthin-deficient	Havaux *et al.*, (2001)
npq2	*npq2*	lacks violaxanthin and neoxanthin	Niyogi *et al.*, (1998)
npq4	*npq4*	PsbS protein knock-out	Li *et al.*, (2000)
var2-2	*var2*	FtsH homologue knock-out	Bailey *et al.*, (2002)
WT	WT	Wild-type (Col-0)	

Table 2.01 List of *Arabidopsis thaliana* genotypes and associated mutant characteristics used in this thesis.

Approximately 50-100 seeds were measured in an Eppendorf, with 1ml of sterilisation solution. Wild-type (WT) and all mutants *Arabidopsis* seeds were sterilised with 0.1 % Triton X-100 and 50% ethanol for 5 min before rinsing three times in water. During the 5 min of sterilisation, Eppendorfs were placed in a rotary wheel to ensure constant agitation. After this, seeds were placed in a fridge for a chilling period (4^{o}C for 72 h) to ensure homogeneous germination (Ware *et al.*, 2015). Sterilised and cold shocked seeds were sown onto a 6:6:1 combination of LevingtonM3 potting compost, John Innes No. 3 soil and perlite (Scotts UK, Ipswich, UK). Seeds were placed in a Sanyo growth cabinet at 100 mol photons m^{-2} s^{-1} for 1 week before being transferred to respective short-day conditions (10 h light) of 40 (LL), 90 (lincomycin treated), 200 (ML) and 450 mol photons m^{-2} s^{-1} (HL) of constant light and 22^{o}C. Seeds and plants were watered directly into trays, with approximately one inch of room temperature water three times per week. Measurements on whole intact leaves were carried out on HL plants between 5–6 weeks old, ML between 6–8, and LL and lincomycin-treated plants at 10–12 weeks old (conditions similar to Tikkanen *et al.* 2006). Once the plants which were to be treated reached the rosette stage of development (8–9 weeks old), lincomycin treatment (0.2 g/l) was started. Lincomycin treatment was then delivered three

times per week until Fv/Fm reached 0.2, by watering plants with dissolved lincomycin, instead of watering alone (Ware *et al.*, 2015).

2.3 *Chlorophyll Content Determination*

Two methods for chlorophyll extraction were used, and this was sample size dependent. For reduced amounts of leaf material, leaves were frozen in liquid nitrogen, and in 1-2 ml of 80% acetone, crushed in a pestle and mortar. Samples were centrifuged at 3,500g to remove unwanted protein. For larger amounts of biomass, extraction was performed per section 2.4 'isolation of chloroplasts'. Total chlorophyll content and chlorophyll *a*/*b* ratio were determined using the method of Porra *et al.* (1989) in 80% acetone (Farber *et al.*, 1997). An Ultraspec 2100 pro spectrophotometer was used to measure sample absorption at 646nm (A_{646}) and 663nm (A_{663}). A cuvette with 80% acetone was used to normalise measurements. Chlorophyll *a*/*b* ratios and chlorophyll concentrations were calculated from absorption measurements on a spectrophotomer:

$$\text{Chl } a = (12.7 * A_{663}) - (2.69 * A_{646}) \qquad \text{(Equation 2.01)}$$

$$\text{Chl } b = (22.9 * A_{646}) - (4.68 * A_{663}) \qquad \text{(Equation 2.02)}$$

2.4 *Isolation of Intact Chloroplasts*

Whole plants were dark-adapted 45 min prior to leaf removal. Intact chloroplasts were prepared by homogenising fresh leaf material (typically 5-20g) in homogenisation buffer (0.45 M Sorbitol, 20 mM Tricine, 10 mM EDTA, 10 mM NaHCO3, 0.1% BSA; pH 8.4) using a polytron blender (Kinematica, Switzerland). Homogenate was filtered through four layers of muslin, followed by four layers of muslin sandwiching one layer of cotton wool. Filtrate was centrifuged for 2 min at 3500g. The supernatant was removed and the chloroplast pellet washed in resuspension buffer (0.3 M Sorbitol, 20 mM Tricine, 5 mM MgCl2, 2.5 mM EDTA; pH 7.6) (Ware *et al.*, 2015). Chloroplast intactness was assessed by Fv/Fm, quenching capacity, or a microscope. Broken chloroplasts are easily observed due to the lack

of a typical ‘halo’ around the structures, as is displayed in the image below (Fig 2.01).

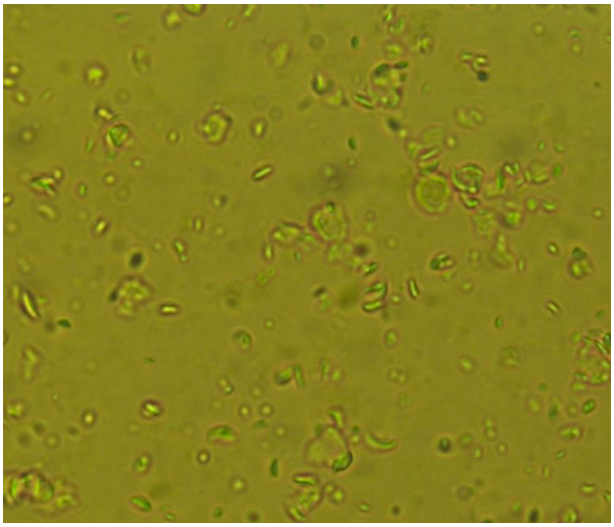

Figure 2.01 A light microscope image of broken chloroplasts taken from a chloroplast preparation when Fv/Fm is lower than 0.6. Very few of the chloroplasts in this picture have the typical ‘halo’ like rig a which is indicative of intactness.

2.5 *Isolation of Thylakoid Membranes*

Isolation of unstacked thylakoids was performed as with intact chloroplast extraction, and for stacked thylakoids 5 mM $MgCl_2$ was added to all buffers. Upon isolation of chloroplasts, 30 ml of resuspension buffer was added to the samples. Chloroplasts were then osmotically shocked by adding 50 ml of breaking medium (10mM HEPES; pH 7.6). After 30s, osmotic potential was restored by adding 50 ml of osmoticum medium (0.66 M Sorbitol, 40 mM MES; pH 6.5). Samples were centrifuged for 10 min at 3500g. Supernatant was poured away before resuspending the pellet in a few drops of resuspension buffer.

2.6 *Leaf Infiltration*

Whole plants were dark adapted for 45 min prior to leaf removal and infiltration. Leaves were placed in a 50 ml syringe with 10 ml of buffer, with the

vacuum created by sealing the nozzle. Vacuum infiltration was then performed on leaves with 10 mM Hepes, 150 mM sorbitol; pH 7.5 and 30 µM DCMU for fast induction measurements, 50 µM nigericin or 1 mM ammonium chloride to inhibit NPQ, or 1 mM lincomycin to inhibit D1 repair.

2.7 *Chlorophyll Fluorescence Measurements*

Chlorophyll fluorescence was measured using Walz JUNIORPAM, DUAL-PAM-100 or IMAGING-PAM fluorimeters (Walz, Effeltrich, Germany). For JUNIOR-PAM measurements, a monitoring leaf clip and fluorescence standard foil was used. Whole leaf measurements were performed after 45 min of dark adaptation. The pNPQ assessment procedure consists of eight increasing actinic light (AL; 435 nm) illumination steps were used, each lasting 5 min (Ruban and Belgio 2014). The AL intensities used were 0, 90, 190, 285, 420, 625, 820, 1150 and 1500 µmol photons m^{-2} s^{-1}. A greater range of intensities was achieved by adjusting the AL integer in the system settings, to correspond to 80, 87 or 90% of the AL values listed. AL intensities were verified by a Walz MQS-B light sensor. The scheme comprises of: (SP)–(AL on)–(120 s)–(SP)–(180 s)–(SP)–(AL off/FR on)–(10 s)–(SP)–(5 s)–(AL on/FR off)–repeat. Here SP the saturating pulse (0.6 s, 6000 µmol photons m^{-2} s^{-1}) and FR is far red light (730 nm). Between 30 and 40 procedure repeats were conducted, with the outermost leaves used, and no plant being used more than twice for any experiment. Methods for other fluorescence induction experiments will be described in text. Parameters were calculated as:

$$NPQ = ((Fm/Fm')/Fm') \qquad \text{(Equation 2.03)}$$

$$Fv/Fm = ((Fm-Fo)/Fm) \qquad \text{(Equation 1.06)}$$

2.8 *Principle of pNPQ Methodology*

ΦPSII is affected by NPQ and RCII photodamage. It was therefore essential to disseminate the ΦPSII reduction attributed to each factor. The following formula thus relates ΦPSII to NPQ, qP_d, and Fv/Fm:

$$\Phi PSII = \frac{qPd*Fv/Fm}{[1+(1-\frac{Fv}{Fm})*NPQ]} \qquad \text{(Equation 1.11)}$$

where qP_d is the photochemical quenching (qP) measured in the dark immediately following a period of illumination; Fm is the maximum fluorescence in the dark-adapted leaf; Fv=Fm–Fo, where Fo is the dark fluorescence level before illumination and Fv/Fm is the maximum quantum yield of PSII. In the absence of photoinhibition, qP_d = 1, and this can be used to estimate the theoretical ΦPSII:

$$Theoretical\ \Phi PSII = \frac{1*Fv/Fm}{[1+(1-\frac{Fv}{Fm})*NPQ]} \qquad \text{(Equation 1.16)}$$

The proportion of open RCII was calculated as:

$$qPd = \frac{(Fm-Fo'act.)}{(Fm-Fo'calc.)} \qquad \text{(Equation 1.17)}$$

where Fm' is the maximum fluorescence after actinic light illumination; Fo'act is the measured dark level of fluorescence after illumination, and Fo'calc is the calculated dark fluorescence level. The latter was calculated using the formula proposed by Oxborough and Baker (1997):

$$Fo'calc. = \frac{1}{(\frac{1}{Fo}-\frac{1}{Fm}+\frac{1}{Fm'})} \qquad \text{(Equation 1.18)}$$

For a detailed guide including the text batch file used to encode the pNPQ assessment procedure, computer programming to extract the data files and the formatting used to present the results, see Appendix Item 4.

The above NPQ parameter is calculated during the last SP in the light at the end of the five-minute AL illumination, and the qPd parameter at P3 during the 10 s dark period. NPQ is protective (pNPQ) when qPd has not dropped below 0.98, thus all RCII are undamaged. This procedure entails an eight-step gradually increasing actinic light illumination of five minute intervals (the light intensities and duration of illumination are explained in Chapter 3.22) as shown below (Fig 2.02).

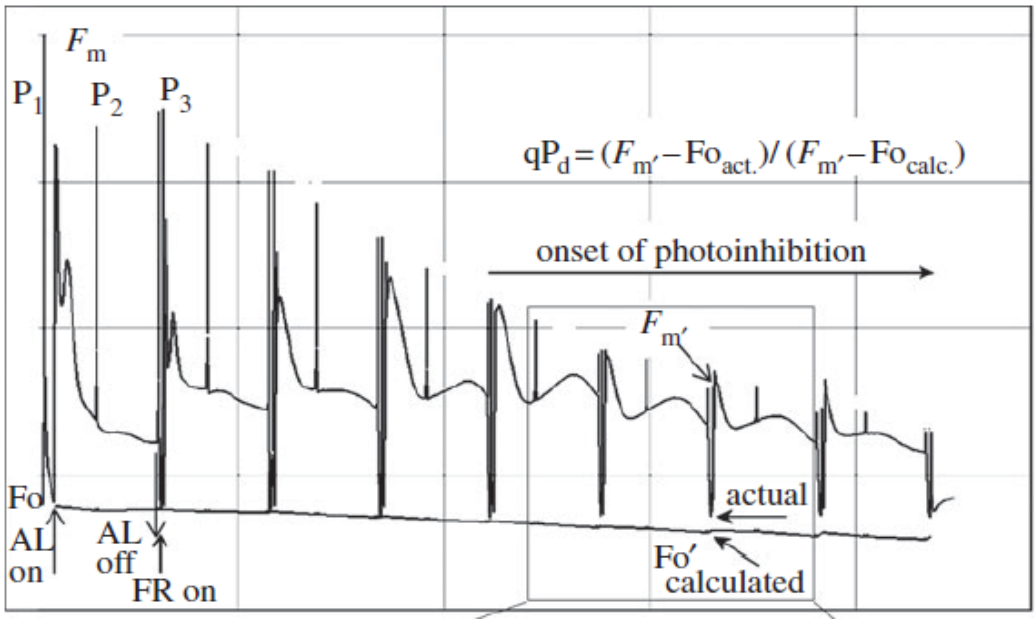

Figure 2.02 Scheme of induction of chlorophyll fluorescence quenching in a WT *Arabidopsis* leaf, with an eight stepwise increasing actinic light levels (figures 3–8): 90, 190, 285, 420, 620, 820, 1150 and 1500 µmol m^{-2} s^{-1}. Vertical arrows on the left of the figure indicate application (AL on) and removal (AL off) of the actinic light treatment. P1, P2, P3 are saturating pulses applied before (P1) and during (P2, P3) the actinic light treatment. Short arrows on the right of the figure indicate levels of calculated (Fo'calc:) and actual (Fo'act:) fluorescence in the dark. The timing scheme for the dark breaks was: (AL off) (FR on)-(7 s)-(P)-(5 s)-(AL on)(FR off), where FR is far-red light; P is the saturating pulse. Taken from Ruban and Belgio (2014).

2.9 *Low Temperature (77K) Fluorescence*

Measurements were carried-out at 77 K using a custom-made cryostat and Jobin Yvon FluoroMax-3 spectrophotometer. Fluorescence spectral resolution was 1 nm, with a 5 nm spectral bandwidth and excitation defined at 435 nm. Absorption spectra were scanned at 5 nm sec-1 from 600 to 800 nm. Grams (Galactic Industries Corporation) software was used to manipulate and present results, as seen in Fig. 2.03 below.

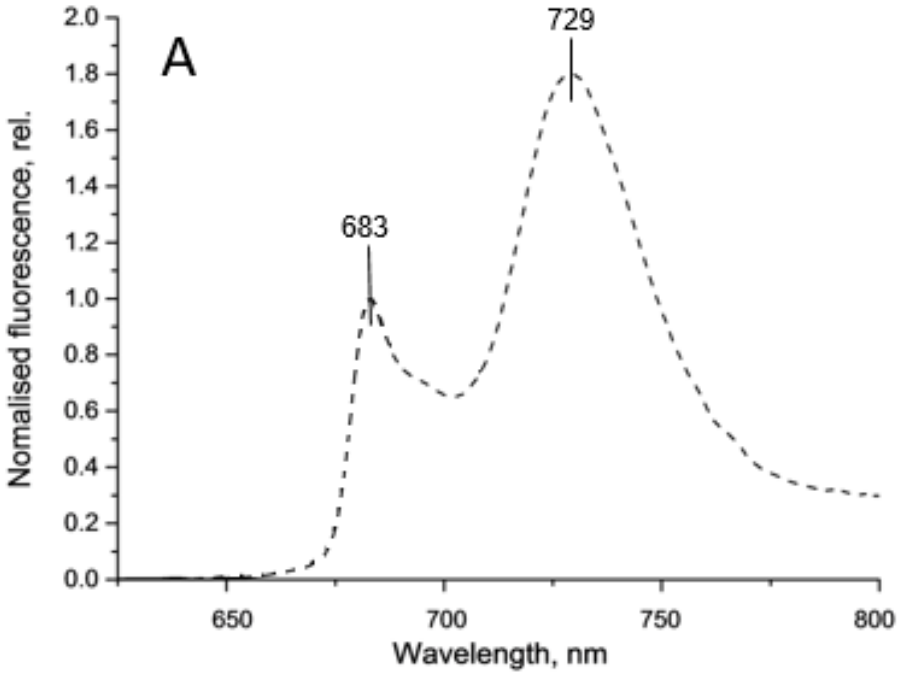

Figure 2.03 Normalised fluorescence trace obtained from 77K fluorescence spectroscopy performed on dark-adapted chloroplasts from a WT plant (Ware *et al.*, 2015b).

2.10 *Time-Correlated Single Photon Counting (TCSPC)*

Fluorescence lifetime decay kinetics were obtained using a FluoTime 200 ps fluorimeter (PicoQuant). A 470-nm laser diode with 10 MHz repetition settings were used for lifetime measurements (Johnson and Ruban, 2009). Instrument response function was 50 ps. Chloroplast fluorescence was detected with a 1 nm slit width at 685 nm. FluoFit software was used to analyse the lifetimes, with the fit quality measured by X2 parameter. Autocorrelation was used as a further control to

judge the quality of fit, with a normal distribution of little fluctuations around zero indicating the fit quality (Ware *et al.*, 2015).

2.11 *Sucrose Gradient Ultracentrifugation*

Membranes corresponding to 500 µg of chlorophyll were washed with 5 mM EDTA. Samples were solubilised with 1 ml solution of 10 mM HEPES and 0.6 % α-dodecyl maltoside (α-DM), pH 7.5 for 45 min on ice. Fractionation by ultracentrifugation (20 h, 4°C, 200,000 g) followed in a 0.06% α-DM, 10 mM HEPES, pH 7.5 and 0.1–1 M sucrose gradient (Dall'Osto *et al.*, 2006; Ware *et al.*, 2015).

2.12 *Freeze Fracture Electron Microscopy (FFEM)*

A dense suspension of chloroplasts was laid down on flat-topped copper specimen plates, and rapidly frozen using slushy liquid nitrogen (-210°C). Fractures were performed at -150 °C with a Polaron E7500 freeze-fracture device (Fisons Scientific Equipment, Loughborough, UK). Replicas were made alternating between carbon and platinum spray-guns. Samples were placed diluted bleach for 30 min. This is ensuring residual protein is removed. Replicas are then washed in distilled water for 30 min. Ultrastructure analysis was performed using a JEM-1230 Electron Microscope (JEOL USA, Inc., Peabody, MA, USA) as previously reported (Johnson *et al.*, 2011).

2.13 *High Performance Liquid Chromatography (HPLC)*

Xanthophyll concentrations were determined using reverse-phase HPLC. A LiChrospher 100 RP-18 column and Dionex Summit chromatography system (Ruban *et al.*, 1994) was used for pigment determination. Two buffers were used and their compositions are: buffer A - 87% acetonitrile, 10% methanol, 3% 0.1 M TRIS pH8; buffer B: 80% methanol, 20% hexane). Chloroplasts with a final concentration of 1 mg mL^{-1} were used for measurements, extracted in 100% acetone or 100%

methanol, and filtered using a 0.5 µm nylon filter. A solvent flow rate of 1 mL/min was used, with typical runs taking ~23 min (Fig. 2.04).

For dark adapted leaves, wholes plants were dark adapted for 45 min before freezing in liquid nitrogen. Three leaves were used for each sample. For light exposed samples, leaves were cut from the plant and frozen in liquid nitrogen immediately after the saturating pulse used to determine the NPQ values at each actinic light intensity.

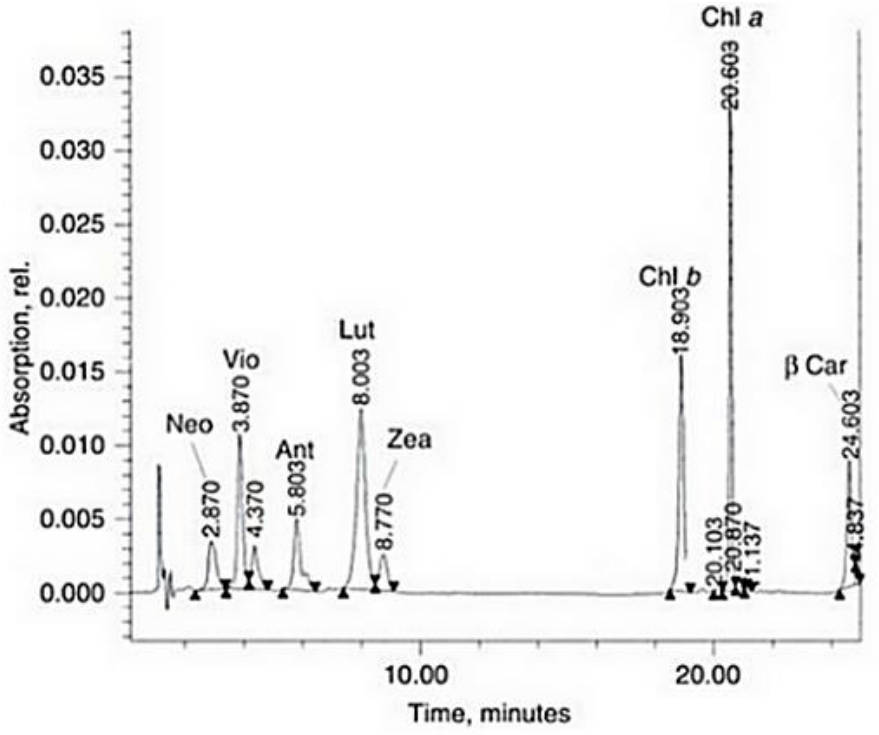

Figure 2.04 Typical HPLC profile of a WT dark-adapted *Arabidopsis* plants. The most polar xanthophylls are eluted first. Xanthophylls and carotenoids displayed are: Neo (neoxanthin), Vio (violaxanthin), Ant (antheraxanthin), Lut (lutein), Zea (zeaxanthin), Chl *b* (chlorophyll *b*), Chl *a* (chlorophyll *a*) and β Car (β carotene) (Ruban, 2012).

2.14 *Sodium Dodecyl Sulfate Polyacrylamide Gel Electrophoresis (SDS-PAGE)*

Glass plates and clamps must be cleaned with water and then with 100% ethanol. The running gel (30% acrylamide mix, 1.5M Tris (pH 8.8), 10% SDS, 10% APS, TEMED) is poured and allowed to set, then stacking gel (30% acrylamide mix,

1.0M Tris (pH 6.8), 10% SDS, 10% APS, TEMED) is set on top of this. Extract unstacked thylakoids according to 2.5 (isolation of thylakoid membranes) with chlorophyll concentration determined according to 2.3 (chlorophyll content determination). Add 10µL of Laemmli buffer (100mM Tris HCl (pH 6.8), 200mM dithiothreitol, 4% SDS (electrophoresis grade), 0.1% bromophenol blue, 20% glycerol) into Eppendorfs with 10µL of sample and mix. Add Eppendorf to Thermoblock (90^{o}C) and leave for 10 min. After this, centrifugate Eppendorf for 5 min at 3500g. Load marker (5-10 µL) and samples (18 µL at 25, 50, 100% concentration) into lanes/wells, close lid. Run at 150 V for 15 mins, then increase to 200 V for a further 60 min. Gels can then be used for coomassie blue staining or Western blot analysis.

Coomassie Blue Staining

Place gels on Petri dishes and cover in 100 ml of Coomassie dye (methanol 45mL, ultrapure H_2O 45mL, acetic acid 10mL, Coomassie Brilliant Blue R250 0.25g) and place on shaker for 60 min. Remove coomassie from gel, pour over destaining buffer (10% ethanol, 10% acetic acid, 80% ultrapure H_2O) and return to shaker for 60 min. Remove destaining buffer and pour over fresh destaining buffer. Detection performed using Western Blotting Detection System (GE Healthcare Life Sciences, Little Chalfont, UK) and analysis with ImageJ software (http://rsb.info.nih.gov/ij/).

Western Blot Analysis

Fill Petri dish with transfer buffer (1.5M glycine, 0.2M Tris) and submerge sandwich equipment in this for 30 min. Remove gel from SDS-PAGE and prepare enclosed sandwich (black cassette wing (-), sponge, blotting paper x2, gel, membrane (nitrocellulose), blotting paper, sponge, clear cassette wing (+)). Place sandwich in holder connecting electrodes, place in BioRad box, add transfer buffer to submerge apparatus, add flea and place on stirrer. Connect lid and apply 400mA current, running for 45 min. Remove membrane from box and cover in Ponceau stain (Ponceau 0.1%, acetic acid 0.5%, ultrapure water) in a Petri dish for 2 min. Remove excess dye with distilled water. Place membrane in Petri dish, cover with solution A (x10 PBS buffer 10%, Tween 20 1%, skimmed milk 5%) for 60 min and place on

shaker. Pour off solution A, add primary antibody and leave in a fridge overnight. Remove primary antibody solution, and pour on fresh solution A for 4 x 10 min. Remove solution A and apply secondary antibody (1µL in 30mL of solution A) for 60 min under agitation on shaker. Remove solution and apply solution B (Tween 20 1%, x10 PBS buffer 10%, ultrapure water) for 2 x 10 min on shaker. In the dark, use developer to generate photographic film.

2.15 *Statistical analysis*

A number of different statistical tests were used to assess whether differences between at least two pieces of data are significantly different. $P < X$ is used to signify there being a less than X% chance that the data is different due to chance. $P < 0.05$ is used as the marker for significance unless otherwise indicated.

Single Factor Analysis of Variance (ANOVA) is used to test whether there is a significant difference between the means of more than two groups of data. The number of inputs, total, average and variance of each group is used to calculate the differences between groups. Significance is indicated by F value > F critical value and $P < 0.05$, as indicated below:

Anova: Single Factor

SUMMARY

Groups	*Count*	*Sum*	*Average*	*Variance*
Row 1	10	9.03	0.903	0.000561
Row 2	10	8.534	0.8534	0.001531
Row 3	10	8.594	0.85946	0.000735

ANOVA

Source of Variation	*SS*	*df*	*MS*	*F*	*P-value*	*F crit*
Between Groups	0.014642	2	0.007321	7.769149	0.002162	3.354131
Within Groups	0.025443	27	0.000942			

	0.04008		
Total	5	29	

Testing for significance between two different groups of data was achieved via a Student *t*-test or Tukeys *t*-test. $P < 0.05$ was used to conclude that datasets were significantly different. For rate constants and averages calculated by regression analysis, a z-test was utilised to test for significance differences. The z-test requires a standard error of the value, frequently the mean, to produce a critical value for the difference between the two parameters. For instance, +/- 1.96 is the critical value that indicates a 95% probability that the differences arose by a reason other than chance. A two-tailed distribution was employed, as results are expected to fall in a normal distribution about the mean and are equally likely to be more positive or negative than the mean (Fig 2.05).

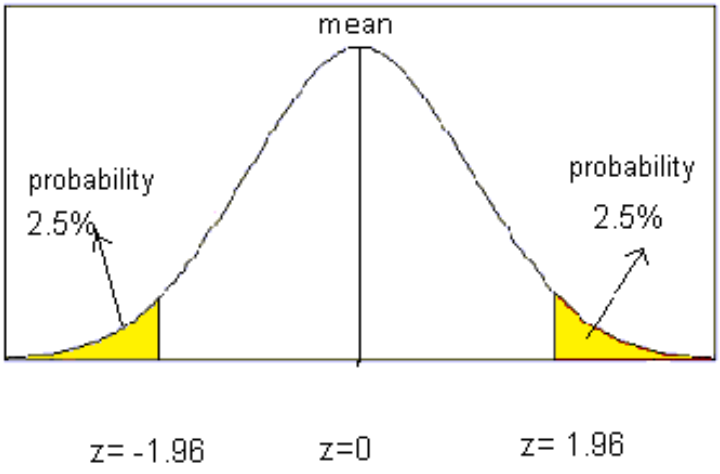

Figure 2.05 Example of a two-tailed distribution with 5% confidence interval and ±1.96 critical value used in z-tests.

Error bars represent the standard deviation (SD), calculated as:

$$SD = \frac{\sqrt{\Sigma\left(x - \overline{x}\right)^2}}{n} \quad \text{(Equation 2.04)}$$

or standard error of the mean (SEM), calculated as:

$$SEM = \frac{SD}{\sqrt{n}}$$ (Equation 2.05)

The statistical analysis employed are explained in figure legends and significance levels are indicated in the figures by asterisks.

2.16 *Measuring photodamage by anthocyanin, ROS and hydrogen peroxide accumulation*

DAB staining for the visualisation of hydrogen peroxide accumulation.

Place leaves in a beaker filled with 0.1% 3,3'-diaminobenzidine (DAB) for 15 min (use HCl to achieve a pH 3.8), making sure they're fully immersed. Remove leaves from beaker and place in tubes containing 0.15% Trichloroacetic acid (TCA) and 4:1 ethanol:chloroform ratio. Ensure leave are fully submerged and leave in the dark for 48 hrs. After removal from solution the leaves were photographed and analysed using ImageJ software (http://rsb.info.nih.gov/ij/) (Thordal-Christensen *et al.*, 1997; Carvalho *et al.*, 2015).

Thiobarbituric acid reactive species (lipid peroxidation)

Use liquid nitrogen to grind 100 mg of leaf material to a fine powder. Add powder to 1 ml of 5% of Trichloroacetic acid (TCA) (diluted with water), and homogenize. Samples are centrifugated (12,000*g*), for 15 min at 4^{o}C. Collect the 250 µL of the supernatant and discard the pellet. 1 ml of 20 % TCA and 0.5% TBA (in water) was added to the supernatant, and the mixture incubated for 1 hr at 95ºC. Samples were placed in an ice bath until returned to room temperature. Samples were then centrifugated (12,000*g*) for 5 min, with the supernatant collected in fresh tubes. Samples were measured using a spectrophotometer at 532 ηm and 660 ηm. ΔL was calculated as (L660ηm – L532ηm), with a molar extinction coefficient being to quantify the MDA-TBA complexes (155 mM^{-1} cm^{-1}). This is then divided by the fresh weight of the leaves used to be expressed as µmol MDA-TBA g-1 fresh weight (FW) (Heath and Packer, 1968; Carvalho *et al.*, 2015).

Anthocyanin accumulation

50–150 mg of fresh leaf material was ground to a fine powder in the presence of liquid nitrogen using a pestle and mortar. 1% HCl in 300 µl of methanol, was added to the powder before being stored at 4°C for 24 hrs. Then 500 µl of chloroform and 200 µl H_2O was added to the homogenate prior to 5 min centrifugation at 14000*g*. The upper band of pigments are anthocyanins with the lower chlorophylls and free pigments. The top layer was therefore carefully removed prior to spectroscopic quantification. The total anthocyanin content is calculated via absorbance at two wavelengths (530 and 657 nm). 530 nm is used to measure anthocyanins, with 657 and chlorophylls present in the sample. The total content expressed as A530–A657 g FW^{-1} (Neff & Chory 1998; Carvalho *et al.*, 2015).

Chapter III –

Optimising the pNPQ

Assessment Procedure

3.1 Introduction

The theory of the pNPQ and qP_d parameters has already been established, but not a reliable procedure to assess these (Ruban and Murchie, 2012). The purpose of the procedure is to have a reliable point of photoinhibition, and one that can also allow us to determine the earliest point of photoinactivation, something that is not afforded using Fv/Fm and qI fluorescence parameters (explained in more detail in Chapter 8). Furthermore, with the procedure, as fast a procedure as possible was desired, but one that also allows the NPQ/pNPQ mechanism to be fully established in each plant, otherwise the results will not offer a true reflection of the extent of photoinhibition in each plant.

The pNPQ assessment procedure and underpinning theory depends on the minimum (Fo) and maximum (Fm) fluorescence levels in the dark, and light (Fo' and Fm' respectively). PAM fluorometers use these four parameters to calculate the ΦPSII and NPQ. Most PAM devices and software's fail to factor into fluorescence measurements the contribution of ΦPSI (Dau, 1994; Lazar, 2013). Indeed, there is even uncertainty as to the amount of fluorescence produced by PSI, and whether this fluorescence is constant or quenchable (Krause and Weis, 1991; Pfündel *et al.*, 2013). The most recent report on the topic was the investigation by Pfündel *et al.*, 2013. Here, the group used a similar fluorescence procedure to assess chlorophyll fluorescence. Nine gradually increasing actinic light values were applied, each of 10 minutes, but performed on a DUAL-PAM-100 (Walz, Germany). Measurements of fluorescence one second after the saturating pulse were used to calculate Fo' with PSI fully reduced. Fo' was also measured after FR light illumination to discern the changes in Fo' with PSI fully oxidised. ΦPSI was calculated from values obtained using Klughammer and Schreiber's (1994) calculation:

$$\Phi\mathrm{PSI} = \frac{\mathrm{Pm}}{\mathrm{Pm}-\mathrm{Po}} \qquad \text{(Equation 3.01)}$$

Where Pm and Po are the maximum and minimum fluorescence signals in P700 measurements. Using this method, the group established that ΦPSI is responsible for 24% of the total fluorescence at Fo. Furthermore, this PSI fluorescence level is not quenched upon exposure to actinic light.

This work is very poignant and potentially very useful in the pNPQ assessment procedure. One of the unique benefits of the technique is the ability to quantify the ΦPSII based on the downregulated and photoinhibited losses of photosynthetic performance in real time (see Materials and Methods). If the fluorescence parameters measured are not a valid representation of ΦPSII, then the investigations and conclusions would be limited in value. Our lab therefore wanted to employ the proposed 24% fluorescence offset and carry out the actinic light procedure to see whether there are any significant changes in the ΦPSII values obtained. Besides minor changes in actinic light values used, there is only one significant change between the experimental set-ups. For the measurements, our group used a JUNIOR-PAM, whereas Pfündel and co-workers (Pfündel *et al.*, 2013) used a DUAL-PAM-100. This difference is important as the DUAL-PAM-100 detects wavelengths longer than 700 nm. This red-shifted detection will result in increased measurements of PSI fluorescence compared to the JUNIOR-PAM (630 nm). The JUNIOR-PAM is used as it is a more versatile PAM fluorometer, with the potential to be used in fields or outdoor environments. Furthermore, the optimal variations in light intensities and illumination had already been established (Chapter 3.22), therefore the qP_d assessments are a true reflection of photoinhibition.

3.2 Results

3.21 Optimising plant growth

Upon starting in the Ruban laboratory, it became apparent that there were a number of elements of the plant growth facility that were not conducive for optimal plant growth. Early fluorescence measurements on plants indicated that Fv/Fm was markedly reduced (Fig 3.01), compared to the desired 0.8-0.83, which signifies healthy plants (Wientjes *et al.,* 2013). It appeared that several techniques employed in the growth of plants could be contributing to this decline. For instance, plants were grown under ~70 µmol m^{-2} s^{-1}, which can lead to the over accumulation of LCHII and reduces Fv/Fm due to the longer energy transfer pathway from LHCII to RCII (Belgio *et al.*, 2014). It was therefore important to establish a light intensity that would allow plants to become healthy. Gradually increasing the light intensity to ~200 µmol m^{-2} s^{-1} produced plants with Fv/Fm of ~0.8. The effect of varying light growth conditions on the health of plants became the research focus in Chapter 7. Increasing the light intensity far beyond this resulted in a much shorter life cycle, reducing the available time to experiment on plants during the adult phase of the life cycle, which also became a focus of research in Chapter 4. Whilst ascertaining the correct light-growth conditions, further plant growth conditions were optimised, including the use of a new type of soil and perlite for better drainage, imbibing seeds and the stratification of seeds to ensure uniform growth, higher light intensities for growth, no thinning during growth to minimise root damage during the separation of plants, and watering plants from below (see Chapters 2 and 3 for further details). These techniques combined to produce plants with higher Fv/Fm values and notably healthier physical characteristics. Taken together, this early work helped to ensure maximum ΦPSII's, so that pNPQ and photoinhibition could, as near as is feasibly possible, be the only factors that affect ΦPSII. Besides plants' health, the new ΦPSII calculations requires Fv/Fm (Equation 1.15). Ensuring reproducible conditions that produce high and stable Fv/Fm values was therefore of paramount importance, as can be seen from the previously published ΦPSII plots (Fig 3.02). Here it can be seen that decreased Fv/Fm manifests as a decrease in ΦPSII.

1:F	1:Fm'	1:PAR	1:Y (II)	1:Fo'	1:qP	1:Fv/Fm
Device Nr: #1, Junior-PAM/II						
Chart Start						
716	2541	0	0.718	-	-	0.718
700	2545	0	0.725	~716	1.009	0.718
1030	1667	90	0.382	~624	0.611	0.718
983	1733	90	0.433	~633	0.682	0.718
604	1791	0	0.663	~640	1.031	0.718

Figure 3.01 Fluorescence parameters measured with a JUNIOR-PAM on whole intact WT leaves. Critically, the 0.718 Fv/Fm value causes a big decline in the ΦPSII, even before any actinic light illumination. In the first dark-phase of the measurements, qP_d is also seen to rise above 1.00 to 1.031, another sign of unhealthy plants.

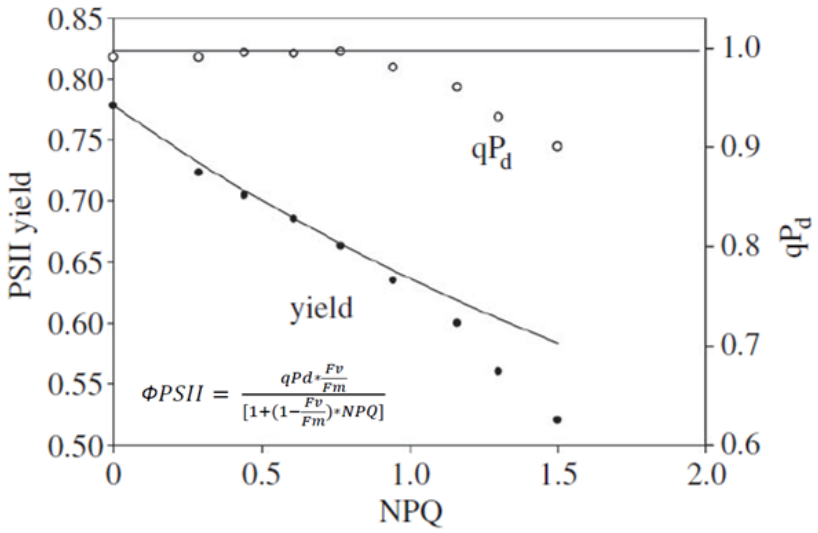

Figure 3.02 The relationship between ΦPSII, qP_d and NPQ in whole intact *npq4* leaves, recorded using the scheme presented in Fig 3.03 (From Ruban and Belgio, 2014). This plot is important for the depiction of the relationships between NPQ, ΦPSII and qP_d. The closed and open circles are taken at the end of each light intensity, and plotted as functions of NPQ vs qP_d, and NPQ vs ΦPSII. The continuous line is the same as the closed circles (equation in graph), except that qP_d is substituted for 1.00, indicative of 100% open reaction centers.

3.22 Optimising the duration and intensity of light to accurately assess the point of photoinhibition

The next step of the protocol establishment project aim was to optimise the pNPQ assessment procedure. Ruban and Belgio (2014) utilised a ~43-minute procedure, the sequence of which is illustrated in Fig 3.03. The pNPQ procedure entails a ~43-minute sequence of gradually increasing actinic light procedure on the JUNIOR PAM fluorometer.

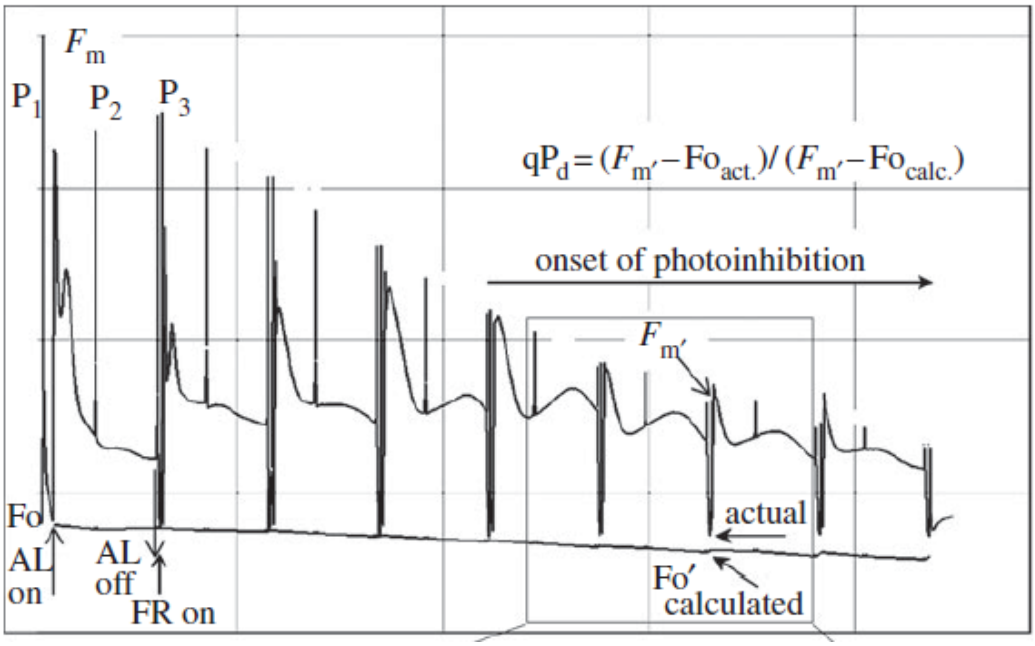

Figure 3.03 Scheme of induction of chlorophyll fluorescence quenching (as depicted in Fig 2.02) in a WT *Arabidopsis* leaf, with an eight stepwise increasing actinic light levels: 90, 190, 285, 420, 620, 820, 1150 and 1500 µmol m^{-2} s^{-1}. Vertical arrows on the left of the figure indicate application (AL on) and removal (AL off) of the actinic light treatment. P1, P2, P3 are saturating pulses applied before (P1) and during (P2, P3) the actinic light treatment. Short arrows on the right of the figure indicate levels of calculated ($Fo'_{calc.}$) and actual ($Fo'_{act.}$) fluorescence in the dark. The timing scheme for the dark breaks was: (AL off) (FR on)-(7 s)-(P)-(5 s)-(AL on)(FR off), where FR is far-red light; P is the saturating pulse. Taken from Ruban and Belgio (2014).

Two key variables in the pNPQ assessment procedure, and PAM fluorescence in general, is the measuring light (ML) and far red (FR) light. Fig 3.04 illustrates the difference between WT plants that have been exposed to different fML intensities. Figs 3.04A and 3.04B have a fML that is too high, which can close RCII. Fig 3.04A displays a fML that is too high leading to quenching of fluorescence, whereas in Fig 3.04B, the minimum amount of fluorescence is gradually increasing, which could be due to photoinhibition, or the activation of photochemical processes after dark-adaptation. These two conditions can elevate Fo, which results in a decreased Fv/Fm compared to leaves exposed to suitable fML intensities (Fig 3.04C). Conversely, a fML intensity that is too low, can result in inaccurate measurements as many other variables use Fo (Fv/Fm and qP_d, see Equations 1.12-1.15). It is therefore important to vary the fML intensity to suit every type of leaf, to reduce the chance of this variable affecting results or conclusions. The FR light is also of vital importance. FR light preferentially excites PSI, as it absorbs light at a longer wavelength. Therefore, the use of FR light is important as it decreases the excitation at PSII, whilst stimulating the ETC, as P700 is oxidised in these conditions. It is important to balance the amount of FR light and the intensity of the light. Varying the length of the FR light illumination should not be too excessive as the ΔpH across the thylakoid membrane may collapse. Furthermore, too little illumination may not effectively relieve the excitation pressure around PSII, resulting in an elevated Fo', making qP_d measurements less reliable. The FR light in Fig 3.05A and Fig 3.05B is too low, as the fluorescence trace is still being quenched at the point of actinic light (AL) illumination, and Fo is not sufficiently quenched in the second-phase of FR light respectively. Fig 3.05C represents an appropriate FR light to relieve the energy accumulation, displayed by two steady-state minimum fluorescence traces, allowing an accurate measurement of $Fo'_{act.}$ and estimation of $Fo'_{calc.}$ In the JUNIOR-PAM settings, a FR integer intensity of eight, for a period of 10 seconds, was the most suitable combination, and incorporated into the pNPQ assessment procedure (Appendix 1).

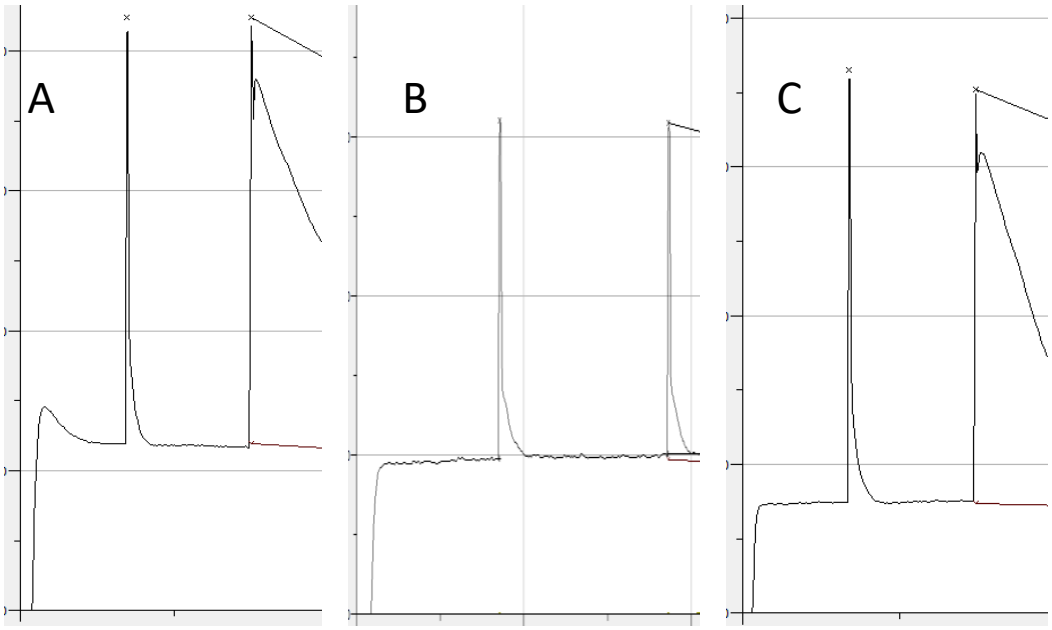

Figure 3.04 Scheme of induction of chlorophyll fluorescence quenching in wild-type *Arabidopsis* leaves. The figures display different fML intensities, and the subsequent effects that are caused from too high fML intensities (A and B), compared to a steady-state fluorescence value obtained in Fig 3.04C.

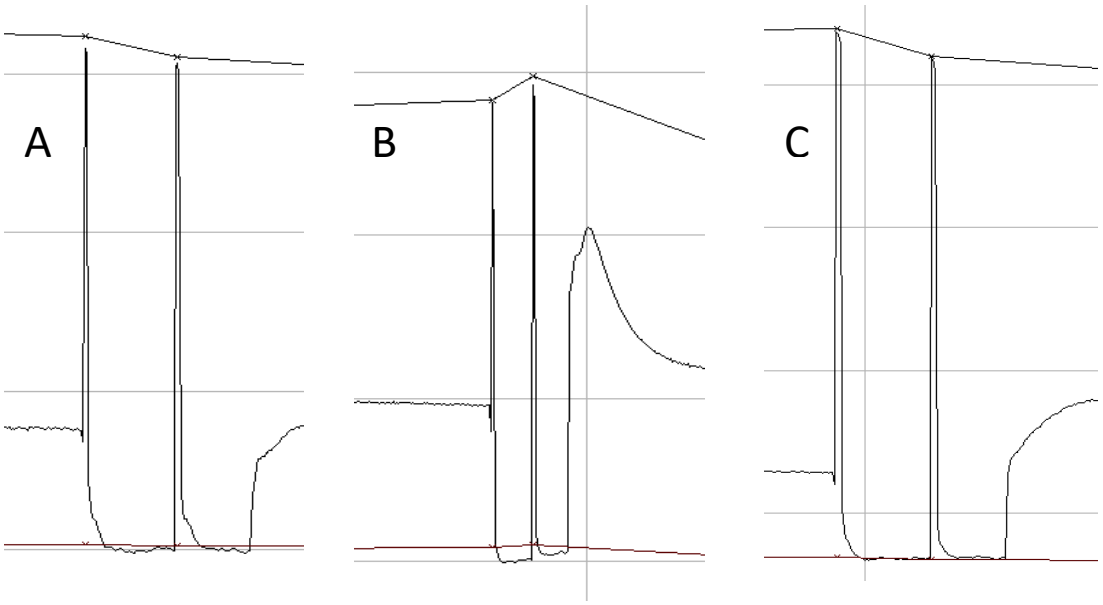

Figure 3.05 Scheme of induction of chlorophyll fluorescence quenching in a wild-type *Arabidopsis* leaf. The figures display different FR light intensities, and the subsequent effects that are caused from too high FR intensities (A and B), compared to a steady-state fluorescence value obtained in Fig 3.05C.

After establishing these variables, the length of the procedure was addressed. The sequence of the procedure was first shortened to 33 minutes, by decreasing the actinic light exposure time for each interval from five minutes to three minutes 40 seconds. The average qP_d values were lower in the 33-min procedure compared to the 43-min procedure, although this was not significant, it was close to being significantly different at 90, 190 and 285 µmol $m^{-2}s^{-1}$ (Fig 3.06A, Table 3.01). NPQ was however significantly lower throughout the course of the procedure (Fig 3.06B, Table 3.01). This suggests that shortening to the pNPQ assessment procedure leads to significantly reduced NPQ levels, and different qP_d levels to the 43-min procedure. In order to ascertain whether the pNPQ procedure was already as short as it can be, without NPQ and qP_d values becoming significantly affected, the procedure was lengthened to 53 min via increasing interval lengths to six minutes 20 seconds. NPQ and qP_d values were not significantly different between the 43 and 53-minute procedure at any actinic light intensity. This suggests that 5 min light intervals were long enough for maximal NPQ formation, and that there is no need to increase the procedure length, as it is important to have it as short as possible.

It is worth noting that the qP_d rise may have had an impact on the results. Plants being used for the procedures were grown under the same light intensity, so the rise was a systematic error for all time variations. Optimising light conditions, as well as changing other growth conditions has stopped this qP_d rise in the majority of cases. As discussed, the qP_d rise became the focus of research in Chapter 7, and will be discussed in greater detail there. importantly, the establishment of an optimal procedure allowed for data collection and extraction with confidence that the chance of other systematic errors occurring being minimal.

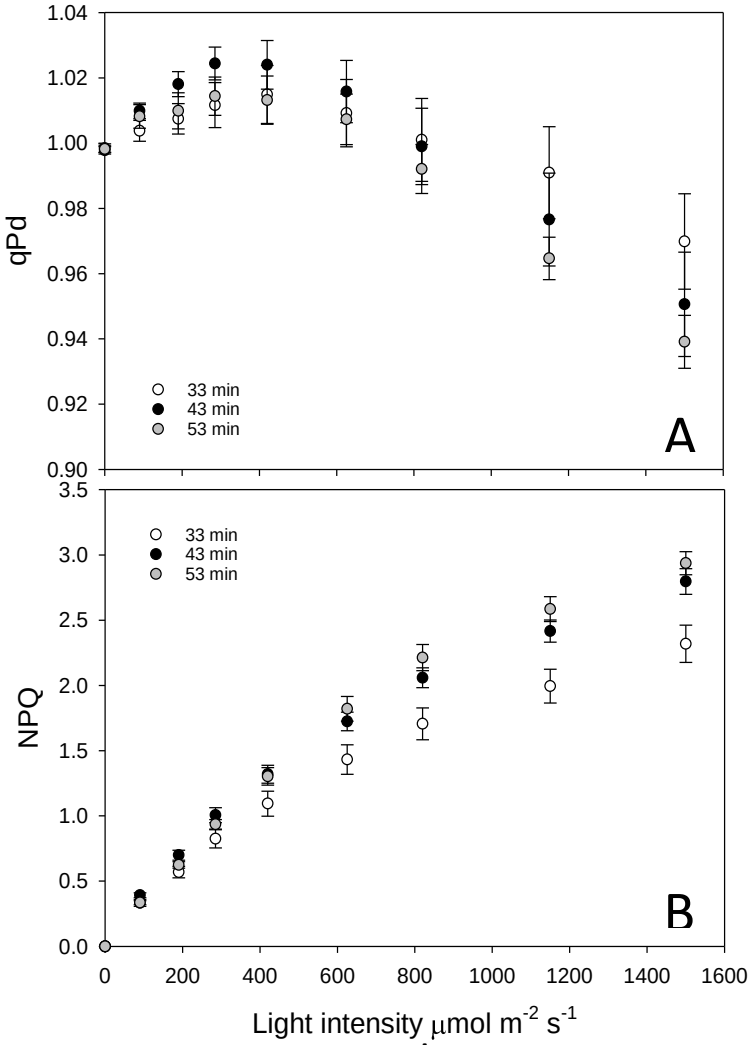

Figure 3.06 A qP_d and B NPQ values obtained by an eight-step actinic light intensity procedure of 33, 43 and 53 min total lengths, with light intensities of 0, 90, 190, 285, 420, 620, 820, 1150 and 1500 µmol m^{-2} s^{-1}. Error bars represent the standard error of the mean (SEM) from 10 repeats (n = 10).

Procedure Length		33-43			43-53			33-53
Light Intensity, mmol m-2 s-1	NPQ	qPd		NPQ	qPd		NPQ	qPd
0	N/A	0.662		N/A	0.794		N/A	0.679
90	0.090	0.116		0.130	0.700		0.949	0.919
190	0.039	0.072		0.117	0.240		0.293	0.913
285	0.061	0.102		0.323	0.212		0.180	0.862
420	0.073	0.391		0.864	0.317		0.092	0.514
625	0.045	0.602		0.428	0.498		0.017	0.534
820	0.027	0.897		0.237	0.627		0.005	0.290
1,150	0.015	0.440		0.204	0.461		0.002	0.047
1,500	0.014	0.345		0.302	0.532		0.002	0.034

Table 3.01 Student *t*-test values for the average NPQ and qP_d values at each of the of 0, 90, 190, 285, 420, 620, 820, 1150 and 1500 µmol m^{-2} s^{-1} light intensities in the 33, 43 and 53-min procedures. The NPQ and qP_d values are those plotted in Fig 3.06A and 3.06B. 33, 43 and 53 represent the length of time of the corresponding procedure.

3.23 *PSI fluorescence contributes to ΦPSII*

In 2013, Dr Pfündel and co-workers published a paper that questioned whether PSI fluorescence should be accounted for during chlorophyll fluorescence measurements (Pfündel et al., 2013). In this paper, the group proposed that a constant offset of 24% of total fluorescence originates from PSI, and that this should be removed to accurately assess the ΦPSII, measure NPQ and Fv/Fm parameters. Furthermore, the group propose that PSI cannot be quenched, therefore its constant contribution will be proportionally greater at Fo compared to Fm. A conclusion of the group's work did not fit with findings of the Ruban laboratory, and indeed the work of Bradbury and Baker (1986) and Oxborough and Baker (1997). A reason for the PSI offset was to correct for the divergence between $Fo'_{act.}$ and $Fo'_{calc.}$ during illumination. Unlike the Ruban groups earlier studies (Ruban and Murchie, 2012; Ruban and Belgio, 2014) and Baker's studies (Bradbury and Baker, 1986; Oxborough and Baker, 1997), the two Fo' values diverged at low light intensities and then gradually became equal at high light intensities. Therefore, before embarking on this study, literature reviews were conducted to compare the findings of the Pfündel research paper (Pfündel et al., 2013). Preliminary findings indicated that PSI fluorescence can be quenched during illumination (Ruban et al., 1991; Trissl et al., 1993; Richter et al., 1999; Holzwarth et al., 2009; Miloslavina et al., 2011; Ballottari et al., 2014), and that a rise in Fo' act. normally indicated photoinhibition, something that should not be occurring at the low light intensities (Bradbury and Baker, 1986; Demmig and Björkman, 1987; Oxborough and Baker, 1997) of Pfündel's research (0, 69, 110, 169, 406 µmol m^{-2} s^{-1}). It was therefore decided to repeat Pfündel's research conditions, using the pNPQ assessment procedure with a 24% constant offset, to perform the pNPQ assessment procedure without a PSI offset, and to test a new offset as calculated from the literature review (a 20% PSI offset that is quenched by 0.4 of qN (described in Equation 3.03 and 3.04)). A control was first established, where potential fluorescence originating from PSI was omitted. As opposed to conducting control experiments and then subsequently adjusting the PSI offset from the values afterwards, fresh plants were used in each condition (no offset, constant 24% offset and reducing 20% offset)

here so that an accurate comparison, to the WT plants with varying PSI fluorescence reductions were used, could be drawn. The standard five min 0, 90, 190, 285, 420, 625, 820, 1150 and 1500 µmol m^{-2} s^{-1} actinic light intensities were employed throughout this experiment (Fig 3.07), with 13 repeats being conducted for each condition. During the experiments, after each increasing five-minute interval, the two Fo' values were measured. Instead of using these to calculated qP_d at each AL intensity, changes in $Fo'_{act.}$ and $Fo'_{calc.}$ were first calculated as a ΔFo'. This is because qP_d expresses the changes between the two Fo' values compared to Fm'. Therefore, for a more accurate reflection of any divergence in the Fo's, ΔFo' was calculated as:

$$\Delta Fo' = \frac{(Fo'act. - Fo'calc.)}{Fo'act.} \qquad \text{(Equation 3.02)}$$

As was established in the early parts of this chapter and subsequent chapters, at low AL intensities, the two Fo'. values matched very well and there is little to no change in ΔFo' (Fig 3.08A). Under high light intensities, $Fo'_{calc.}$ becomes gradually lower than $Fo'_{act.}$ (Fig 3.08B). This is due to the reduced quenching of Fo' by NPQ compared to Fm' quenching, and when RCII become photodamaged and closed, the neighbouring LHCII cannot be photochemically quenched by the bound RCII. This elevates the minimum fluorescence levels (when photochemical quenching and fluorescence are the predominant pathways for de-excitation of excited P680), thus the minimum fluorescence levels are higher at Fo' than predicted using the calculated Fo of Oxborough and Baker (1997; $Fo'_{calc.}$). Consequently, at high light intensities, there is an increase in ΔFo' and it becomes progressively more positive with increasing AL intensities (Fig 3.08B). A divergence in Fo' values also manifests as a decrease in qP_d. At approximately 750 µmol m^{-2} s^{-1}, qP_d becomes lower than 0.98, the point that is indicative of photoinhibition (Fig 3.08C). The AL intensity, and the 2.0 NPQ value that was still protective (pNPQ), were similar to Ruban and Belgio (2014). The average Fv/Fm for the leaves tested was 0.80 ± 0.01, which indicates healthy leaves. This provided confidence that the WT plants were behaving as expected and would be valid to test the PSI offset measurements, and that a valid control could be compared to with the new conditions.

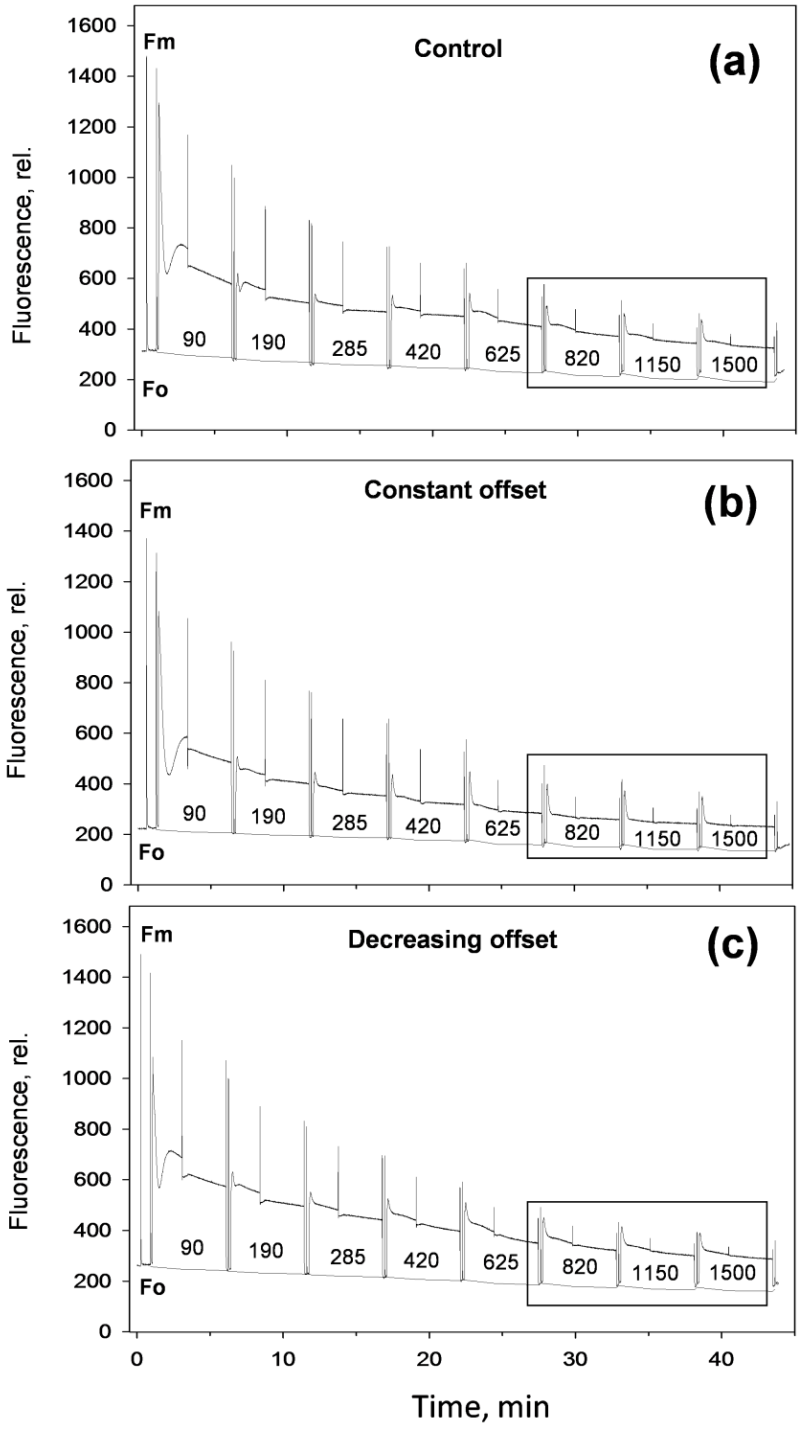

Figure 3.07 Typical chlorophyll fluorescence scheme of induction traces for (a) control (b) constant 24% fluorescence offset (c) 20% fluorescence offset at Fo, subsequently quenched by 0.40 of qN. The default JUNIOR-PAM (Walz) actinic light intensities used were 0, 90, 190, 285, 420, 625, 820, 1150, 1500 µmol m^{-2} s^{-1}. Each illumination period lasted 5 min with the total course of the routine lasting ~43 min (Giovagnetti *et al.*, 2015).

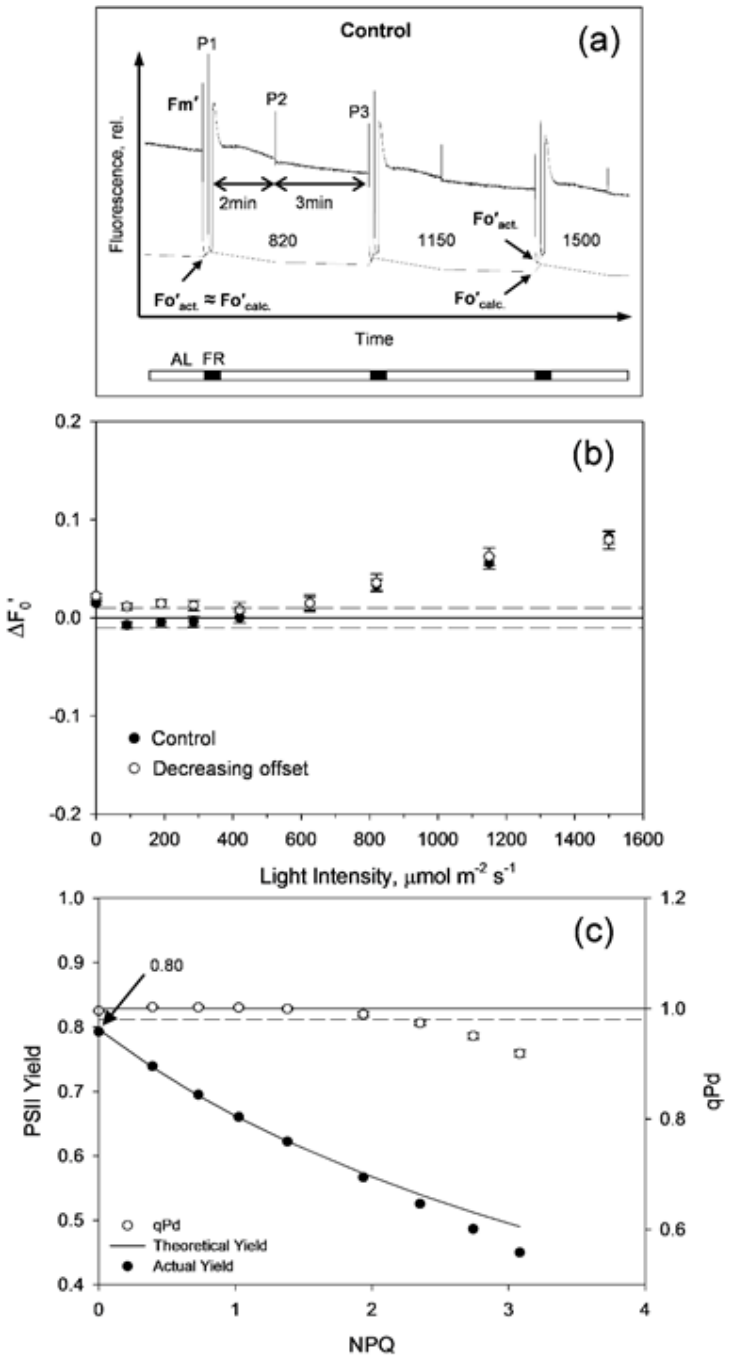

Figure 3.08A A representative chlorophyll fluorescence trace exert (from Fig. 3.07) for 820-1500 µmol m^{-2} s^{-1} actinic light (AL) intensities under control conditions (see Materials and Methods for a complete scheme description). B At lower AL, $Fo'_{act.}$ and $Fo'_{calc.}$ values are similar, but at intensities $Fo'_{calc.}$ becomes lower. b Average ΔFo' [($Fo'_{act.}$- $Fo'_{calc.}$)/ $Fo'_{act.}$] values calculated from 21 repeats of the gradually increasing AL scheme of induction. C Relationship between NPQ and qP_d (open circles) and NPQ and actual PSII yield (closed circles) ascertained using the Fv/Fm value indicated, at the light intensities presented in B. Averages were calculated from 21 repeats with error bars representing SEM. The theoretical PSII yield (continuous line) was calculated using Equation 1.16 (Giovagnetti *et al.*, 2015).

In order to try and measure, and then correct for the fluorescence contribution of PSI, the percentage contribution suggested by Pfündel and co-workers was employed (Pfündel et al., 2013). A constant 24% decrease in Fo was therefore used to correct for PSI fluorescence. Before the start of the pNPQ assessment procedure, the fluorescence offset was manually changed, in the Walz JUNIOR-PAM software, to reduce fluorescence by 24%. This resulted in some immediate changes in NPQ, ΦPSII and qP_d behaviour. A 24% of Fo decrease in fluorescence roughly equates to a 4.8% decrease in fluorescence at Fm. As NPQ is calculated as a change in Fm' compared to Fm, this means that NPQ is effectively a much greater quencher of PSII fluorescence. The average NPQ value at the end of the offset pNPQ assessment procedure significantly increased to 3.9 (Fig 3.09C) compared to the 3.1 in the control (z-test; $P < 0.05$). The parameters dependent on Fo showed even greater changes. $Fo'_{calc.}$ became instantly higher than $Fo'_{act.}$ throughout the measurement (Fig 3.09A, 3.09B). This negative ΔFo' resulted in a qP_d rise above 1.00 over the course of the procedure (Fig 3.09C), resulting in a significant change in qP_d (*t*-test, $P < 0.01$) and effectively rendering the measurement of photoinhibition redundant. As qP_d values did not decline below 1.00 in the majority of the leaves tested, the phototolerance light curves could not be calculated (Fig 3.12) compared to the control experiments results (Fig 3.11). According to the results obtained with the constant PSI offset, 800 µmol m^{-2} s^{-1} would be required to cause photodamage in 10% of leaves, and 1500 µmol m^{-2} s^{-1} would not damage more than 15% of leaves. Furthermore, as the actual ΦPSII depends on qP_d, this measurement was also affected, and $ΦPSII_{act.}$ was greater than $ΦPSII_{theor.}$, which is not possible as more than 100% of RCII cannot be open. This is because the constant offset causing a rise in $Fo'_{act.}$ above $Fo'_{calc.}$, which masks the subtle changes in $Fo'_{act.}$ values and nullifies the qP_d measurements (Fig 3.09B). However, Fv/Fm values were similar to those achieved by the Pfündel team (Pfündel et al., 2013), and significantly increased the PSII quantum yield compared to the control measurements (*t*-test, $P < 0.001$). The average Fv/Fm using this offset was 0.83, reflecting a ~4% increase compared to the 0.8 Fv/Fm in control measurements.

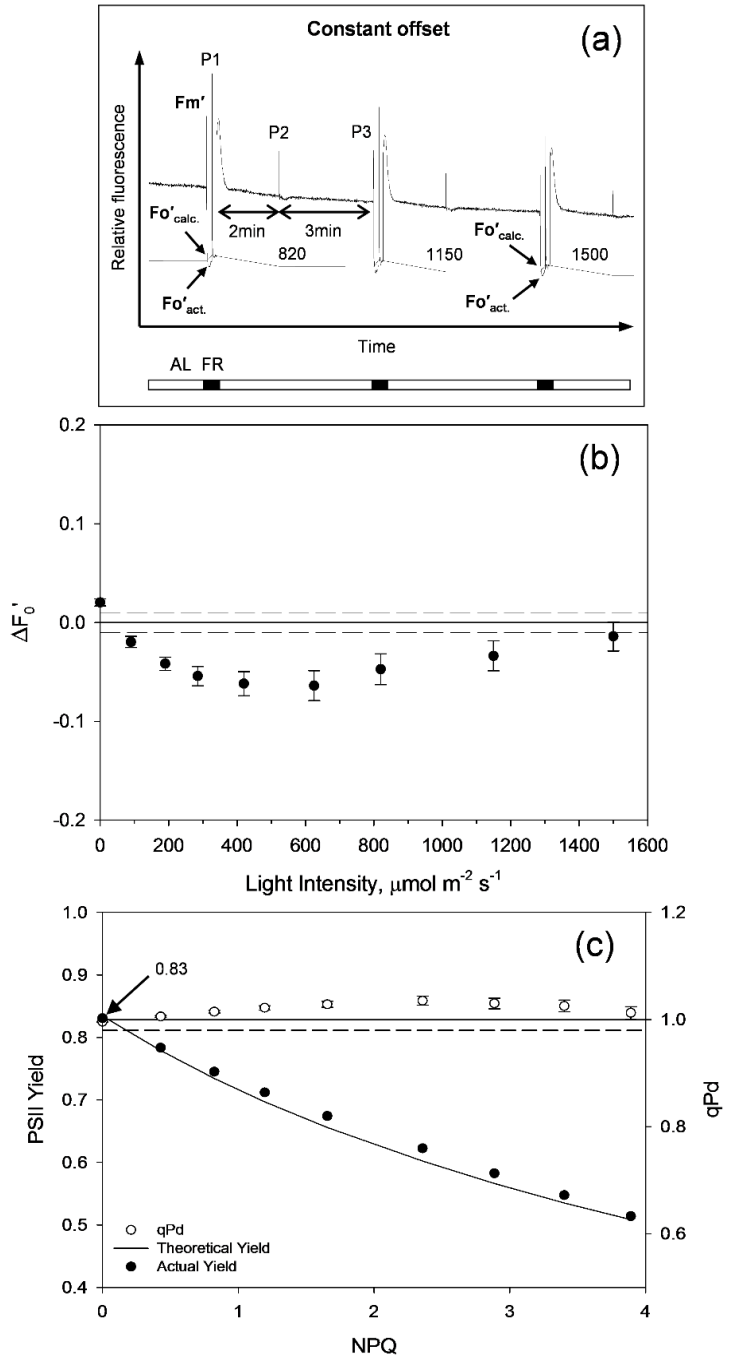

Figure 3.09 A representative chlorophyll fluorescence trace exert (from Fig. 3.07) for 820-1500 µmol m^{-2} s^{-1} actinic light (AL) intensities conducted with a constant 24% fluorescence offset at Fo level (see Materials and Methods for a complete scheme description). At lower AL, $Fo'_{act.}$ and $Fo'_{calc.}$ values are similar, but at intensities $Fo'_{calc.}$ becomes lower. B Average ΔFo' [($Fo'_{act.}$- $Fo'_{calc.}$)/ $Fo'_{act.}$] values calculated from 21 repeats of the gradually increasing AL scheme of induction. C Relationship between NPQ and qP_d (open circles) and NPQ and actual PSII yield (closed circles) ascertained using the Fv/Fm value indicated at the light intensities presented in B. Averages were calculated from 21 repeats with error bars representing SEM. The theoretical PSII yield (continuous line) was calculated using Equation 1.16 (Giovagnetti *et al.*, 2015).

As the constant PSI fluorescence contribution offset invalidated the $Fo'_{calc.}$, qP_d and ΦPSII, an assessment of literature pertaining to PSI fluorescence was performed, and a new PSI offset calculated. A 20% PSI fluorescence contribution was calculated at Fo, with 4% at Fm. These were calculated from:

$$\mathrm{PSI_{(Fo)}}\ (\%) = \frac{0.1\ \mathrm{ns}(\tau_{\mathrm{Av\ PSI}}) \times 0.445_{(\mathrm{PSI})}}{0.4\ \mathrm{ns}(\tau_{\mathrm{Av\ PSII}}) \times 0.555_{(\mathrm{PSII})}} \times 100 \qquad \text{(Equation 3.03)}$$

$$\mathrm{PSI_{(Fm)}}\ (\%) = \frac{0.1\ \mathrm{ns}(\tau_{\mathrm{Av\ PSI}}) \times 0.445_{(\mathrm{PSI})}}{2\ \mathrm{ns}(\tau_{\mathrm{Av\ PSII}}) \times 0.555_{(\mathrm{PSII})}} \times 100 \qquad \text{(Equation 3.04)}$$

In these two equations, τ_{Av} represents the excited state lifetimes of open PSI, PSII and the closed RC of PSI and PSII. In the Fo state, RCI and RCII are open. PSII lifetimes in the Fo state have been calculated as 0.4 ns, but in the Fm and thus closed state the lifetime of PSII increases fivefold to 2 ns (Engelmann *et al.,* 2005; Johnson and Ruban 2009; Belgio *et al.,* 2012; Caffarri *et al.,* 2014). Conversely, PSI fluorescence in the Fo and Fm states measured by picosecond time-resolved fluorescence remains constant at 100 ps or 0.1 ns (Wagner *et al.,* 1996; Richter *et al.,* 1999; Moise and Moya 2004; Engelmann *et al.,* 2005; Johnson and Ruban 2009). Factoring in the PSI:PSII ratio of 0.8 for plants grown under ~200 µmol m^{-2} s^{-1} (Ware *et al.*, 2015; Wientjes *et al.*, 2013), this results in 4 and 20% PSI fluorescence contributions at Fm and Fo. It is worth noting that this is solely in the Fo and Fm state, and not in the Fm' or Fo' states. Contrary to the work of Pfündel *et al.,* (2013), there is ample literature which supports the notion of NPQ acting on PSI (Ruban *et al.,* 1991; Richter *et al.,* 1999; Holzwarth *et al.,* 2009; Miloslavina *et al.,* 2011; Ballottari *et al.,* 2014). The work of Alfred Holzwarth's group have suggested that increasing NPQ levels correspond to increased PSI quenching, and that lifetimes can be reduced by 50 ps (Richter *et al.,* 1999; Holzwarth *et al.,* 2009; Miloslavina *et al.,* 2011). The Horton lab also demonstrated the quenching of PSI fluorescence in 77K fluorescence experiments on thylakoids, suggesting that PSI can be quenched by up to 50% of the value of PSII quenching (Ruban *et al.*, 1991). It was therefore decided from the literature review that the 20% contribution of PSI to PSII fluorescence at Fo should be progressively decreased depending on the NPQ formed at each light intensity.

A decrease in PSI fluorescence of 0.4 the quantum coefficient of NPQ (qN) was chosen as this fitted well with the 30-50% quenching capacity of PSI fluorescence observed independently by the Horton and Holzwarth labs (Ruban *et al.,* 1991; Trissl *et al.,* 1993; Holzwarth *et al.,* 2009; Miloslavina *et al.,* 2011). The PSI fluorescence contribution was performed in real time during the pNPQ assessment procedure, by altering offset after each light intensity during the pNPQ assessment procedure in the Walz software. As the offset was only marginally reduced in the Fo and Fm state, the Fv/Fm values were still on average 0.83 (Fig 3.10C), and not statistically different from the 24% offset values, but significantly greater than the control average (*t*-test, $P < 0.001$). The only other parameter that showed a difference to the control conditions was the average NPQ at the procedure end. This was 3.5, however the increase was not significantly different to the control or constant offset (*t*-test, $P > 0.05$). Importantly, from the perspective of accurately quantifying photoinhibition and pNPQ, the $Fo'_{act.}$ and $Fo'_{calc.}$ parameters matched at low light intensities, before a positive ΔFo at higher light intensities (Fig 3.10B). This means that qP_d did not rise above 1.00 during the procedure, and declined below 0.98 at high light intensities, thus effectively measuring the first signs of photoinhibition. Furthermore, the qP_d values were not significantly different to those measured during the control experiments (*t*-test, $P < 0.05$). This was reflected in the two ΦPSII being closely matched at low light intensities, with the actual ΦPSII deviating from the ΦPSII calculated when RCII became damaged (Fig 3.10C). The function of the light tolerance curves, which are calculated by plotting the percentage of leaves which show the first signs of photoinhibition ($qP_d < 0.98$) at each light intensity, was also restored by the regained ability to use qP_d as an effective marker to measure photoinhibition (Fig 3.11). The constant PSI contribution had removed this function of the pNPQ assessment procedure (Fig 3.12). But, by decreasing the PSI contribution offset, the light intensity required to close RCII in 50% of leaves was calculated as being increased by ~125 µmol m^{-2} s^{-1} to 850 µmol m^{-2} s^{-1}. Although this was an increase, it was not significant (z-test, $P > 0.1$). This is due in part to the same light intensities being tolerated by 100% of leaves (285 µmol m^{-2} s^{-1}) and the same light intensity being required to damage 100% of leaves (1500 µmol m^{-2} s^{-1}).

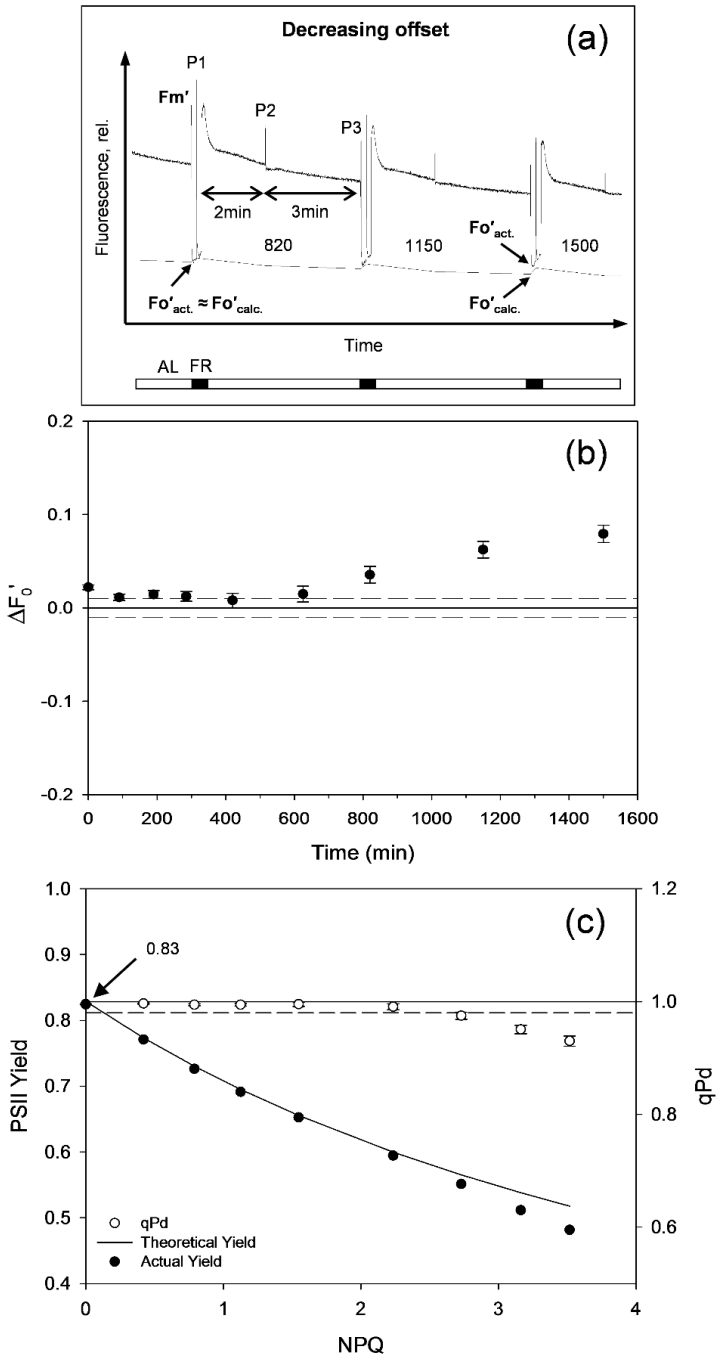

Figure 3.10 A representative chlorophyll fluorescence trace exert (from Fig. 3.07) for 820-1500 µmol m^{-2} s^{-1} actinic light (AL) intensities conducted with a 20% fluorescence offset at Fo, subsequently quenched by 0.40 of qN (see Materials and Methods for a complete scheme description). At lower AL, $Fo'_{act.}$ and $Fo'_{calc.}$ values are similar, but at intensities $Fo'_{calc.}$ becomes lower. b Average ΔFo' [($Fo'_{act.}$- $Fo'_{calc.}$)/ $Fo'_{act.}$] values calculated from 21 repeats of the gradually increasing AL scheme of induction. c Relationship between NPQ and qP_d (open circles) and NPQ and actual PSII yield (closed circles) ascertained using the Fv/Fm value indicated. Averages were calculated from 21 repeats with error bars representing SEM. The theoretical PSII yield (continuous line) was calculated using Equation 1.16 (Giovagnetti *et al.*, 2015).

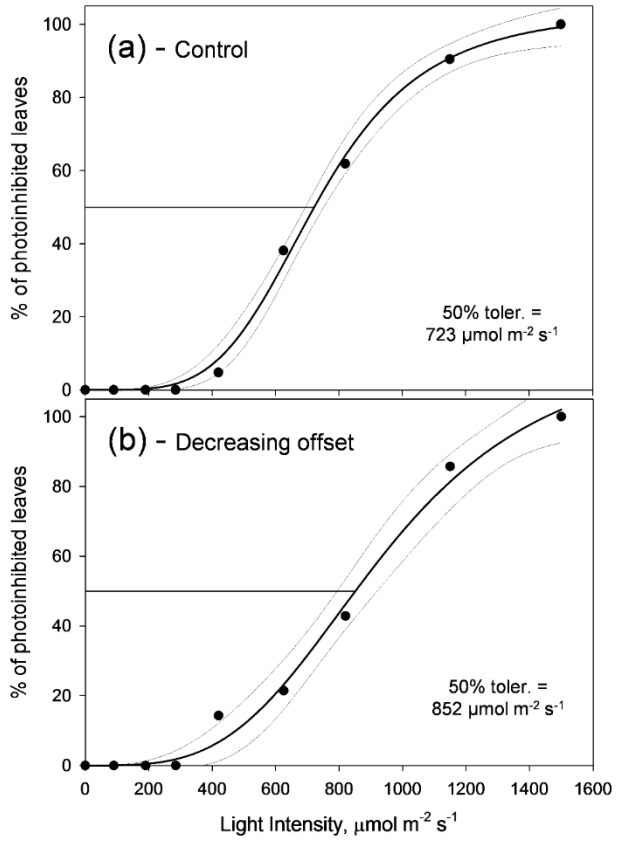

Figure 3.11 Relationship between photoinhibited leaves and corresponding light intensity for a 21 control and b 14 decreasing offset 2 (20% PSI fluorescence contribution – 0.4 qN) experiments. Leaves were considered photoinhibited when qP_d < 0.98. Light tolerance curves were plotted using SigmaPlot12.5 software (Systat Software, Inc., Chicago, USA; Sigmoidal Hill 3 Parameter, f = a*x^b/(c^b+x^b)) with 95% confidence intervals (Giovagnetti *et al.*, 2015).

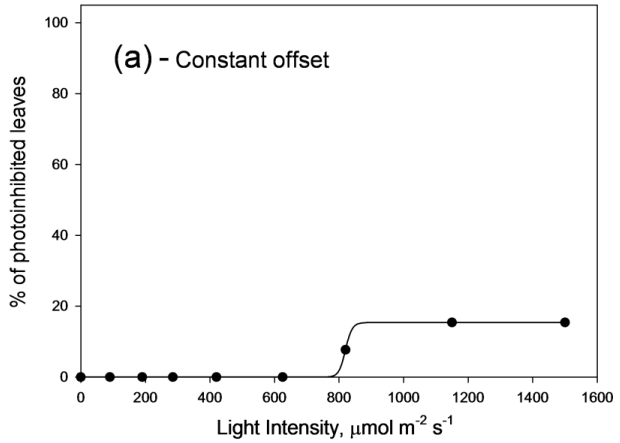

Figure 3.12 Relationship between photoinhibited leaves and corresponding light intensity for constant 24% fluorescence offset experiments. Leaves were considered photoinhibited when qP_d < 0.98. Light tolerance curves were plotted using SigmaPlot12.5 software (Systat Software, Inc., Chicago, USA; Sigmoidal Hill 3 Parameter, f = a*x^b/(c^b+x^b)) with 95% confidence intervals (Giovagnetti *et al.*, 2015).

3.3 Discussion

- Plant growth conditions were optimised to ensure that plants had average Fv/Fm values above 0.80.
- A reliable and reproducible chlorophyll *a* fluorescence procedure was established to assess pNPQ, NPQ, qP_d and ΦPSII.
- PSI fluorescence contributions during fluorescence measurements should be considered as this yields more precise material on the ΦPSII.
- The model of a constant 24% contribution of PSI fluorescence to the Fo level, as proposed by Pfündel *et al.*, (2013), was found to invalidate qP_d measurements and light tolerance curves, as well as significantly increasing NPQ and Fv/Fm values.
- A decreasing 20% contribution of PSI fluorescence to the Fo level by 0.4 qN, was found to be the optimum correction for PSI fluorescence contributions, as well as ensuring increased Fv/Fm values, qP_d values that did not rise above 1.00 and allowing light tolerance curves to be constructed.

Chapter IV – The Capacity for High Phototolerance is Dependent on Leaf Age

4.1 Introduction

The effects of varying abiotic conditions on plant health was documented in Chapter 3. After improving the average Fv/Fm values of plants, it became apparent that there is heterogeneity in these values throughout the rosette. Fv/Fm appeared to depend on plant age, particularly in the very young and senescing plants. Indeed, that is why a 40-60 day after sowing selection criterion was used when selecting plants to test. It was also observed that younger and older plants suffered declines in qP_d earlier than healthy adult plants. Indeed, these observations have been previously reported by Krause *et al.*, (1995) and Manetas *et al.*, (2002) who independently observed increased photoinhibition of juvenile and mature plants, compared to adult plants. Vegetative and reproductive growth phases are known to vary depending on plant age and environmental stimuli (Schurr *et al.*, 2006). Perhaps, the greatest changes are those in the width, depth and weight of leaves during the four different phases of ontogenesis: juvenile, adult, reproductive and senescent (Hopkinson, 1964; Milthorpe, 1959; Avery, 1933). The juvenile phase consists of radicle, hypocotyl and cotyledon appearance; the leaves undergo vegetative growth becoming rounded and trichomes emerging on the adaxial side (Kerstetter and Poethig 1998; Boyes *et al.*, 2001; Tsukaya, 2013). In the next phase, rosettes develop with leaves increasing in size and number, and trichomes also emerging on the abaxial side (Kerstetter and Poethig 1998; Boyes *et al.*, 2001; Tsukaya, 2013). The reproductive phase starts with inflorescence, and occurs until the senescent phase sets in, defined by necrosis and abscission (Noodén, 1988; Matile *et al.*, 1992; Woo *et al.*, 2001; Amasino, 2010). Previous experiments that have measured the susceptibility of photodamage in relation to the stage of ontogenesis, have used Fv/Fm, D1 degradation and changes in CO_2 rates (Oquist *et al.*, 1982; Siffel *et al.*, 1993; Barker *et al.*, 1997; Thiele *et al.*, 1997; la Porta *et al.*, 2006; Radochová and Tichá, 2008; Liu *et al.*, 2009; Nath *et al.* 2013), have certain limitations as previously mentioned. Using qP_d as an assessment of photoinhibition can overcome this, therefore it was used to test for an ontogenesis-photoinhibition correlation. qP_d as a marker of photoinhibition was also validated against peroxidase and hydrogen peroxide accumulation in leaves from the four different phases of ontogenesis.

The life cycle of higher plants can be divided into four phases: juvenile, adult, reproductive and senescent (Fig 4.01). Previous techniques (Fv/Fm, D1 protein degradation, oxygen evolution) used to measure photosynthetic changes in plants during their life cycle are discussed throughout this thesis and their accuracy or efficiency debated. It was therefore decided that the true changes in phototolerance and pNPQ capacity should be quantified during ontogenesis. An assessment of the reactive oxygen species (ROS) would also be performed to corroborate or discredit the measurements performed. Plants of different ages were used, but also plants of the same age with the leaves from the three different rosette structures measured (inner, intermediate and outer).

4.2 Results

Plants from 1-13 weeks old has the pNPQ assessment procedure applied (Fig 4.01, Materials and Methods). 30 tests were used for each age group. Plants aged 1-2 weeks are classed as juvenile, 3-6 weeks as adult, 7-8 weeks as reproductive and 9-13 as senescent. The first plants to be exposed to the pNPQ assessment procedure (as depicted in Fig 2.02) were the one then two-week-old plants. Fig 4.02A shows that one week old plants are only able to form a pNPQ capacity of ~0.5. This caused $\Phi PSII_{theor.}$ and $\Phi PSII_{act.}$ to deviate almost instantly. From Fig 4.02C it can be seen from the proportion of closed circles, that very few leaves showed no signs of photoinhibition during the course of the increasing light routine. In fact, the most common symbol was the open rhomboid indicative of qP_d values < 0.9. Using the qP_d values of each leaf obtained against each light intensity, Fig 4.02E shows that the light intensity that inhibits 50% of one week old leaves is 73 µmol photons m^{-2} s^{-1}. Two-week-old plants however have a significant improvement in ΦPSII and phototolerance compared to one week old plants (Fig 4.02B, 4.02D). NPQ was protective until ~1.5, meaning that $\Phi PSII_{theor.}$ and $\Phi PSII_{act.}$ are much more closely matched at higher light intensities. This increased pNPQ capacity is significantly higher than one week old plants (Tukey's test; $P < 0.05$). This manifested in a seven-fold increased light intensity required to cause photodamage to 50% of the leaves (Fig 4.02F), which is significantly higher (z-test; $P < 0.05$).

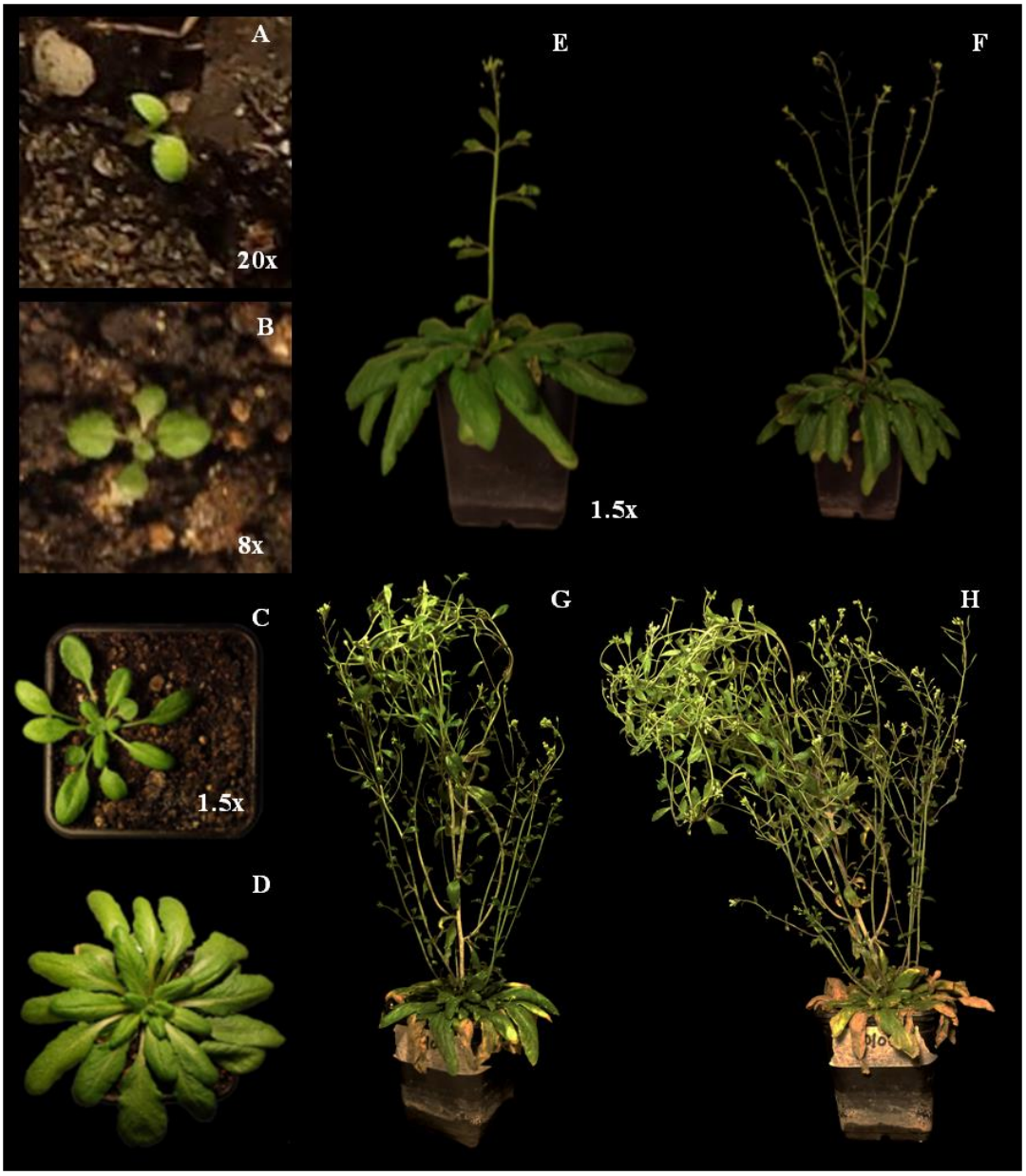

Figure 4.01 Visual aspect of *Arabidopsis thaliana* plants aged (A) 1, (B) 2, (C) 4, (D) 6, (E) 7, (F) 8 (G) 11 and (H) 13 weeks (Carvalho *et al.*, 2015). This displays the size and qualities of the plants used at the different stages of ontogenesis during the *Arabidopsis* plants life cycle.

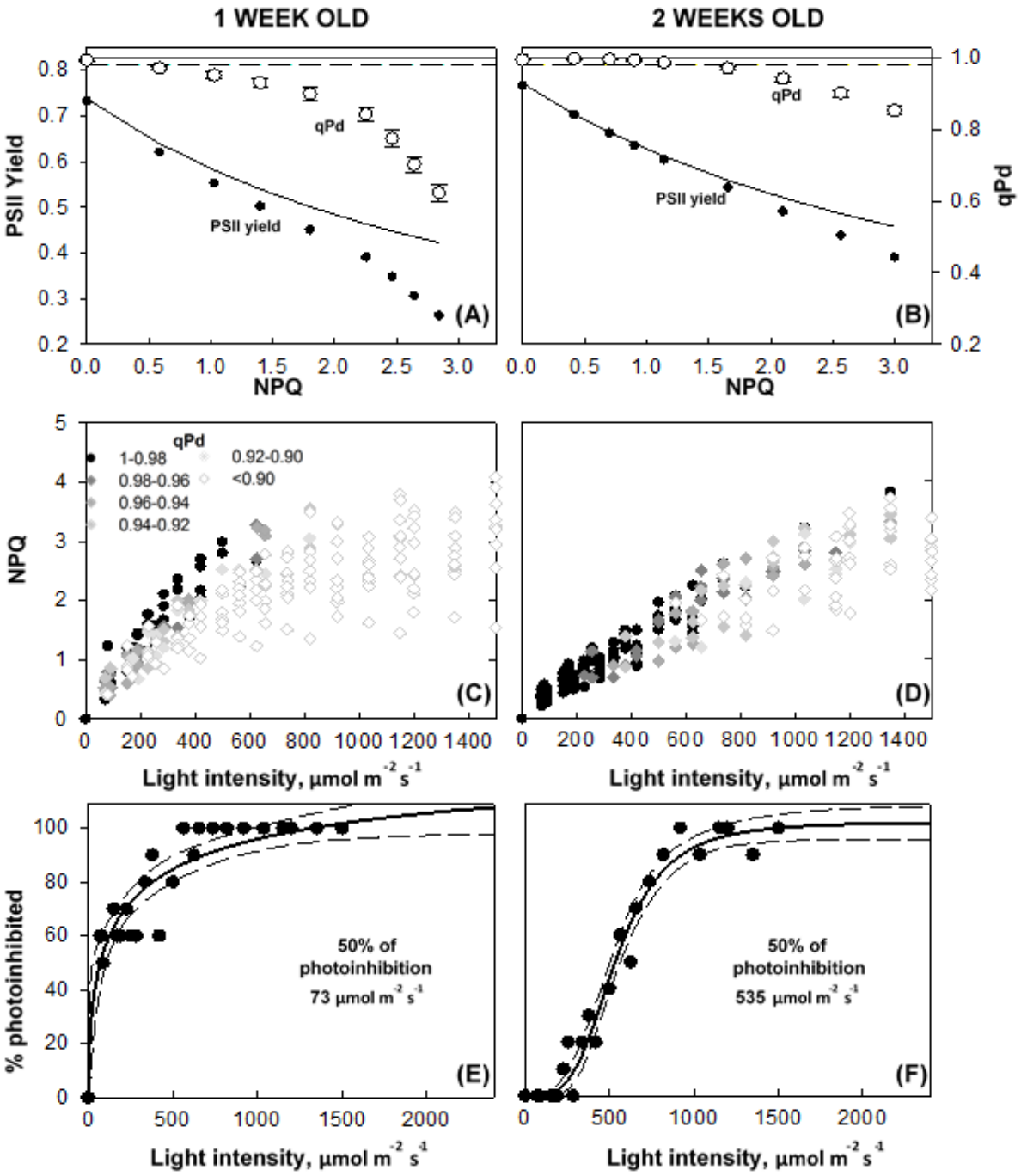

Figure 4.02 (A, B) Relationship between PSII yield, NPQ and qP_d parameters; (C, D) relationship between NPQ, light intensity and qP_d parameters and (E, F) percentage of photoinhibited leaves of 1 (A, C, E) and 2 (B, D, F) week old *Arabidopsis thaliana* plants. Error bars show the SEM (n=30). The theoretical yield (continuous line) was calculated using qP_d always equal to 1.00 (Carvalho *et al.*, 2015).

The adult phase of the plants lives was also marked by further significant increases in ΦPSII, pNPQ and phototolerance (Fig 4.03A, Fig 4.03B, Fig 4.04A, Fig 4.04B). 3-6-week-old plants had an average pNPQ capacity of ~1.9, 2.1, 2.2 and 2.4 respectively. $\Phi PSII_{act.}$ is ~0.45 in the three and four-week-old plants, and increases to ~0.5 in the five and six week olds. Individual pNPQ and NPQ plots against light intensities also shows that the leaf populations were increasingly protected at the higher light intensities (Fig 4.03C, Fig 4.03D, Fig 4.04C, Fig 4.04D). The proportion of filled circles increases at higher light intensities, and the amount of white rhomboids decreasing almost to the point of there being none at 1500 µmol photons m^{-2} s^{-1}. The actinic light intensity required to cause photodamage in 50% of leaves increases from 760 in the three and four-week-old plants to 1008 and 960 in the five and six-week-old plants (Fig 4.03E, Fig 4.03F, Fig 4.04E, Fig 4.05F).

The reproductive phase of the life cycle showed increased qP_d values at the procedure end, and higher pNPQ capacities (Fig 4.05A, Fig 4.05B). The seven-week-old plants had an average pNPQ of 2.5, with eight week olds even greater at 2.8. These values are significantly higher than the juvenile pNPQ averages (Tukey's test, $P < 0.05$). The average qP_d barely dropped below 0.98 for both types of plants, which was reflected in $\Phi PSII_{act.}$ matching $\Phi PSII_{theor.}$ until almost the very highest light conditions. Individual leaves showed a consistent pNPQ and NPQ forming capacity (Fig 4.05C, Fig 4.05D). The seven and eight-week-old plants didn't have any leaves with greater than 10% closed RCII for the first time in the plants life cycle. The result of this was the highest light intensity required to induce photodamage in 50% of the leaves, with 1,135 and 1,385 µmol photons m^{-2} s^{-1} required respectively (Fig 4.05E, Fig 4.05F). These light intensities were the highest recorded in the study, with the following senescence phase associated with a decline in photoprotection.

From nine weeks onwards, there was a decrease in the photoprotective capacities of the senescing plants. The average pNPQ value had an overall decrease from 1.9 to 2.2, 2.0, 1.6, and 1.2 in the nine to 13-week-old plants (Fig 4.06A, Fig 4.06B, Fig 4.07A, Fig 4.07B, Fig 4.08A). Although there was a slight increase in pNPQ during this time, $\Phi PSII_{act.}$ successively decreased from ~0.47 in the nine week olds to 0.35 in those aged 13 weeks (Fig 4.06A-B, Fig 4.07A-B, Fig 4.08A). There was also an

increase in the total degree of photoinhibition, displayed as grey and open rhomboids, throughout the pNPQ procedure as the plants aged, with fewer plants without photoinhibition (closed circles) at the higher light intensities. The reduced pNPQ capacities showed in the decreasing light intensities that closed 50% of RCII. Nine week olds tolerated 940 µmol photons m^{-2} s^{-1}, with 10-13 week olds becoming damaged at 1058, 682, 403, 332 µmol photons m^{-2} s^{-1} (Fig 4.06E, Fig 4.06F, Fig 4.07E, Fig 4.07F, Fig 4.08C).

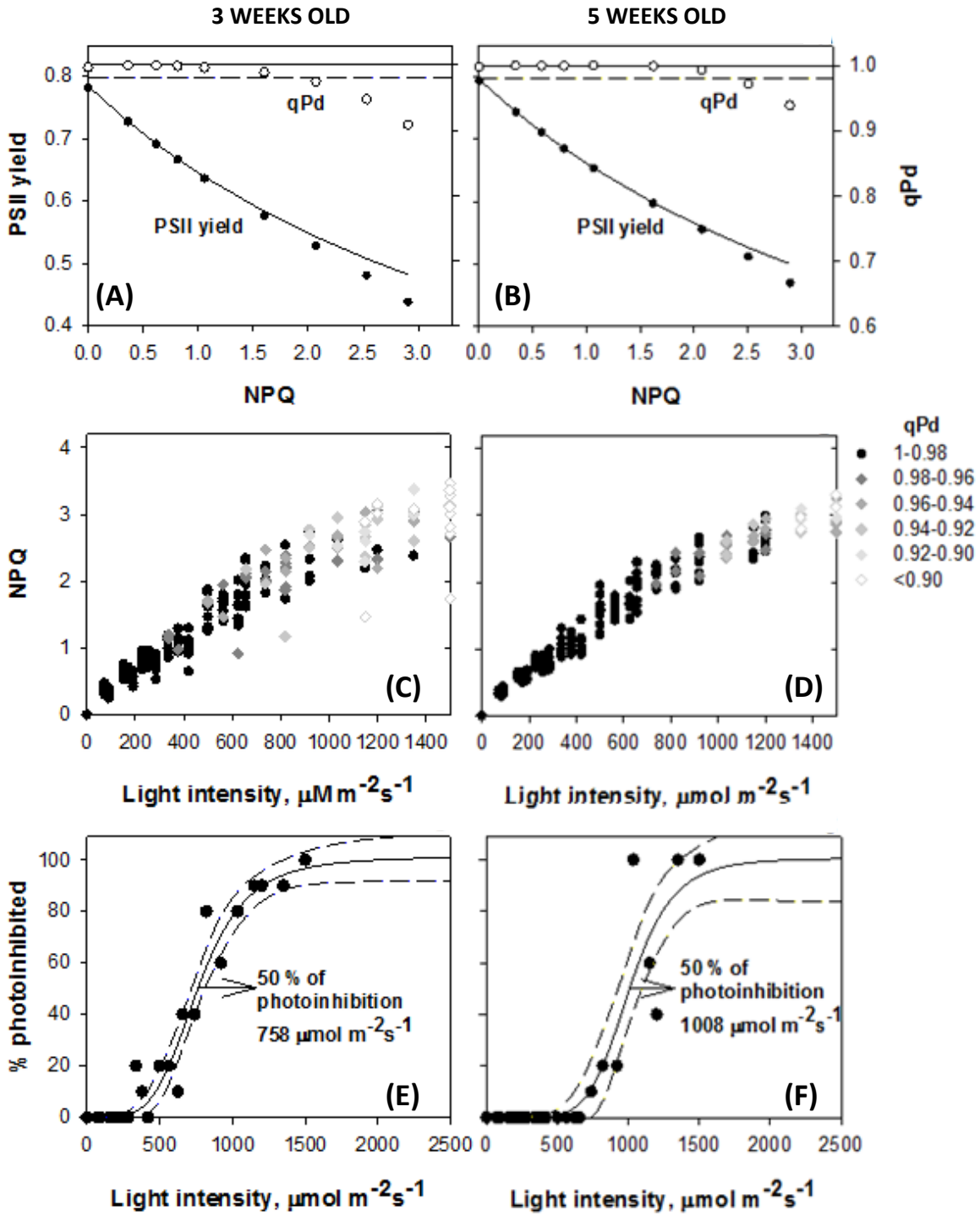

Figure 4.03 (A, B) Relationship between PSII yield, NPQ and qP_d parameters; (C, D) relationship between NPQ, light intensity and qP_d parameters and (E, F) percentage of photoinhibited leaves of 3 (A, C, E) and 5 (B, D, F) week old *Arabidopsis thaliana* plants. Error bars show the SEM (n=30). The theoretical yield (continuous line) was calculated using qP_d always equal to 1.00 (Carvalho *et al.*, 2015).

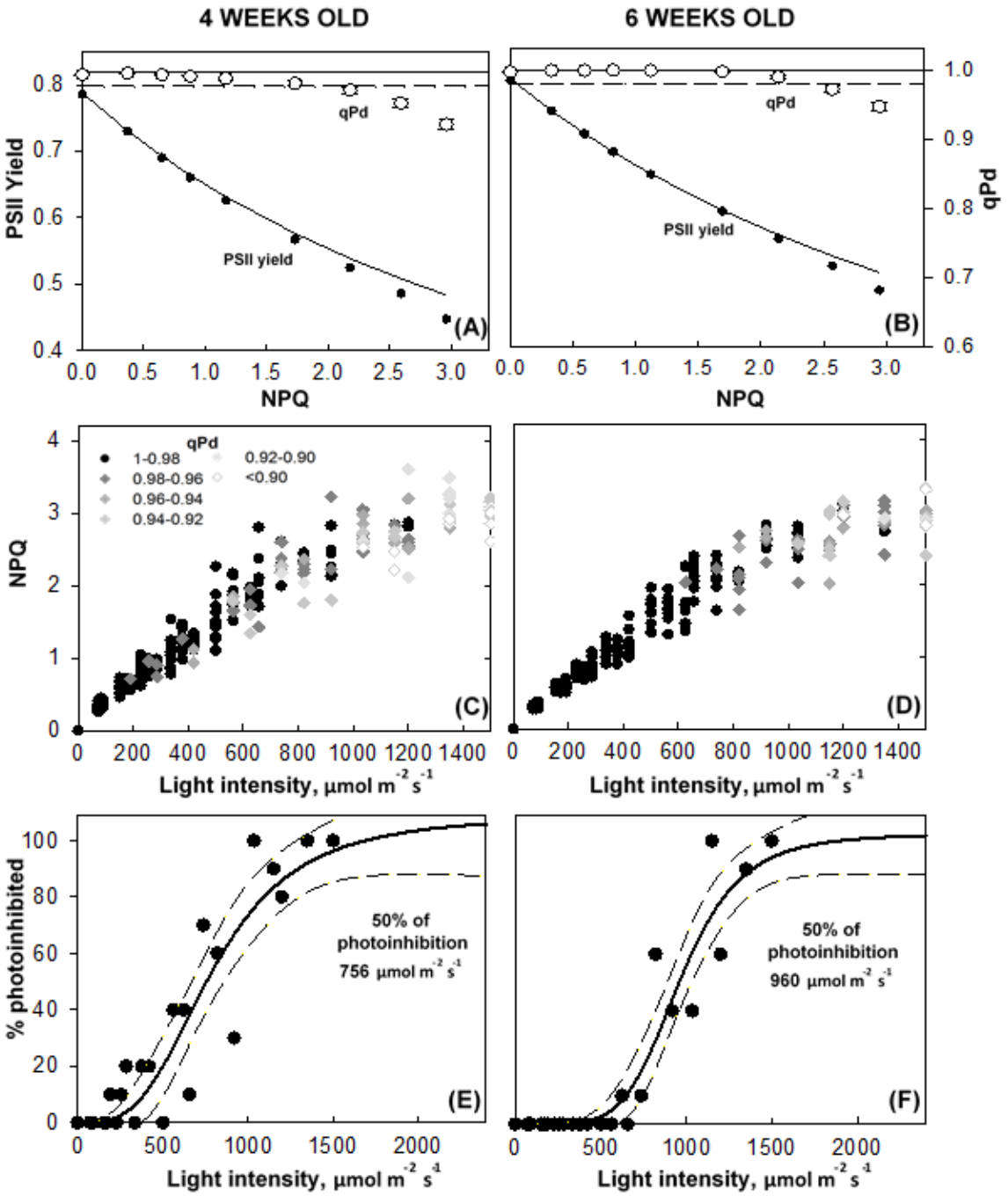

Figure 4.04 (A,B) Relationship between PSII yield, NPQ and qP_d parameters; (C,D) relationship between NPQ, light intensity and qP_d parameters and (E,F) percentage of photoinhibited leaves of 4 (A,C,E) and 6 (B,D,F) week old *Arabidopsis thaliana* plants. Error bars show the SEM (n=30). The theoretical yield (continuous line) was calculated using qP_d always equal to 1.00 (Carvalho *et al.*, 2015).

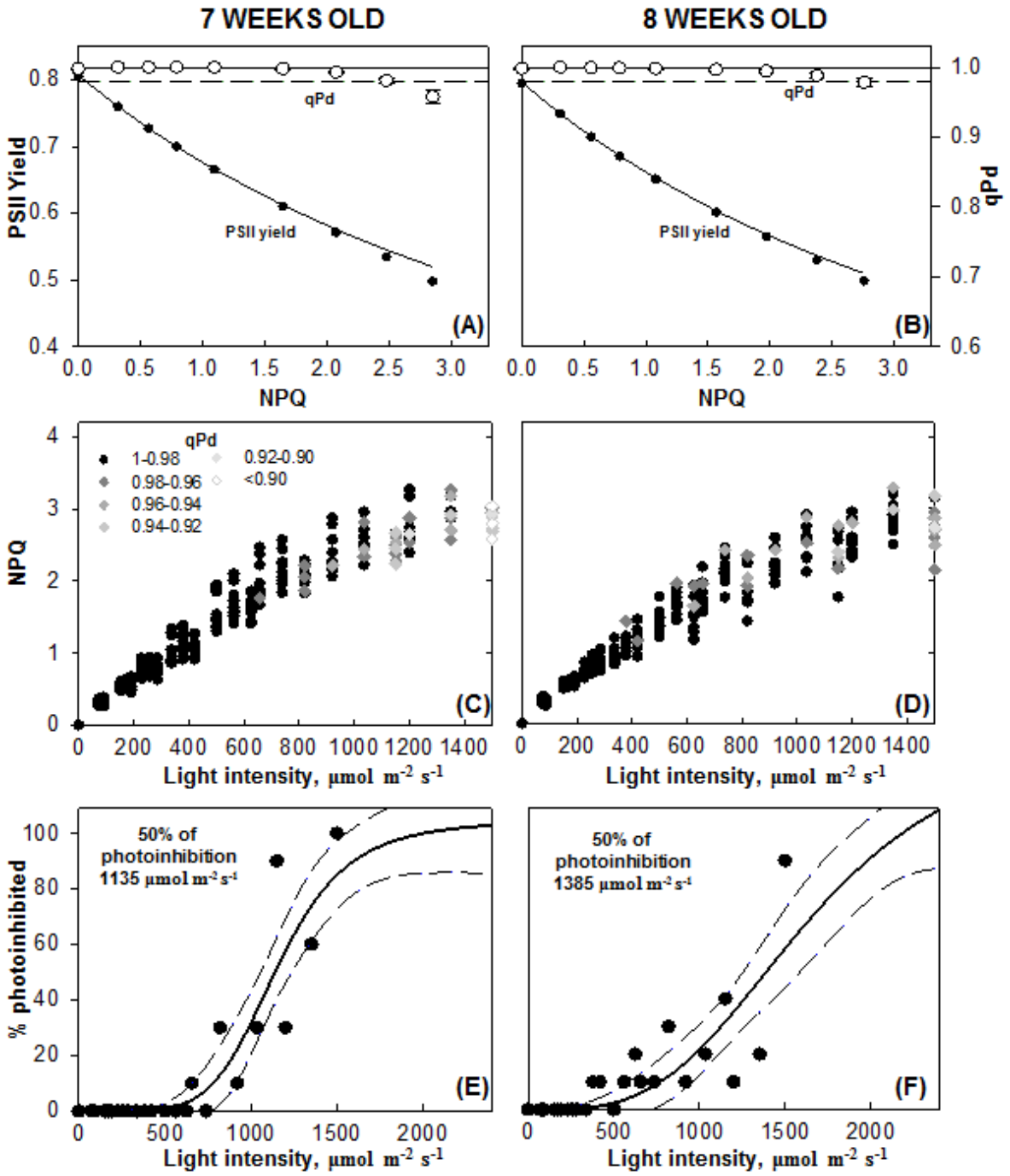

Figure 4.05 (A,B) Relationship between PSII yield, NPQ and qP_d parameters; (C,D) relationship between NPQ, light intensity and qP_d parameters and (E,F) percentage of photoinhibited leaves of 7 (A,C,E) and 8 (B,D,F) week old *Arabidopsis thaliana* plants. Error bars show the SEM (n=30). The theoretical yield (continuous line) was calculated using qP_d always equal to 1.00 (Carvalho *et al.*, 2015).

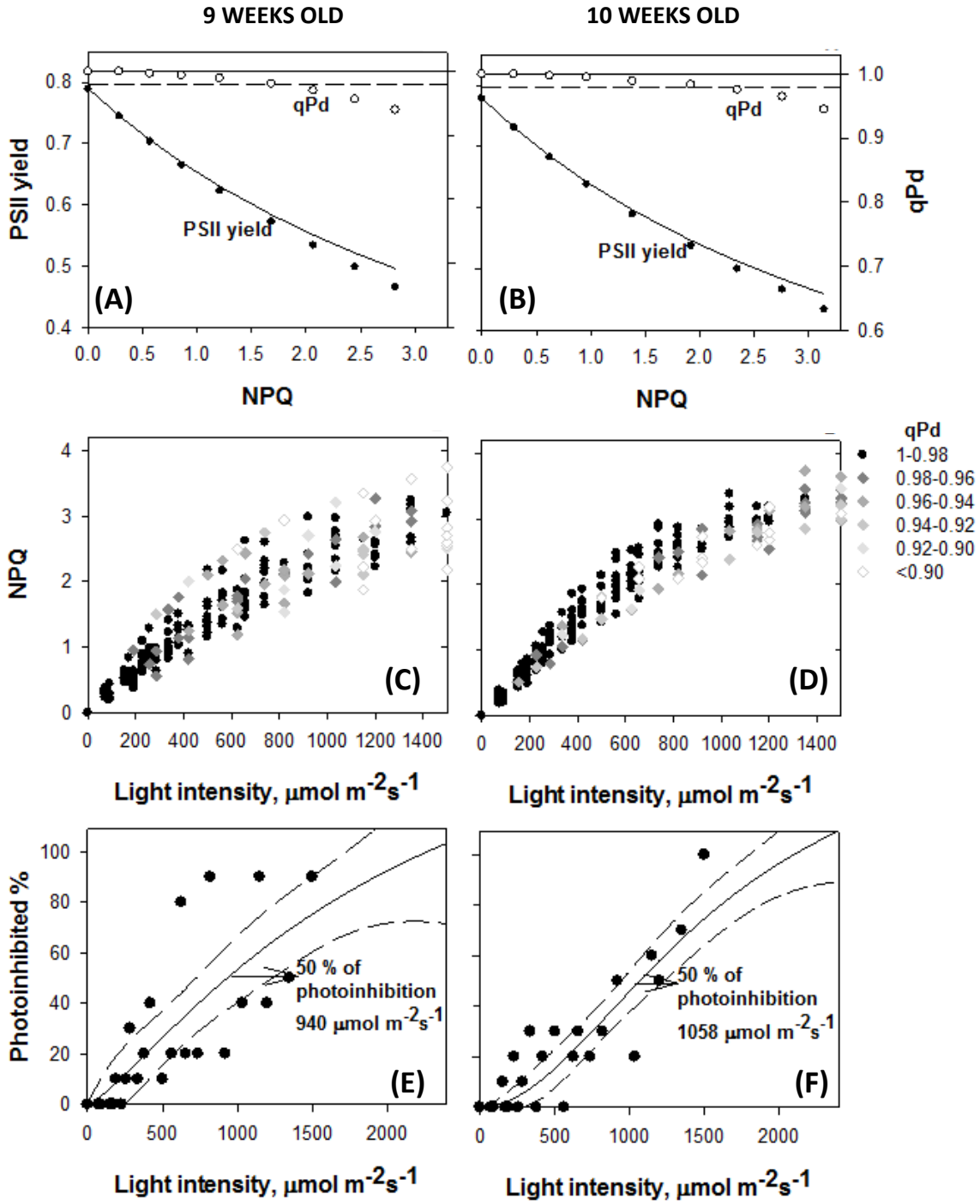

Figure 4.06 (A,B) Relationship between PSII yield, NPQ and qP_d parameters; (C,D) relationship between NPQ, light intensity and qP_d parameters and (E,F) percentage of photoinhibited leaves of 9 (A,C,E) and 10 (B,D,F) week old *Arabidopsis thaliana* plants. Error bars show the SEM (n=30). The theoretical yield (continuous line) was calculated using qP_d always equal to 1.00 (Carvalho *et al.*, 2015).

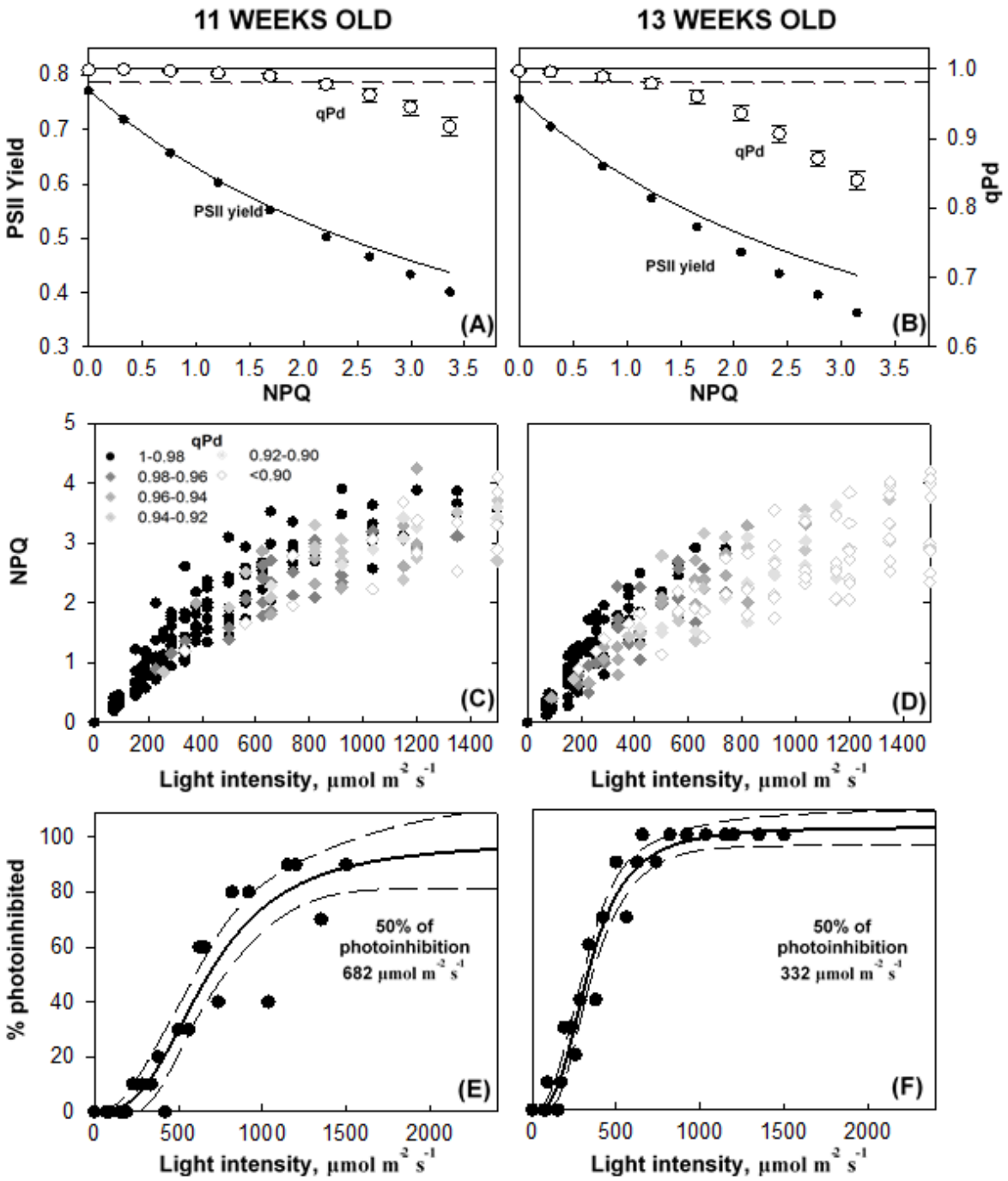

Figure 4.07 (A,B) Relationship between PSII yield, NPQ and qP_d parameters; (C,D) relationship between NPQ, light intensity and qP_d parameters and (E,F) percentage of photoinhibited leaves of 11 (A,C,E) and 13 (B,D,F) week old *Arabidopsis thaliana* plants. Error bars show the SEM (n=30). The theoretical yield (continuous line) was calculated using qP_d always equal to 1.00 (Carvalho *et al.*, 2015).

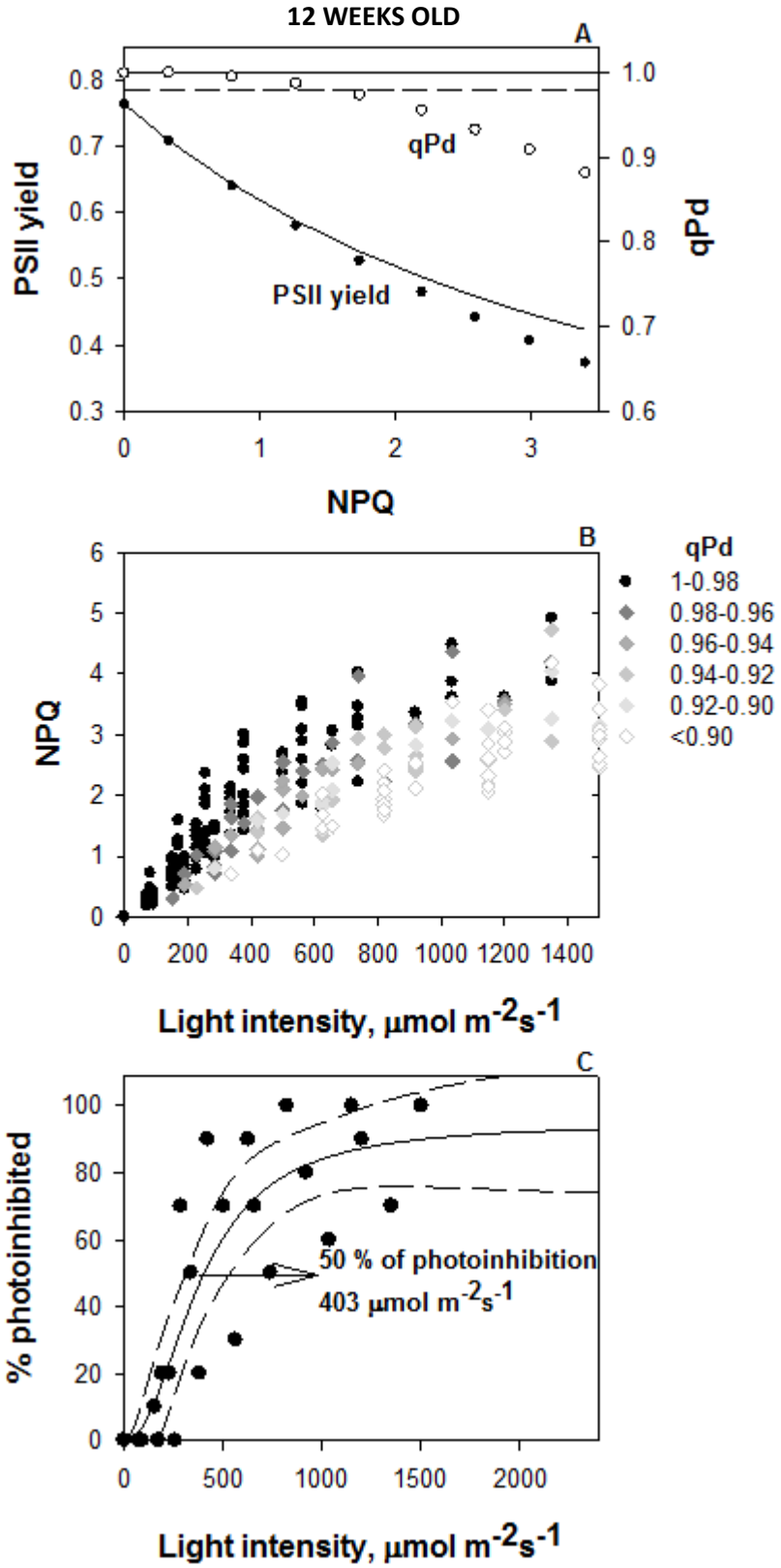

Figure 4.08 (A) Relationship between PSII yield, NPQ and qP_d parameters; (B) relationship between NPQ, light intensity and qP_d parameters and (C) percentage of photoinhibited leaves of 12 weeks old *Arabidopsis thaliana* plants (Carvalho *et al.*, 2015).

To better visualise the increase, plateau and decrease in photoprotective capacities of *Arabidopsis* plants, the data obtained during the pNPQ assessment procedures was presented in a number of different ways (Figs 4.09A-C). Firstly, the light intensity at which 50% of RCII were closed was plotted against the plants age. An almost symmetrical peak and trough curve was the result, showing a rise until almost eight weeks old, followed by a decline in high light tolerance. The letters illustrate significant differences between tolerated light intensities. This curve is matched extremely well by the highest NPQ value of each plant age that protected 100% of RCII. Here, these are significant increases in the maximum pNPQ capacities from the juvenile to adult and adult to reproductive phases, followed by a significant decrease from the reproductive to senescent phases (Tukey's test, $P < 0.05$). This overlap, coupled with the average pNPQ capacities of the plants at each week, suggests that the tolerated light intensity is directly dependent on the pNPQ capacity. The pNPQ process also seems to become more finely tuned as the plants develop to the reproductive phase, before decreasing in the senescent phase. The efficiency of pNPQ is taken from plotting the lowest pNPQ values at each light intensity for the plants of different ages. As pNPQ is protective, it is also wasteful if it is unnecessarily great as it has a large reduction effect on the ΦPSII. Eight-week-old plants have the most efficient pNPQ, with one week olds the least. Calculating the pNPQ efficiency is also useful, as it provides an estimate for the amount of pNPQ that would be required for plants to survive higher light intensities. For instance, all of the one week old plants exhibited photodamage after ~625 µmol photons m^{-2} s^{-1}, but they could survive 1500 µmol photons m^{-2} s^{-1} if they could form pNPQ of ~7.

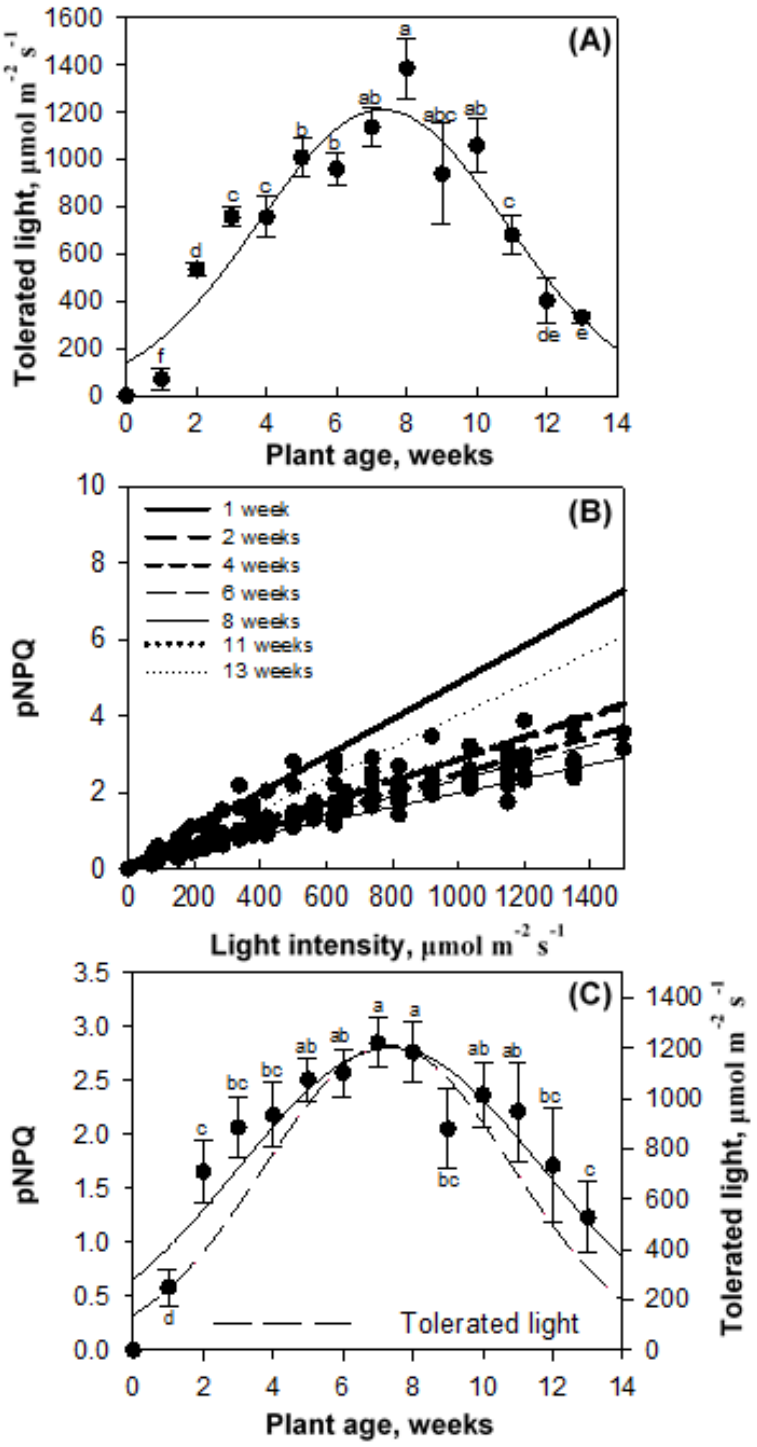

Figure 4.09 (A) Light intensity which caused photoinhibition in 50% of leaf populations; (B) relationship between the most efficient pNPQ and light intensity and (C) relationship between the maximum pNPQ capacity and plant age. The data were obtained from leaves from 1 to 13 weeks old *Arabidopsis thaliana* plants. Error bars show the SD. Different letters represent a significant difference by Z-test, P<0.05 or Tukey's test, P<0.05 (pNPQ *vs* plant age) (Carvalho *et al.*, 2015).

A fluorescence based approach was then used to test two other markers of plant fitness, and see whether the Fv/Fm values or electron transport rates (ETR) could have affected the light tolerance of the plants. Fv/Fm was measured at the start of each procedure, so can accurately assess the maximum quantum photosynthetic yield of each plant. The Fv/Fm values however had no correlation with the tolerated light intensities, and in fact showed remarkable consistency between the plants from 1-13 weeks old (Fig 4.10A). There was only an increase of 0.74-0.81 in the first seven weeks of growth, follow by a decrease from 0.8 to 0.76 in weeks eight to 13. The plants from each age group were not statistically different to more than six others at any one time suggesting that Fv/Fm played no role in light tolerance. ETR was also measured during the course of the procedure. ETR peaked at seven weeks old, but there was an observable difference in ETR in the plants aged 3-8 weeks old compared to the rest (Fig 4.11). A plateau was reached at ~500 µmol photons m^{-2} s^{-1} for most of the plants, therefore the ETR at 500 µmol photons m^{-2} s^{-1} was also compared. This profile of ETR is similar to the tolerated light intensities (4.10B). There is an increase from 26 to 79 µmol photons m^{-2} s^{-1} during 2-8 weeks of development, followed by a significant decrease in the 9-13-week period from 61 to 25 µmol photons m^{-2} s^{-1} (Tukey's test, $P < 0.05$). ETR therefore also appears to play a role in the tolerated light intensities of plants during ontogenesis.

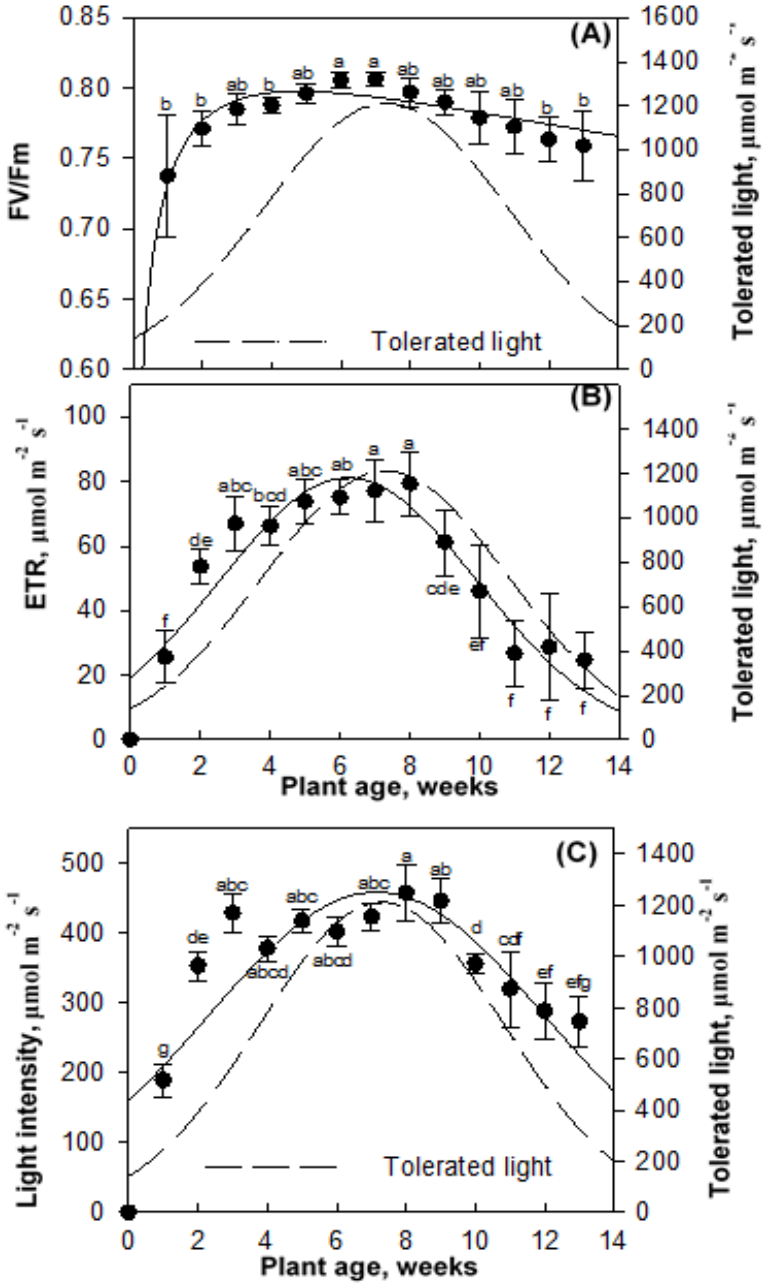

Figure 4.10 (A) Maximum quantum yield [Fv/Fm] vs. plant age and (B) ETR at 500 µmol m^{-2} s^{-1} of actinic light intensity vs. plant age (C) Tolerated light intensity when pNPQ equals 1, related to plant age. The measurements were obtained on *Arabidopsis thaliana* plants between 1 and 13 weeks old. Error bars show the SEM (n=30). Different letters represent significant differences by Tukey's test, P<0.05 (Carvalho *et al.*, 2015).

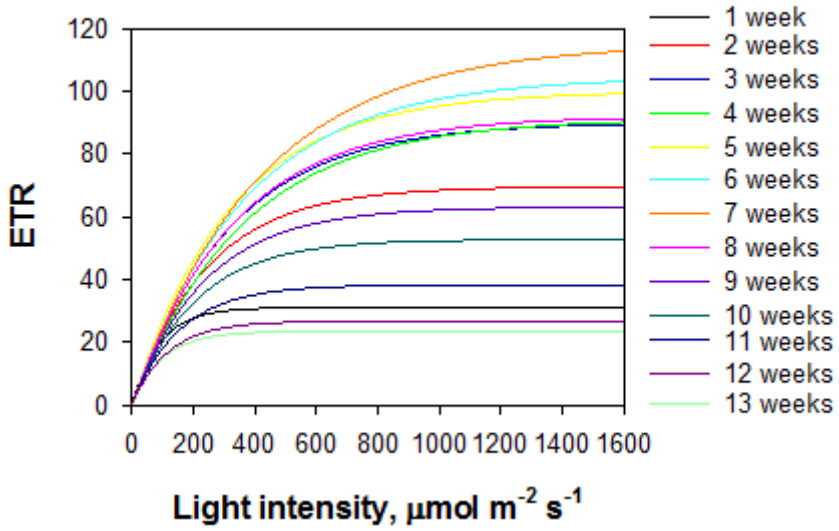

Figure 4.11 ETR vs light intensity measured in *Arabidopsis thaliana* plants from 1 to 13 weeks old (Carvalho *et al.*, 2015). ETR was measured by applying a saturating pulse at the end of each five-min AL step throughout the course of the eight-step pNPQ assessment procedure.

The chlorophyll content, anthocyanin content and thickness of leaves were also tested to investigate whether any of these other age-related components play a decisive role in the phototolerance of leaves during ontogenesis. The total chlorophyll content of leaves displayed a consistent pattern to the age-related light intensity (Fig 4.12A). Although the total contents seem to follow stepwise increases and decreases, the rise from 15.5 to 55.8 µg cm^{-2} during the first eight weeks, followed by a five-week decrease to 15.2 µg cm^{-2} does illustrate a correlation to phototolerance. Interestingly, the Chl *a*/*b* ratios did not follow the same pattern as total chlorophyll or phototolerance, but instead reflect the Fv/Fm variation (Fig 4.12B). The peak here though was reached at four weeks old, with a ratio of 3.7, before decreasing through the reproductive and senescent phases to 3.00 at 13 weeks. Vastly different was the trend of anthocyanin formation. Anthocyanins peaked in the juvenile and senescent phases of plant growth. After the initial

formation at two weeks old (28 Abs530-Abs657 g FW^{-1}), there were no significant changes in the following 7 weeks, before the highest peak of 64 Abs530-Abs657 g FW^{-1} in week 11, and another decrease to week 13 (4.12C). Due to the unusual accumulation pattern, the anthocyanin pigments extracted were checked by spectrophotometry to confirm that no other pigments were affecting the result. However, due to the clean traces of samples tested, it would appear that there were not (Fig 4.13). It was therefore hypothesised that the changes in anthocyanin levels might be due to the decreased photoprotective capacities on NPQ, and thus required for anti-oxidative purposes. The formation of hydrogen peroxide (H_2O_2) and subsequent MDA formation/lipid peroxidation (TBARS) were tested. The results show that there is an increased area of brown spots in the juvenile and senescent leaves, indicative of the presence of H_2O_2 (Fig 4.14). Furthermore, TBARS displayed a significant increase in lipid peroxidation again for the juvenile and senescent plants (Tukey's test, $P < 0.05$). The final test was the light absorption properties of the different leaves. A continuous irradiation from 400-750 nm was conducted, as well as discontinuous irradiation of 440 and 680 nm (Fig 4.15A). The first test showed that besides the two-week-old plants which had a markedly reduced absorbance capacity, the remaining leaves were similar. The second test demonstrated that the absorption profiles were dissimilar to the phototolerance capacities of the different leaves (Fig 4.15B). These two tests seem to indicate that changes in leaf thickness were not responsible for the changes in light tolerance during ontogenesis.

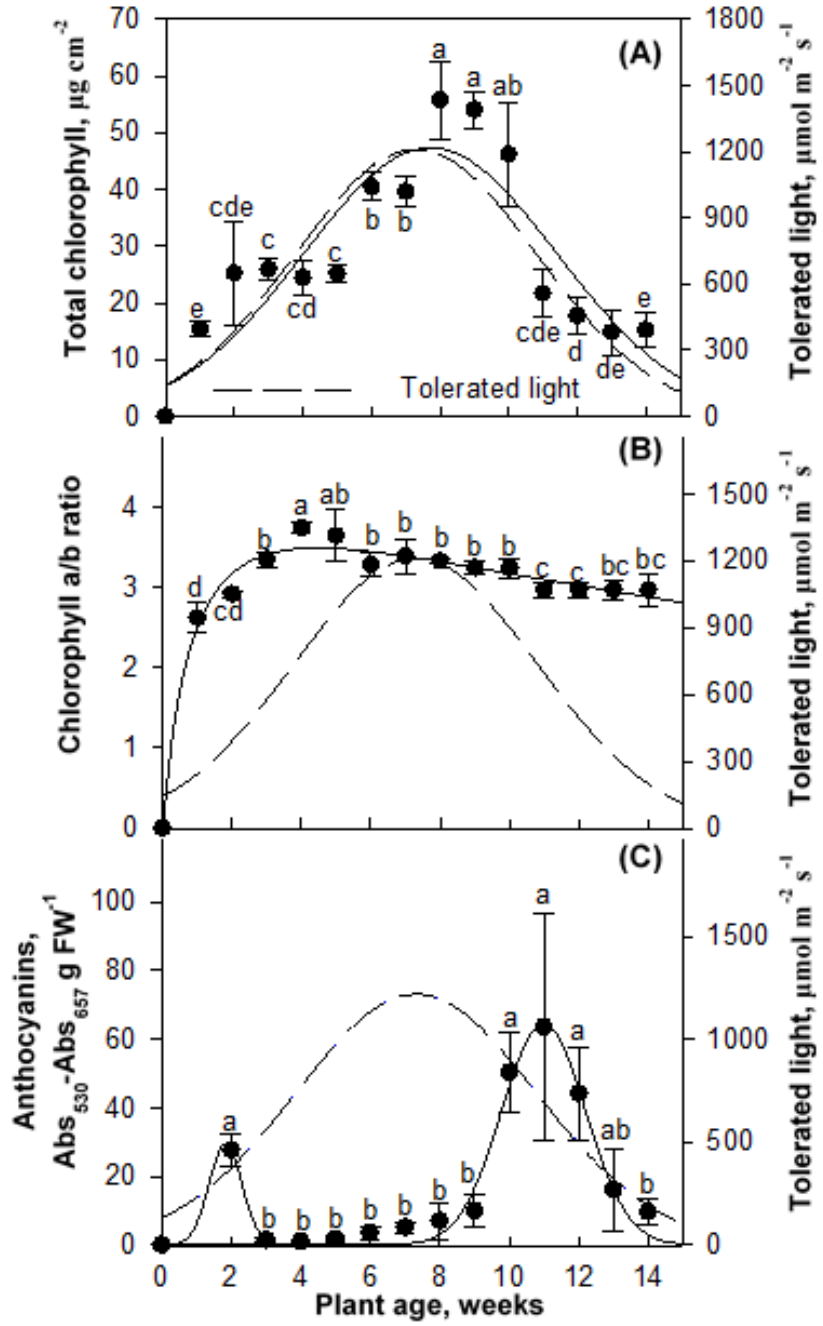

Figure 4.12 (A) Total chlorophyll; (B) chlorophyll *a*/*b* ratio and (C) total anthocyanins content. The data were obtained from leaves from *Arabidopsis thaliana* plants aged between 1 and 2 weeks to 14 weeks old. Error bars show the SEM (n=6). Different letters represent significant difference by Tukey's test, P<0.05 (Carvalho *et al.*, 2015).

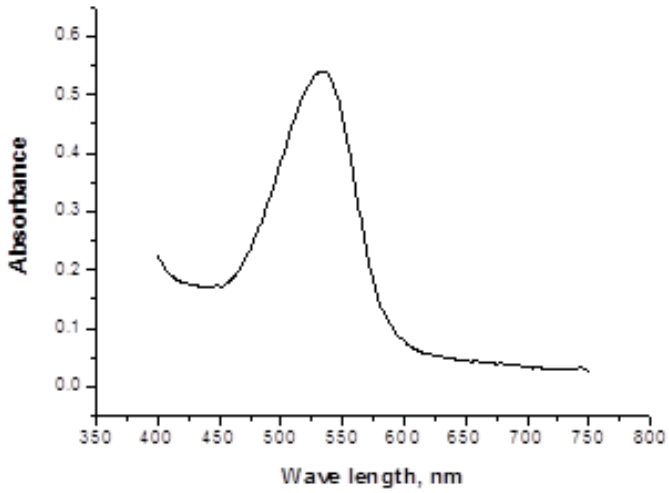

Figure 4.13 (A) Anthocyanins visible spectra profile measured in leaves of 7-week-old *Arabidopsis thaliana* plants. Each measure represents the average of 6 independent leaves (Carvalho *et al.*, 2015).

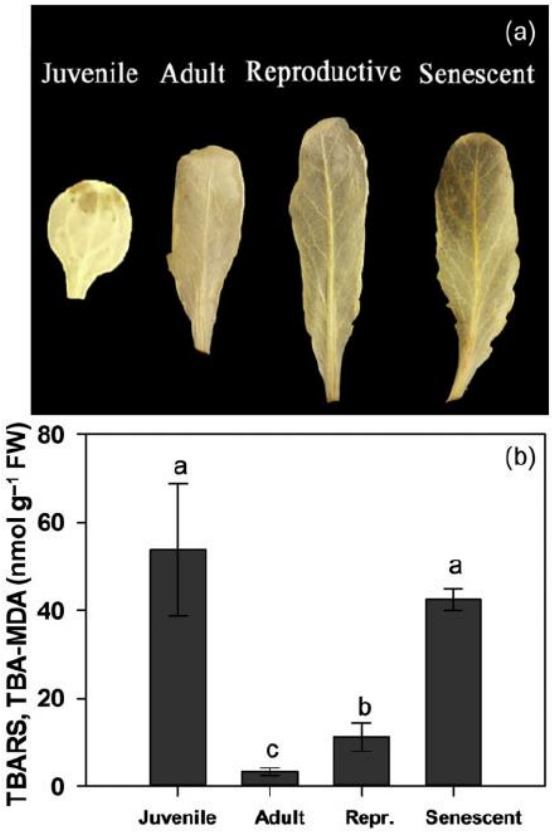

Figure 4.14 Age-dependent reactive oxygen species (ROS) accumulation indicators in leaves of *Arabidopsis thaliana*. (A) In situ H_2O_2 detection assessed by 3,3'-diaminobenzidine (DAB) staining. (B) Lipid peroxidation, as indicated by thiobarbituric acid-reactive substances (TBARS). Error bars show the standard deviation (n = 3). Different letters represent significant differences by Tukey's test, $P < 0.05$. The leaves used in the assays were always the most externally positioned in the rosette at respective ontogenetic phases: juvenile (2 weeks), adult (5 weeks), reproductive (8 weeks) and senescent (11 weeks) (Carvalho *et al.*, 2015).

Due to the significant changes observed in leaves during ontogenesis, different aged leaves were tested on the same plant in order to see whether they showed the same behaviour as different aged outer leaves. The pNPQ assessment procedure was applied to 30 internal, intermediate and external rosette leaves. These results corroborated the findings observed in aging outer leaves, that the adult leaves are the most phototolerant, and that juvenile leaves are more susceptible to photodamage. The average qP_d dropped below 0.98 at 1.9, 2.4 and 2.8 pNPQ as the leaves get older (Fig 4.05A, 4.16A, Fig 4.16B). The light intensities increased significantly from 643 to 856 and 1385 µmol photons m^{-2} s^{-1} as you move outwards through the rosette (Fig 4.17A). Furthermore, it appears that these changes are again independent of the average Fv/Fm values which do not significantly change from the innermost to outermost parts of the rosette (Fig 4.17B).

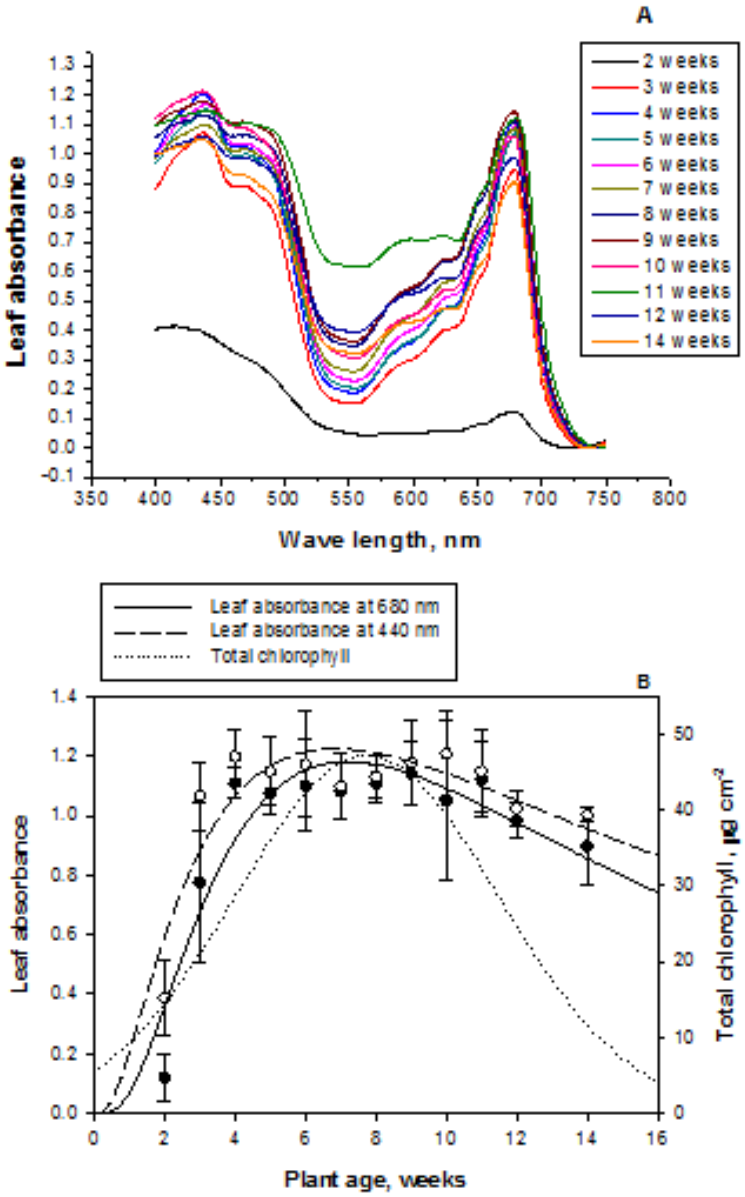

Figure 4.15 (A) Leaf absorbance in a range of wave length from 400 nm to 750 nm measured from *Arabidopsis thaliana* plants from 2-14 weeks old and (B) leaf absorbance at 440 and 680 nm vs plant age. Closed circles represents the leaf absorbance at 440 nm and open circles represents the leaf absorbance at 680 nm in respective plant ages. The leaf absorbance measures were obtained with an Olis® DW2000 spectrophotometer (Olis, Inc. Bogart, USA) according (Bauerle *et al.* 2004) with modifications. The leaves were previously dark adapted for 20 min, detached and quickly used for spectrophotometric scan of absorbance. Six different spectra were obtained from independent leaves from each age and an average of these spectra was utilized as representative spectra for each plant age (Carvalho *et al.*, 2015).

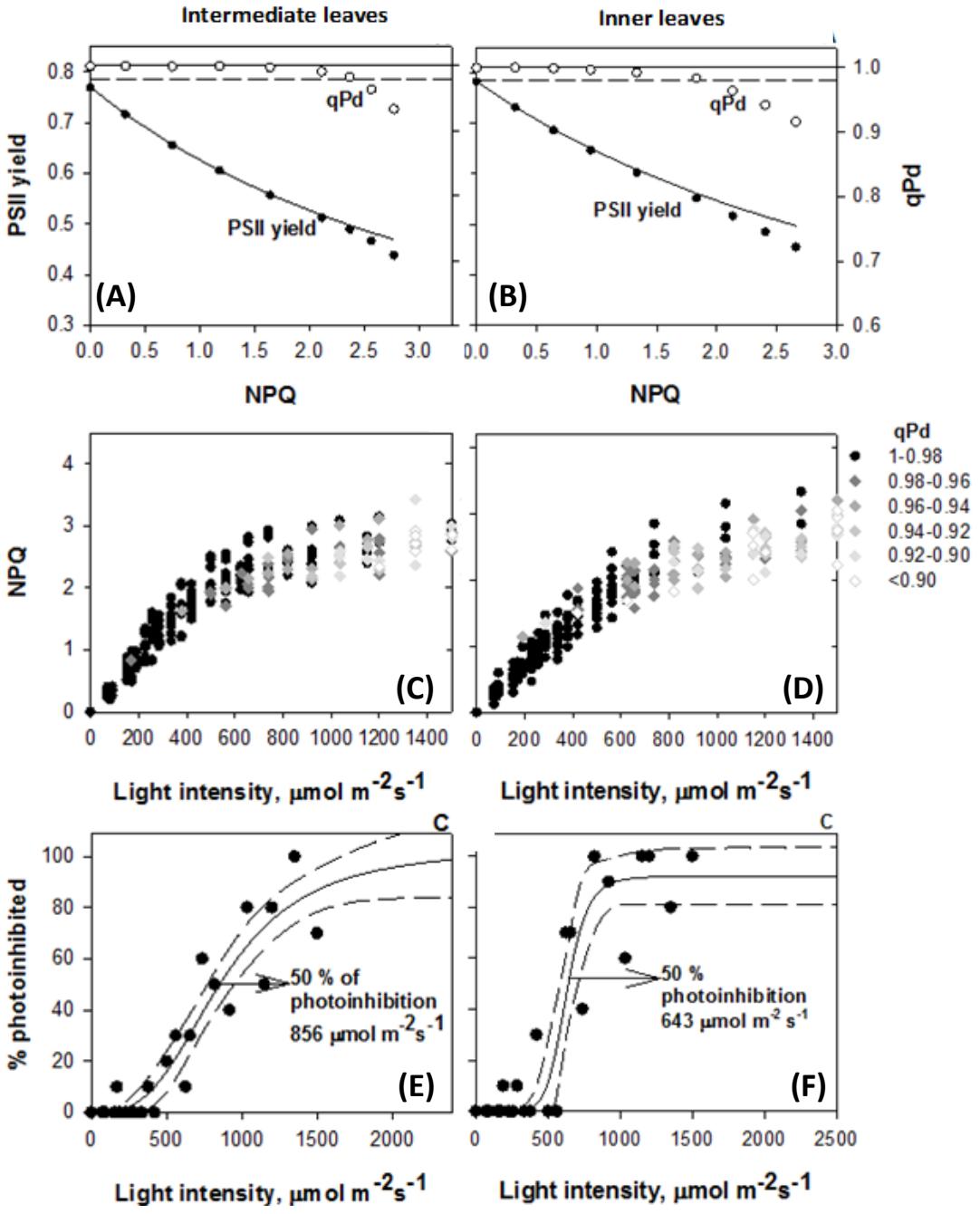

Figure 4.16 (A,B) Relationship between PSII yield, NPQ and qP_d parameters; (C,D) relationship between NPQ, light intensity and qP_d parameters and (E,F) percentage of photoinhibited leaves of 8-week old *Arabidopsis thaliana* plants intermediate (A,C,E) and inner (B,D,F) leaves. Error bars show the SEM (n=30). The theoretical yield (continuous line) was calculated using qP_d always equal to 1.00 (Carvalho *et al.*, 2015).

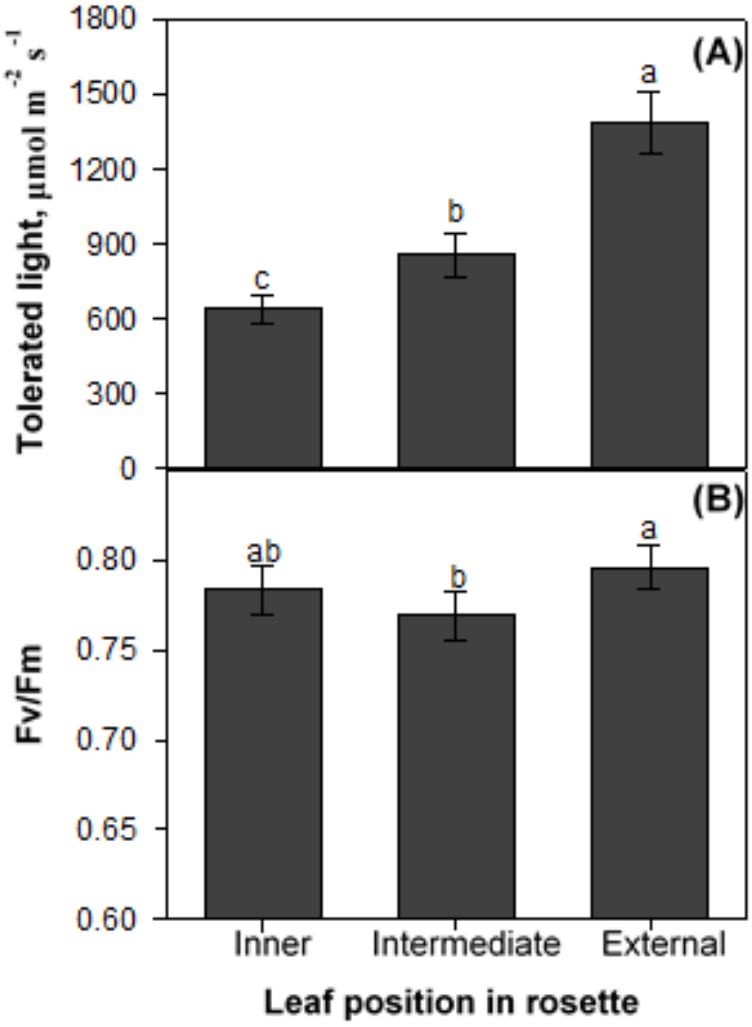

Figure 4.17 (A) Light intensity related to photoinhibition in 50% of leaf populations; (B) Fv/Fm from inner, intermediate and external leaves from 8-week-old *Arabidopsis thaliana* plants. Error bars show the SD. Different letters represent significant difference by z-test, $P < 0.05$ (50% photoinhibition light) or Tukey's test, $P<0.05$ (Fv/Fm) (Carvalho *et al.*, 2015).

4.3 Discussion

- The fluorescence parameter qP_d was used to quantify the amount of light required to cause the first signs of photoinhibition in *Arabidopsis* plants during a compete life cycle.
- Light tolerance was shown to be age dependent, with juvenile and senescent phases were the most susceptible to damage, and adult and reproductive phases the most tolerant.
- Eight-week old plants were found to have the highest tolerance, with 1,385 µmol photons m^{-2} s^{-1} required to cause the first signs of photoinhibition in 50% of leaves.
- Juvenile and senescent plants have the highest NPQ levels during the actinic light procedure, but they were also the most susceptible to photodamage.
- pNPQ capacity, ETR, and total chlorophyll content were shown to correlate with photoprotection indicating that these are the most important processes conferring phototolerance.
- Chl *a*/*b* ratios, anthocyanin levels, Fv/Fm, leaf thickness and ROS accumulation were shown to be independent of phototolerance trends, suggesting that they do not contribute significantly to high light tolerance.
- The dependency of pNPQ formation on age is also true of leaves of different ages on the same plant.

Chapter V – Discerning Role of the PsbS Protein in pNPQ

5.1 Introduction

Non-photochemical Chl *a* fluorescence quenching serves to counteract the accumulation of excess energy arising in PSII during saturating light conditions. The name originates from the readily available experimental procedure that can be used to indirectly measure the dissipation of excess energy as heat. NPQ is ΔpH dependent, and for many years was also thought to be dependent upon violaxanthin de-epoxidation and the PsbS protein (Demmig-Adams, 1990; (Li *et al.*, 2000; Dreuw *et al.*, 2003; Niyogi et al, 2004). However, it has been subsequently shown that NPQ can form in knockouts of either zeaxanthin (Rees *et al.*, 1989; Niyogi *et al.*, 1997) or PsbS (Johnson and Ruban, 2011; Ruban and Belgio, 2014). Indeed, titration and 9-aminoacridine (9-aa) experiments performed on isolated LHCII trimers and chloroplasts has shown that the relationship between quenching and ΔpH is affected by zeaxanthin and PsbS (Johnson and Ruban, 2011). Despite this *in vitro* approach illustrating that NPQ can be triggered without PsbS, it has yet to be shown *in vivo*. Furthermore, a quantification of the photoprotective capacity contributed by PsbS has not yet been performed in healthy *Arabidopsis* plants. In order to quantify the contribution of PsbS protein to photoprotection in *Arabidopsis thaliana*, plants grown with no PsbS (*npq4*), control amounts of PsbS (WT) and overexpressing PsbS (L17) were grown. A total of 40 WT and *npq4*, and 12 L17 leaves were exposed to the gradually increasing actinic light (AL) procedure (Fig 5.01). Fig 5.01 shows a typical fluorescence induction trace using the pNPQ assessment procedure. This figure illustrates the closeness of the calculated Fo' ($Fo'_{calc.}$) and actual Fo' ($Fo'_{act.}$) at low light intensities. However, at high light, the closure of RCII's leads to an increase in $Fo'_{act.}$, which causes the two Fo' parameters to diverge, and causes a decline in qP_d (Equation 1.13). The pNPQ capacity, light intensity which induces photoinhibition in 50% of leaves and ΦPSII were measured and compared. This allowed for quantification of PsbS protein to photoprotection in positive and negative controls. Further to this, the effects of varying PsbS concentrations to NPQ were ascertained using the lincomycin-treatment model. Lincomycin inhibits the synthesis of the chloroplast genome. A gradual application of the antibiotic to mature plants allowed for the removal of RCII, thus creating a

LHCII majority membrane composition. Plants with reduced ratios of RCII:LHCII have been shown to have a much greater quenching capacity than control plants. This system is advantageous as thylakoid membranes consist of almost exclusively LHCII, carotenoids and the PsbS protein, the most important components for NPQ (Demmig *et al.*, 1987; Ruban and Horton, 1994; Li *et al.*, 2000), and the subject of this experiment. WT, *npq4* and *L17* chloroplasts were treated with light, and the NPQ states compared between them using 77K fluorescence, time-correlated single photon counting (TCSPC) and freeze-fracture electron microscopy (FFEM). The results of these two experimental approaches complemented each other's findings, and revealed for the first time the *in vivo* presence of a 700 nm aggregation band in the NPQ state.

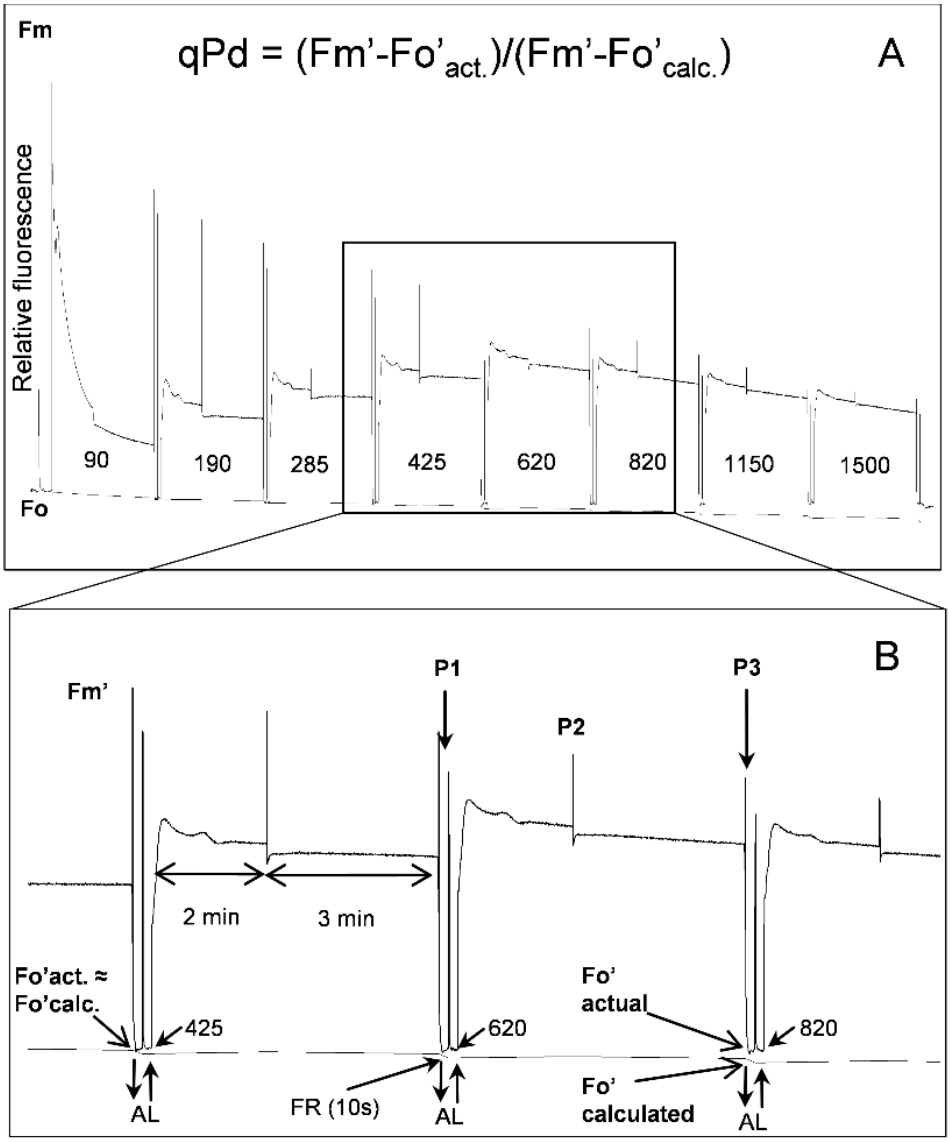

Figure 5.01 A Typical high light acclimated plant chlorophyll fluorescence scheme of induction (as depicted in Fig 2.02) with an eight-step increasing actinic light (AL) routine. In this example 0, 90, 190, 280, 420, 625, 820, 1150, 1500 µmol m^{-2} s^{-1} AL intensities were used. B Zoomed in region of the fluorescence scheme (A) illustrating the timing and application of 625, 820 and 1150 µmol m^{-2} s^{-1} AL (upward arrow and downward arrow demonstrate the turning of AL on and off respectively), along with saturating pulses (SP, P1, P2, P3). P1 indicates an SP in the dark, or after 10 sec of far red (FR) light, P2 during AL illumination, and P3 at the end of AL. The difference between $Fo'_{act.}$ and $Fo'_{calc.}$ is determined at P1, and subsequently used to calculate qP_d.

5.2 Results

5.21 Quantifying the contribution of PsbS protein to phototolerance

Fig 5.02A shows the relationship between qP_d, NPQ and AL intensity for WT plants. The degree of photodamage was then represented using grey rhomboids with increasingly pale fillings (Fig 5.2A). This method of representation allowed for a 3D visualisation using a 2D plot. qP_d and NPQ values measured at each AL intensity were then used to calculate $\Phi PSII_{theor.}$ and $\Phi PSII_{act.}$ (Fig 5.2B). Results show that WT plants can form a maximum NPQ of 3.1 during the course of the procedure (Fig 5.02A). Furthermore, they are able to form a maximum pNPQ of 2.4. The closeness of pNPQ maxima and NPQ maxima is reflected by the small deviation between the $\Phi PSII_{theor.}$ and $\Phi PSII_{act.}$ (Fig 5.2B). The average qP_d value drops below 0.98 at around 1.5 NPQ, thus meaning that the average pNPQ capacity of WT plants is 1.5. At this point, the ΦPSII is ~0.61. At the end of the procedure, $\Phi PSII_{act.}$ is 0.5, whereas the $\Phi PSII_{theor.}$ is 0.54. This means that 7% of the reduced ΦPSII is due to photodamage and may take many hours to repair. Using this methodology to distinguish between the components reducing ΦPSII is a novel and unique result. Previous methods of measuring Fv/Fm and NPQ have been unable to disentangle the photoinhibitory and photoprotective components, let alone ascertain how this manifests as a reduction in ΦPSII.

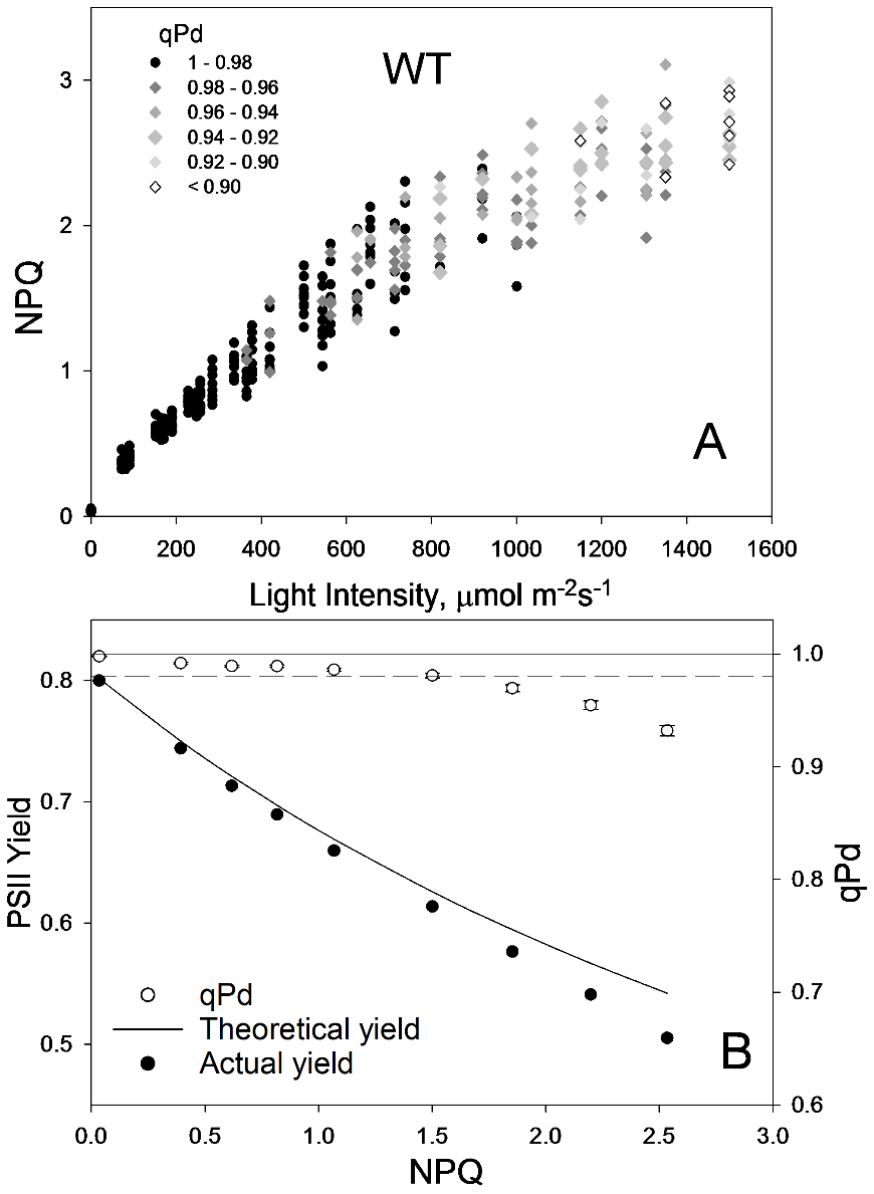

Figure 5.02 A Relationship between light intensity and NPQ, and the subsequent effect on qP_d for 40 WT *Arabidopsis* intact leaves. Data points were taken during the fluorescence routine explained in Fig 5.01. The Figure key explains the grayscale relationship of symbols to qP_d. B Relationship between NPQ, PSII actual yield (closed circles) and qP_d (open circles). At each light intensity NPQ and qP_d data points were taken from (A) and averaged. Error bars show the SEM (n = 40). The theoretical yield (continuous line) was calculated using a qP_d value of 1.00 (Ware *et al.*, 2014).

The procedure was applied to *L17* plants, and it became apparent that the relationship between NPQ and light intensity was very different from that of the WT (Fig 5.03A). By the end of the procedure, some *L17* leaves managed to reach NPQ values of over 5. The higher NPQ capacity in the *L17* leaves translated as a higher pNPQ capacity as some leaves can reach 1200 µmol photons m^{-2} s^{-1} without any RCII damage. Furthermore, the maximum pNPQ capacity of an *L17* leaf during the procedure was 4.3, which is higher than 3.1 pNPQ maxima of the WT leaves. It was not just individual leaves where pNPQ was greater in the PsbS overexpressing plants, Fig 5.03B shows the average qP_d value only dropped below 0.98 at around 3.75. The pNPQ capacity of *L17* plants was significantly higher than in the WT plants (*t*-test; $P < 0.05$). This enhanced pNPQ capacity is reflected in the closeness of $\Phi PSII_{act.}$ and $\Phi PSII_{theor.}$ until 0.45. By the procedure end, $\Phi PSII_{theor.}$ is 0.41 and $\Phi PSII_{act.}$ is 0.38, which is a difference of 7%. This means that *L17* plants have ~1% less photoinhibition than the WT leaves, despite having a significantly reduced $\Phi PSII_{act.}$ compared to WT plants (*z*-test; $P < 0.05$). The reduction in photodamage is achieved by greater pNPQ, this however causes a reduction in ΦPSII as well, and $\Phi PSII_{act.}$ is 0.12 lower in *L17* plants than WT. This is a huge reduction, and means that WT plants are in fact able to convert a greater amount of light into photosynthetic by-products than *L17* plants at high light intensities.

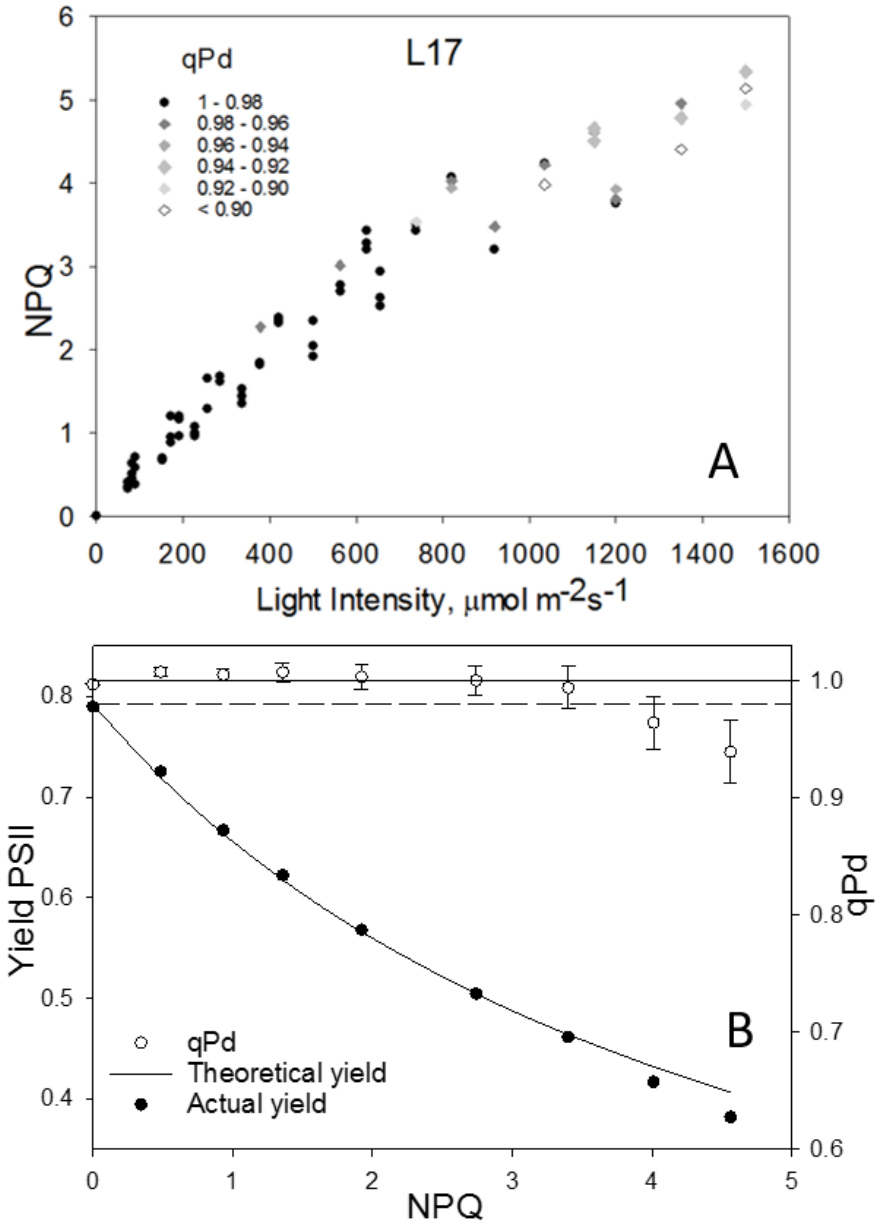

Figure 5.03 A Relationship between light intensity and NPQ, and the subsequent effect on qP_d for 12 *L17 Arabidopsis* intact leaves. Data points were taken during the fluorescence routine explained in Fig 5.01. The Figure key explains the grayscale relationship of symbols to qP_d. B Relationship between NPQ, PSII actual yield (closed circles) and qP_d (open circles). At each light intensity NPQ and qP_d data points were taken from (A) and averaged. Error bars show the SEM (n = 12). The theoretical yield (continuous line) was calculated using a qP_d value of 1.00.

npq4 whole intact leaves were then exposed to the pNPQ assessment procedure (Fig 5.04A). Leaves from this genotype experienced photoinhibition earlier than the WT and *L17* plants. Indeed, 190 µmol photons m^{-2} s^{-1} is enough to cause RCII closure in one leaf. There is also a greater proportion of open rhomboids by the end of the procedure, which indicates that 90% of leaves had a reduction in photochemical capacity of at least 10%. *npq4* leaves are also only able to achieve an NPQ capacity of 2 and pNPQ of 1.4 during the pNPQ assessment procedure; this is less than the NPQ and pNPQ maxima of both the WT and *L17* leaves. $\Phi PSII_{act.}$ and $\Phi PSII_{theor.}$ deviate at a significantly lower NPQ value than in both the WT and *L17* plants (*z*-test; $P < 0.01$), this indicates that *npq4* plants are not able to achieve the same pNPQ capacities of the other genotypes. Indeed, the point of deviation for the two ΦPSII's in the *npq4* plants is less than 1. It is not just the first point of RCII damage to which *npq4* plants are more susceptible, but under high light conditions as well. qP_d at the procedure end was significantly lower in the *npq4* leaves than the WT and *L17* leaves (*t*-test; $P < 0.001$).

qP_d values obtained for individual leaves at each light intensity during the pNPQ assessment procedures (Figs5.02-04A) can be used to calculate percentages of leaves which are inhibited at each light intensity (Fig 5.05). Here, the percentage of leaves with $qP_d < 0.98$ was plotted against the corresponding light intensity at which the SP was applied. Sigmoidal regression analysis (Hill, three parameter; $f=ax^b/c^b+x^b$) was used to extrapolate between the data points and calculate the point at which 50% of leaves became photoinhibited in each genotype. The different relationships between pNPQ, qP_d, $\Phi PSII_{act.}$ and $\Phi PSII_{theor.}$ observed between the genotypes over the course of the procedure manifested in significantly different patterns of population phototolerance. In WT plants, 50% of leaves showed signs of photodamage at 700 µmol photons m^{-2} s^{-1}. *L17* plants are able to tolerate 250 µmol photons m^{-2} s^{-1} more than WT leaves before 50% of leaves showed the first signs of photoinhibition ($qP_d < 0.98$). This difference in phototolerance is significant (*z*-test; $P < 0.05$) compared to WT leaves, and significantly greater than the 450 µmol photons m^{-2} s^{-1} which causes photoinhibition in 50% of *npq4* leaves (*z*-test; $P < 0.0001$). The difference between *npq4* leaves and

WT was also significant (*z*-test; P < 0.01). This therefore means that *L17* plants are the most tolerant of high light, followed by WT and *npq4* plants.

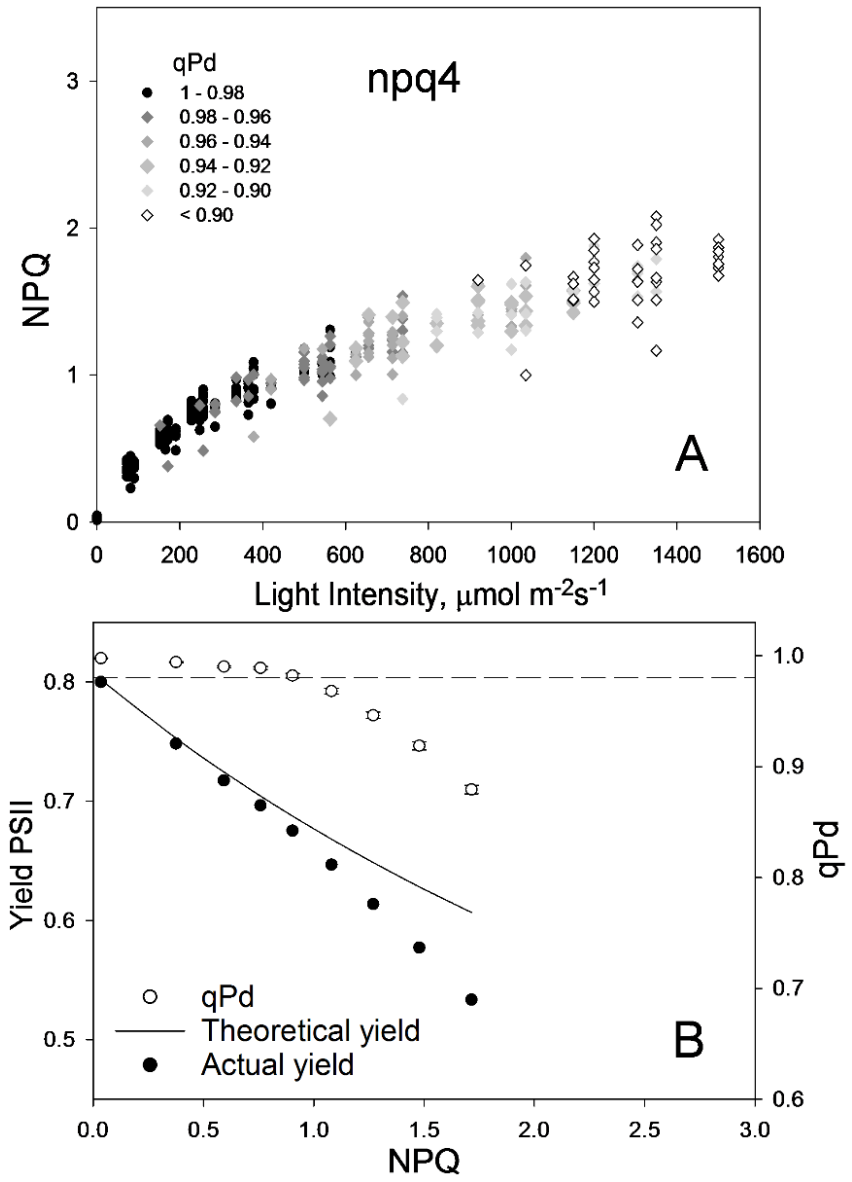

Figure 5.04 A Relationship between light intensity and NPQ, and the subsequent effect on qP_d for 40 *npq4 Arabidopsis* intact leaves. Data points were taken during the fluorescence routine explained in Fig 5.01. The Figure key explains the grayscale relationship of symbols to qP_d. B Relationship between NPQ, PSII actual yield (closed circles) and qP_d (open circles). At each light intensity NPQ and qP_d data points were taken from (A) and averaged. Error bars show the SEM (n = 40). The theoretical yield (continuous line) was calculated using a qP_d value of 1.00 (Ware *et al.*, 2014).

qP_d values obtained for individual leaves at each light intensity during the pNPQ assessment procedures (Figs5.02-04A) can be used to calculate percentages of leaves which are inhibited at each light intensity (Fig 5.05). Here, the percentage of leaves with $qP_d < 0.98$ was plotted against the corresponding light intensity at which the SP was applied. Sigmoidal regression analysis (Hill, three parameter; $f=ax^b/c^b+x^b$) was used to extrapolate between the data points and calculate the point at which 50% of leaves became photoinhibited in each genotype. The different relationships between pNPQ, qP_d, $\Phi PSII_{act.}$ and $\Phi PSII_{theor.}$ observed between the genotypes over the course of the procedure manifested in significantly different patterns of population phototolerance. In WT plants, 50% of leaves showed signs of photodamage at 700 µmol photons m^{-2} s^{-1}. *L17* plants are able to tolerate 250 µmol photons m^{-2} s^{-1} more than WT leaves before 50% of leaves showed the first signs of photoinhibition ($qP_d < 0.98$). This difference in phototolerance is significant (*z*-test; $P < 0.05$) compared to WT leaves, and significantly greater than the 450 µmol photons m^{-2} s^{-1} which causes photoinhibition in 50% of *npq4* leaves (*z*-test; $P < 0.0001$). The difference between *npq4* leaves and WT was also significant (*z*-test; $P < 0.01$). This therefore means that *L17* plants are the most tolerant of high light, followed by WT and *npq4* plants.

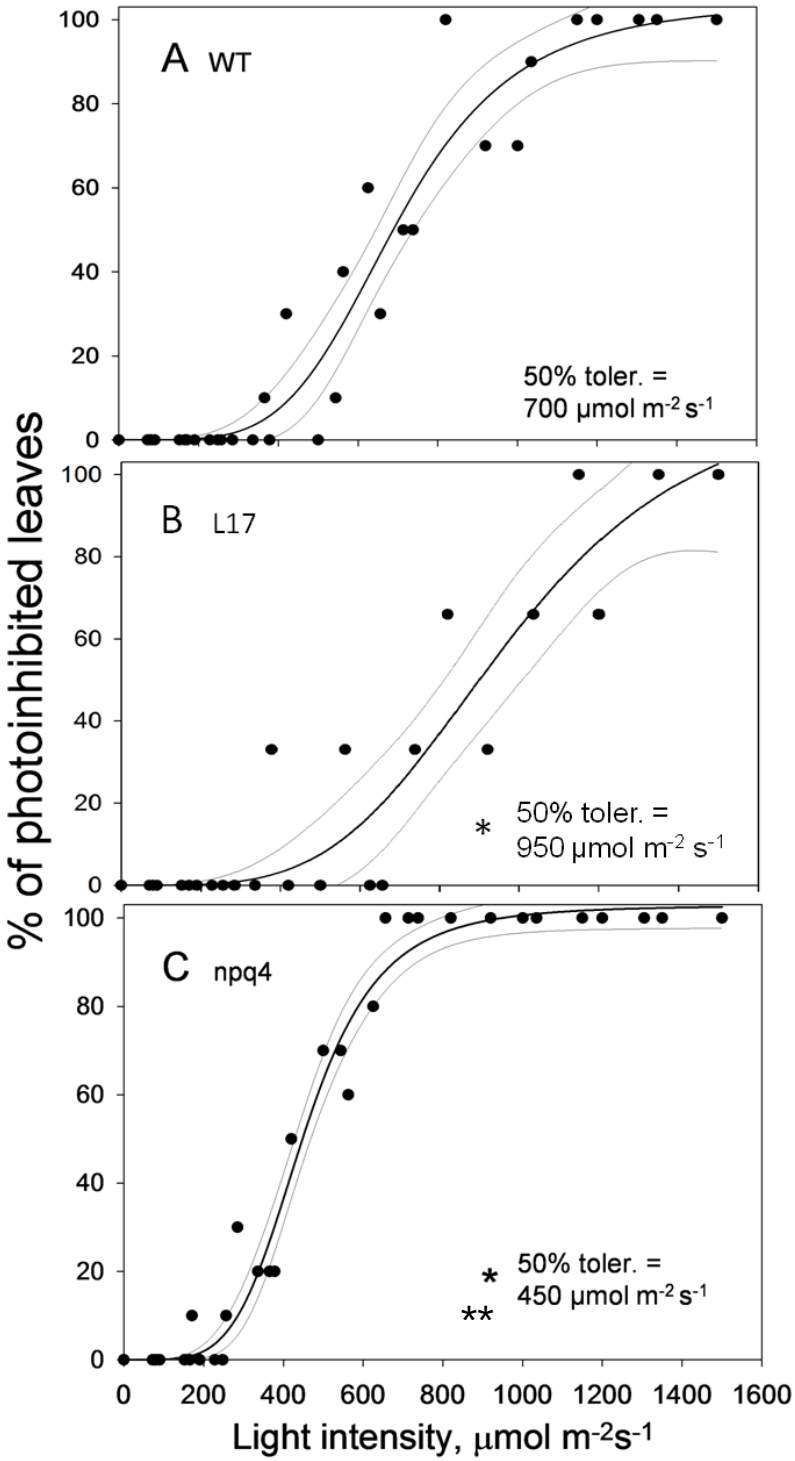

Figure 5.05 Relationship between the percentage of photoinhibited leaves and light intensity for A WT, B *npq1* and C *npq4 Arabidopsis* plants. Data points are derivatives from Fig 5.02A-4A for WT, *L17* and *npq4* respectively. Lines represent regression fit curves (Sigmoidal, Hill, 3 Parameter; f =axb/cb+xb)) with 95% confidence values plotted using SigmaPlot12 (Systat Software, Inc., Chicago, USA). A single asterisk is used to signify this significant difference between mutants and WT plants, with a double asterisk representing a significant difference between *L17* and *npq4* plants ($P < 0.05$).

Increased PsbS protein concentration therefore manifests in increased phototolerance. There is almost a liner relationship between the maximum pNPQ capacity of each genotype and the light intensity, which supports the conclusion that absolute pNPQ capacity if the determining factor affecting phototolerance (Fig 5.06). However, this is not the sole factor governing photoprotection, and the effects of varying PsbS concentration in different systems and the examination of its dynamics through different techniques was performed.

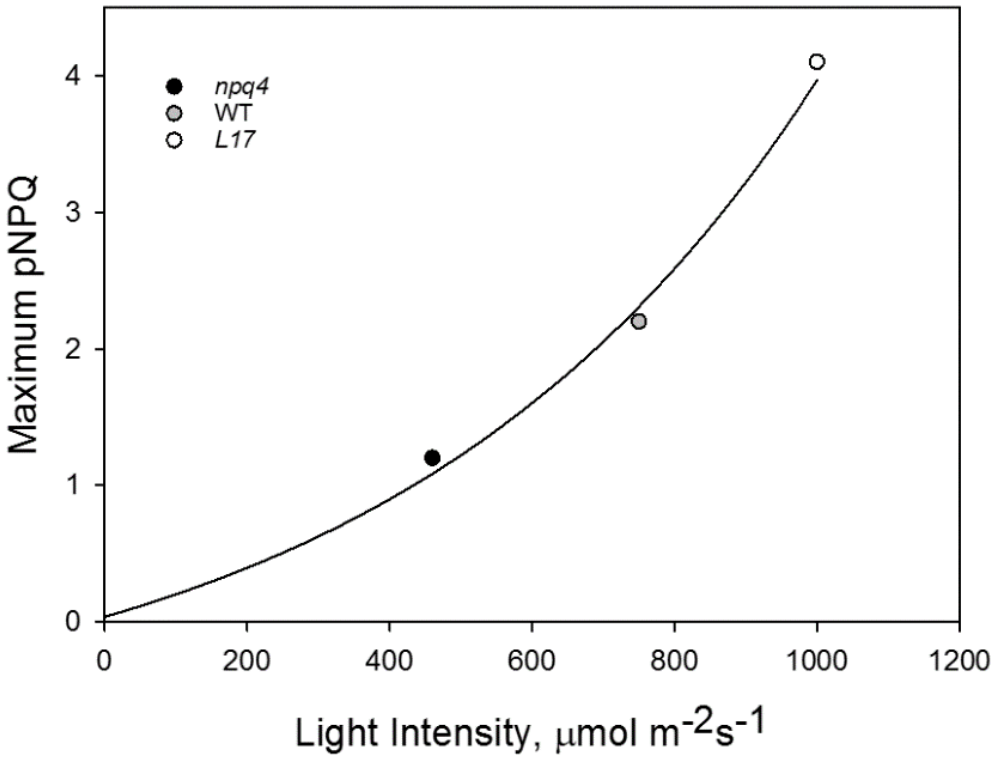

Figure 5.06 Comparison of maximum pNPQ and the corresponding light intensity that it protected 100% of RCII up to for WT, *L17* and *npq4* plants measured over the course of the pNPQ assessment procedure.

5.22 Assessing PsbS-dependent dynamics on pNPQ formation

In a gradually increasing procedure as described above, the absolute pNPQ capacity is the determining factor. However, the selection pressure can be changed if the pNPQ assessment procedure is also changed. In order to also assess the speed of pNPQ formation, and see whether this selection pressure is important in PsbS mutants, a constant 1500 µmol photons m^{-2} s^{-1} procedure was applied. As all plants showed signs of photoinhibition in the first five minutes of illumination (Fig 5.07), the dynamics of qP_d decline and NPQ formation are the focus of the results. Unfortunately, owing to the timing of paper publications, *L17* plants are not included in this section. However, results are similar to those seen in Chapter 8 (Fig 8.12).

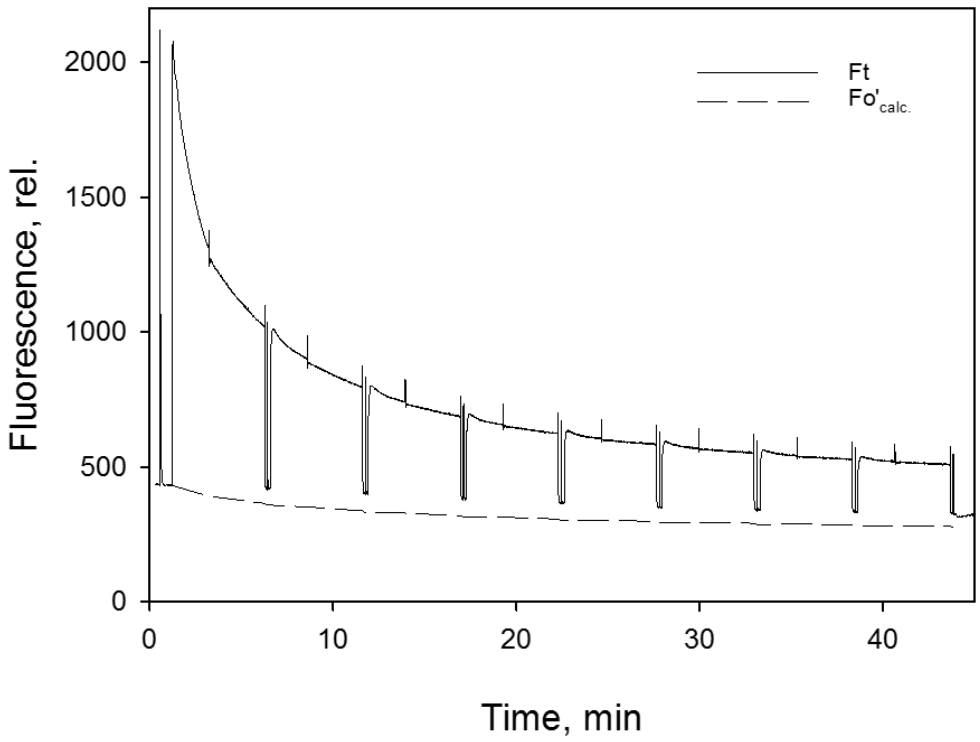

Figure 5.07 A typical chlorophyll induction fluorescence trace performed on a whole intact WT leaf. The AL was 1500 µmol photons m^{-2} s^{-1} for the whole 43 minutes. Illumination with a constant high light causes a deviation between $Ft/Fo_{act.}$ and $Fo'_{calc.}$ from the start of the procedure.

Upon exposure to high light (Fig 5.07), there was an immediate difference in the average qP_d values between *npq4* and WT plants (Fig 5.08A). Whereas under a gradually increasing AL procedure, qP_d values were similar between *npq4* and WT plants until around 300 µmol photons m^{-2} s^{-1}, the slower forming NPQ in PsbS-less plants resulted in severe photodamage from the start. By the end of the procedure, *npq4* plants were significantly more photoinhibited than the WT counterparts (*t*-test; $P < 0.01$). Interestingly, from around 22 mins, there was no further decline in qP_d in the *npq4* plant. From around 17 min, this was the same pattern with the WT plant. This result indicates that once the plants are able to achieve the amount of NPQ which was able to prevent further photodamage, further qP_d decline was halted.

The average NPQ values obtained during the constant 1500 µmol photons m^{-2} s^{-1} actinic light procedures are presented in Fig 5.08B. It is clear that NPQ formation is much quicker in the WT plants, yet after the greater quenching formed over the first five min, the difference in NPQ between the two genotypes changed very little. Taken in context of the qP_d decline results (Fig 5.08A), an interesting comparison to the results from the gradually increasing AL procedures can be drawn. In the WT, there is no real net change in qP_d decline from 17 min onwards, the same is true of the *npq4* plant but after 22 min. At 17 min, the WT plants have on average formed 2.2 NPQ. Now at 22 min, the *npq4* plants on average have formed 2.1 NPQ. This result shows that PsbS is required to form rapid NPQ, without which, plants can suffer enormously when exposed to sudden high light. However, once again, it is the absolute amount of NPQ which governs photoprotection, rather than any one specific component which is present.

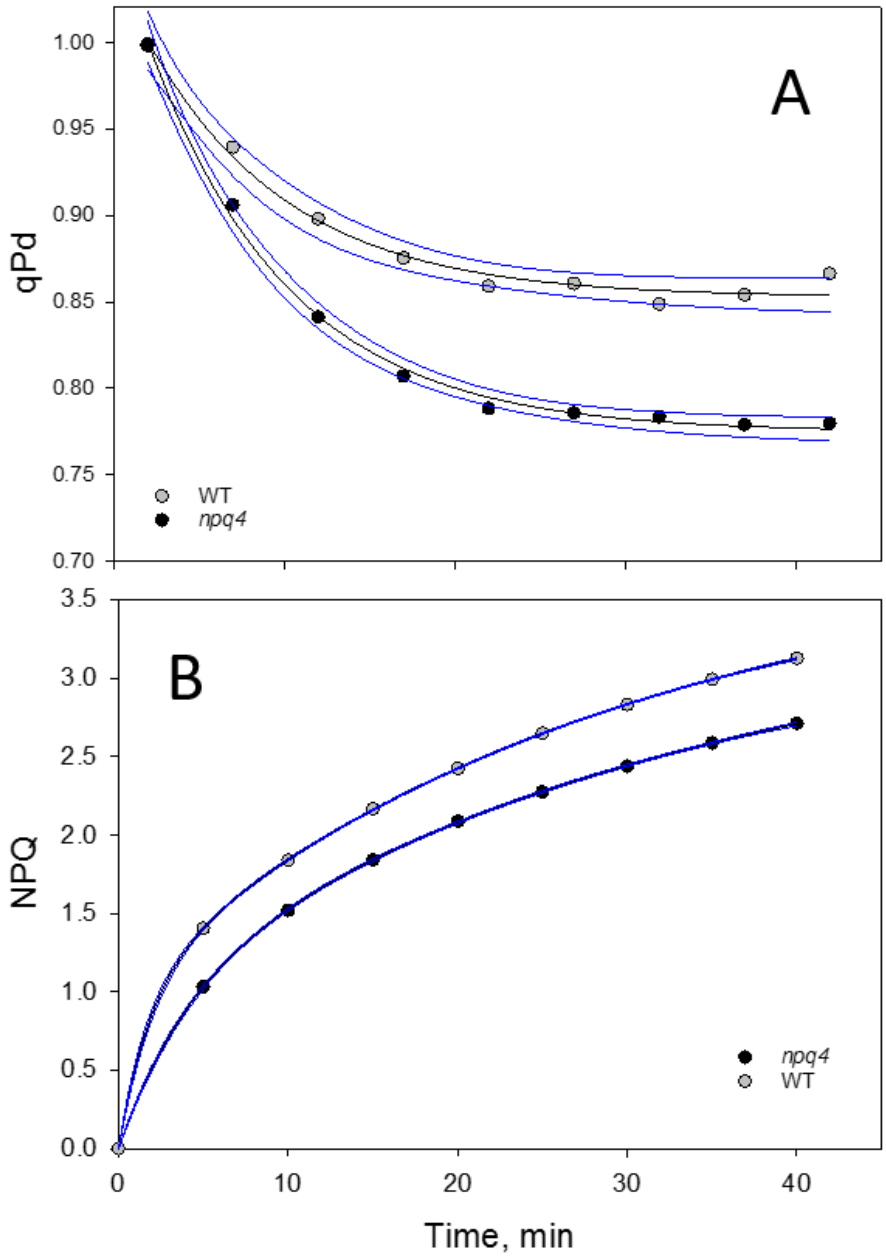

Figure 5.08 Onset of (A) qP_d and (B) NPQ formation over a constant 1500 µmol m^{-2} s^{-1} light routine, illustrated in Fig 5.08. Grey circles indicate WT, and black *npq4* *Arabidopsis* leaves. The darker lines indicate regression fit curves. A = Exponential Decay, Single, 3 Parameter; f = y0+a*exp(-bx)), and the lighter lines represent 95% confidence intervals, all plotted using SigmaPlot12 (Systat Software, Inc., Chicago, USA). B = Exponential Rise to Maximum, Single, 3 Parameter; f = y0+a(1-exp(-bx))) (Ware *et al.*, 2014).

5.23 PsbS protein modulates NPQ in plants devoid of RCII

Here, plants were watered with 0.2 g/L lincomycin, three times per week, until Fv/Fm reached approximately 0.2, represented by Fig 5.09. This Fv/Fm value was chosen as Belgio *et al.,* (2015) found this to be the lowest Fv/Fm value which did not compromise the maximum NPQ capacity.

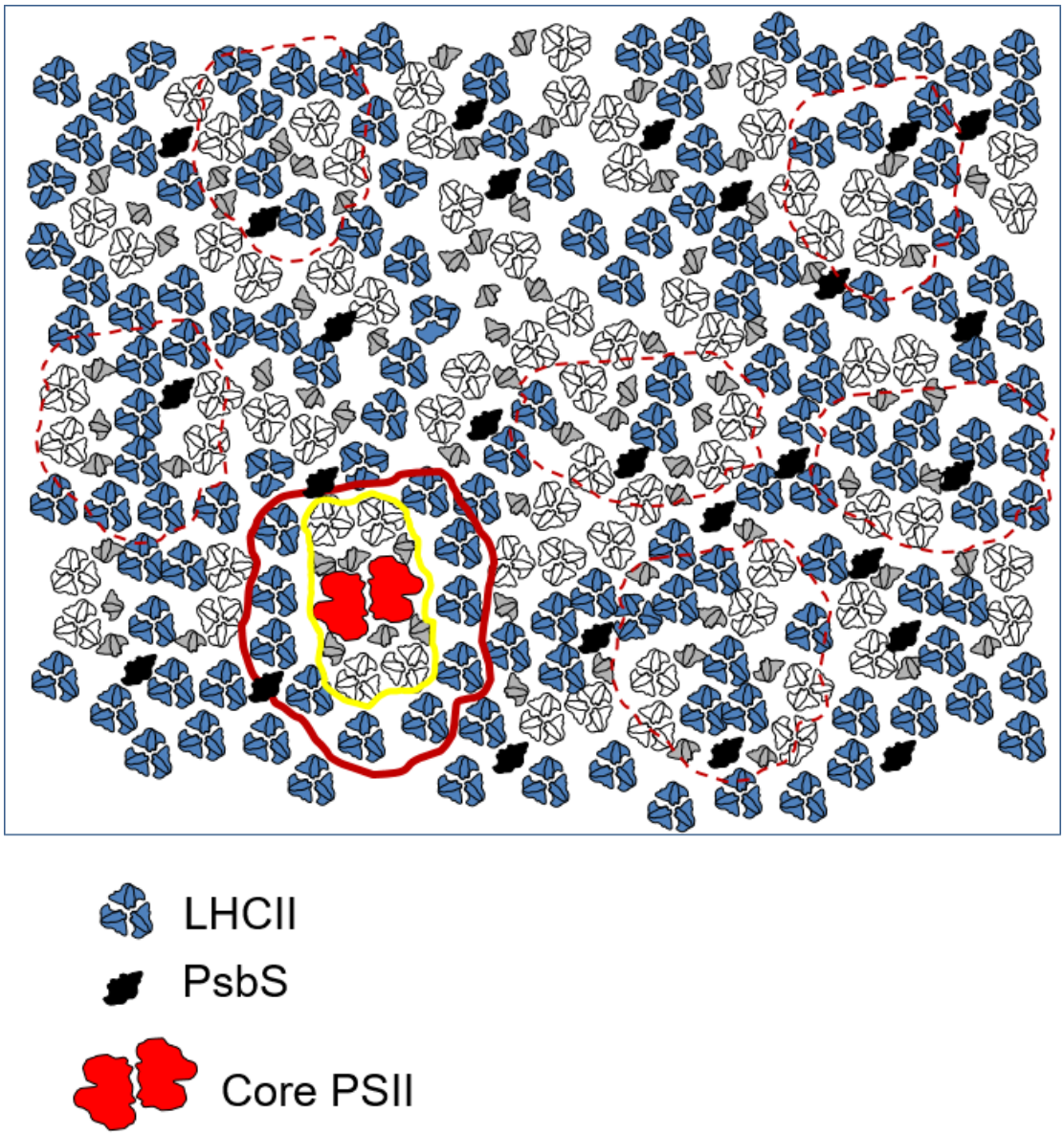

Figure 5.09 Theoretical structures of the PSII membrane in lincomycin-treated plants. Represents the enlarged antenna (LHCII) system found in lincomycin-treated plants, with many of them poorly connected, displayed by the bold and dashed red lines (Ware *et al.*, 2015b).

Lincomycin treatment revealed an interesting result regarding energy transfer between LHCII and PSII in the thylakoid membrane. There are two main competing models of energy transfer, the 'lake model' and 'puddle model'. These two differ as the former predicts many connected antenna and reaction centers, therefore RCII can quench energy absorbed anywhere in the membrane. The latter model stipulates distinct supercomplexes, with PSII only able to quench energy absorbed by LHCII to which it is directly connected. Fig 5.10A shows the arrangement of PSII particles by FFEM in thylakoid membranes of WT plants with an Fv/Fm of ~0.2. Counting the number of PSII particles at 0.2 Fv/Fm intervals unequivocally showed support for the puddle model. The solid line in Fig 5.10B displays an almost linear relationship between the number of PSII particles within a 50 nm radius and Fv/Fm. The dashed line represents the result expected if a lake model were true. In this scenario, even a few RCII would be enough to quench the excitation pressure in the membrane, which is generated by the measuring light applied to assess the Fv/Fm. This is indicated by the plateau at 0.8 Fv/Fm until a sudden collapse in Fv/Fm upon the removal of all PSII particles. As the number of LHCII does not change with lincomycin application at this light intensity, the almost linear relationship between Fv/Fm and PSII particle number represents an increased number of uncoupled antenna, relative to the number of PSII particles. This result supports the findings of Belgio *et al.,* (2014), who indicated that the puddle model is a more accurate reflection of energy quenching in the membrane.

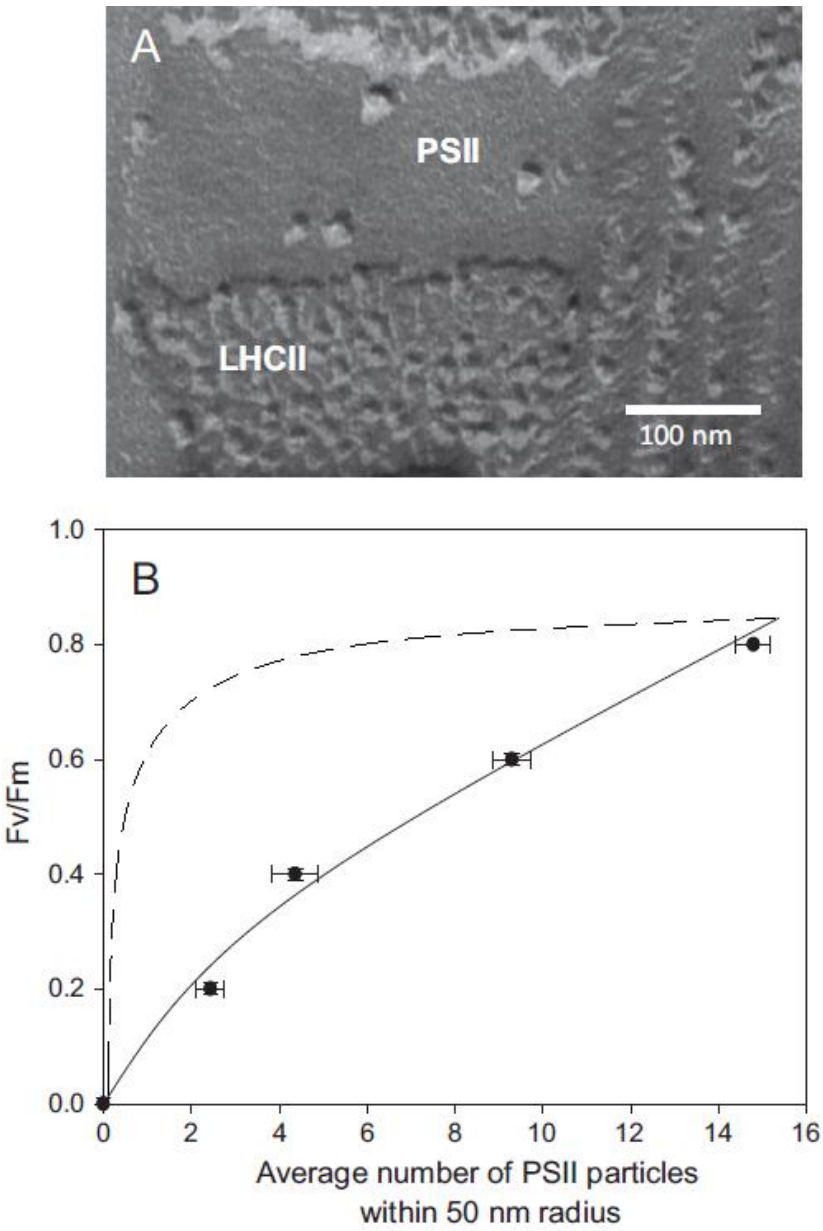

Figure 5.10 A freeze fracture electron micrograph of thylakoid membranes from lincomycin-treated WT *Arabidopsis* plants. Fv/Fm was ~0.15; (B) Closed circles represent the relationship between the PSII yield (Fv/Fm) and concentration of RCII particles, calculated using Image Pro Plus. Error bars represent SEM (n = 3). The solid line represents regression analysis was performed using SigmaPlot12. The dashed line depicts the relationship between Fv/Fm and PSII particle number predicted by the 'Lake Model' (Ware *et al.*, 2015b).

Once the lincomycin treatment protocol had been established, intact leaves from WT, *npq4*, *L17* and detached leaves infiltrated with a control buffer (20 µM HEPES; pH 7.0) or buffer and 100 µM nigericin. They were then exposed 5 min constant 1150 µmol photons m^{-2} s^{-1} actinic light, followed by 10 min with the measuring light in the dark (Fig 5.11).

Fig 5.11 illustrates the dependency of quenching capacity on the PsbS protein. *L17* leaves have the greatest degree of quenching in 5 min, with the relative fluorescence levels dropping to ~0.2 (Fig 5.11B). WT leaves had the next lowest fluorescence level at 0.3 (Fig 5.11A), with *npq4* showing very little quenching ability, and only dropping to ~0.6 (Fig 5.11C). The leaf infiltrated with nigericin has a similar quenching capacity to *npq4* leaves in the light. However, upon removal of light, it becomes apparent that Fm' is not quenched. This therefore illustrates that NPQ in plants treated with lincomycin is also ΔpH dependent, thus adding further evidence to its validity as a model.

Using the lincomycin model to investigate the dynamics of NPQ is extremely useful, as it reflects the mechanism's action almost exclusively in the antenna, rather than in the reaction centers. This means that the slowly reversible component of NPQ can be investigated, largely without photoinhibition (qI), which is reaction center dependent. Lincomycin treated WT leaves had an average NPQ of 1.9, with ~80% of this relaxing in 10 min in the dark (Fig 5.12). *L17* plants overexpressing PsbS form much larger NPQ (z-test, $P < 0.001$), reaching NPQ of ~3.0. Conversely, *npq4* leaves lacking PsbS only form 0.7 NPQ during illumination, with almost none of this quenching relaxing in the dark (Fig 5.12).

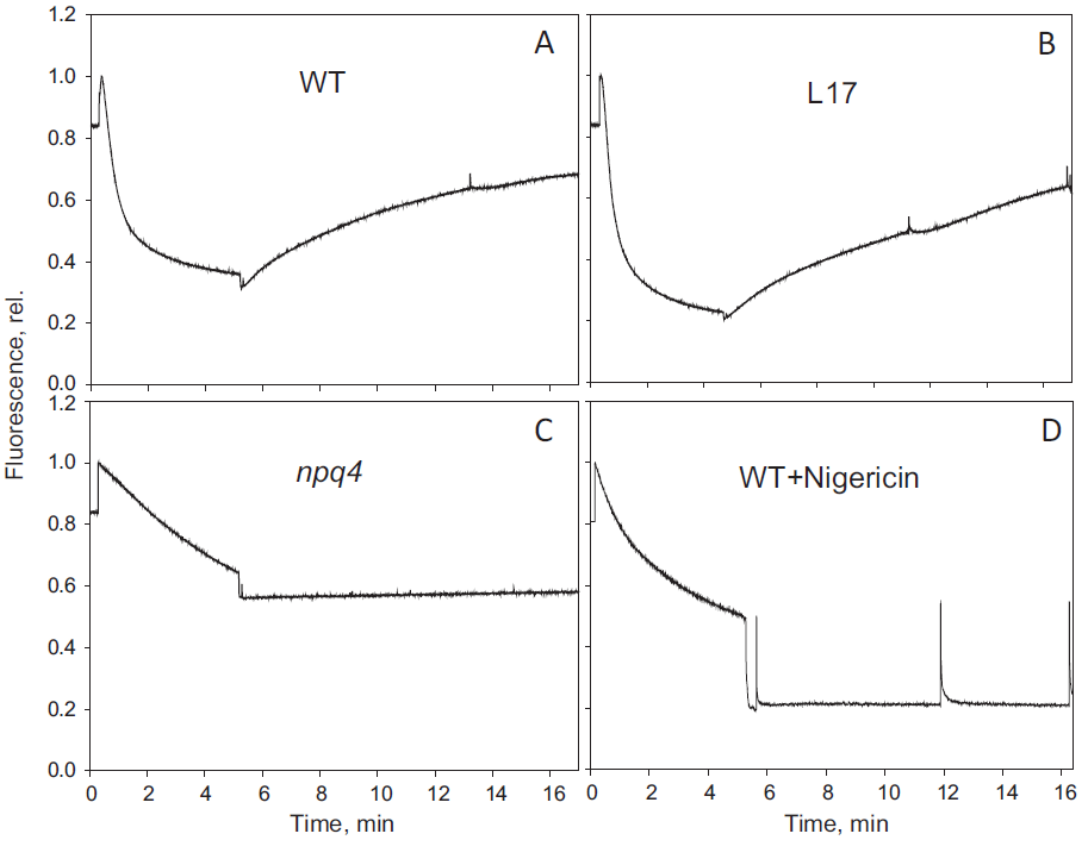

Figure 5.11 A typical PAM fluorescence quenching traces for A) WT, B) *L17*, C) *npq4* and D) WT leaves infiltrated with nigericin. All plants were treated with lincomycin until Fv/Fm reached ~0.2. The procedure consists of 5 min constant illumination at 1150 µmol m^{-2} s^{-1}, followed by ~10 min of dark recovery (Ware *et al.*, 2015b).

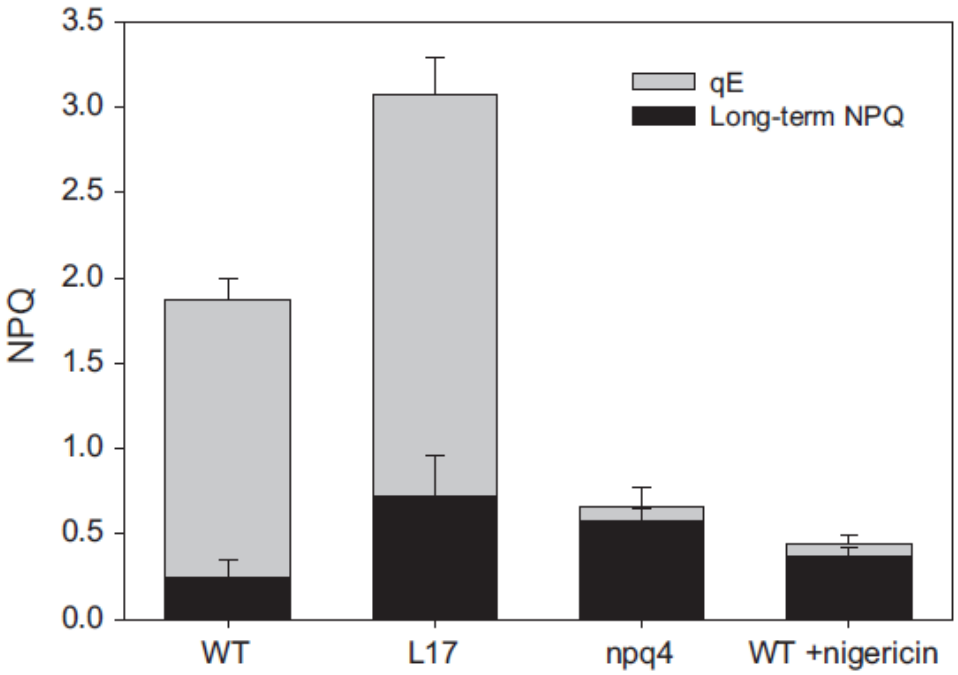

Figure 5.12 The amplitude of NPQ components recorded after 5 min constant actinic light treatment at 1150 µmol m^{-2} s^{-1} (see Fig 5.11). Non-reversible NPQ was measured in the dark, 10 min after the end of actinic light exposure. Error bars represent the standard error of the mean from three independent repeats (Ware *et al.*, 2015b).

This result offers new evidence on NPQ formed in the antenna. It has been previously stated that irreversible or slowly reversible NPQ, qI, was solely attributed to closed RCII (Osmond, 1994). It was shown here however that sustained quenching can be also be attributed to LHCII, or in this case, solely attributed to the antenna. Another interesting result is that the sustained component of quenching is significantly greater in the *L17* leaves compared to the WT (z-test, $P < 0.05$). Increased amount of PsbS would be expected to reverse the Fm' state achieved during illumination, it seems however that the greater quenching in the light caused a more pronounced sustained component. This result is similar to that observed by Ruban *et al.,* (2004), who found that greater NPQ in diatoms resulted in a slower reversal of this quenching.

5.24 Super-quenching reveals a fluorescence peak at 700 nm

Room temperature fluorescence experiments on whole leaves are sometimes open for criticism owing to potential reabsorption and unaccounted transmission from chloroplast movements (Dall'Osto *et al.*, 2014). In order to generate a more rounded picture of quenching dynamics in the thylakoid membrane and understand the NPQ dependency on PsbS in lincomycin treated plants, 77K fluorescence, TCSPC and FFEM experiments were performed on intact chloroplasts.

L17, *npq4* and WT plants were grown under 100 µmol photons m^{-2} s^{-1}, as this light environment has been shown to encourage healthy plant growth whilst the antibiotic was being applied (Belgio *et al.*, 2012). Intact chloroplasts were then extracted, and intactness was judged by comparing the Fv/Fm measured using the JUNIOR-PAM, prior to extraction, to the DUAL-PAM-100 measurements. If the Fv/Fm of the chloroplasts differed by less than 0.1, then further experiments were allowed to proceed. No artificial enhancers of NPQ, such as diaminodurene (DAD) or methylviologen (MV) were used, as these have a great effect on NPQ and affect its correlation with light intensity. Furthermore, it was desirable to have ΔpH dependency and ETRs as close to the *in vivo* conditions as possible. Upon dilution of the chloroplast in resuspension buffer, a final 3 µM chlorophyll concentration of was used to ensure minimal reabsorption in the 77K fluorescence measurements and an optimum concentration for TCSPC.

Upon exposure to 25 min of actinic light (AL, 1600 µmol photons m^{-2} s^{-1}), NPQ of between 6 and 7 was reached in the *L17* chloroplasts (Fig 5.13). With a syringe, the sample was quickly extracted, injected into a holder and then immediately frozen in liquid nitrogen. The 77K spectra was then recorded and compared to the dark-adapted state, which was measured in the same way, just with AL exposure omitted. There is a clear and striking difference between the two spectra (Fig 5.14). The DA sample, consistent with previous findings shows two bands at 683 (LHCII) and 729 nm (PSI). The illuminated sample also has two peaks, one also at 683 nm, however, it reveals a new band at 700 nm (Ware *et al.*, 2015). This presents *in vivo* evidence for the aggregation of PSII causing a 700 nm peak for the first time, and

supports the previous findings of the Horton laboratories *in vitro* experiments from the early 90's (Ruban *et al.*, 1991; 1994). There is also evidence for the quenching of PSI fluorescence in strong NPQ states. Indeed, this was argued by Giovagnetti *et al.,* (2015) in their new method for calculating the true ΦPSII. Here, the 729 nm band from PSI has been almost completely quenched. To confirm the differences in the spectra, and present the differences with greater clarity, analysis by a second derivative was performed (Fig 5.14B). This again confirms that there was a true difference between the two spectra, and not just a difference in P680 quenching and concordantly the normalisation. The experiment was also repeated on *npq4* and WT chloroplasts. After 25 min of illumination however, NPQ of ~1.5 and ~5 could only be achieved in the *npq4* and WT chloroplasts. This was to be expected and added support to the conclusions and correlation of NPQ dependency on PsbS in whole leaves. 77K fluorescence spectra in these treated chloroplasts added to the picture of fluorescence quenching. The WT and *L17* spectra had little difference in spectra, with the WT also having a peak of 700 nm, although this was marginally lower than *L17*, but PSI was also heavily quenched (Fig 5.15). The spectra from *npq4* chloroplasts demonstrates partial aggregation of PSII by the formation of a slight band at 700 nm (Fig 5.15). It is clear here though that the 729 nm peak has not been quenched. This suggests that the aggregation of PSII occurs before the quenching of PSI fluorescence. This was tested by repeating the experiment, but with 75 min of AL exposure, on *npq4* chloroplasts which resulted in NPQ levels of 4. The result supports this conclusion as PSI is now majorly quenched in comparison to the bands at 680 and 700 nm (Fig 5.16).

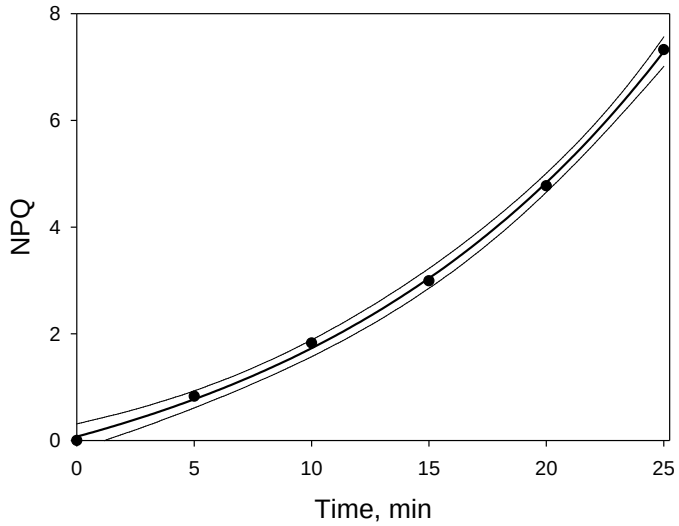

Figure 5.13 - Legend on the following page

Figure 5.13 The time course of NPQ induction in intact *L17* lincomycin-treated chloroplasts using 2000 µmol m^{-2} s^{-1} of actinic light. Regression analysis and the 95% confidence interval were plotted using SigmaPlot 12.0 (Stirling Model; f=a(e^bx-1)) (Ware *et al.*, 2015b).

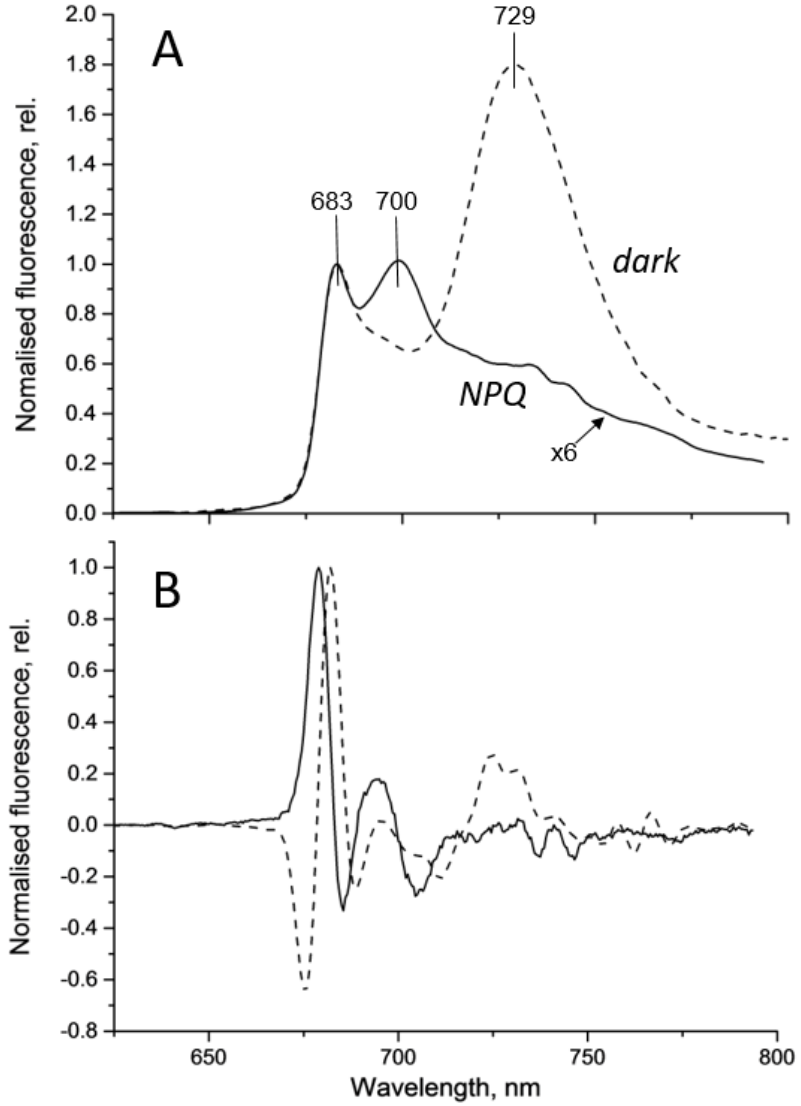

Figure 5.14 77K fluorescence spectra of intact chloroplasts from the lincomycin-treated *L17* plants in the Fm (dashed line) and Fm' (NPQ, solid line) states. The NPQ state was achieved via high light illumination in a Dual PAM. All spectra were normalised at 680 nm. 2000 µmol m^{-2} s^{-1} actinic light intensity at 435 nm excitation for 25 min was used. B) Second derivative of fluorescence spectra (Fm (dashed line) and Fm' (solid line) plotted using GRAMS spectroscopy software (Thermo Scientific, USA). Fv/Fm of samples was ~0.2. NPQ of ~6 was achieved in the illuminated sample (Ware *et al.*, 2015b).

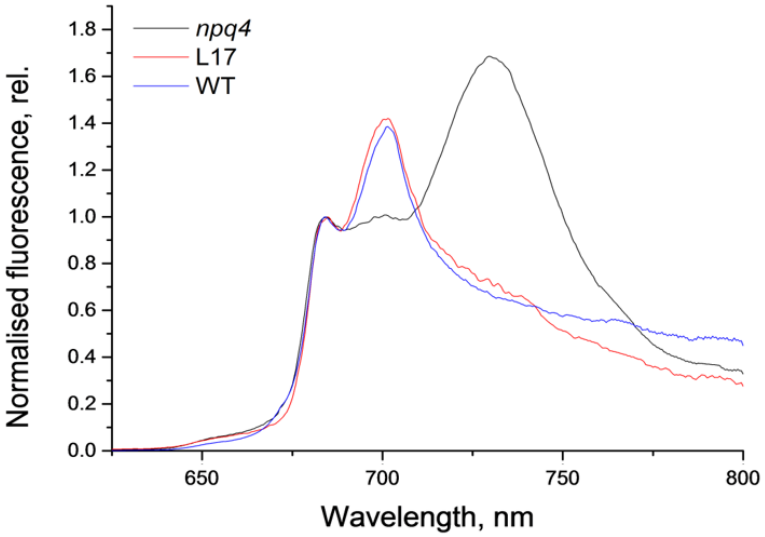

Figure 5.15 77K fluorescence spectra of intact chloroplasts from the lincomycin-treated *npq4*, *L17* and WT plants in the Fm' state. The NPQ state was achieved via high light illumination in a Dual PAM. All spectra were normalised at 680 nm. 2000 µmol m^{-2} s^{-1} actinic light intensity at 435 nm excitation for 25 min was used (Ware *et al.*, 2015b).

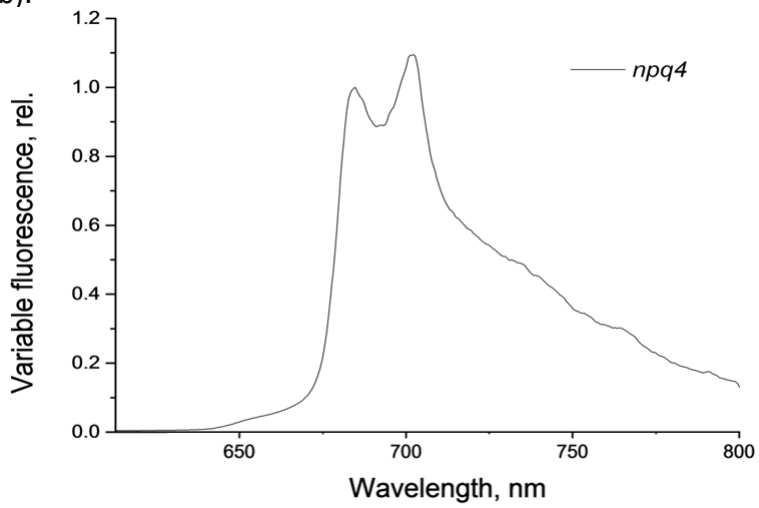

Figure 5.16 77K fluorescence spectra of intact chloroplasts from the lincomycin-treated *npq4* plants in the Fm' state. The NPQ state was achieved via high light illumination in a Dual PAM. All spectra were normalised at 680 nm. 2000 µmol m^{-2} s^{-1} actinic light intensity at 435 nm excitation for 75 min was used (Ware *et al.*, 2015b).

Owing to the novelty of these results, the fluorescence lifetime profiles of the dark and quenched states were measured via TCSPC. *L17* chloroplasts were used for this as they offered the most extreme differences between the Fm and Fm' states. The average fluorescence lifetimes measured were 1.9 ns and 0.34 ns in the Fm and Fm' states respectively. It should be firstly noted that the average lifetime in the Fm state is close to the commonly cited 2.0 ns lifetime for dark adapted thylakoids and chloroplasts (Belgio *et al.*, 2012). It is also close to the 2.0 ns dark adapted lifetime measured by Belgio *et al.,* (2012) in WT chloroplasts which had been treated with lincomycin. Taken together, this result suggests that PsbS concentration exerts no quenching effects in the Fm state. This is contrary to the effects of zeaxanthin, which effect the degree of quenching in both the Fm and Fm' states (Johnson *et al.*, 2010). Furthermore, it shows that lincomycin has no effect on the lifetimes of chloroplasts. This is in agreement with the conclusion of Belgio *et al.,* (2012), who stated that lifetimes are controlled by LHCII and not RCII. Here, it is shown again that lincomycin treatment, which depletes the chloroplast encoded RCII but has no effect on LHCII, does not affect the average Fm lifetime. The most novel finding of this experiment was the confirmation of the 'super quenched state' of LHCII in lincomycin treated chloroplasts. The reduction in average lifetime from 1.9 to 0.34 ns is approximately a six-fold decrease. Albeit slightly lower than the corresponding NPQ of 7 achieved with the DUAL-PAM-100, it shows again the great degree of quenching achieved. The slight lower NPQ level is also to be expected given that NPQ could not be fixed after the AL exposure, so with transfer to the pico-quant TCSPC machine and time required to expose the sample to 10,000 photons, six-fold quenching is still very good. It is also much greater than the previously reported 0.5-0.9 ns lifetimes (Belgio *et al.*, 2012). The components of the reduced average lifetime are different between the Fm and Fm' states. The Fm state has three components between 0.3 and 2.65 ns, with the greatest components amplitude occurring at 1.4 ns. In contrast, the Fm' state's components were all shorter than 1.0 ns. The greatest component, comprising of more than 50% of the total lifetime amplitude, was 0.1 ns. Both samples also appear to be free from photoinhibition owing to the absence of a >3.0 ns lifetime component. This adds further evidence

for the degree of quenching achieved, and almost rules out the chance that it was due to an artefact of the DUAL-PAM-100.

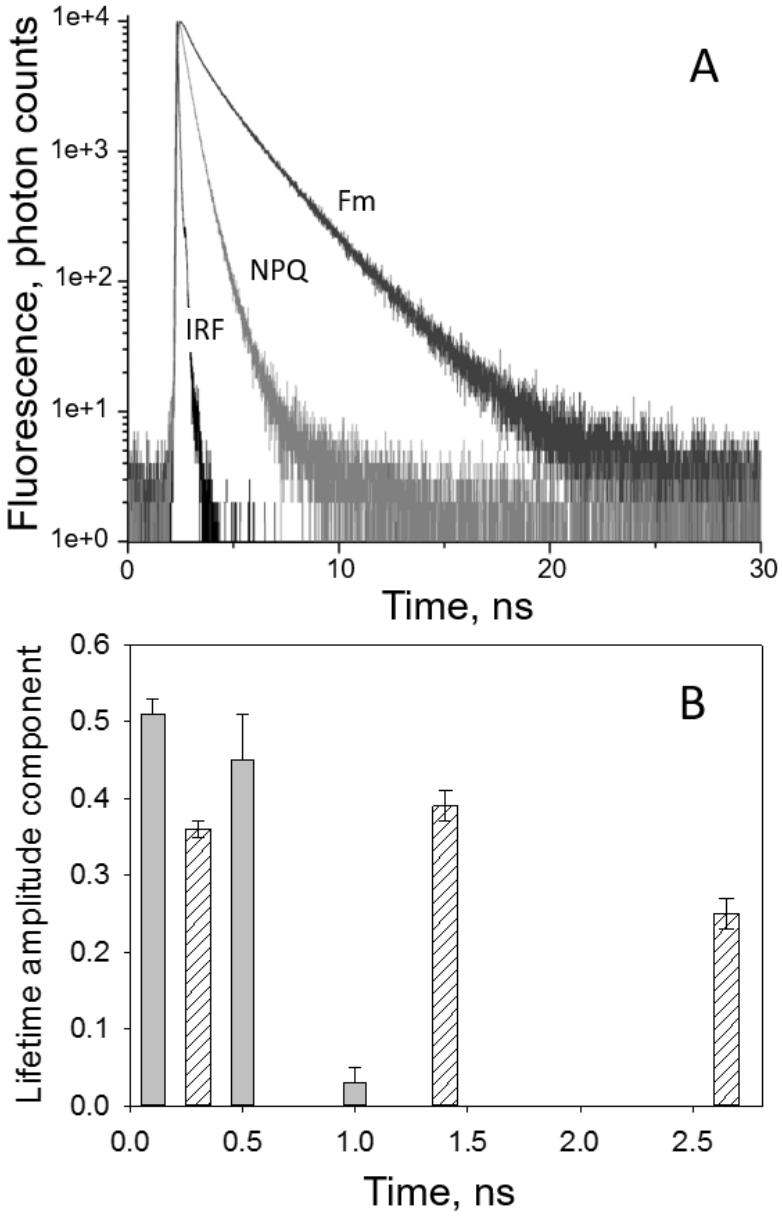

Figure 5.17 Time resolved fluorescence decay kinetics of *L17* intact chloroplasts from the lincomycin-treated *L17* plants in the Fm (black) and quenched states (light grey). The average intensity weighted lifetimes were ~1.9 ns ± 0.04 (Fm state) and 0.34 ns ± 0.06 (NPQ state). The quenched state was achieved by sample illumination in a Dual PAM (see Fig 5.14 legend). IRF stands for Instrumental Response Function. B) Components of fluorescence lifetimes in the Fm (white chequered bars) and NPQ state (grey bars) of *L17* chloroplasts. Error bars represent SEM (n = 3). Excitation was provided at 435 nm with detection at 685 nm (Ware *et al.*, 2015b).

The final method used to quantify the degree of quenching and measure the differences between Fm and Fm' states was freeze-fracture electron microscopy (FFEM). This method was also employed as it is a non-fluorescence based approach and should offer another insight into the RCII independent NPQ component, and see whether the 700 nm 'aggregated band' manifested as a physical aggregation of LHCII.

Chloroplasts were extracted as previously described. Chloroplasts were either frozen in the DA state or after 25 min AL exposure in slushy liquid nitrogen. This splitting technique is extremely useful as the core of the lipid bilayer is split revealing the internal state of the protoplasmic and exoplasmic membranes. Transmission electron microscopy (TEM) was used to visualise the replicas made of the membranes. Although LHCII have a distinguishable shape and outline, particles suspected of being the antenna protein were measured prior to being counted. 8 nm, being the widely-cited diameter of LHCII, was the reference by which LHCII was measured against and checked for correctness.

The results from the FFEM experiment offered physical confirmation of the aggregation results obtained using fluorescence based approaches. In the Fm state, particle picking and subsequent Weibull regression analysis (Fig 5.18) showed that the average number of LHCII in a 25 nm radius was 5.8 ± 0.5. Measurements of LHCII particles in the Fm' state showed on average 16.9 ± 0.3 LHCII (Fig 5.18). This indicates an approximate three-fold increase in LHCII aggregation from the Fm to Fm' state. The results here were achieved with an NPQ of ~6 in the Fm' state. This is much higher than NPQ measured in other experiments, however Johnson *et al.,* (2011) achieved NPQ of ~2.5 in spinach chloroplasts, and from the Fm to Fm' state measured a 2.15-fold increase in LHCII aggregation. Therefore, the FFEM results seem to be in line with previous findings. The novelty of this result is that it supports the opinions formed here, that a 700 nm peak is indicative of 'super-quenching' and LHCII aggregation. Furthermore, RCII is not required for NPQ, and the aggregated state achieved here is so strong that it quenches the excitation energy.

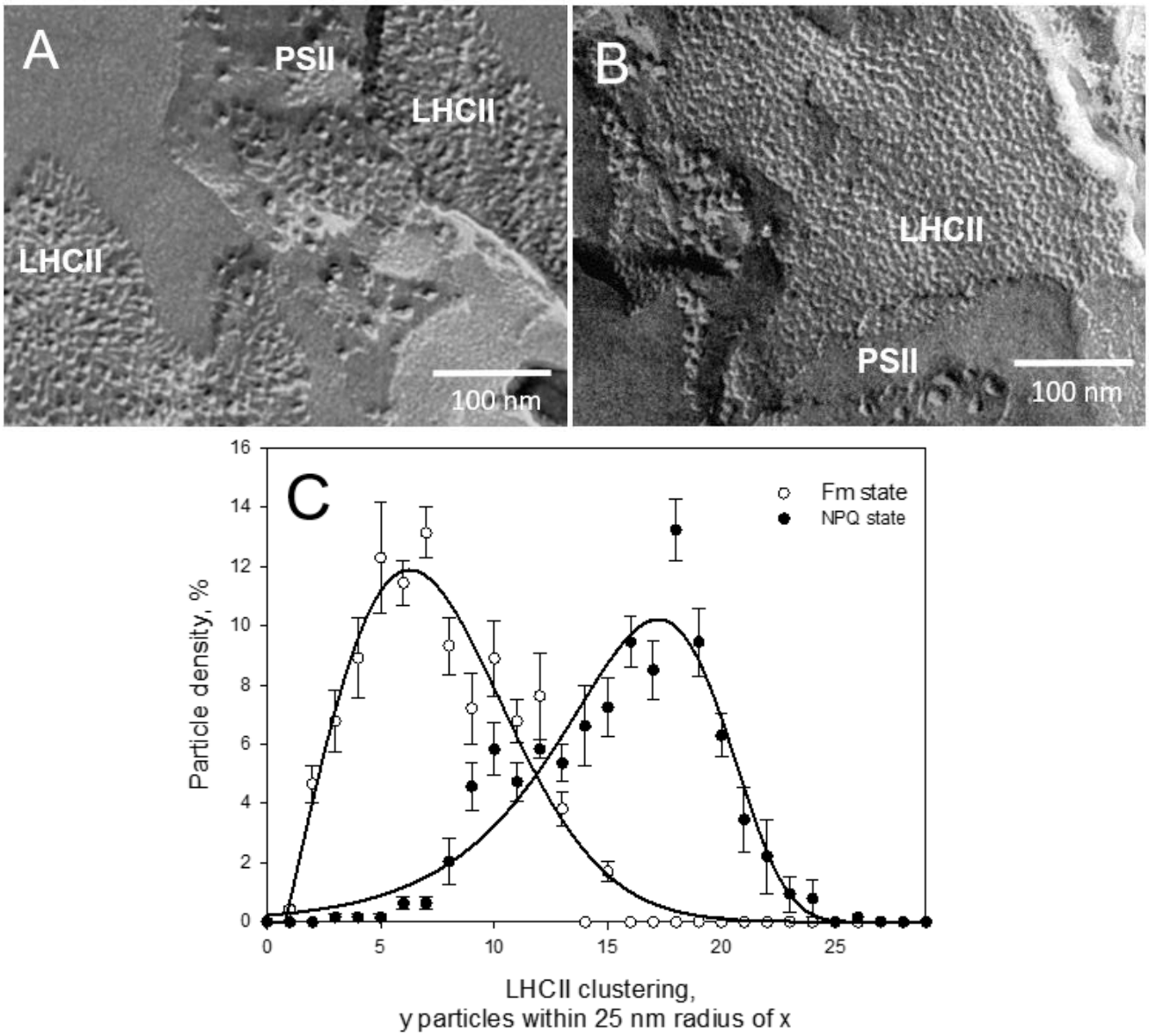

Figure 5.18 Freeze fracture transmission electron micrographs performed on intact chloroplasts from the lincomycin-treated *L17* plants in the Fm (A) and NPQ state (B). Scales are 100 nm where indicated. Fv/Fm of samples was ~0.2. NPQ of ~6 was achieved in the illuminated sample in a Dual-PAM. C) LHCII particle density analysis of Fm (open circles) and Fm' (closed circles) state using ImagePro Plus software. Weibull parameter regression analysis was plotted using SigmaPlot 12.0. Error bars represent SEM (n = 4) (Ware *et al.*, 2015b).

5.3 Discussion

- Arabidopsis plants overexpressing PsbS protein (L17) form higher pNPQ and NPQ capacities than WT or PsbS protein knock-outs (npq4).
- L17 plants were the most phototolerant, able to tolerate 950 µmol photons m^{-2} s^{-1} before 50% of leaves showed the first signs of photoinhibition.
- WT plants have the highest ΦPSII in the strongest light intensities.
- NPQ causes a physical aggregation of LHCII trimers in the photosynthetic membrane, as measured by FFEM.
- The aggregation of LHCII trimers causes a 700 nm fluorescence peak, whilst quenching the PSI fluorescence peak.

Chapter VI –

An *in vivo* quantification of the pNPQ capacity of *Arabidopsis* xanthophylls

6.1 Introduction

LCHII are the primary light harvesting proteins in the PSII super complex. As well as chlorophylls *a* and *b*, LCHII monomers bind four xanthophylls each: one neoxanthin, two luteins and either one violaxanthin, antheraxanthin or zeaxanthin depending on the degree of de-epoxidation. Xanthophylls play a number of important roles as accessory pigments to LHCII. The first function involves light harvesting. Xanthophylls absorption spectra differs greatly from Chl *a* and *b*. Although xanthophylls are spectrally diverse, the xanthophylls bound to LHCII enhance absorption as their 475 nm peak occurs in the Soret band region (Fuciman *et al.*, 2012). This provides a useful complementation to the chlorophylls in LHCII. However, xanthophylls have a much shorter, ~500 times, excited state lifetime than chlorophylls. This means that for them to effectively contribute to light harvesting in the thylakoid membrane, xanthophylls must rapidly distribute the absorbed energy to neighbouring chlorophylls via singlet energy transfer.

The second and major role of xanthophylls entails excess energy dissipation. The importance of xanthophylls in NPQ was truly demonstrated by Demmig-Adams work in 1990, when she showed a correlation between the presence of zeaxanthin and the degree of quenching the thylakoid membranes. Zeaxanthin had been discovered in green plants before then, with Wraight and Crofts (1970) and also Krause (1974) showing that it was rapidly accumulated after exposure to light, but it was Demmig-Adams work that lead to zeaxanthin being pursued as the primary quencher of the thylakoid membrane. Since then, a debate in the field as to which xanthophyll is the primary quencher has ensued. More recent research by Ruban *et al.* (2007) and Chemliov *et al.* (2015), have proposed that chl-lutein energy transfer is the main dissipative pathway of excess energy. Niyogi *et al.* (1997) also showed that removal of lutein (*lor1*) caused a greater reduction in quenching capacity than zeaxanthin-less *Chlamydomonas* (*npq1*). Despite this, the importance of zeaxanthin has also been well documented, with Rees *et al.* (1989, 1990) showing that the presence of zeaxanthin in LHCII causes the harvesting proteins to have a greater affinity to acidification of the thylakoid lumen. Indeed, a pH of only 5.7-6.2 is required to induce qE when zeaxanthin is present, compared to the 4.5-5.0

required without it (Johnson *et al.*, 2012). Despite the search for a specific quencher, the role of xanthophylls as quenchers is widely accepted. Xanthophylls serve the purpose of accepting energy from excited state chlorophylls, as the S_1 state of zeaxanthin and lutein is energetically lower than the S_1 state of chlorophyll (Polivka *et al.*, 1999). This means that they are able to accept energy from excited chlorophylls readily, removing energy before triplet or singlet state chlorophylls can form.

The third and final significant role of the xanthophylls is a structural one. There are four binding sites in LHCII: V1, N1, L1 and L2, which violaxanthin/zeaxanthin, neoxanthin and two luteins occupy. The former appears to play the smallest structural role in LHCII, owing to the peripheral position it occupies. As this is the only bound xanthophyll which undergoes structural changes in the de-epoxidation cycle, an accessible and loosely bound site, as is the case, would be preferable. The N1 site is of more mechanistic importance for LHCII than V1. Located next to helix C in the chlorophyll *b* concentrated area of LHCII, the most polar of the xanthophylls is required for the binding of more than two xanthophylls to LHCII (Croce *et al.* 1999a; 1999b). Dall'Osto *et al.*, (2006) however found that neoxanthin is not required to occupy the N1 site in order for LHCII to form trimers, yet LHCII was unable to without lutein. There are many reports alluding to the importance of lutein in LHCII form and function. The L1 and L2 sites that lutein occupies are located in the centre of the LHCII monomer, with their trans-configurations leading to the binding of both A and B central helices. The occupancy of such a central location can explain why several *in vitro* reports that support the *in vivo* results of Dall'Osto *et al.*, (2006), and demonstrate that lutein is required for LHCII trimerisation (Bishop, 1996; Polle *et al.*, 2001; Havaux *et al.*, 2004).

Xanthophylls play many diverse and important roles in green plants. Yet, despite the vast research conducted in the field of NPQ, the quantification of xanthophyll protectiveness has never been accomplished. The purpose of this chapter was therefore to try and quantify the contribution of each xanthophyll to NPQ.

6.2 Results

6.21 HPLC analysis confirms compositions of xanthophyll mutants

A number of *Arabidopsis* plants (Col-0) with different xanthophyll compositions were kindly generated and donated by Dr Luca Dall'Osto. See Table 2.01 for a list of abbreviations, and Table 6.01 for Fv/Fm and Chl *a*/*b* ratios of mutants used in this chapter. Prior to using plants for fluorescence experiments, high-performance liquid chromatography (HPLC) was carried out; this was to ensure that the seeds were composed of certain xanthophylls as described. HPLC was performed on chloroplasts that had been extracted intact, before being ruptured in liquid nitrogen and ultracentrifugated in 100% methanol to remove any accessory proteins (see Materials and Methods for further details).

A typical run using the reverse-phase HPLC LiChrospher 100 RP-18 column and Dionex Summit chromatography system is around 23 minutes. The most polar xanthophylls are excluded from the system first, so in a typical run (Fig 6.01) the xanthophylls are excluded in the order of neoxanthin, violaxanthin, antheraxanthin, lutein, zeaxanthin, chlorophyll *b*, chlorophyll *a* and finally β-carotene.

Indeed, all of the xanthophyll deficiencies were as previously recorded by Fiore *et al.* (2006), such as the *lute* plant here, which clearly only shows the one peak that can be clearly attributed to lutein (Fig 6.02). Table 6.02 shows the xanthophyll compositions of mutants used in this chapter. The percentage of each xanthophyll in each genotype was calculated as [mmol of a xanthophyll specie/(mmol of total xanthophylls)]*100. Three chloroplasts samples were used for each genotype, and three plants were used for a chloroplast sample. As was the case with Havaux & Niyogi (1999), only xanthophylls which were the focus of the research were presented. From the table it is evident that xanthophyll compositions were in line with those previously reported. Of the changes in xanthophyll concentrations, zeaxanthin is also the biggest changer. There were no traces of zeaxathin present after dark-adaptation, but with increases in this xanthophyll after exposure to light.

Genotype	Abbreviation	Xanthophyll composition	Fv/Fm	Chl *a*/*b*
lut2	*lut2*	NVZ	0.83±0.0	3.2±0.1
npq2	*npq2*	LZ	0.79±0.0	3.3±0.1
aba4npq1lut2	*viol*	V	0.80±0.0	3.8±0.2
chy1chy2lut5	*lute*	L	0.80±0.0	4.4±0.4
lut2npq2	*zea*	Z	0.75±0.0	3.0±0.1
WT	WT	LNVZ	0.83±0.0	3.3±0.0

Table 6.01 The xanthophyll composition of each plant: L, lutein; N, neoxanthin; V, violaxanthin, and Z, zeaxanthin. Fv/Fm measurements were performed on intact leaves after 45 min dark adaptation (SEM, n = 30 leaves). The chlorophyll *a*/*b* ratios extracted in 80% acetone according to Porra *et al.* (1989). (SEM, n = 3).

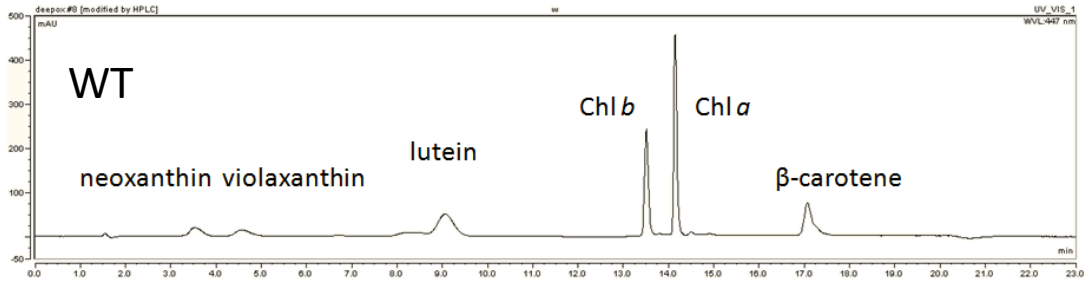

Figure 6.01 Typical reverse-phase HPLC profile of chloroplasts from the WT plant, using a LiChrospher 100 RP-18 column and Dionex Summit chromatography system (Ruban *et al.* 1994). Carotenoid identification was performed in 100% methanol.

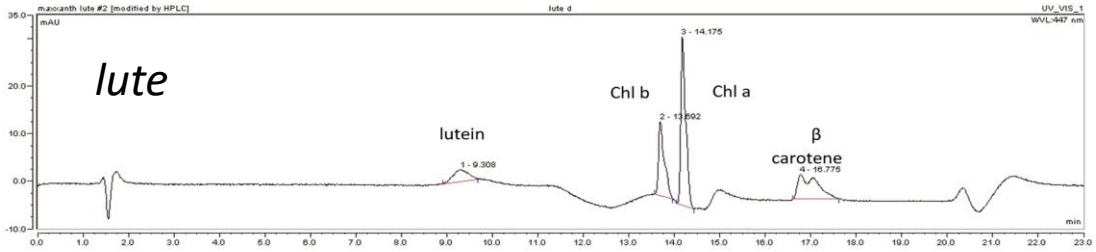

Figure 6.02 Typical reverse-phase HPLC profile of chloroplasts from the *lute* plant, using a LiChrospher 100 RP-18 column and Dionex Summit chromatography system (Ruban *et al.* 1994). Carotenoid identification was performed in 100% methanol (Ware *et al.*, 2016).

	Genotype	% violaxanthin	% zeaxanthin	% lutein
Dark adapted (1-hr)	WT	12.5	0	69
	lut2	76.5	0	0
	npq1	13.8	0	66.2
	npq2	0	42.6	57.4
	viol	100	0	0
	lute	0	0	100
	zea	0	100	0
Light adapted (800 µmol m^{-2} s^{-1})	WT	14.7	15.7	54.5
	lut2	62.9	21.6	0
	npq1	19.6	0	66.6
	npq2	0	65.6	34.4
	viol	100	0	0
	lute	0	0	100
	zea	0	100	0

Table 6.02 HPLC was performed on intact chloroplasts in 100% methanol. Xanthophyll percentages were calculated as [mmol of a xanthophyll specie/(mmol of total xanthophylls)]*100. Chloroplast preparations were performed from three plants of each genotype, with results from a single representative experiment. Violaxanthin, zeaxanthin, lutein and neoxanthin were the only xanthophylls measured, with violaxanthin, zeaxanthin and lutein used when expressing percentages, as these are the focus of this research and correspond to previous publications (Havaux & Niyogi, 1999).

6.22 Quantifying the effect of xanthophyll composition on ΦPSII

A gradually increasing actinic light procedure was used as previously described (as depicted in Fig 2.02, Fig 6.03). Applying this procedure to each genotype revealed some very striking patterns about the trends in NPQ protectiveness of certain xanthophylls (Fig 6.04 and 6.05A). Indeed, analysis of variance (ANOVA) testing showed that NPQ, pNPQ and qP_d parameters were significantly different between all species ($P < 0.0001$).

lut2 have the greatest degree of photodamage by the procedure end, represented by the greatest proportion of closed circles out of all the mutants. 500 µmol photons m^{-2} s^{-1} was required to cause the first signs of photodamage in the *lut2* genotype ($qP_d < 0.98$). No other mutant plant could have all leaves tolerate as great a light intensity without having any leaves become photoinhibited. The first light intensity to cause photodamage to all leaves was 820 µmol photons m^{-2} s^{-1} which is also the highest tolerance for all the mutants. Interestingly with the *lut2* mutant, there is very little difference between the highest pNPQ capacity and NPQ capacity. The maximum pNPQ of 2.2 is only 0.8 shorter than the 3.0 NPQ maxima. These pNPQ and NPQ values are higher than all others, except the WT which has a 0.6 higher pNPQ forming capacity (Fig 6.04A-F, Fig 6.05A)).

The single knock-out of zeaxanthin de-epoxidase (*npq1*) showed the first signs of RCII damage as 152 µmol photons m^{-2} s^{-1}, yet it took 740 µmol photons m^{-2} s^{-1} to damage 100% of leaves. *npq1* plants were able to form NPQ of 2.3, but only pNPQ up to 1.3. Therefore, the protective capacity of this mutant does not go as deep as *lut2*. This is reflected in the fact that 90% of leaves have more than 10% of RCII permanently closed at 1500 µmol photons m^{-2} s^{-1}.

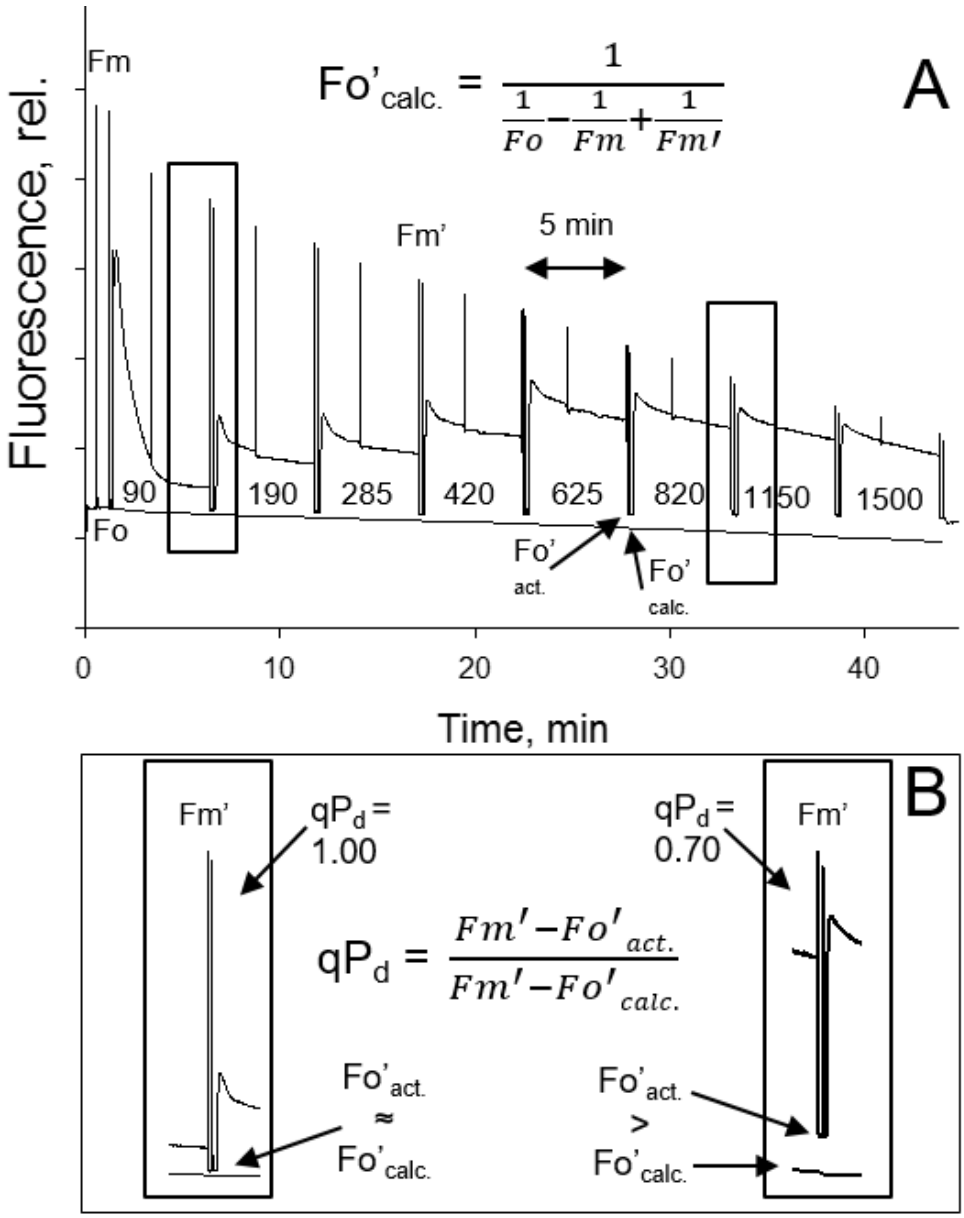

Figure 6.03 A Typical high light acclimated plant chlorophyll fluorescence scheme of induction with an eight-step increasing actinic light (AL) routine (as depicted in Fig 2.02). In this example 0, 90, 190, 280, 420, 625, 820, 1150, 1500 µmol m^{-2} s^{-1} AL intensities were used. B Zoomed in region of the fluorescence scheme (A) illustrating the timing and application of 625, 820 and 1150 µmol m^{-2} s^{-1} AL (upward arrow and downward arrow demonstrate the turning of AL on and off respectively), along with saturating pulses (SP, P1, P2, P3). P1 indicates an SP in the dark, or after 10 sec of far red (FR) light, P2 during AL illumination, and P3 at the end of AL. The difference between $Fo'_{act.}$ and $Fo'_{calc.}$ is determined at P1, and subsequently used to calculate qP_d (Ware *et al.*, 2016).

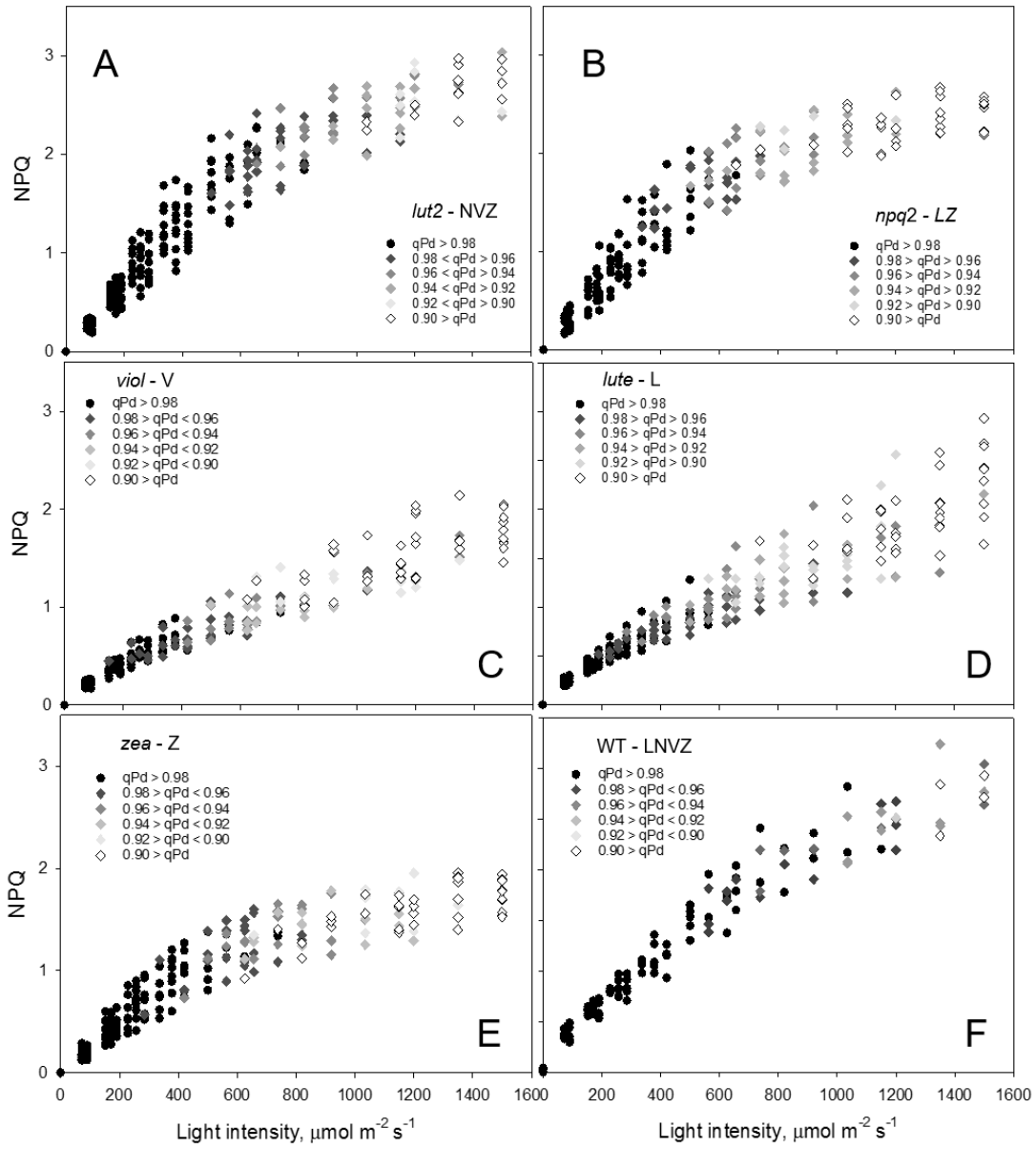

Figure 6.04 A 3-dimensional representation of the openness of reaction centers, with the corresponding protectiveness of NPQ and actinic light intensity. Black circles represent leaves where 98-100% of reaction centers are open at a particular light intensity; here NPQ is protective (pNPQ). Greyscale rhomboids represent the degree of reaction center closure. 30 repeats were conducted for each genotype. (A) *lut2* – no lutein, (B) *npq2* – no violaxanthin and neoxanthin, (C) *viol* – violaxanthin only, (D) *lute* – lutein only, (E) *zea* – zeaxanthin only, (F) WT – wild type (Ware *et al.*, 2016).

The final single knock-out of one xanthophyll was *npq2*. The constitutive zeaxanthin expresser is able to form NPQ of 2.7 and pNPQ of 2.0 (Fig 6.04B). The constitutive zeaxanthin expression might have contributed the tolerance of the relatively high 378 µmol photons m^{-2} s^{-1}, and it took 656 µmol photons m^{-2} s^{-1} to close all the RCII in all leaves tested. *viol* plants are able to form NPQ of over 2.0, yet had the lowest maximum pNPQ capacity of 1.1. All leaves had over 10% RCII closure by 1500 µmol photons m^{-2} s^{-1}, this was the only genotype to suffer photodamage to such a degree. It is not just the degree of damage at the procedure end when the damage is more pronounced, 152 µmol photons m^{-2} s^{-1} is enough to cause the first signs of photoinhibition, the lowest of all studied (Fig 6.04C). This behaviour is different even to *npq4* (no PsbS) plants, which although slow in forming pNPQ, they were able to protect plants into the very high light intensities, even though they were slow in forming pNPQ.

Despite a clearly visible greater NPQ capacity at the higher light intensities of the *lute* genotype compared to the viol, pNPQ and qP_d values were similar. Although the minimum light intensity to cause photoinhibition in all leaves was higher in the *lute* plants, 190 µmol photons m^{-2} s^{-1} is the second lowest light intensity to induce RCII closure in any leaf of all genotypes tested. Indeed, *lute* plants have a low pNPQ capacity yet of 1.3, but a much higher NPQ maximum of 3.0 (Fig 6.04D). The gulf between these types of NPQ would be an interesting future research topic. Why the NPQ capacity is much greater at the high light intensities compared to *viol* and *zea* plants, yet limited at low light intensities and unable to stop the earliest signs of photodamage, could be an interesting avenue of future research. It seems to be a similar story to the *npq4* plants (Ware *et al.*, 2014). The lack of zeaxanthin appears to be a problem in initiating the NPQ process, but lutein seems to encourage a deep NPQ when expressed instead of violaxnathin or zeaxanthin. PsbS is also required for a quick NPQ initiation, but high quenching capacities can be achieved without it.

The final mutant, *zea*, is completely protected to 285 µmol photons m^{-2} s^{-1}, and a high 738 µmol photons m^{-2} s^{-1} is required to close RCII in all leaves. Upon reaching this light intensity, there is almost no increase in NPQ, a stark contrast to lute. This is reflected in the little difference between its pNPQ maxima of 1.4 and NPQ of 2.0.

The most tolerant of all the xanthophyll composition plants tested was the one with the complete set, the WT. All leaves were free from photoinhibition until 562.2 µmol photons m^{-2} s^{-1}, and had the highest light tolerance for any leaf with 1150 µmol photons m^{-2} s^{-1}. The NPQ formed was 3.2, which is only 0.1 higher than the highest mutant, as mentioned, the 2.8 pNPQ was 0.6 higher than the next genotype. The plant with the smallest difference between pNPQ and NPQ maxima had the lowest degree of photodamage, represented by the amount of open diamonds (qP_d < 0.9) by the procedure end, and shows again the importance of absolute pNPQ capacity (Ware *et al.*, 2014; Carvalho *et al.* 2015).

qP_d and NPQ both have an effect on ΦPSII, the latter of which is quickly reversible, the former of which takes hours. Two ΦPSII are calculated to take this into account, $ΦPSII_{act.}$ and $ΦPSII_{theor.}$, whereby in the latter, only NPQ is taken into consideration. However, with the true ΦPSII, the minimum amount of pNPQ is the desired outcome, as RCII closure is also factored in. With *npq1* plants, qP_d dropped below 0.98 when NPQ was 0.95, whereupon the two ΦPSII deviated. The $ΦPSII_{theor.}$ average was the joint highest with 0.6 by procedure end (Fig 6.05B). This NPQ in this genotype was not that protective however, and $ΦPSII_{act.}$ was 0.53 on average at the procedure end. Other single knock-outs, *lut2* and *npq2*, have lower $ΦPSII_{act.}$ and $Φ$ $PSII_{theor.}$ than *npq1* (Fig 6.06A and B). In fact, *npq2* plants have significantly lower $ΦPSII_{act.}$ than the single xanthophyll mutants *viol* and *lute* (*t*-test; P < 0.001). *npq2* plants $ΦPSII_{act.}$ was only 0.45, whereas *lut2* plants have 0.52.

Reflected in the lowest pNPQ forming capacity yet, *viol* plants were the only other mutant beside *npq1* to have a $PSII_{theor.}$ average above 0.6 (Fig 6.06C). The higher NPQ in *lute* plants compared to *viol* plants (Fig 6.06C and D) manifested in a lower $Φ$ $PSII_{theor.}$, and despite having a higher qP_d at procedure end, *lute* plants also have a lower $ΦPSII_{act.}$ than *viol* plants. The marginally higher average pNPQ was not therefore able to transfer into a greater photosynthetic capacity at 1500 µmol photons m^{-2} s^{-1}. The final mutant, *zea*, has the joint lowest $ΦPSII_{act.}$ with 0.45. This is the result of a large decline in qP_d by procedure end, and a significantly lower Fv/Fm at the start of the routine (P < 0.05). Despite a higher pNPQ average than *viol*

and *lute,* these results coupled together indicate poor photosynthetic performance in high light intensities for zeaxanthin only plants.

The best performing plant, with the both the highest Φ $PSII_{theor.}$ and $\Phi PSII_{act.}$ was the WT. With an average pNPQ of 2.1, this was the highest of any of the plants (Fig 6.06F). As displayed in Fig 6.06F, there is little disparity between the average pNPQ and NPQ maxima. This resulted in very little decline in qP_d, and both these factors resulted in the smallest deviation of any genotype between the two ΦPSII's. The final factor contributing to the high photosynthetic rate was the Fv/Fm average being above 0.8. Therefore, as well as having the least RCII damage, WT has the highest performing plant upon exposure to high light.

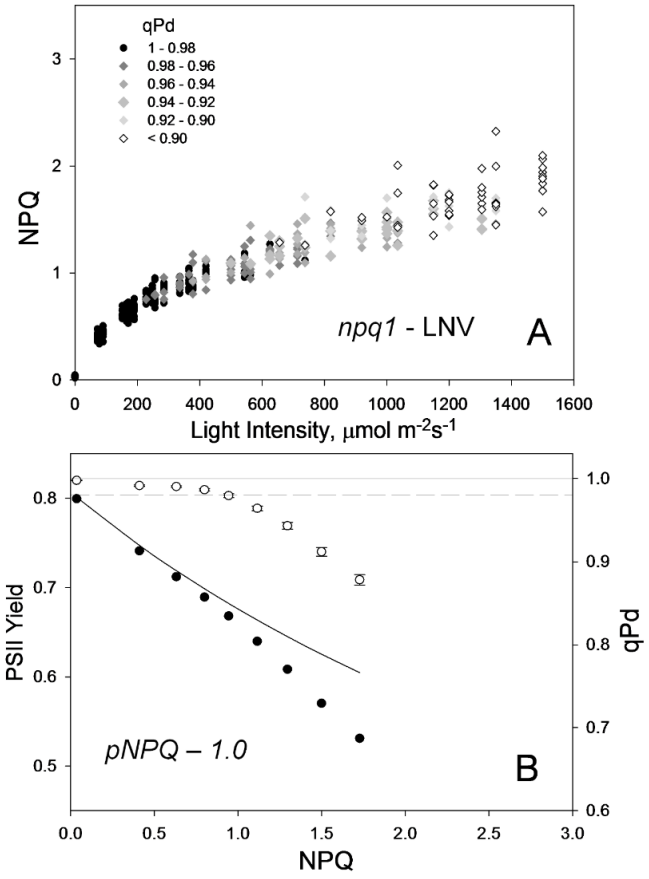

Figure 6.05A Relationship between light intensity and NPQ, and the subsequent effect on qP_d for 40 *npq1 Arabidopsis* intact leaves. Data points were taken during the fluorescence routine explained in Fig. 6.03. The Figure key explains the grayscale relationship of symbols to qP_d. B Relationship between NPQ, PSII actual yield (closed circles) and qP_d (open circles). At each light intensity NPQ and qP_d data points were taken from Fig. 2A and averaged. Error bars show the SEM (n = 40). The theoretical yield (continuous line) was calculated using qP_d as equal to 1.00 (Ware *et al.*, 2014).

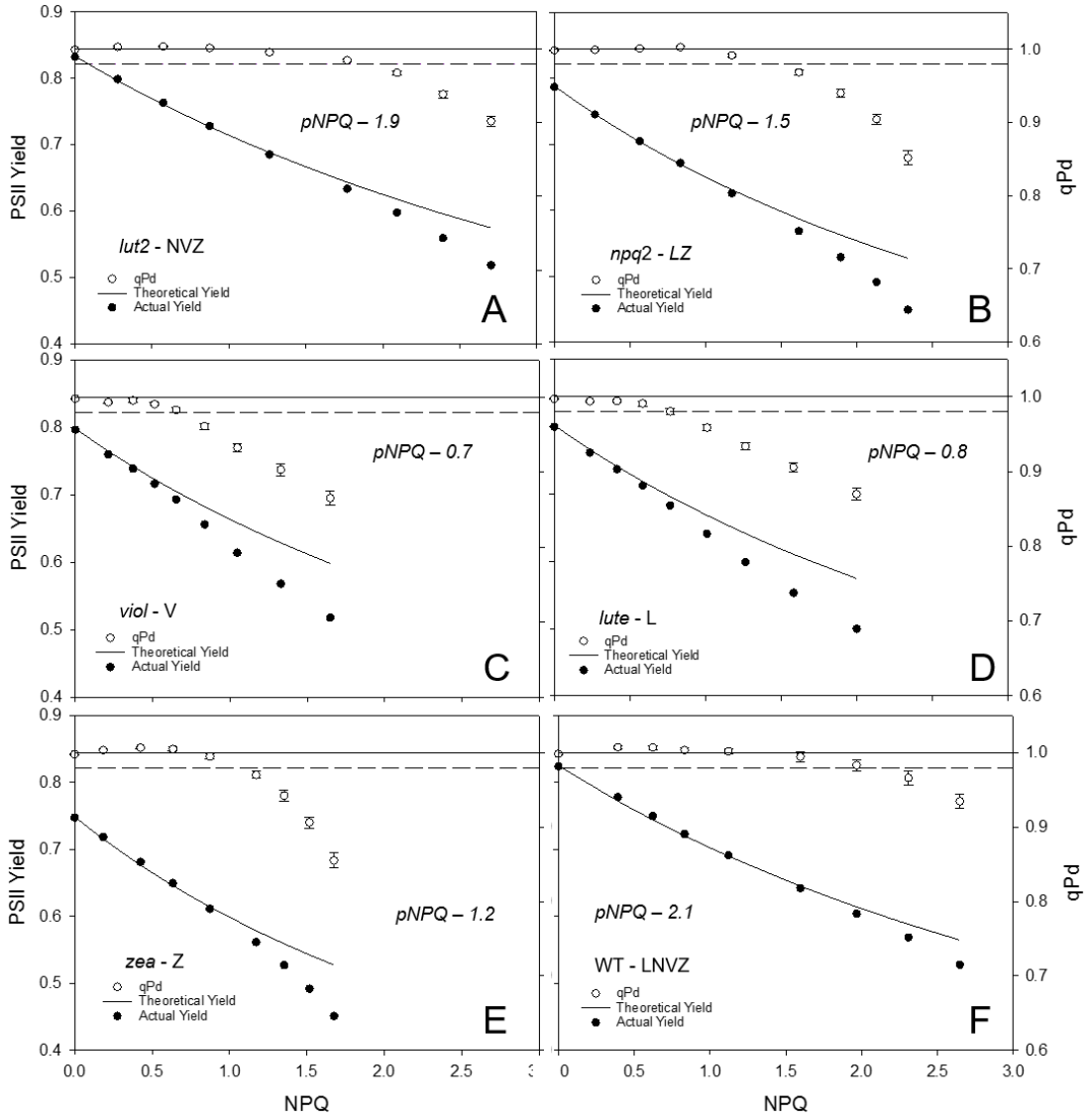

Figure 6.06 displays the actual (closed circles) and theoretical (black line) yields of PSII (ΦPSII) in function of NPQ and qP_d. In the theoretical yield calculation, qP_d is always equal to 1.00 (open circles, see Materials and Methods). Data points are the average of 30 repeats conducted on whole intact leaves using the pNPQ assessment procedure (Fig 6.03). Error bars represent the standard error of the mean. (A) *lut2* – no lutein, (B) *npq2* – no violaxanthin and neoxanthin, (C) *viol* – violaxanthin only, (D) *lute* – lutein only, (E) *zea* – zeaxanthin only, (F) WT – wild type (Ware *et al.*, 2016).

6.23 Calculating the phototolerance of xanthophyll mutants

The most accurate way of determining the phototolerance is by constructing leaf population light tolerance curves (Fig 6.07). This involves plotting the percentage of leaves with some degree of photodamage ($qP_d < 0.98$) against the corresponding light intensity (Figs6.04-05A) and extrapolating the data points, using a sigmoidal regression fitting (SigmaPlot 12.0; sigmoidal, Hill, three parameter; $f=ax^b/c^b+x^b$). This then allows the light intensity which causes photoinhibition in any percentage of leaves to be worked out, which in this case was 50% of leaves.

The light intensities causing the first signs of photoinhibition in 50% of leaves is significantly different between all the genotypes here (ANOVA; $P < 0.00001$). The point of 50% photoinhibition was also significantly different between all genotypes (*z*-test; $P < 0.01$), except for tests between *viol, lute* and *npq1* plants, which were not significantly different (*z*-test; $P > 0.05$). The 415, 410 and 400 µmol photons m^{-2} s^{-1} correspondingly required to close partially close 50% of leaves in these mutants (Figs 6.07C, D and 6.08), means that all three have the worst light tolerance capacities of all the plants tested here. WT plants were again the best performing genotype and required 750 µmol photons m^{-2} s^{-1} before 50% of leaves showed the first signs of photodamage (Fig 6.07F). *lut2* was the most tolerant of all the mutants, with 615 µmol photons m^{-2} s^{-1} required to close RCII's in 50% of leaves (Fig 6.07A), with *npq2* and *zea*'s corresponding 575 and 535 µmol photons m^{-2} s^{-1} showing them to be the next most tolerant plants (Fig 6.07B, C).

As was the case with PsbS concentration, it is important to see whether the absolute pNPQ capacity is the most important factor conferring phototolerance. Fig 6.09 shows the relationship between maximum pNPQ capacity and the light intensity which induces photodamage in 50% of leaves. This weakly positive correlation relationship indicates the same conclusions as was previously found (Ware *et al.*, 2014; Carvalho *et al.*, 2015), and again points to pNPQ capacity as being the paramount factor in photoprotection.

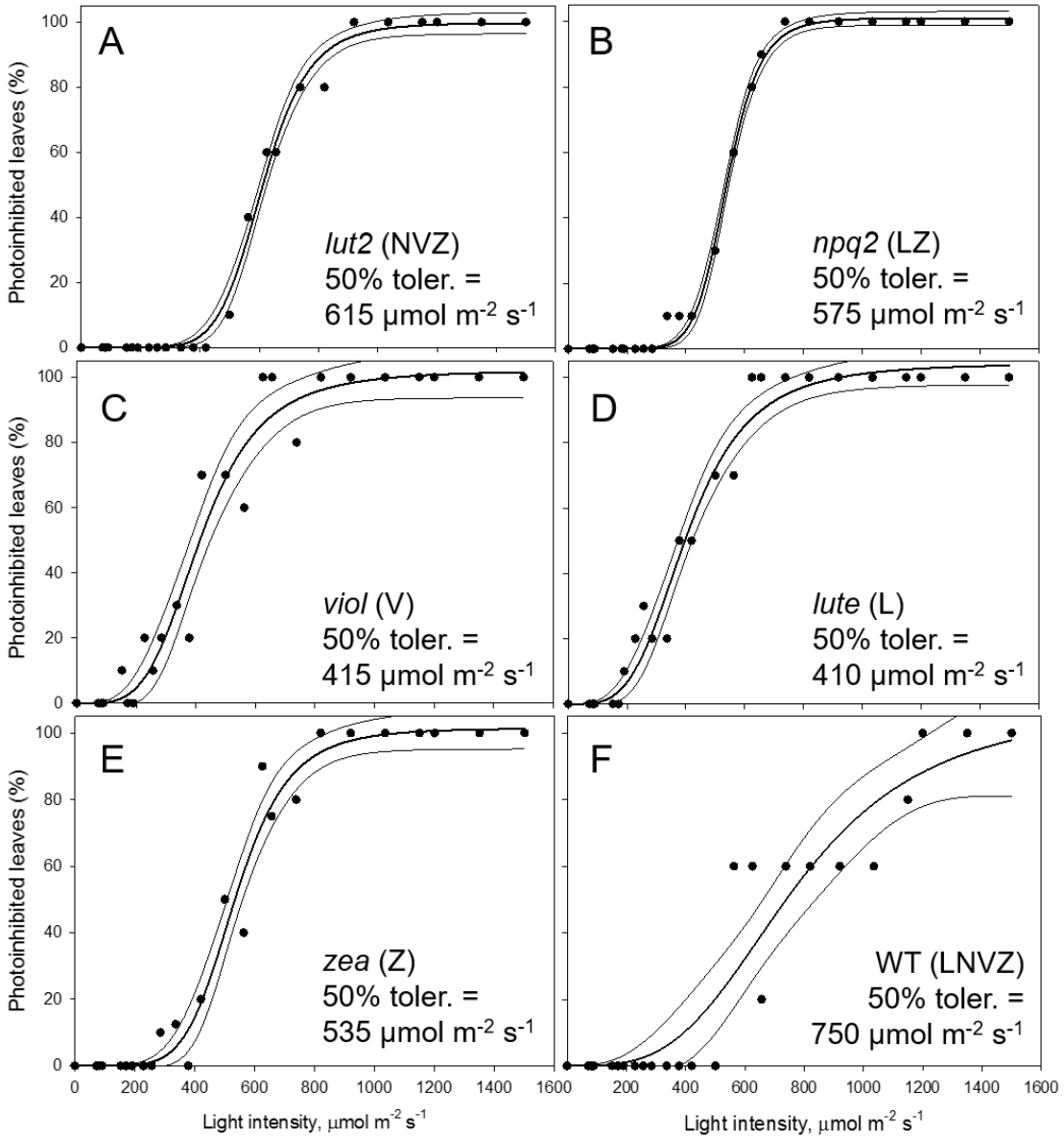

Figure 6.07 Leaf population tolerance curves calculated using the pNPQ assessment procedure. Each closed circle represents the percentage of closed reaction centers at each actinic light intensity. The % of photoinhibited leaves was calculated from Fig. 6.04 as 100×Nrhombs/Ntotal. Regression analysis and 95% confidence intervals were performed using SigmaPlot12.0 (Sigmoidal fit, Hill 3 parameter, f = a*x^b/[c^b+x^b]) (A) *lut2* – no lutein, (B) *npq2* – no violaxanthin and neoxanthin, (C) *viol* – violaxanthin only, (D) *lute* – lutein only, (E) *zea* – zeaxanthin only, (F) WT – wild type (Ware *et al.*, 2016).

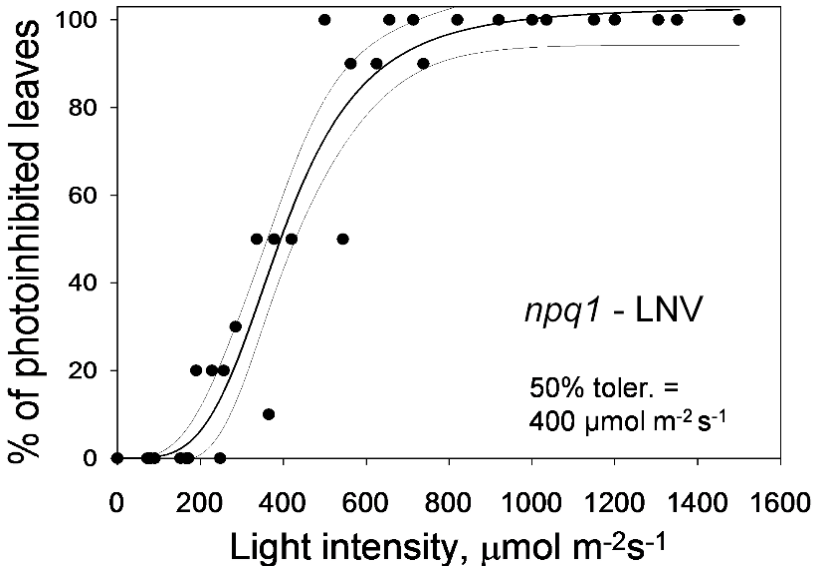

Figure 6.08 Relationship between the percentage of photoinhibited leaves and light intensity for *npq1 Arabidopsis* plants. Data points are derivatives from Fig. 6.05. Lines represent regression fit curves (Sigmoidal, Hill, 3 Parameter; f =axb/cb+xb)) with 95% confidence values plotted using SigmaPlot12 (Systat Software, Inc., Chicago, USA) (Ware *et al.*, 2014).

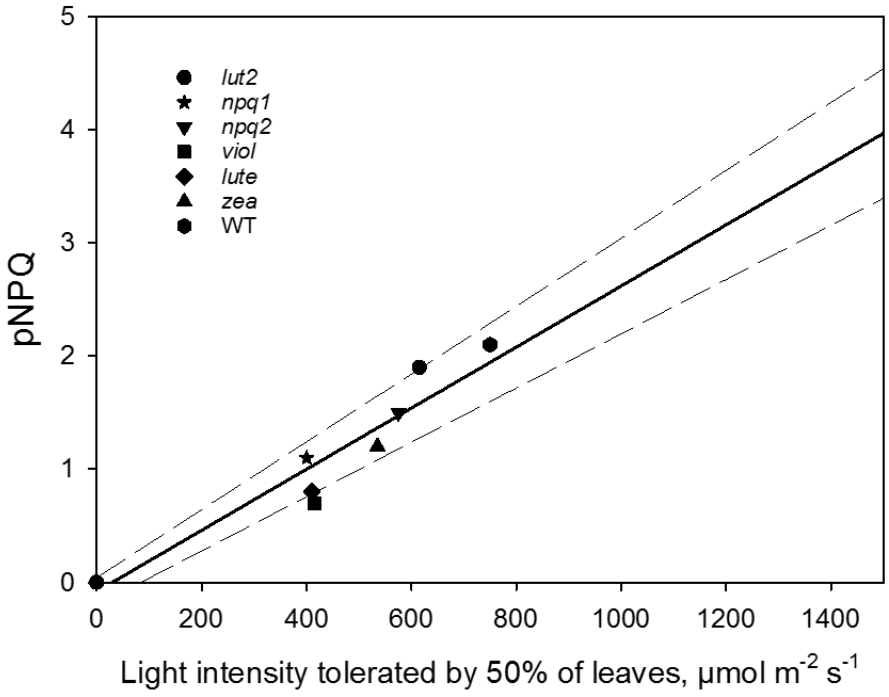

Figure 6.09 The pNPQ value which protects each genotype, taken from Figs. 6.05B and 6.06, and the light intensity which causes photoinhibition in 50% of leaves for that genotype. Regression analysis was performed using SigmaPlot 12.0 (Linear, f = y0+a*x). *lut2* – no lutein, *npq1* – no zeaxanthin, *npq2* – no violaxanthin and neoxanthin, *viol* – violaxanthin only, *lute* – lutein only, *zea* – zeaxanthin only, WT – wild type.

Albeit a slightly crude method of establishing the most important xanthophyll for light tolerance, Table 6.03 allows for the direct comparison between different xanthophyll composition mutants, and the average light intensity tolerated by each xanthophyll. This shows that, of the xanthophylls studied, that zeaxanthin is the most important xanthophyll for light tolerance. The average light intensity which causes photoinhibition in 50% of leaves that contain zeaxanthin is ~620 µmol photons m^{-2} s^{-1}. Rather surprisingly, given the documentation supporting the hypothesis that lutein is the primary quencher of excess energy (van Grondelle and Novoderezhkin, 2006; Ruban *et al.*, 2007; Wentworth *et al.*, 2003), it seems to be less important in conferring phototolerance than violaxanthin. However, there is one big factor that needed to be investigated before this conclusion could be made. In the introduction, the structural roles of xanthophylls was listed as one of their major functions. There have been numerous reports also, that detail the requirement of lutein for the correct organisation of LHCII. Therefore, using the data already obtained, a number of other parameters were investigated to see whether this is also an important variable here.

		Xanthophyll		
		lutein	zeaxanthin	violaxanthin
Genoptype	WT	750	750	750
	lut2		615	615
	npq1	400		400
	npq2	575	575	
	viol			415
	lute	410		
	zea		535	
	Total	533.75	618.75	545

Table 6.03 Relationship between the light intensity (µmol photons m^{-2} s^{-1}) which induces photoinhibition in 50% of leaves of *lut2* – no lutein, *npq1* – no zeaxanthin, *npq2* – no violaxanthin and neoxanthin, *viol* – violaxanthin only, *lute* – lutein only, *zea* – zeaxanthin only, WT – wild type plants.

6.24 A varied lutein composition impairs electron flow

As well as the NPQ, pNPQ and qP_d parameters which were measured during the course of the procedure, a number of other useful ones were calculated alongside these. Relative electron transport rates (ETR) offer an insight into the amount of photons which are absorbed by light harvesting pigments, that go on to generate electrons and photochemical by-products. Thus, ETR gives a lot of useful information about the rates of photochemistry in each mutant plant. ETR were measured in the light phase of the pNPQ assessment procedure (Fig 6.10A), at the point when NPQ is also measured (Fig 6.03). The results show a clear difference between plants with lutein mutations compared to other xanthophylls. It is perhaps not surprising the *lut2* plants have a lower ETR than WT and almost all other xanthophylls, given the reported retardation of LHCII in these mutants (Dall'Osto *et al.*, 2006). A change in protein structure may perturb the photon and electron transfer pathways, and the result here seems to support this idea. It may be surprising though, that the one plant with a lower ETR than *lut2*, was the *lute* plant, and it was significantly lower (*z*-test; $P < 0.05$). Sole expression of lutein does also have an effect on LHCII structure as well, and of all the plants tested, the leaves on the plant with this genotype were much smaller than any other, as was the case with Dall'Osto *et al.* (2006). Therefore, a similar explanation as with the *lut2* plants is possible here. There were no significant differences between the *viol, npq2* and *zea* ETR rates (*z*-test; $P > 0.05$), but *npq1* plants had significantly reduced ETRs compared to *viol* and *zea* plants (*z*-test; $P < 0.05$), but there was not a significant difference between *npq2* and *npq1* ETRs. This result would add evidence to the idea that violaxanthin/zeaxanthin do not play much of a structural role in LHCII, but owing to their location on the periphery of the protein complex, their main role is to convert between the light harvesting and light quenching forms. WT plants, as well as having the highest pNPQ and light tolerance capacities, they also have significantly higher ETR and photochemistry rates (*z*-test; $P < 0.05$).

The final parameter taken into consideration during the pNPQ assessment procedure is excitation pressure, measured via the 1-qP parameter. As with the ETR and NPQ parameters, this is measured during the illumination phase of the

procedure. The 1-qP parameter gives a quantum coefficient of the number of RCII closed during illumination. Whereas qP_d shows the number open after the removal of light, 1-qP also incorporates those RCII which are temporarily saturated, as well as those permanently closed. The two factors which minimise excitation build up are pNPQ and high rights of photochemistry. The 1-qP parameter therefore offers a valuable insight into the efficiency of light harvesting during illumination by the different genotypes.

As WT plants had the highest pNPQ and ETRs, it is not surprising that Fig 6.10B shows WT plants to have the lowest excitation pressure in the membrane. From ~100 µmol photons m^{-2} s^{-1}, the WT has a lower excitation pressure, which continually decreases compared to all other mutants until it reaches the greatest difference at 1500 µmol photons m^{-2} s^{-1}. At the final light intensity of the procedure, 1-qP is significantly lower than all mutants (*z*-test; $P < 0.001$). Even the overall rate of 1-qP accumulation from 0-1500 µmol photons m^{-2} s^{-1} is significantly lower in the WT compared *lut2*, *lute, npq1* and *viol* plants (*z*-test; $P < 0.01$). In contrast to this, the *lute* plants had a significantly higher average excitation pressure over the course of the procedure than all other plants (*z*-test; $P < 0.05$). There are then two other distinct groups of xanthophylls based on excitation pressure. *lut2*, *npq1* and *viol* plants have similar trends of excitation pressure accumulation up to ~1000 µmol photons m^{-2} s^{-1}. The final two mutants, *zea* and *npq2*, also display a very similar trend in increasing 1-qP. Upon reaching ~1000 µmol photons m^{-2} s^{-1}, there appear to be two different group trends. Taking this observation into account, an extrapolation by regression analysis from 1500 to 2500 µmol photons m^{-2} s^{-1} was performed, and the results supported the initial observations.

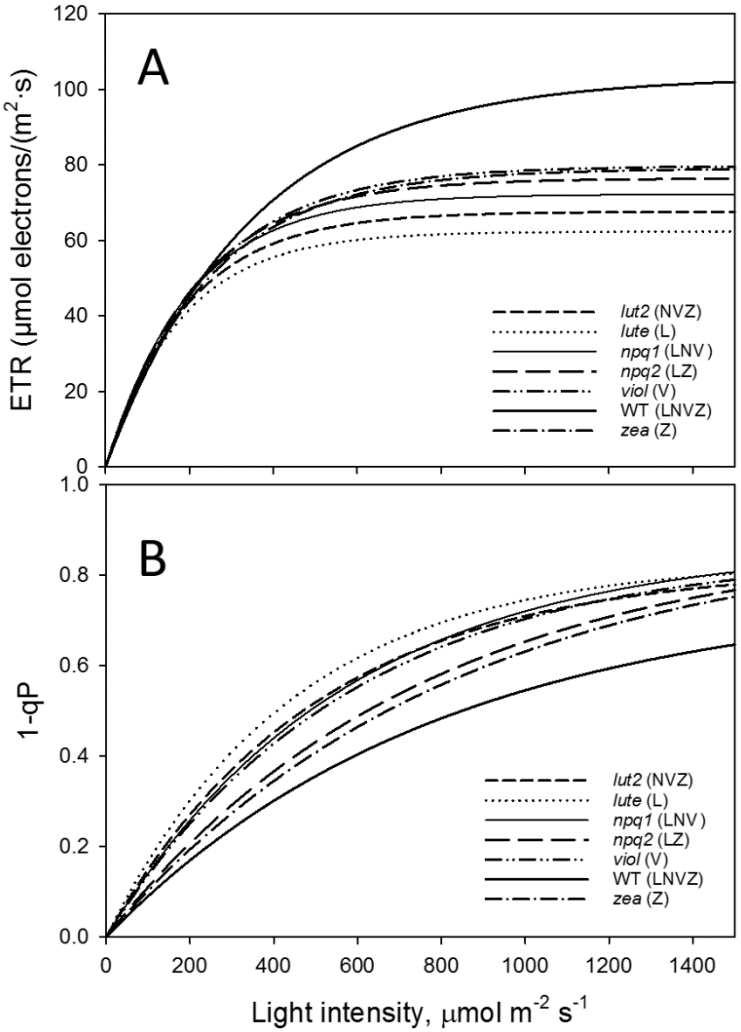

Figure 6.10A Electron transport rates (ETR) and (B) excitation pressure (1-qP) taken from the 2nd saturating pulse after each 5 min actinic light (AL) illumination period (see Fig. 6.03A). Regression analysis was performed using SigmaPlot12 (Exponential Rise to Maximum, Single 2 Parameter, f = a*[1-exp(-b*x)]). Data points are the average of 10 independent experiments (n=10). Fig 6.10B Regression analysis was performed using SigmaPlot12 (Exponential Rise to Maximum, Single 2 Parameter, f = a*[1-exp(-b*x)]). Data points are the average of 10 independent experiments (n=10).

Fig 6.11 shows the extended plots of energy accumulation in the plants. A reason for extending the plot theoretically rather than using higher AL values was due to one of the limiting factors of the pNPQ assessment procedure. With the JUNIOR-PAM, there are set intervals between actinic light values. Although the device can be manually increased from 1500 to 2500 µmol photons m^{-2} s^{-1}, it would mean that the procedure would not use the same gradually increasing AL values as was used here. Furthermore, it would mean that only one 1-qP value between 1500 and 2500 µmol photons m^{-2} s^{-1} would be applied, which would not offer much more information than the theoretical extension excitation pressure. Indeed, the additional AL values would be at 1900 µmol photons m^{-2} s^{-1}, and this would still leave a large gap between 1900 and 2500 µmol photons m^{-2} s^{-1}, and this would require careful fitting anyway.

What the results do confirm though is that the *lute* and *lut2* plants have reduced excitation pressure at the highest light intensities (Fig 6.11). It might seem strange that the plants with only lutein or conversely no lutein have the smallest excitation pressure, but they do have a common feature, and that is the retardation of LHCII. The smaller protein complexes may be not be able to absorb as much light as intact LHCII timers. This might explain why the WT and de-epoxidase mutants have a steeper rising excitation pressure beyond 1500 µmol photons m^{-2} s^{-1}, that the *lute* and *lut2* mutants. Furthermore, it illustrates that the structural roles that xanthophyll's play are essential for LHCII function. Swapping xanthophyll's to improve the photoprotection of plants cannot be achieved without significant reorganisation of the proteins they are bound to. This limits the effectiveness of this approach to improving the photoprotective capacities of mutant plants, as the pNPQ capacities and ΦPSII are seriously undermined. However, protein complex variations seem to be independent from pNPQ behaviour, as the ratios in Table 6.04 do not match those of Table 6.03. Therefore, this work appears to have only scratched the surface on the complex relationships between xanthophyll composition, membrane organisation and photoprotection.

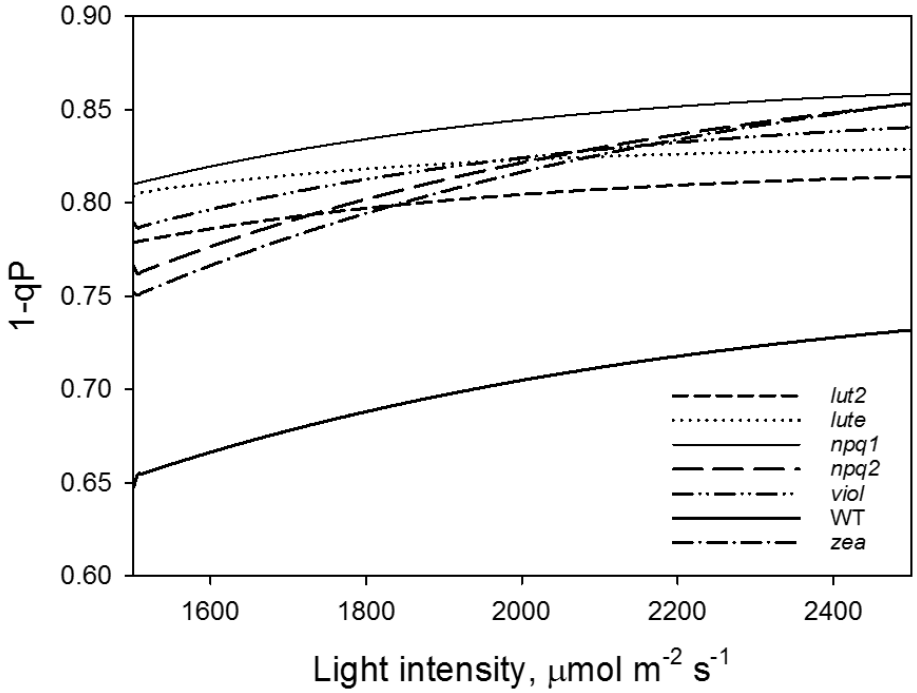

Figure 6.11 An extrapolation of Fig 6.10B, where the excitation pressure was recorded at each 2nd saturating pulse after each 5 min actinic light (AL) illumination period (see Fig 6.03). Regression analysis was performed using SigmaPlot12 (Exponential Rise to Maximum, Single 2 Parameter, f = a*[1-exp(-b*x)]). *lut2* – no lutein, *npq1* – zeaxanthin only; *npq2* – no violaxanthin and neoxanthin, *viol* – violaxanthin only, *lute* – lutein only, *zea* – zeaxanthin only, WT – wild type.

Genotype	PSI/PSII	LHCII/PSII
lut2	112 (±19)	97 (±13)
npq2	73 (±9)	89 (±14)
viol	101 (±14)	97 (±7)
lute	53 (±11)	69 (±18)
zea	41 (±11)	48 (±5)
WT	100 (±12)	100 (±8)

Table 6.04 PSI-LHCI, PSII core and LHCII content were evaluated upon solubilisation of thylakoids with 0.4% α-DM and fractionation of pigment-protein complexes by non-denaturing Deriphat-PAGE. PSI/PSII and LHCII/PSII ratios were normalised to the corresponding WT values. (Ware *et al.*, 2016).

6.25 Visualising reaction center damage at rosette level

The dependency of pNPQ and qP_d on leaf age and position in the canopy was previously documented (Chapter 4, Carvalho *et al.*, 2015). Therefore, it is important to be consistent when selecting leaves to test with the JUNIOR-PAM. In light of this, the pNPQ assessment procedure was adapted to be used with the IMAGING-PAM. This apparatus illuminates the whole leaf area, and presents the NPQ and qP_d parameters over a spectrum of colours, which creates a novel picture of photoinhibition across the whole rosette. Fig 6.12 shows the values qP_d over the whole rosettes. With purple and grey colours illustrating the highest qP_d values, and blue/green representing greater degrees of photodamage, it is apparent that *lut2* and *lute* plants (Fig 6.12) have the lowest qP_d values. WT plants again have the highest qP_d value at procedure end, and photodamage is homogeneous across the leaf types. *zea*, *npq2* and *viol* rosettes are progressively more blue/green, which indicates reduced phototolerance in these genotypes compared to the WT.

The most striking result of the IMAGING-PAM experiments is the NPQ capacity of each genotype. Fig 6.13A shows a remarkable and unique pattern of NPQ formation in the *lut2* plant. There is a clear disparity between the amount of NPQ formed in the outer leaves compared to leaves in the centre of the rosette. The younger leaves of this mutant are only able to form around half of the NPQ in the outer and older leaves. All mutants had reducing quenching capacities in the inner leaves, but not to the same extent of the lutein deficient plant (Fig 6.12 and 13). Despite the vast care taken to ensure that similar leaves were chosen in each experiment, the heterogeneity of the *lut2* canopy cannot be excluded as a contributing factor to the reduced ETR and increased 1-qP of *lut2* plants (Fig 6.12). As the images do show pronounced differences in NPQ within the rosettes of *lut2* plants, with more time, exploring the age-dependent role of lutein in these and other mutants would have been an interesting avenue of research. Unfortunately, there was not enough time to pursue this result further. However, the results of the IMAGING-PAM experiments did add support to the conclusions of Carvalho *et al.* (2015), and leaf age and type should be taken into consideration when performing fluorescence measurements.

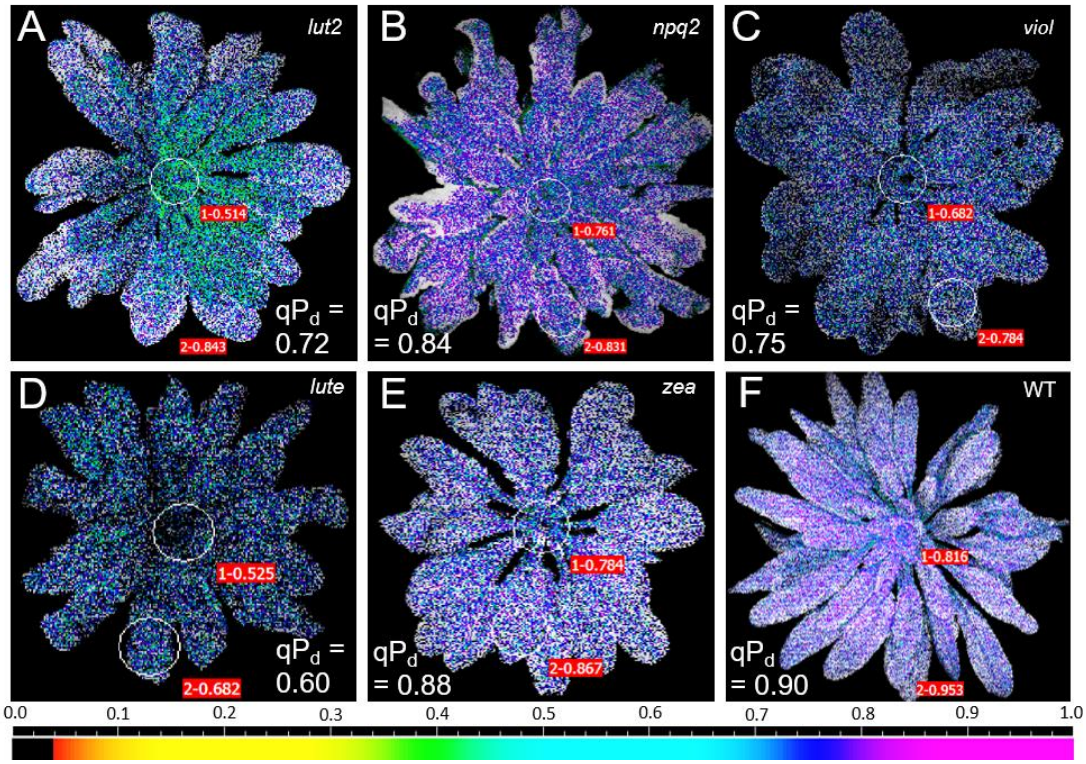

Figure 6.12 pNPQ assessment procedure performed using an IMAGING-PAM (Walz, Effeltrich, Germany). Actinic light intensities of 0, 81, 186, 281, 396, 611, 801, 1076, 1250 µmol m^{-2} s^{-1} were used. Fluorescence image represents the average qP_d value for the whole leaf area at 1250 µmol m^{-2} s^{-1}. *lut2* – no lutein, *npq2* – no violaxanthin and neoxanthin, *viol* – violaxanthin only, *lute* – lutein only, *zea* – zeaxanthin only, WT – wild type. White circles are 9mm, indicating that WT plants are the largest at 50 days old and *lute* the smallest (Ware *et al.*, 2016). A key difference in the IMAGING-PAM procedure compared to the DUAL-PAM and JUNIOR-PAM procedures is the lack of a FR light dark period. Due to the lack of a FR light function in the IMAGING-PAM, a 30 second dark period was employed to relieve the excitation pressure from the previous AL intensity, before proceeding with the next AL step. The scale represents 0-1.00 for qP_d.

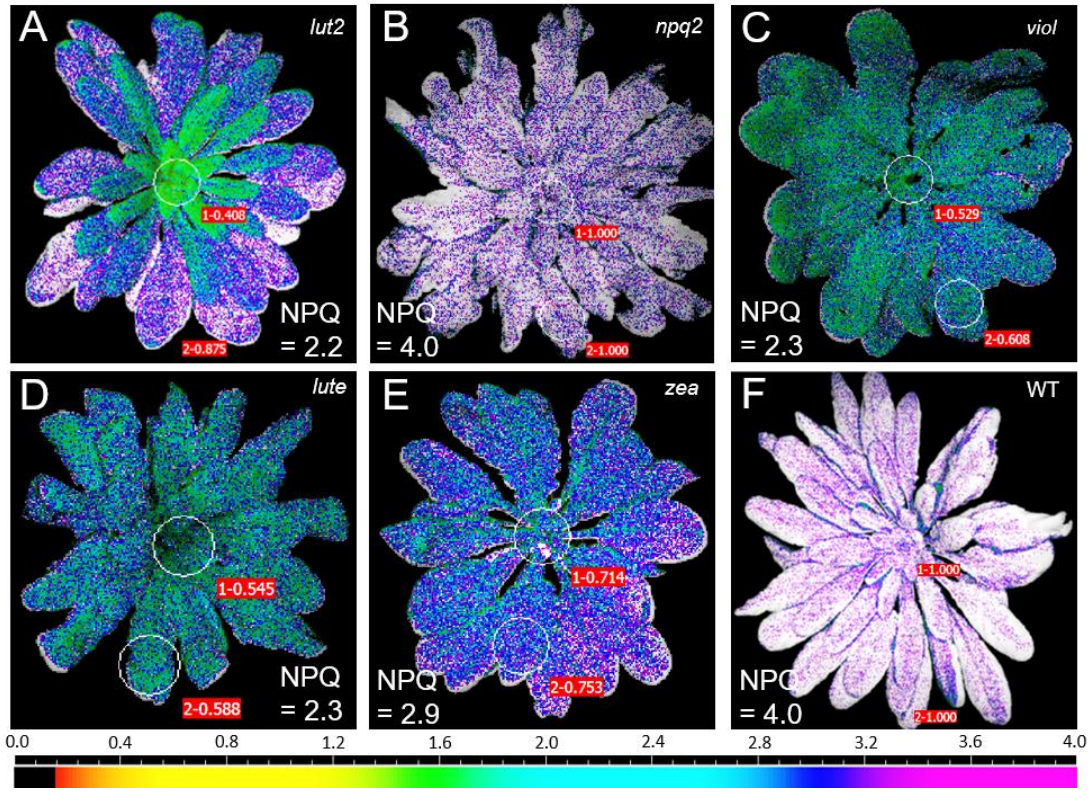

Figure 6.13 pNPQ assessment procedure performed using an IMAGING-PAM (Walz, Effeltrich, Germany). Actinic light intensities of 0, 81, 186, 281, 396, 611, 801, 1076, 1250 µmol m^{-2} s^{-1} were used. Fluorescence image represents the average NPQ value for the whole leaf area at 1250 µmol m^{-2} s^{-1}. *lut2* – no lutein, *npq2* – no violaxanthin and neoxanthin, *viol* – violaxanthin only, *lute* – lutein only, *zea* – zeaxanthin only, WT – wild type. White circles are 9mm, indicating that WT plants are the largest at 50 days old and *lute* the smallest (Ware *et al.*, 2016). A key difference in the IMAGING-PAM procedure compared to the DUAL-PAM and JUNIOR-PAM procedures is the lack of a FR light dark period. Due to the lack of a FR light function in the IMAGING-PAM, a 30 second dark period was employed to relieve the excitation pressure from the previous AL intensity, before proceeding with the next AL step. The scale represents 0-4.00 for NPQ.

6.3 Discussion

- Plants with different xanthophyll compositions were assessed for phototolerance capacities via chlorophyll fluorescence.
- WT plants were demonstrated to have the highest phototolerance capacity, the highest ΦPSII and the highest pNPQ capacity.
- Of the three groups of mutants, plants expressing lutein, violaxanthin and/or zeaxanthin, the ones expressing zeaxanthin has the highest phototolerance.
- Of the mutant plants tested, *lut2* and *viol* plants had the joint highest ΦPSII, with *lut2* plants also having the highest light tolerance capacity.
- WT plants, followed by single knock-out mutants, then multiple knock-outs had the highest photoprotective capacities.
- Structural changes to LHCII manifested in altered Chl *a*/*b*, PSI/PSII and LHCII/PSII ratios, with *zea* plants having significantly smaller antenna sizes than all mutants.
- The mutants with smaller antenna sizes have increased excitation pressure (1-qP) compared to the WT.
- WT plants have the highest ETR, with *lute* plants the lowest ETR.

Chapter VII – Photoprotection in Plants Acclimated to Different Light Intensities

7.1 Introduction

As documented in Chapter 3, upon starting in the Ruban laboratory, plants had reduced Fv/Fm values below 0.8. Furthermore, one of the most important observations given the reliance of ΦPSII calculations on qP_d, was the rise of qP_d values above 1.00 during actinic light exposure. qP_d is a quantum coefficient, therefore it should only range between 0 and 1.00. However, when plants became illuminated, qP_d began to rise above 1.00, sometimes in the range of 1.05 and 1.10. This would represent a 105-110% rate of photochemistry in the dark, which is theoretically impossible. Carrying out further tests on a range of plants, it was observed that the unhealthiest looking plants had the largest rises in qP_d. Furthermore, the light intensities used to grow plants were very low, which was reflected in Fv/Fm values in the range of 0.7-0.75, which is much lower than the 0.8 typically measured in healthy plants (Wientjes *et al.* 2013). This is indicative of poorly coupled LHCII-RCII in the supercomplexes, which reduces the photochemical quenching of these plants. This causes a rise in Fo, which concomitantly reduces Fv (Fm-Fo), and reflects a reduced ΦPSII. Based on this combination, it seemed that the conditions were directly affecting the rise in qP_d and it was decided that it would be a good theory to test. Using the gradually increasing pNPQ assessment procedure (Fig 7.01A), plants grown under low (~40 µmol photons m^{-2} s^{-1}), lincomycin-treated (~90 µmol photons m^{-2} s^{-1}), medium (~200 µmol photons m^{-2} s^{-1}) and high light (~450 µmol photons m^{-2} s^{-1}) conditions were assessed for their photoprotective capacities. As previously mentioned (Chapter 2), the eight actinic light intensities in the pNPQ assessment procedure are 100, 90 or 80% of: 0, 90, 190, 280, 420, 625, 820, 1150, 1500 µmol m^{-2} s^{-1} with the eight light intensities at each step lasting for five minutes. This procedure allows NPQ to form without the velocity of formation being a defining factor, which allows the effectiveness of NPQ in each subject to be assessed. NPQ gradually increases under the pNPQ assessment procedure, and NPQ that protects 100% of RCII from photoinhibition is termed pNPQ. The point of photoinhibition is normally defined as $qP_d < 0.98$. qP_d drops below 0.98 when the normally well matched $Fo'_{act.}$ and $Fo'_{calc.}$ deviate at high light intensities. As RCIIs become progressively more closed, the minimum level of

fluorescence ($Fo'_{act.}$) rises, ΔFo increases and qP_d drops below one (Fig 7.01B). There are a number of physiological changes in plants depending on their acclimation history, such as Chl *a*/*b* ratio, LHCII accumulation, and PSI/PSII stoichiometry (Leong and Anderson 1984b; Seeman *et al.*, 1987; Chow *et al.*, 1990; Bailey *et al.*, 2001; Bailey *et al.*, 2004; Ballottari *et al.*, 2007; Kouril *et al.*, 2013; Wientjes *et al.*, 2013). The first section of this chapter displays the relationship between the acclimation history of plants and the qP_d rise phenomenon. The remainder of the chapter used fast rise kinetics and sucrose gradient techniques to quantify the degree of connectivity between PSII supercomplexes and qP_d rise.

7.2 Results

In high light (Fig 7.02) and most medium light grown plants (Fig 7.03), this relationship of matching Fo's until high actinic light intensities causes a deviation, allows for the easy quantification of RCII photodamage. For instance, Fig 7.06A shows that in high light grown plants there is little to no ΔFo at low actinic light values. Under higher AL values, ΔFo becomes more positive. This manifests as a drop in qP_d (Fig 7.06B). Low light grown plants (Fig 7.04) and lincomycin-treated plants (Fig 7.05) however exhibited a different relationship in ΔFo behaviour. Under low AL irradiance, ΔFo became increasingly negative (Fig 7.06B, 7.06C). Upon reaching the highest AL values, this ΔFo trend starts to recover and move back towards positive ΔFo. However, there was still only one light intensity that had an average ΔFo that was positive. ML grown plants exhibited a trend in between both of these, a negative ΔFo at low light intensities followed by an increasingly less negative ΔFo at higher light intensities, but it was most similar to their HL grown counterparts (Fig 7.07A, 7.06A).

A negative ΔFo is a highly unusual result, given that ΔFo should be 0 or a positive result. In theory, $Fo'_{calc.}$ should either be the same as $Fo'_{act.}$ or lower than the actual when plants become photodamaged (Oxborough and Baker, 1997; Ruban and Murchie, 2012; Ware *et al.*, 2015). The differences in the two Fo values are used to calculate qP_d (Fig 7.01).

Applying the pNPQ assessment procedure to plants grown under HL, ML, LL and LT irradiances yielded very different relationships between NPQ, qP_d and light intensities (Figs 7.02-05 respectively). Seemingly in contradiction to previous literature, HL plants had the least NPQ and the greatest amount of photodamage. NPQ increased and photodamage decreased in the lower light acclimated plants. However, qP_d is essential for assessing the degree of photodamage. qP_d is a quantum coefficient for the rate of photochemistry in the dark, and thus, should not be greater than 1.00, as this represents 100% efficiency of RCII. Consequently, due to the negative ΔFo obtained in these measurements, qP_d became greater than 1.00 in all of the plants measured. As expected from the ΔFo calculations, the smallest increase in qP_d was in the HL grown plants, which was almost non-existent

(Fig 7.08A), followed by the ML (Fig 7.07A) and LL (Fig 7.08B) acclimated plants. The differences in qP_d at each light intensity between the differently acclimated plants was significant (ANOVA, $P < 0.001$; *t*-test, $P < 0.001$). The only marginal rise of qP_d in the HL plants resulted in little deviation between the theoretical and actual ΦPSIIs (Fig 7.08A) at low light intensities, before photoinhibition became more pronounced at high actinic light intensities, and the $\Phi PSII_{act.}$ dropped below the $\Phi PSII_{theor.}$. In contrast, ML and LL grown plants had a disparity between the two ΦPSIIs, but with $\Phi PSII_{act.}$ becoming higher than $\Phi PSII_{theor.}$ (Figs 7.07B, 7.08B). The ML grown plants did reflect the expected trend of a lower $\Phi PSII_{theor.}$ than $\Phi PSII_{act.}$ towards the procedure end, but LL acclimated plants did not, even though the leaves would be expected to have suffered a large amount of photoinhibition at this point based on previous experiments (Ruban and Belgio, 2014). Given that qP_d measurements have worked on greenhouse and wild plants, these three results suggest that artificial plant growth history affects qP_d measurements.

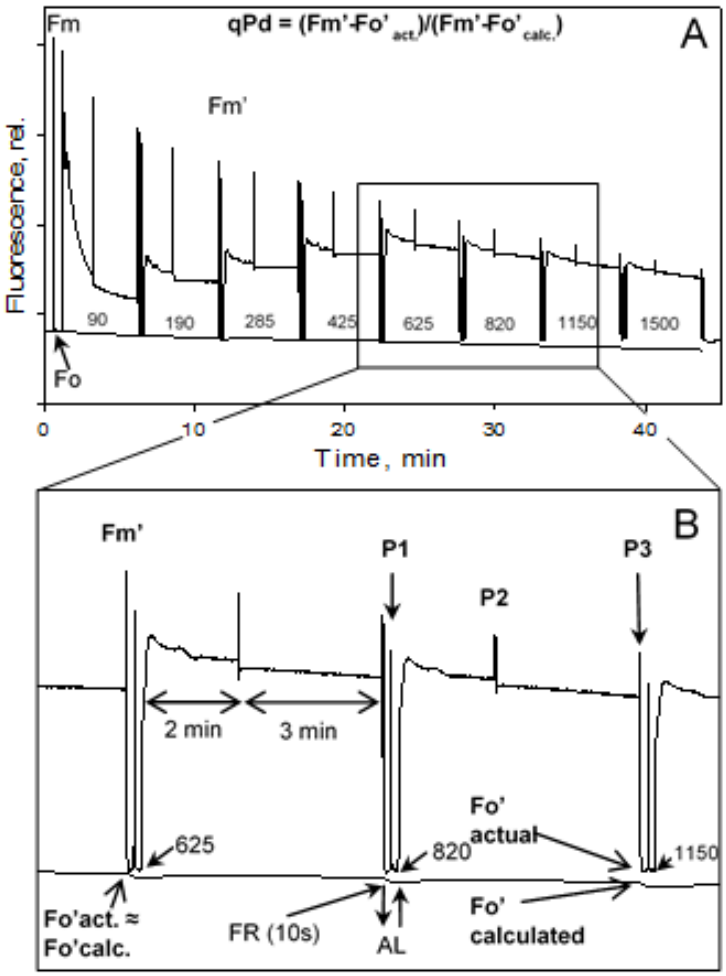

Figure 7.01 A Typical high light acclimated plant chlorophyll fluorescence scheme of induction (as depicted in Fig 2.02) with an eight-step increasing actinic light (AL) routine. In this example 0, 90, 190, 280, 420, 625, 820, 1150, 1500 µmol m^{-2} s^{-1} AL intensities were used. 80 and 90% AL intensities of the aforesaid values were achieved by carefully extracting the fibre-optic from the emitting diode and determining the AL intensity with a Walz MQS-B sensor. This allowed a more accurate reflection of PSII susceptibility to photodamage to be realised. For detailed explanation of routine development see Ruban & Belgio (2014). B Zoomed in region of the fluorescence scheme (a) illustrating the timing and application of 625, 820 and 1150 µmol m^{-2} s^{-1} AL (upward arrow and downward arrow demonstrate the turning of AL on and off respectively), along with saturating pulses (SP) (P1, P2, P3). P1 indicates an SP in the dark, or after 10 sec of far red (FR) light, P2 during AL illumination, and P3 at the end of AL. The difference between $Fo'_{act.}$ and $Fo'_{calc.}$ is determined at P1, and subsequently used to calculate qP_d. At low AL intensities, there is little to no difference between $Fo'_{calc.}$ and $Fo'_{act.}$, but under increasing AL intensities the two values diverge. See also 'Materials and Methods' for a detailed description. The timing scheme in the dark was: (AL off)(FR on)-(10 s)-(FR off/SP)-(5 s)-(AL on) (Ware *et al.*, 2015a).

It is widely accepted that the light conditions which plants are grown under affects the relative antenna size (Mäenpää and Andersson, 1989; Walters *et al.*, 1995; Kouril *et al.*, 2012; Hogewoning *et al.*, 2012; Wientjes *et al.*, 2013). In order to test the correlation between increased antenna size and qP_d rise, plants were grown under low light conditions but whilst simultaneously being watered with lincomycin solution (0.2 g/l). Plants watered with lincomycin have been shown to have increased amounts of LHCII together with reduced amounts of RCII (Belgio *et al.*, 2012). This is because RCII, along with several other photosynthetic membrane protein complexes are encoded by the chloroplast genome, whereas LHCII are nucleus-encoded (see Fig 1.04A). Furthermore, the light intensities that the lincomycin-treated plants are grown under is not high enough to stop the enzymatic conversion of Chl *a* to Chl *b* by chlorophyllide oxidase, which contributes to the further accumulation of LHCII, the Chl *b* containing protein complexes (Espineda *et al.*, 1999). Once these plants reached a similar size to the LL grown non-treated *Arabidopsis*, the pNPQ assessment procedure was applied to 30 individual leaves (Figs 7.05, 7.09). The pNPQ assessment procedure illustrated an even greater qP_d rise compared to LL grown plants (Figs 7.04, 7.08B), reaching between 2.5 and 3.0 in plants by the procedure end (Fig 7.09). Belgio *et al.*, (2012) had previously shown using the lincomycin model that disconnected LHCII had enhanced NPQ capacities. In order here, HL, ML, LL then lincomycin treated plants had increased NPQ values by the procedure end. Therefore, it was decided to test whether the decoupling of LHCII from RCII could be causing the rise in qP_d.

High Light

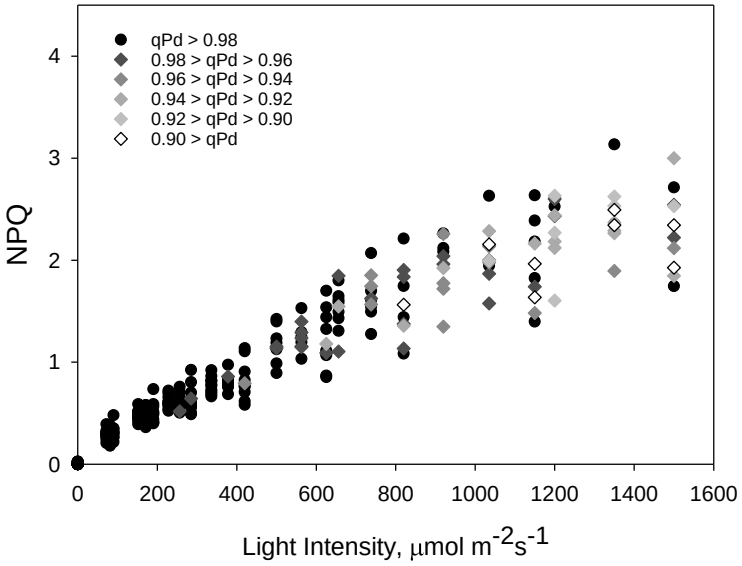

Figure 7.02 A 3-dimensional representation of the openness of reaction centers, with the corresponding protectiveness of NPQ and actinic light intensity in HL acclimated plants. Black circles represent leaves where 98-100% of reaction centers are open at a particular light intensity; here NPQ is protective (pNPQ). Greyscale rhomboids represent the degree of reaction center closure. 30 repeats were conducted.

Medium Light

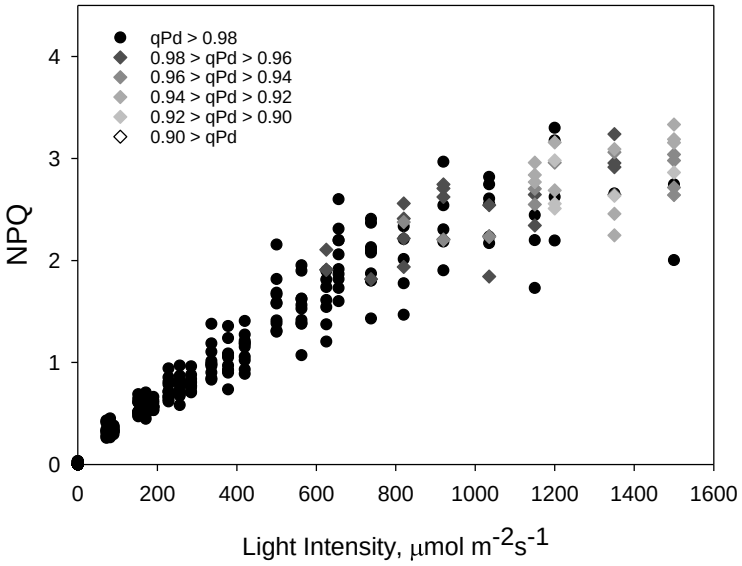

Figure 7.03 A 3-dimensional representation of the openness of reaction centers, with the corresponding protectiveness of NPQ and actinic light intensity in ML acclimated plants. Black circles represent leaves where 98-100% of reaction centers are open at a particular light intensity; here NPQ is protective (pNPQ). Greyscale rhomboids represent the degree of reaction center closure. 30 repeats were conducted.

Low Light

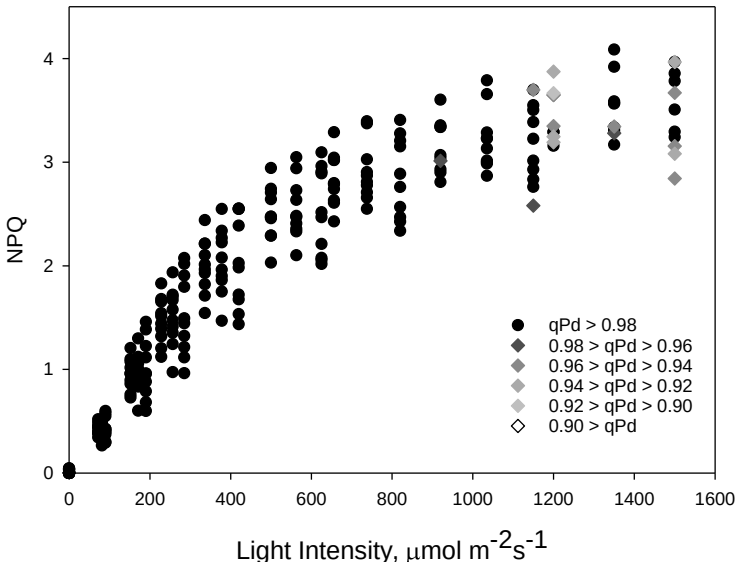

Figure 7.04 A 3-dimensional representation of the openness of reaction centers, with the corresponding protectiveness of NPQ and actinic light intensity in LL acclimated plants. Black circles represent leaves where 98-100% of reaction centers are open at a particular light intensity; here NPQ is protective (pNPQ). Greyscale rhomboids represent the degree of reaction center closure. 30 repeats were conducted.

Lincomycin Treated

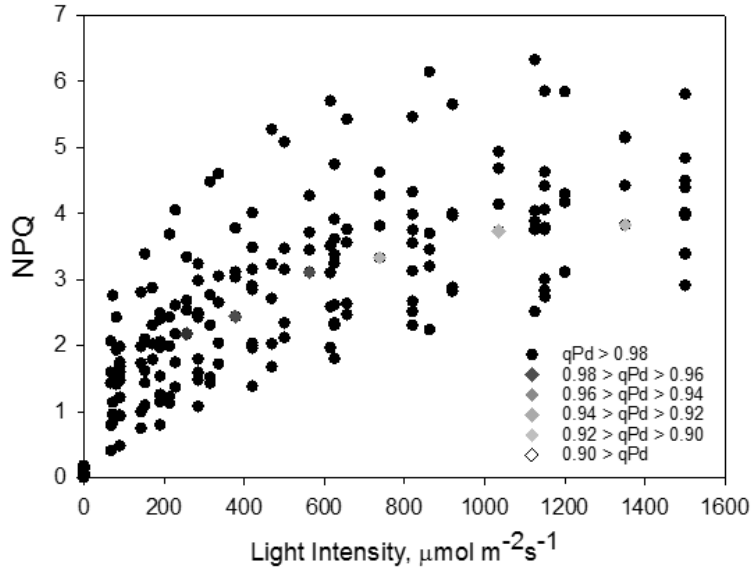

Figure 7.05 A 3-dimensional representation of the openness of reaction centers, with the corresponding protectiveness of NPQ and actinic light intensity in lincomycin-treated plants. Black circles represent leaves where 98-100% of reaction centers are open at a particular light intensity; here NPQ is protective (pNPQ). Greyscale rhomboids represent the degree of reaction center closure. 30 repeats were conducted.

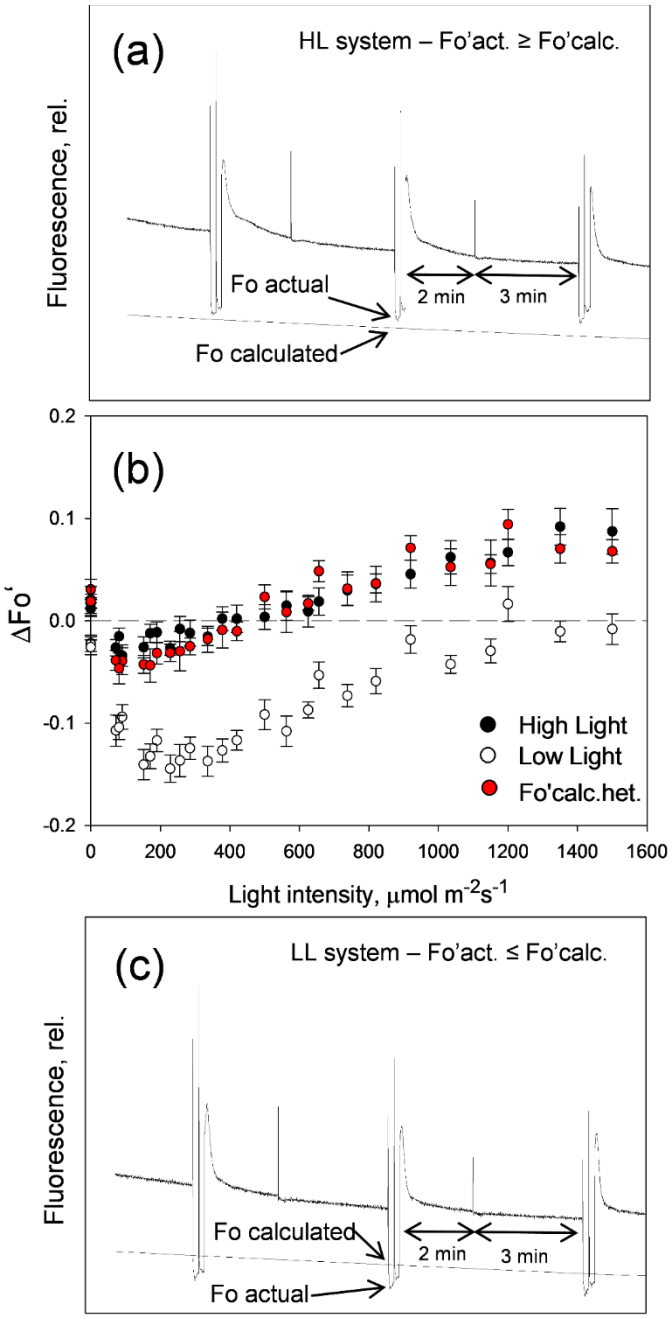

Figure 7.06A Extract of a typical chlorophyll fluorescence routine conducted on a high light acclimated leaf using a JUNIOR PAM fluorimeter (Walz, Germany). The gradually increasing actinic light (AL) routine induces photoinhibition which can be readily observed as a divergence between $Fo'_{act.}$ and $Fo'_{calc.}$ B Average ΔFo' data obtained in HL and LL acclimated plants. C An extract of a typical chlorophyll fluorescence routine conducted on a low light acclimated leaf using a JUNIOR PAM fluorimeter (Walz) (Ware *et al.*, 2015a).

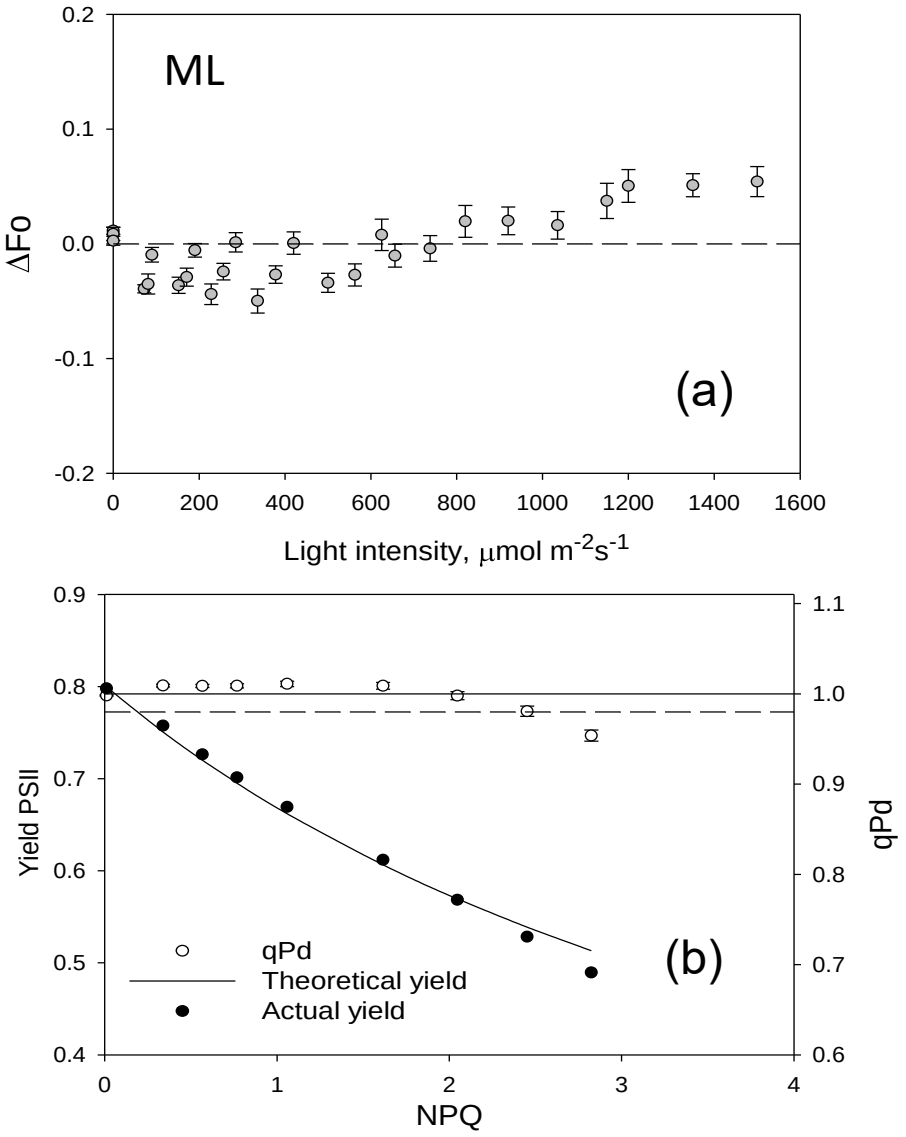

Figure 7.07A ΔFo' [(Fo'$_{act.}$-Fo'$_{calc.}$)/Fo'$_{act.}$] results obtained from fluorescence traces for each AL intensity were averaged for medium light grown plants. Error bars show SEM (n = 10). B Relationship between NPQ and qP_d (open circles) and NPQ and PSII actual yield (closed circles) for medium light grown plants. Data points were averaged from 30 repeats on whole intact leaves. Error bars show the standard error of the mean (n = 30). The theoretical yield (continuous line) was calculated using Equation 1.16 (Ware *et al.*, 2015a).

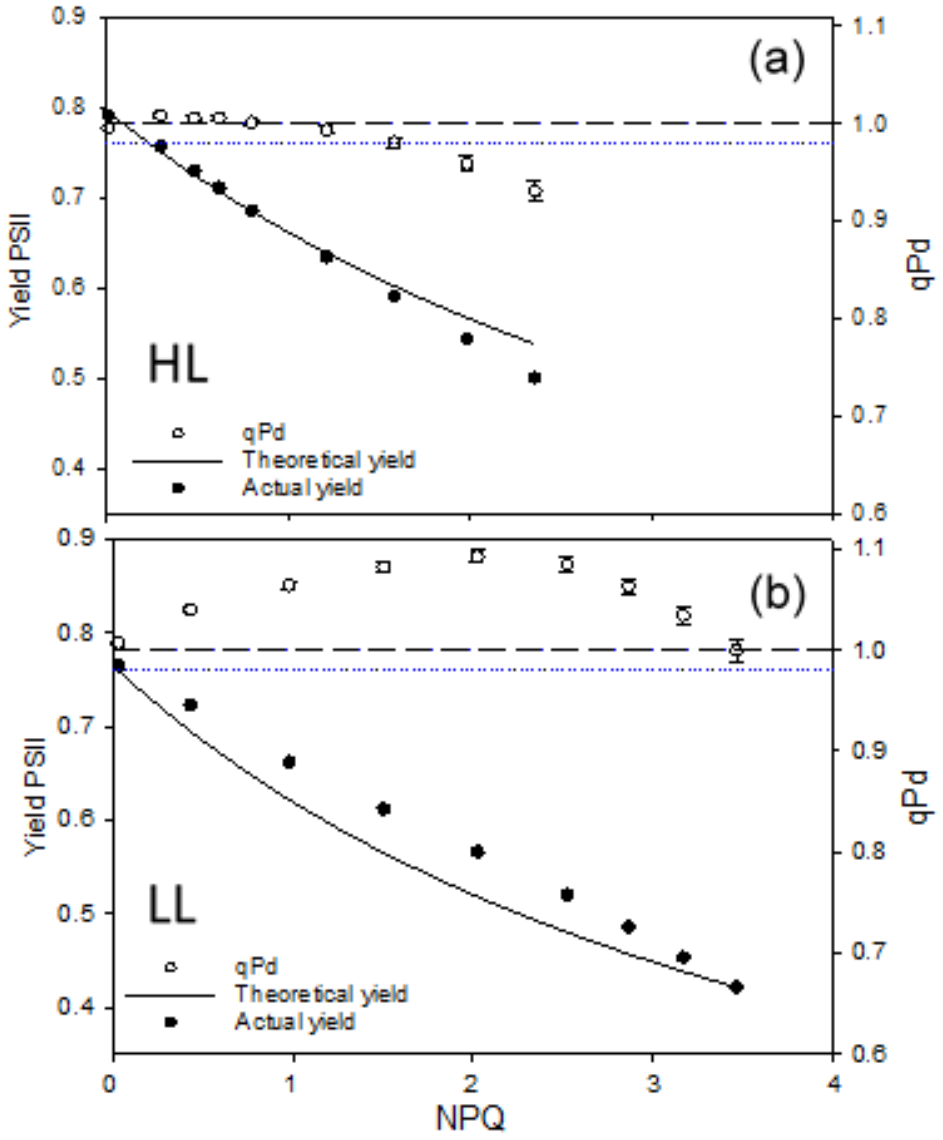

Figure 7.08 Relationship between NPQ and qP_d (open circles) and NPQ and PSII actual yield (closed circles) for (A) high light and (B) low light grown plants. Data points were averaged from 30 repeats on whole intact leaves. Error bars show the standard error of the mean (n = 30). The theoretical yield (continuous line) was calculated using a qP_d value of 1.00 (Ware *et al.*, 2015a).

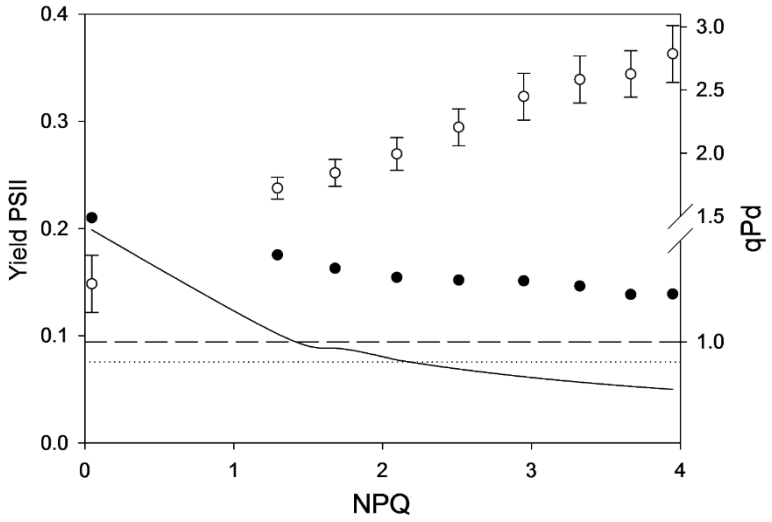

Figure 7.09 Relationship between NPQ and qP_d (open circles) and NPQ and PSII actual yield (closed circles) for lincomycin-treated plants. Data points were averaged from 25 repeats on whole intact leaves. Error bars show the standard error of the mean (n = 25). The theoretical yield (continuous line) was calculated using a qP_d value of 1.00.

A number of different techniques were used to measure the physical and functional PSII cross sections of plants acclimated to different light intensities. Firstly, Chl *a/b* ratios were calculated. As expected, there was a significant difference between the plants grown at different light intensities (ANOVA, $P < 0.001$; Table 7.01). This is owing to the phenotypic response of shade acclimated plants, which have a greater proportion of LHCII and therefore a greater amount of Chl *b* and a reduced ratio of Chl *a*/*b*. There were also significant differences between individual populations. HL grown plants had significantly higher Chl *a*/*b* ratios than LL and lincomycin-grown plants, and ML acclimated plants had significantly higher ratios than lincomycin-treated plants as well.

Table 7.01 Antenna properties of plants grown under different intensities (Ware *et al.*, 2015a)

Antenna properties of plants grown under high-, medium- and low-light conditions

Conditions	F_v/F_m[a]	Chl a/b[b]	PSII total antenna size (%)[c]	PSII relative absorption cross section (%)[d]	Required total protective NPQ (%)[e]
High light	0.80 ± 0.003	3.81 ± 0.18	100	100	100
Medium light	0.80 ± 0.001	3.40 ± 0.05	118	112 ± 0.04	113.9
Low light	0.76 ± 0.002	2.80 ± 0.17	139	128 ± 1.57	182.0
Lincomycin treated	0.21 ± 0.035	2.4 ± 0.07		140 ± 1.1	228.0

[a] Standard error of the mean (SEM), $n = 30$

[b] Chlorophyll *a/b* ratios were estimated from absorption spectra of 80 % final acetone extract of leaf material (Porra et al. 1989); SEM, $n = 5$

[c] Total antenna chlorophyll from normalised bands 3, 4 and 5 obtained in sucrose gradients (Fig. 4) was calculated and compared to HL plants

[d] The area under each normalised fast induction fluorescence kinetic trace (Fig. 5) was analysed and compared to the obtained HL area (Malkin et al. 1981); SEM, $n = 3$

[e] The difference in protective capacity was estimated by calculating the area under each minimum pNPQ gradient and comparing it to the HL area (Fig. 6); SEM, $n = 20$

After growing enough plants at the right age for each light intensity (see Materials and Methods), sucrose gradient separations were executed on HL, ML and LL acclimated groups of plants. The beauty of this technique is that it uses centrifugations to separate different components of $C_2S_2M_2L_2$ complexes, depending on how well each of the proteins are bound together, and the subsequent different weight results in discrete rows as occurred here (Fig 7.10). The amounts of each band must be quantified in order to compare their relative amounts. Before this however, it is clear to see that the Band 3, therefore LHCII trimers, decreases from LL to ML and HL plants, which was expected given the Chl *a*/*b* ratio experiment results. Although the bands matched those previously published (Dall'Osto *et al.*, 2006), each band was confirmed by performing absorption spectra measurements on the isolated bands (Fig 7.11). Band 1 contains free pigments and was omitted from the image; Band 2 contains monomeric antenna proteins; Band 3 is trimeric LHCII proteins; Band 4 contains minor antenna proteins bound to LHCII; Band 5 are RCII bound proteins; and Band 6 are exclusively PSI supercomplexes. The volume of each band was then calculated using the relative area of the absorption spectra (Fig 7.12), multiplying this by the volume of each band, the dilution factor used for the measurement, and dividing this by the amount of chlorophyll proteins in each of the individual complexes from each band. The amount of chlorophyll molecules in each band was: 42 chls per LHCII trimer, 66 per LHCII-CP29-CP24 complex, and 35 per PSII core complex (Pessarakli 2005; Dall'Osto *et al.* 2006; Caffarri *et al.* 2009; Amunts *et al.* 2010). These complexes

correspondingly refer to bands 3, 4 and 5. These results showed a similar amount of C2:LHCII ratios as previously reported (van Oort *et al.* 2010; Kouril *et al.* 2012; Wientjes *et al.* 2013), which assured us that the protocol was viable. Following on from this the amount of harvesting proteins bound to each dimeric core was calculated. Table 7.01 shows the increase in total antenna size of 18 and 38% in the ML and LL grown plants compared to the HL. The work of Wientjes *et al.* (2013) compared the antenna sizes between plants grown under 20, 100 and 800 μmol photons m^{-2} s^{-1}. Here they found a 23 and 40% increase LHCII relative to RCII. With another groups' research supporting this biochemical technique, the novel part of this experiment could now proceed, and a comparison between the physically attached and functionally attached PSII supercomplex.

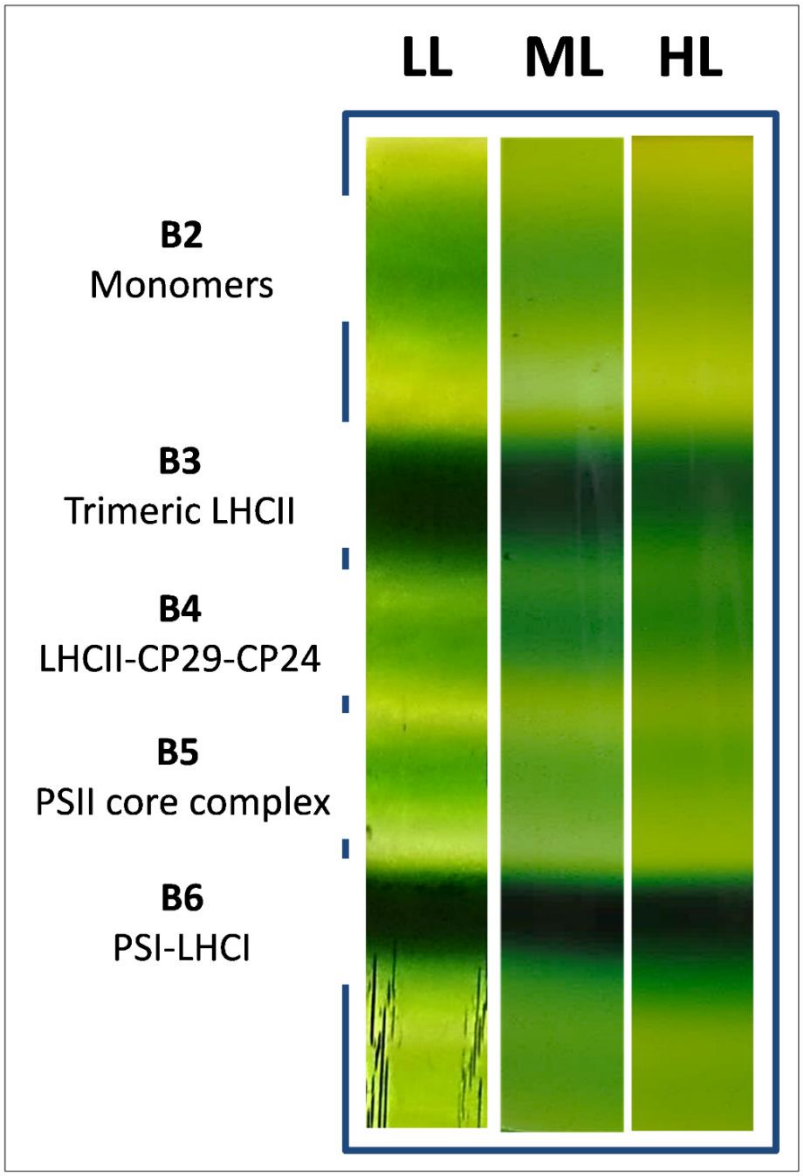

Figure 7.10 Sucrose gradients performed on plants grown under low (LL), medium (ML) and high light (HL) conditions. Thylakoid membranes corresponding to 0.6 µg of chlorophyll were solubilised with 0.6% α-dodecyl maltoside (α-DM) before loading onto 0.1-1 M sucrose gradients. Bands were confirmed by absorbance spectroscopy (Ware *et al.*, 2015a).

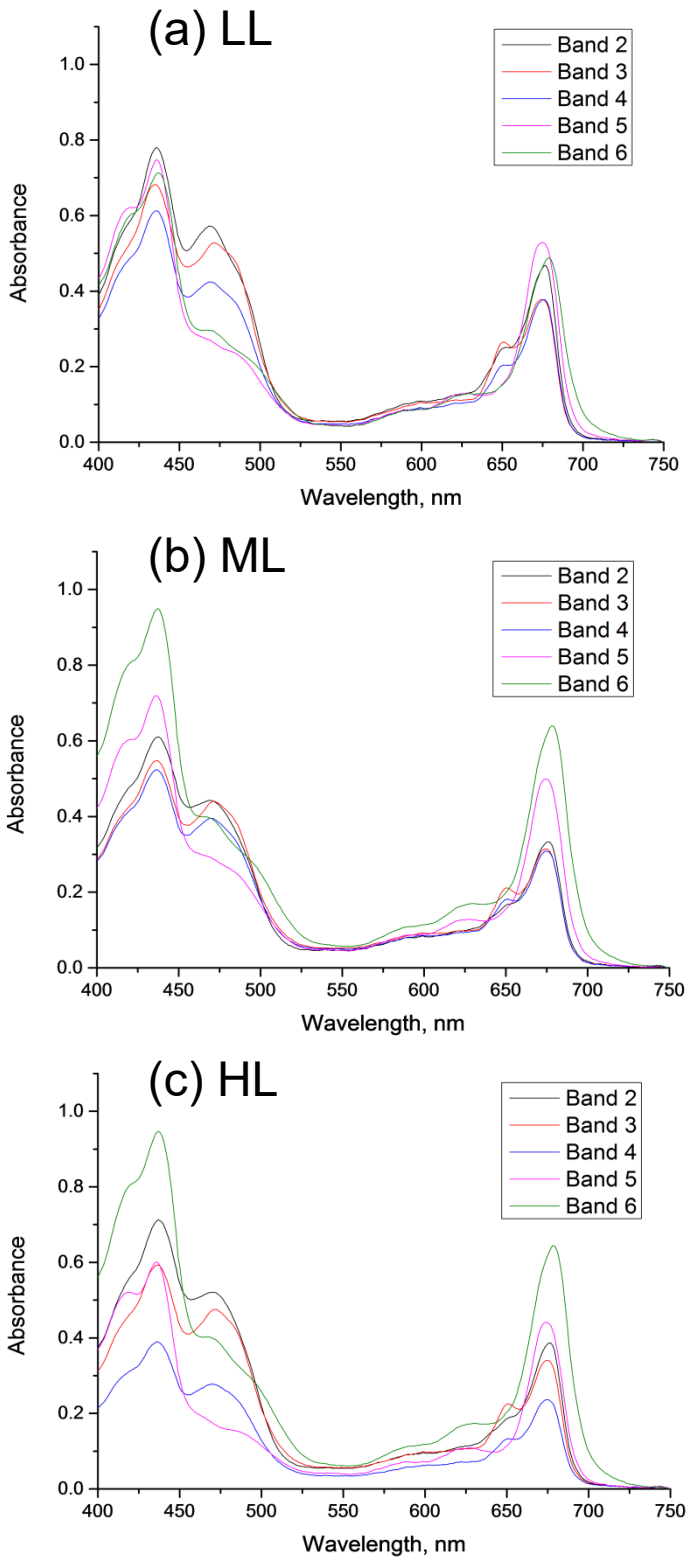

Figure 7.11 Absorbance spectra (Hitachi, U-3310 spectrophotometer) conducted on bands obtained from sucrose gradients (Fig. 7.06) for (A) low light (B) medium light (C) high light grown plants. All bands were normalised to 0 at 750 nm. Band 2-6 correspond to monomers, trimeric LHCII, LHCII-CP29-CP24, PSII core, and PSI-LHCI complexes respectively. Band 1 was measured and recorded as free pigments (Ware *et al.*, 2015a).

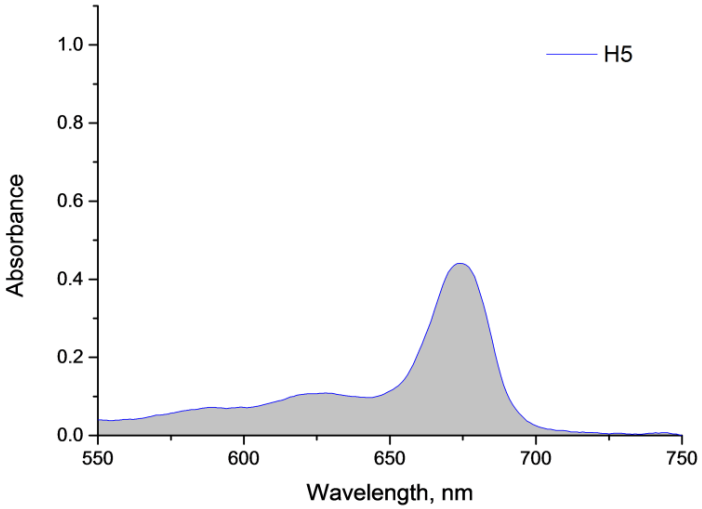

Figure 7.12 An example band absorbance spectra from Fig 7.11, with traces again zeroed at 750 nm. Using OriginPro 9.0, the mathematical area under each trace was calculated using the integrate function between 550 and 750 nm. This area was used to calculate the total amount of arbitrary chlorophyll. This was achieved by multiplying the total amount of the band extraction from the sucrose gradient (ml) by the dilution factor of solution used to perform the absorbance spectra, and by the area measured under the trace. This arbitrary chlorophyll value was divided by the number of chlorophylls per complex in each band (42 chlorophylls per LHCII trimer (Band 3), 66 per LHCII-CP29-CP24 complex (Band 4) and 35 per PSII core complex (Band 5)) to ascertain the amount of complexes present (Ware *et al.*, 2015a).

Belgio and co-workers in the Ruban laboratory had shown the adaptability and accuracy of fast fluorescence kinetics as a method for estimating PSII cross sections (Belgio *et al.*, 2012; 2014). In 2012, it was used to compare the functional cross sections in lincomycin-treated plants, and in 2014, it was used to compare PSII cross section changes during NPQ formation and relaxation (Belgio *et al.* 2012; 2014). The rise from Fo to Fm in a fast fluorescence induction kinetic measurement is directly dependent upon the amount of chlorophylls that are energetically couple to RCII (Malkin *et al.* 1981; De Bianchi *et al.* 2008). The technique displays the amount of time taken to saturate 100% of RCII in the illuminated sample (Fig 7.13). Normalising the trace as a rise from 0 (Fo) to 1 (Fm), over time, allows a direct comparison to be performed between different plant types. The area below the

trace and above the x-axis, is used to give a relative comparison between the saturation times. As it is a relative comparison, the plant with the acclimation history that rendered it the slowest saturation time is considered to have a 100% cross section. Fig 7.13 illustrates that HL acclimated plants had the slowest RCII saturation, with ML the second quickest, and LL the quickest to become saturated. The total functional cross sections are ascertained by measuring the grey area below the 1.00 Fv line and above the saturation curve. The total areas of ML and LL plants were calculated to be 12 and 18% greater than HL plants respectively, and these differences were significant (z-test, $P < 0.01$). Although sucrose gradients were not successfully performed on lincomycin-treated plants, fast rise kinetics were. Indeed, the trend of increasing functional cross section continued here and lincomycin-treated plants have an estimated cross section that is 40% larger than HL plants. These results confirm that lower light conditions increase the functional cross sections of plants, as the saturation of the photosynthetic membrane occurred more quickly in the lower light adapted plants. Coupled with the sucrose gradients, the fast rise fluorescence experiments show that the functional cross section is not as large as the physical cross section of the PSII supercomplex. Comparing the LL and ML sucrose gradient experiments to the fluorescence experiments suggests approximately 10 and 6% of the antenna is respectively uncoupled.

Having partially disconnect antenna could cause NPQ to rise dramatically. Belgio *et al.*, (2012) showed that in lincomycin-treated plants NPQ is approximately two-fold higher than WT plants. However, a conclusion of the Ruban groups' following paper was that the quenching capacity in free LHCII is higher than RCII-bound LHCII (Belgio *et al.*, 2014). What if the unbound LHCII is not quenching the excitation energy acting on PSII? This theory arose from the idea that in low and high light conditions, the acclimation history of plants would have different selection pressures on the plants. In LL conditions, a large light harvesting network would help to drive photosynthesis by increasing the amount of energy absorbed for photochemistry. However, in high light conditions, such as those in the pNPQ assessment procedure, RCII would be saturated, and LHCII would merely increase the amount of excess

energy and excitation pressure. It would be interesting to see how effective unbound LHCII would be at relieving this overexcitation. With the new pNPQ assessment approach, a quantification of the protectiveness of this NPQ was performed.

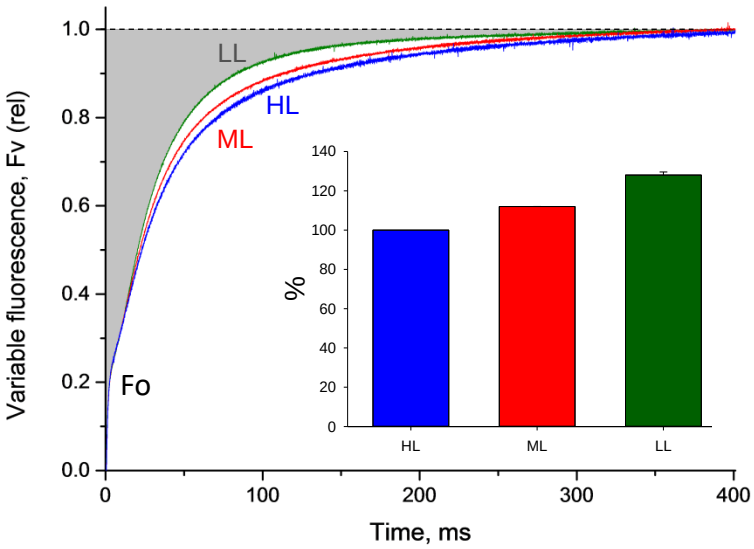

Figure 7.13 PSII fast fluorescence induction traces performed on detached low, medium and high light acclimated leaves. Vacuum infiltration with 30 µM DCMU was performed 20 sec before exposure to 7 µmol m^{-2} s^{-1}. Traces are the mean values for 3 repeats. All traces were zeroed at Fo and normalised to 1 at Fm. Inset shows the difference in average absorption cross-sections obtained by calculating the area under each fluorescence trace compared to HL cross-section area (see Materials and Methods) (Ware *et al.*, 2015a).

The data obtained in the pNPQ assessment procedure, which was presented in Figs 7.02-7.04, can be used for this. The NPQ values obtained at the end of each five-minute illumination period were obtained. The corresponding qP_d values, recorded 10 seconds after each of the five minute intervals, were plotted against the NPQ values. Then for each light intensity, the lowest NPQ value that had a corresponding qP_d value of 0.98-1.00, was obtained. This represents the most efficient pNPQ value for each type of acclimated plant. The results (Fig 7.14) show that the minimum amount of pNPQ required at each light intensity was higher for each type of plant than the HL. In fact, the pNPQ values required were 28, 82 and 128% higher for ML, LL and lincomycin-treated plants than the HL (Table 7.01). The differences between all plant types are significant (ANOVA, $P < 0.0001$) and these are also significantly higher pNPQ values when individually compared to HL plants (z-test, ML - $P < 0.05$; LL and LT – $P < 0.001$). The average increase in pNPQ values measured at the end of the procedure, where NPQ still protects 98-100% of RCII, was not as great as the increase in the NPQ values at the procedure end (Fig 7.15). This supports the idea that increased antenna accumulation leads to increased NPQ, but that this NPQ is not protective. The more uncoupled antenna in the photosynthetic membrane, the less protective the NPQ is there. There could be a number of contributing reasons for this phenomenon. In lincomycin-treated plants, a highly heterogeneous system of free or grouped LHCII, and PSII supercomplexes arises (Belgio *et al.*, 2014). In this system, NPQ is much less effective at dissipating excess energy, in fact it was shown that it is three times less effective at quenching than photochemistry.

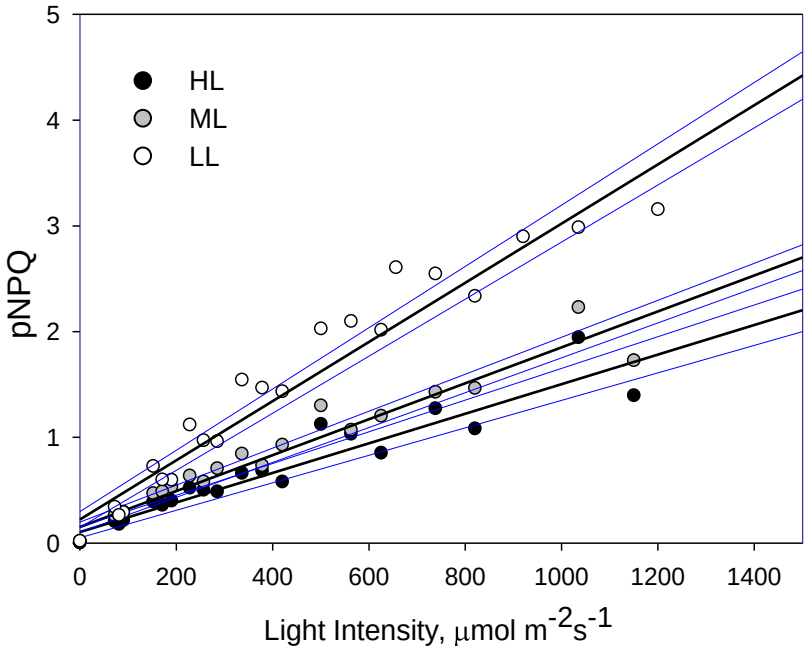

Figure 7.14 Relationship between light intensity and maximum protective capacity during a gradually increasing routine (see Figs 7.02-7.05). Regression analysis (Standard Curves, Linear Curve; f = y0+a*x) was plotted using SigmaPlot12 (Systat Software, Inc., Chicago, USA). Data points were taken for the lowest pNPQ value at each light intensity, thus representing the lowest NPQ value corresponding to qP_d > 0.98. Gradients were calculated as f = 0.1032+0.0015*x (HL), f = 0.1519+0.0017*x (ML) and f = 0.2224+0.0028*x (LL). The gradient can therefore be used to estimate the minimum NPQ needed for 100% RC protection at each actinic light intensity. The difference in protective capacity was estimated by calculating the area under each pNPQ gradient and comparing it to the HL area. Blue lines correspond to the standard deviation (Ware *et al.*, 2015a).

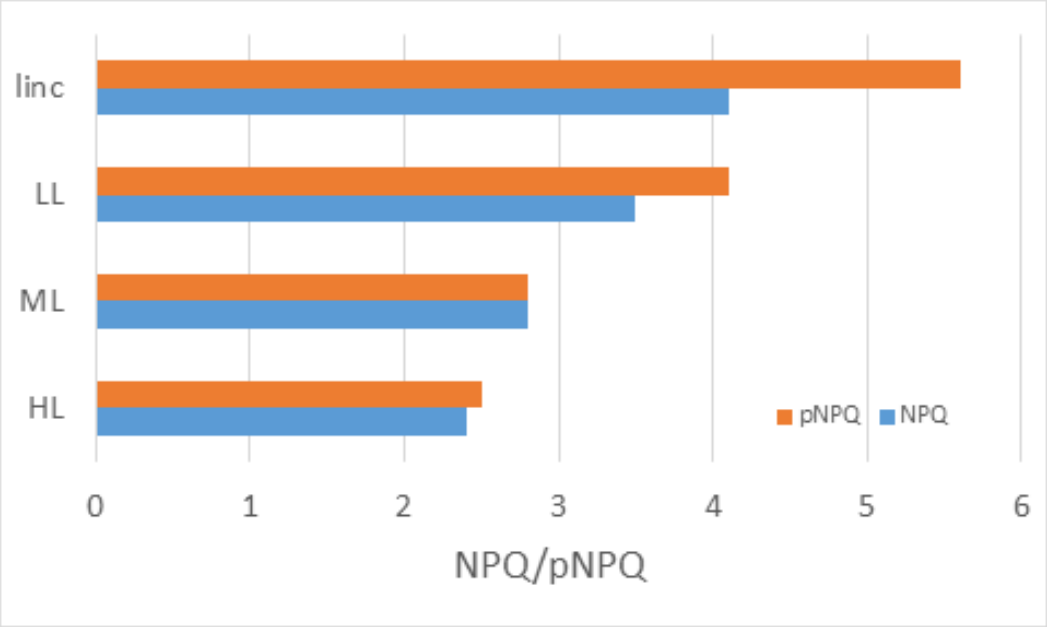

Figure 7.15 Maximum NPQ and pNPQ capacity of HL, ML, LL and LT leaves measured after the last actinic light illumination step of 1,500 µmol photons m^{-2} s^{-1} at the end of the pNPQ assessment procedure.

This is made the more exceptional, because qP is less efficient in shade adapted plants. Plants acclimated to conditions of less than 200 µmol photons m^{-2} s^{-1} have significantly reduced amounts of plastoquinone than plants grown above this light intensity, thus reducing the photosynthetic capacity of these plants (Leong and Anderson, 1984a; 1984b). Englemann and co-workers showed that exciton capture by RCII was dependent on the amount of uncoupled antenna (Englemann *et al.*, 2005). Taking these results in combination, an increase in uncoupled antenna decreases the photochemical capacities of LL adapted plants, which at the same time reduces the effectiveness of NPQ. It seems rather surprising then that the qP_d measurements collected during the actinic light procedure suggests enhanced photochemical capacities in LL plants. This conclusion could be drawn because the point of photoinhibition ($qP_d < 0.98$) is not breached, as qP_d continues to rise in the increased AL irradiance. One may draw the conclusion that the Oxborough and Baker (1997) formula does not work for heterogeneous systems. Based on the information gathered during these experiments, a new way of calculating qP_d in systems where LHCII is not completely coupled to RCII was developed, but with the

primary aim that it can still produce accurate analysis of qP_d decline and thus measure the first points of photoinhibition.

Predicting what might be happening in heterogeneous systems, such as the LL plants, compared to homogeneous ones, such as HL plants, a figure was constructed to better conceptualise the problem (Fig 7.16). Here it can be seen that a homogeneous system has PSII supercomplexes surrounded by a small amount of free LHCII (Fig 7.16A). In the Fm state, the total system is fluorescing and this is measured by a fluorometer (Fig 7.16A). Conversely in the dark, or Fo state, photochemical quenching is able to quench the system (Fig 7.16B). Importantly, in the formula of Oxborough and Baker, $Fo'_{calc.}$ is based upon Fo, Fm and Fm'. Fm' is dependent on the amount of NPQ present, and in a HL adapted plant, NPQ is pNPQ, and effectively relieves the excitation pressure on the energetically connected supercomplexes (Fig 7.16C). This is also true in the $Fo'_{act.}$ state, as NPQ and qP both quench the same illuminated area. $Fo'_{calc.}$ and $Fo'_{act.}$ can thus be compared for the same connected system to calculate a qP_d value and measure the amount of closed RCII compared to the original Fo and Fm states (Fig 7.16D). In plants that have been grown under LL or lincomycin-stress conditions, this is not the case. Illustrated by Fig 7.16E, it is evident that these conditions cause a large amount of LHCII to be synthesised relative to RCII. When measuring the Fm state of the leaf, this is not an issue as disconnected LHCII fluoresce the same amount as the connected LHCII (Belgio *et al.*, 2012). However, in Fo state, this is a different scenario (Fig 7.16F). connected LHCII (Belgio *et al.*, 2012). However, in Fo state, this is a different scenario (Fig 7.16F).

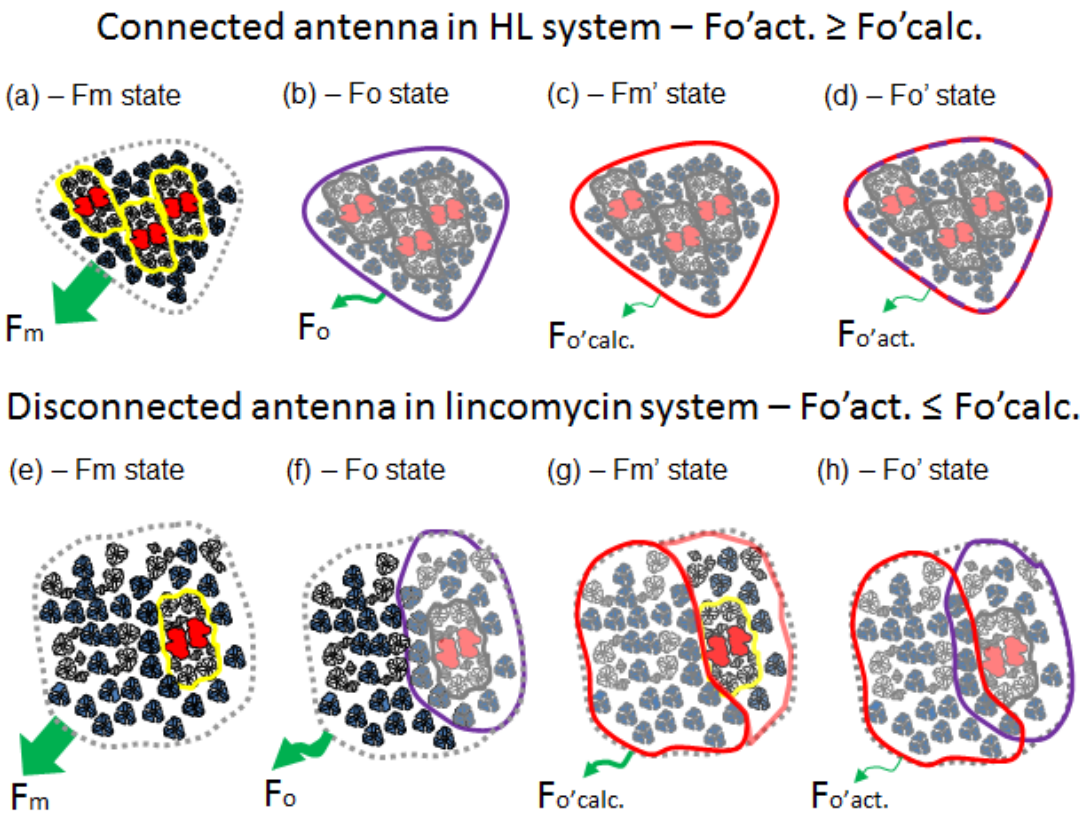

Figure 7.16 Theoretical structures of the PSII membrane in high light (Fig. 7.16A-D) and lincomycin (Fig. 7.16E-H) treated plants. Green arrows represent relative fluorescence emission, purple lines the quenching effect of photochemistry (qP) and red lines the scope of NPQ. A There are no dissipation mechanisms in the Fm state, hence maximum fluorescence is observed here. B In the Fo state only photochemical quenching (qP) is relieving fluorescence from the membrane. C In the Fm' state, the application of a saturating pulse closes the qP pathway and NPQ is the only dissipation mechanism acting on quenching fluorescence. d After previous illumination but in the dark, NPQ and qP_d are both quenching fluorescence in the same interconnected system. Here $Fo'_{act.}$ and $Fo'_{calc.}$ are well matched in the homogeneous HL membrane. Only at high light intensities, $Fo'_{act.}$ starts to increase above $Fo'_{calc.}$ E Represents the enlarged antenna (LHCII) system found in lincomycin treated plants, with many of them poorly connected. This causes a high level of minimum fluorescence (Fo) which cannot be quenched by reaction centers (RCII) in the dark. G Shows that the enhanced NPQ from free LHCII fails to act evenly across the PSII membrane. There is still some NPQ acting directly on PSII but this is lower than the NPQ in isolated LHCII. This results in Fm' and $Fo'_{calc.}$ being lower than they should. H The effect of NPQ and qP_d appear enhanced in this heterogeneous complex compared to the overlapping systems of (D) due to the higher levels of NPQ originating in unbound LHCII (Ware *et al.*, 2015a).

The Fo level of plants with increasingly disconnected LHCII is higher than plants with more connected systems (Fig 7.16G). RCII can only quench the absorbed light of functionally connected LHCII. There are therefore a large number of LHCII that are fluorescing in the Fo state. These free LHCII have a greater quenching capacity than the bound LHCII. When a leaf has been illuminated, these LHCII form a deep NPQ, which is not acting evenly across the photosynthetic membrane. This causes Fm' to be heavily quenched (Fig 7.16G). The formula of Oxborough and Baker (Equation 1.18) was created to predict the values of Fo' at a time when fluorometers could not accurately measure the minimum fluorescence levels in the dark after prior light exposure (Oxborough and Baker, 1997). Before this calculation, many studies used Fo to replace Fo', which leads to the incorrect estimations of Fv'/Fm' and qP (Quick and Horton, 1984; Weiss and Berry, 1987; Oxborough and Baker, 1997). The calculation of qP_d (Equation 1.17) relies on an accurate comparison between the measure $Fo'_{act.}$ and the predicted Fo' based on NPQ ($Fo'_{calc.}$) to estimate the amount of closed RCII. NPQ acts more in the Fm' state, therefore the formula predicts that it will not be as strong a quencher on RCII. However, in the Fo' state, NPQ still heavily quenches the free LHCII, which means that $Fo'_{act.}$ is lower than $Fo'_{calc.}$, thus causing qP_d to become higher than 1.00 (Fig 7.16H).

Based on the experimental data that has been obtained, the task was to alter the Oxborough and Baker (1997, Equation 1.18) formula to accommodate heterogeneous light harvesting systems.

$$Fo'_{calc.} = \frac{1}{\left(\frac{1}{Fo} - \frac{1}{Fm} + \frac{1}{Fm'}\right)} \qquad \text{(Equation 1.18)}$$

The formula of Oxborough and Baker above was transformed to remove the variable Fm'. As Fm' can be expressed in terms of Fm and NPQ (Fm' = Fm/(NPQ+1)), the equation was expressed as:

$$Fo'_{calc.} = \left(\frac{1}{Fo} - \frac{1}{Fm} + \frac{(NPQ+1)}{Fm}\right)^{-1} \qquad \text{(Equation 7.01)}$$

Then, the components of the equation were split into those the homogeneous system element, represented by n, and those of the heterogeneous system, called m. The above equation can then be written for a heterogeneous system as:

$$\mathrm{Fo'_{calc.het.}} = \left(\frac{1}{(n*Fo+(1-n)*Fm} - \frac{1}{Fm} + \frac{(NPQ+1)(mNPQ+1)}{Fm(n(mNPQ+1)+(1-n)(NPQ+1)}\right)^{-1}$$

(Equation 7.02)

If n equals the proportion of coupled antenna, (1-n) is the fraction of uncoupled antenna. mNPQ is the amount of NPQ attributed to the disconnected LHCII, which has been shown to be greater than NPQ, but inefficient at quenching PSII. The increasing amount of uncoupled antenna is reflected in a drop of Fv/Fm below 0.8, as was correlated by sucrose gradients here. The Fv/Fm value of 0.8 is the benchmark for a healthy plant, and the measured value here for HL plants with no qP_d rise. As a quantum expression, this means that Fm can be represented by 1.00 and Fo as 0.2:

$$\frac{Fv}{Fm} = \frac{Fm-Fo}{Fm} = \frac{1.00-0.2}{1.00} = 0.8 \qquad \text{(Equation 7.03)}$$

Representing Fo as 0.2 and Fm as 1.00, Equation 7.02 can be transformed to:

$$\mathrm{Fo'_{calc.het.}} = \left(\frac{1}{0.2n*(1-n)} - 1 + \frac{(NPQ+1)(mNPQ+1)}{(n(mNPQ+1)+(1-n)(NPQ+1)}\right)^{-1}$$

(Equation 7.04)

n can be represented as a fraction of uncoupled to coupled antenna:

$$n = \frac{(Fm-Fou)}{(Fm-Fo)} \qquad \text{(Equation 7.05)}$$

where Fo_u represents fluorescence contribution due to the uncoupled antenna and Fo the coupled antenna. Experimental data was then used to calculate the n and m values. As the NPQ in HL plants was shown to be pNPQ. m was calculated as the average NPQ in HL plants subtracted from the average NPQ in LL plants. The average m was calculated as 2.00. n was calculated as [(5-(Fo/0.2))/4]. Therefore, if Fo was 0.2, n would be 1.00 and the contribution of uncoupled antenna would be 0. However, the average n for LL acclimated plants estimated to be 0.963, and

consequently (1-n) to be 0.037. This means that using the data obtained from the pNPQ assessment procedure, $Fo'_{calc.het.}$ can be estimated, and a qP_d utilised as the assessment for photoinhibition. Fig 7.17 shows the effect of reducing the contribution of the uncoupled antenna, and that $Fo'_{calc.het.}$ instead drops below $Fo'_{act.}$ at high light intensities.

This new positive ΔFo at high light intensities resulted in a qP_d average that barely rises above 1.00 during the procedure (Fig 7.18B). In the lower light conditions, coupling may not be the same as in the dark or in higher light conditions. Indeed, Belgio *et al.*, (2014) showed that the effective antenna size changes in light exposed, and dark recovering plants. This may be why the new $Fo'_{calc.}$ heterogenous system fit curve does not rectify the qP_d rise at all light intensities in the procedure. With more time, investigating the coupling at each light intensity may rectify this, rather than taking an average coupling as demonstrated here. In addition to this, individual qP_d values plotted against light intensities can be plotted and light tolerance curves drawn. ANOVA shows significant changes between the three sets of acclimated plants ($P < 0.01$). The LL plants had significantly smaller light intensities than both the HL and ML plants, with 500 µmol photons m^{-2} s^{-1} being required to close RCII in 50% of plants (Fig 7.19C). The HL and ML acclimated plants were not significantly different and were able to tolerate 660 and 740 µmol photons m^{-2} s^{-1} (Fig 7.19A, 7.19B). Interestingly, the ML plants higher light intensities than the HL counterparts. This could be due to the stepwise increments of the pNPQ assessment procedure, as both sets of plants had 100% leaves showing signs of RCII damage at 1200 µmol photons m^{-2} s^{-1}.

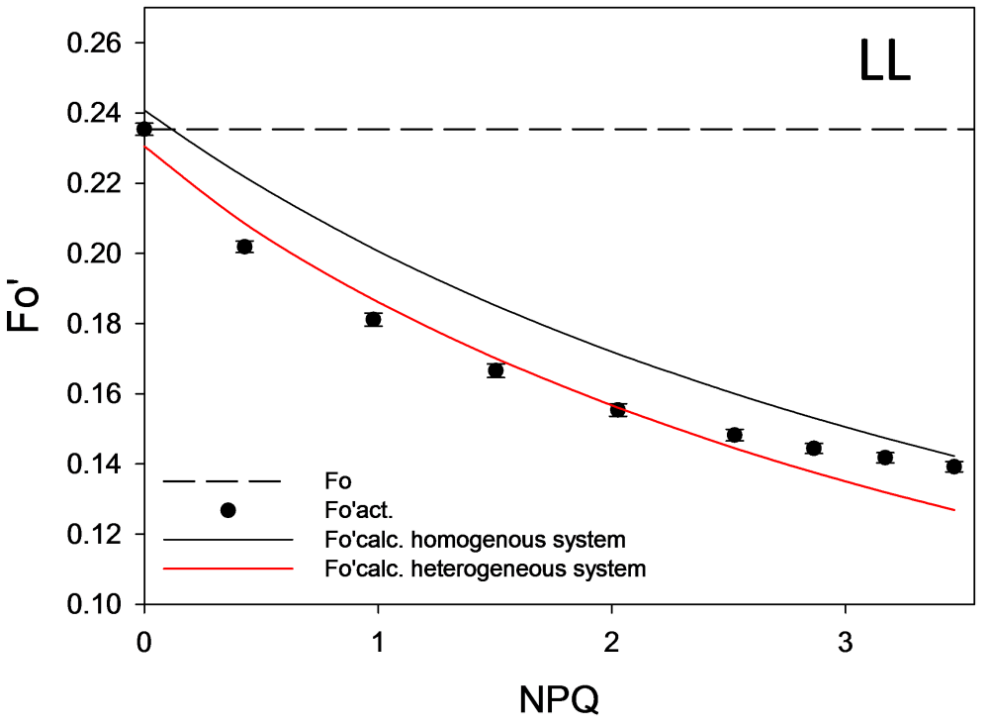

Figure 7.17 Association of NPQ and $Fo'_{act.}$ recorded during a gradually increasing actinic light routine performed on whole intact leaves from low light grown plants. Error bars show the standard error of the mean (n = 30). The continuous black line was plotted using the formula of Oxborough and Baker (Equation 1.18). The continuous red line was plotted using a modified formula for a heterogeneous photosynthetic membrane system (Ware *et al.*, 2015a).

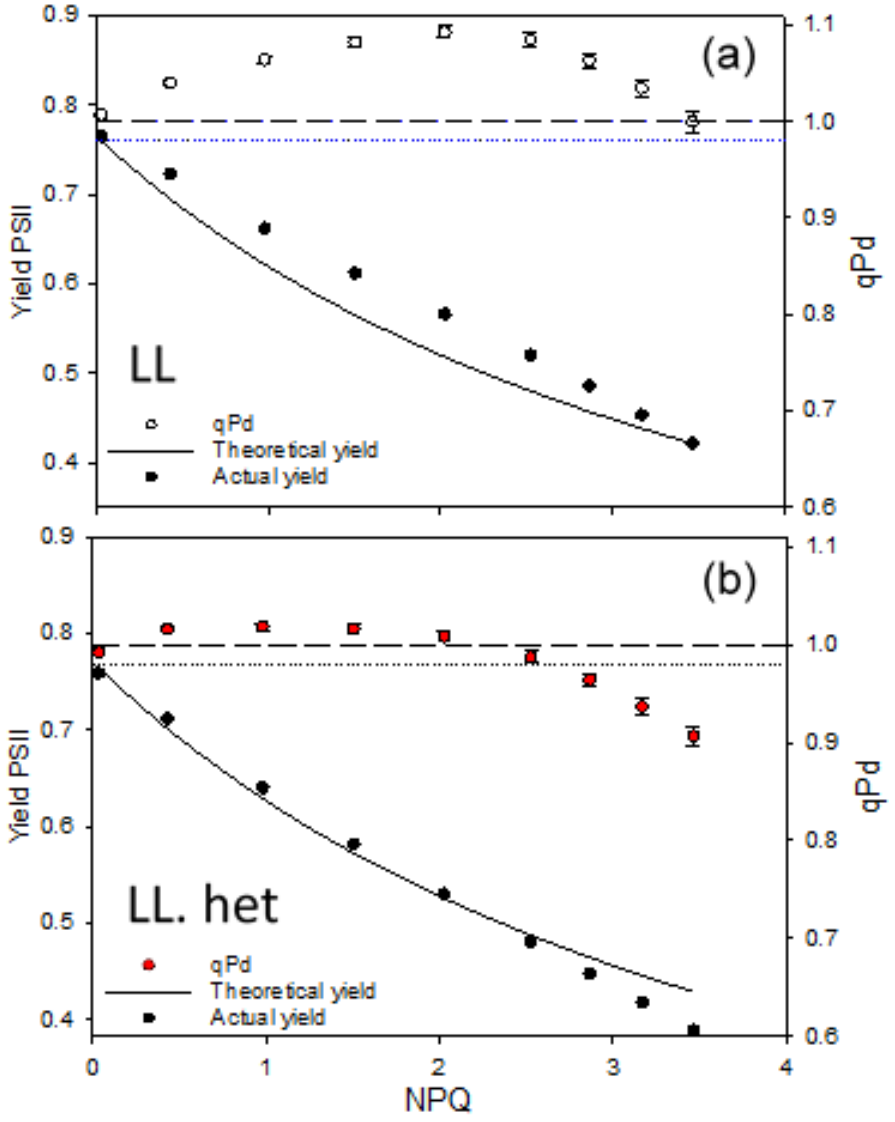

Figure 7.18 Relationship between NPQ and qP_d (open circles) and NPQ and PSII actual yield (closed circles) for (A) low light grown plants (B) corrected low light grown plants using the modified formula of Oxborough and Baker (Equation 7.01). Data points were averaged from 30 repeats on whole intact leaves. Error bars show the standard error of the mean (n = 30). The theoretical yield (continuous line) was calculated using qP_d always equal to 1.00 (Ware *et al.*, 2015a).

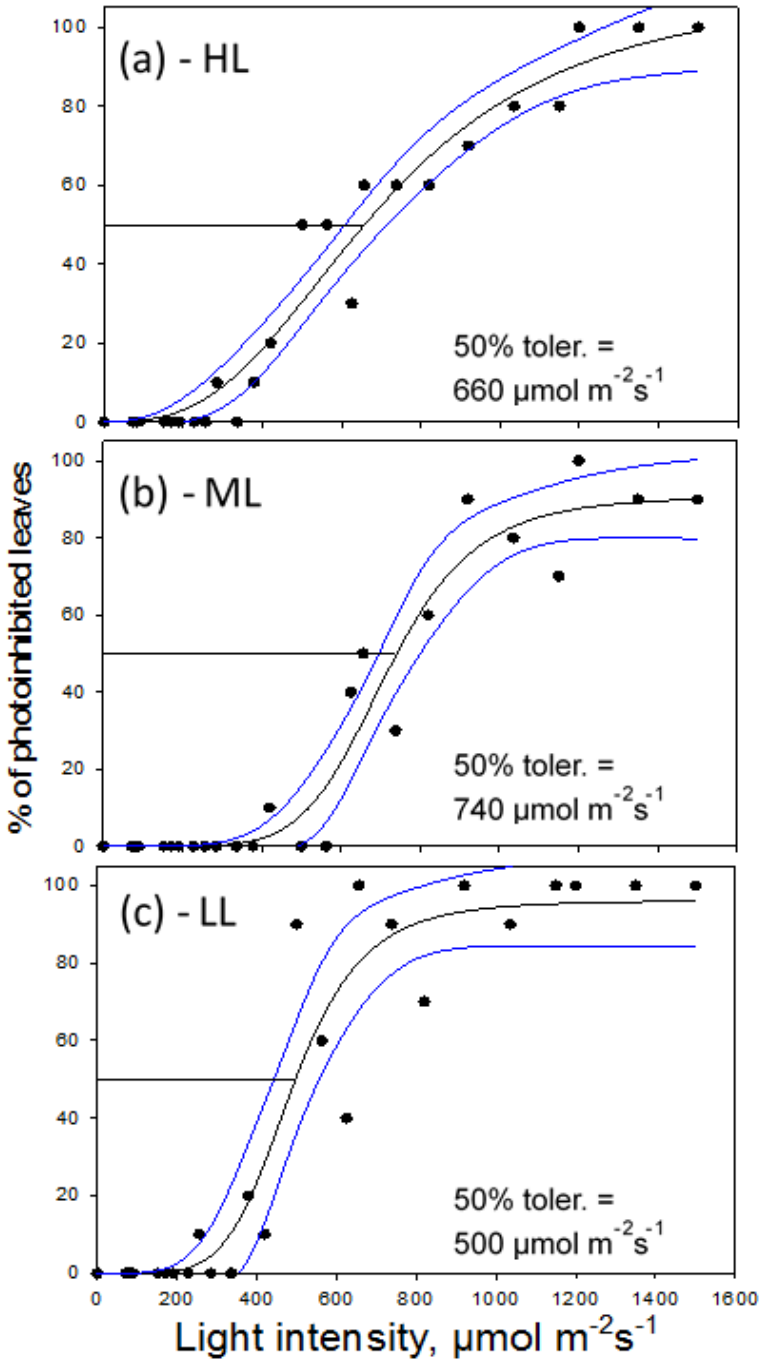

Figure 7.19 Association between actinic light intensities and the percentage of photoinhibited leaves (qP_d < 0.98) for (a) HL, (b) ML and (c) LL *Arabidopsis* leaves. Percentage data points were calculated from 10 gradually increasing light routine experiments (Fig. S1) for 80, 90 and 100% actinic light intensities of 0, 90, 190, 280, 420, 625, 820, 1150, 1500 µmol m^{-2} s^{-1}. Regression fit curves (Sigmoidal, Hill, 3 Parameter; f =axb/cb+xb)) and 95% confidence intervals were plotted using SigmaPlot12 (Systat Software, Inc., Chicago, USA) (Ware *et al.*, 2015a).

7.3 Discussion

- Lincomycin-treated plants and low light treated plants exhibit qPd rises above 1.00 during fluorescence measurements.
- High light acclimated plants are the most tolerant to photoinhibition, having the lowest qP_d values at the procedure end, and the highest ΦPSII.
- Average Fv/Fm values are significantly reduced in LL acclimated plants, indicative of an increased antenna network.
- Medium light plants had the highest light intensity required to cause the first signs of photoinhibition ($qP_d < 0.98$) in 50% of leaves, at 740 µmol photons m^{-2} s^{-1}.
- Lincomycin-treatment exacerbates the increased LHCII:RCII ratio, with treatment resulting in a 150% increase in LHCII compared to high light acclimated plants, but only 10-20% increased energetic coupling of LHCII-RCII.
- Compared to HL acclimated plants, LL plants had a 38% increase in physically bound LHCII, but there was only a 28% increase in the functional cross section.
- The formula of Oxborough and Baker (1997) was modified to rectify the discrepancy between energetically and functionally coupled antenna.
- The discrepancy between $Fo'_{calc.}$ and $Fo'_{act.}$ can be rectified using our new formula, allowing the pNPQ assessment procedure to be successfully applied to plants that are acclimated to different light intensities, or plants that are exposed to abiotic stresses to be compared.

Chapter VIII – Disentangling Photoprotection and Photorepair

8.1 Introduction

The final results section of my thesis concerns the repair rates of the reaction center D1 protein. During the course of my PhD, I presented the theory and findings of the pNPQ methodology at an internal University of London seminar. Professor Nixon, a reaction center specialist, proposed the idea that D1 protein repair rates could affect the conclusion made using the pNPQ assessment procedure and qP_d measurements. If the D1 protein is repaired more quickly in certain mutants, then pNPQ might not be the determining factor governing light tolerance. Although D1 protein repair has been calculated to take place over longer timescales than the pNPQ assessment procedure (Tyystjarvi *et al.*, 1994, Sacharz, 2015), it was imperative to test whether it was a contributing factor of light tolerance, and if so, how much it contributes to it. Fluorescence techniques and Western blot analysis was used to test infiltrated chloroplasts, infiltrated leaves and on genetic mutants that have impaired D1 protein repair cycles and NPQ formation (Table 2.01). Whilst the use of uncouplers can incite criticism, as they can disrupt the intermolecular bonds of the proteins that they are bound to (Fan *et al.*, 2015). The combination of all these experiments and the extremely close pattern of results yielded conclusive evidence as to which mechanism is more important in maintaining ΦPSII in short light treatments, and what the repair rate of PSII reactivation during dark-phase recovery is.

8.2 Results

For around 30 years, classical fluorescence parameters have been used without a review on what they actually tell us. Fv/Fm, qI and qE are common measures of NPQ and photoinhibition (Fig 8.01), yet they are ambiguous, misleading and in some cases, have lead the wrong conclusions in the photoprotective characterisation of mutant plants. Here classic conditions used to measure photoinhibition and NPQ were recreated and compared to the new parameters qP_d and pNPQ. It is proposed that these as the only true means of measuring the real protective capacity of NPQ and ascertaining the state of reaction centers without disrupting light treatments. Furthermore, reaction center repair, mostly in the form of the D1 protein is considered the most important factor in maintaining a high PSII yield. Here it is demonstrated through a variety of methods that although RC repair is important, pNPQ is actually the factor which protects plants in high light conditions and is essential for maximum PSII yield.

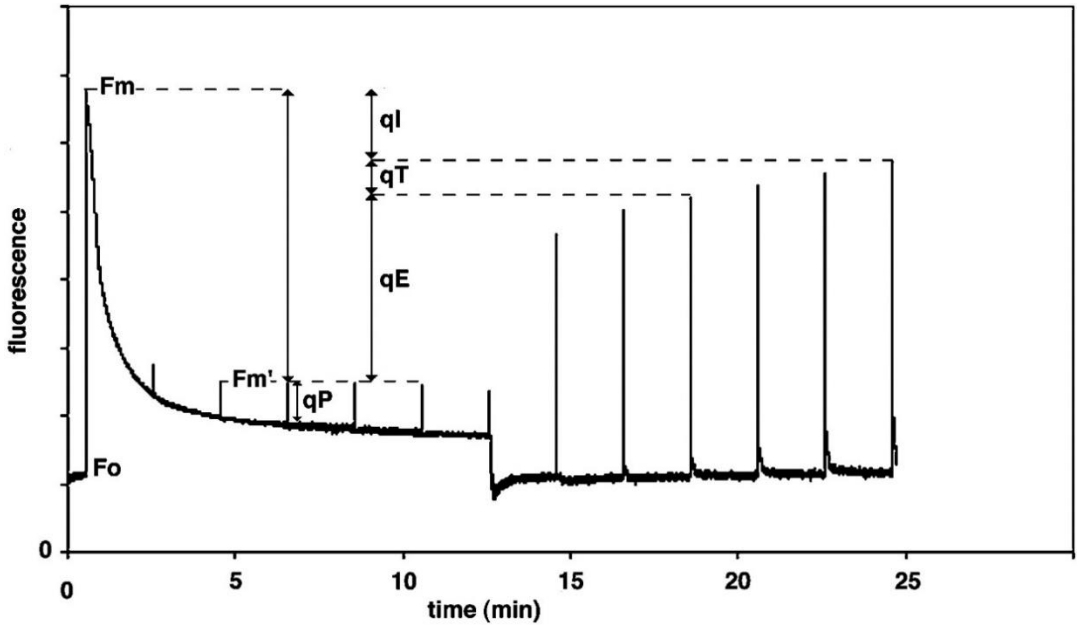

Figure 8.01 Chlorophyll fluorescence induction trace. The difference between Fm and Fm' (e.g. qE = Fm/Fm'-1) is used to calculate qP, qE, qT and qI, depending on the recovery period after the removal of actinic light (From Muller et al., 2001).

Two main experimental procedures have been employed, fluorescence and biochemical methods. Fv/Fm has been the principally used parameter in fluorescence to measure plant fitness and photodamage. A problem with using Fv/Fm, is that is mainly dependent on Fm, which in turn is affected by NPQ. Fv/Fm has a hyperbolic relationship with NPQ, small amounts of NPQ from 0-5 cause a decrease in Fv/Fm of 0.6. However, once reaching ~0.2, NPQ does not cause Fv/Fm to decrease any further (Fig 8.02B). qI is also measured using fluorescence and sometimes used as a marker for photoinhibition. qI is measured after a period of dark relaxation, and the sustained decrease in Fm' is attributed to qI. Employing a typical NPQ induction experiment, 190 µmol m^{-2} s^{-1} AL for 30 min before 15 min dark recovery, and measuring changes in fluorescence, it is evident that Fv/Fm and qI can provide alternative conclusions for the same experiment (Fig 8.02A). Here, using qI, WT plants suffer significantly less photoinhibition than *npq2* and L17 plants during a 30-min low light experiment (*t*-test, $P < 0.05$). Using the same data set, the use of Fv/Fm proposes that *npq2* leaves are significantly more photodamaged than L17 and WT leaves (*t*-test, $P < 0.05$). This is a contradictory conclusion, despite these two parameters being used to apparently measure the same phenomenon, photoinhibition. qP_d on the other hand is dependent on ΔFo, which reflects the state of reaction centers. qP_d did not decline below 1.00 in any of the different genotypes, showing a sharp inconsistency to the conclusions presented using Fv/Fm and qI. This illustrates a fundamental problem of using the qI parameter, when it does not have a consistent timeframe for measurement. Even so, using a timeframe would not negate the problem that different mutations affecting the dynamics of NPQ formation and relaxation causes. A parameter that does not depend on the NPQ of maximal fluorescence is vital, if the state of RCII is to be accurately measured. Some of the experiments conducted during my PhD have supported the notion that pNPQ is the determining factor in photoprotection. The used of qP_d as a measure of photoinhibition has been vital in this. However, qP_d is a measurement of the state of RCII, and RCII can undergo a repair process when it becomes damaged. Therefore, using a variety of methods, the repair rates of RCII were tested to ascertain whether the light tolerance of plants is affected by D1 protein repair during the pNPQ assessment procedure.

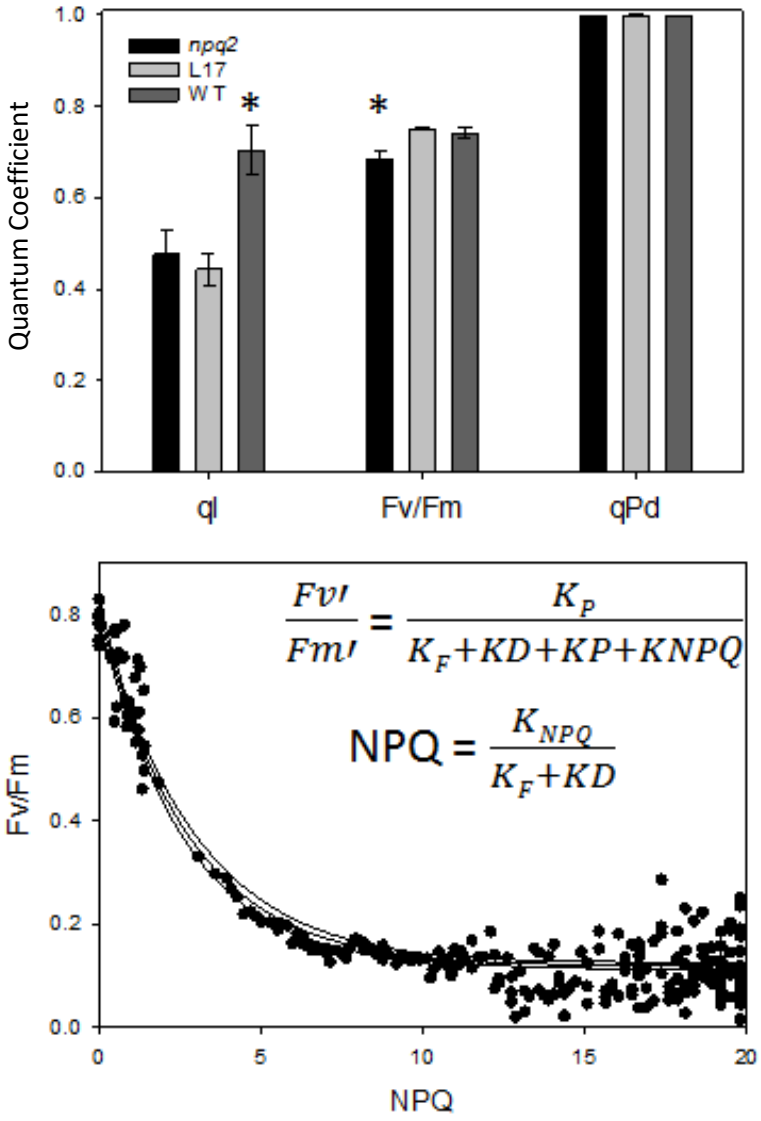

Figure 8.02 A *npq2*, L17 and WT plants were exposed to 190 µmol m^{-2} s^{-1} for 30 min, prior to 15 min dark relaxation. Saturating pulses (SP) were applied 10 seconds after light exposure to measure qP_d, and 15 min after illumination to assess qI and Fv/Fm. Error bars represent SEM, with four repeats performed for each genotype (n = 4). An asterisk represents a significant difference between one genotype and the other two genotypes (*t*-test, $P < 0.05$). B represents the relationship between NPQ and Fv/Fm for 12 hr illumination experiments under 2000 µmol m^{-2} s^{-1}. SP was applied every 30 min in the dark after a brief 10sec of far red (FR) light. Regression analysis was performed using SigmaPlot12.0 (Exponential Decay, Single, 3 Parameter, f = y0+a*exp(-b*x). Equations represent NPQ and Fv/Fm parameters expressed as rate constants.

The pNPQ assessment procedure was adapted for use on the DUAL-PAM-100 (see Appendix Item 3), but with the DUAL-PAM actinic light settings being slightly different to the JUNIOR-PAM, the actinic light intensities were 0, 95, 170, 286, 448, 698, 865, 1076 and 1667 µmol m^{-2} s^{-1} (Fig 8.03). Despite this slight change, the DUAL-PAM is an extremely useful PAM device as it can be used on leaves but also chloroplasts. Chloroplasts are 'clean' photosynthetic apparatus, that are unaffected by leaf thickness, are free from chloroplast migration, and can also have uncouplers easily applied to the solution they are in. There are a number of uncouplers that can be used to isolate different mechanisms of the NPQ and D1 repair processes. lincomycin, has been previously mentioned as an inhibitor of the chloroplast genome, and this can be used to inhibit the D1 repair cycle. Ammonium chloride (NH_4Cl) and nigericin are uncouplers and inhibit the formation of a transmembrane ΔpH, thus inhibiting pNPQ (Hipkins and Baker, 1986; Cao *et al.*, 2013). Diaminodurene (DAD) increases the cyclical electron flow around Cyt *b6/f* and PSI, enhancing ΔpH, and increasing NPQ (Wraight and Crofts, 1970; Mills and Barber, 1975; Johnson and Ruban, 2011). Performing the procedure on intact chloroplasts yielded some interesting results. The photoinhibitory light intensity varied between every set of chloroplast (z-test, $P < 0.05$). The light intensities that damaged 50% of chloroplasts in the control, lincomycin, NH_4Cl, DAD and DAD + lincomycin treated chloroplasts is 600, 125, 460, 990 and 900 µmol m^{-2} s^{-1} respectively (Fig 8.04A). qP_d at the end of the procedure also showed the same pattern with 0.79, 0.45, 0.74, 0.96 and 0.93 (Fig 8.04B). Not all of the conditions yielded significantly different qP_d values at the end of the procedure though. Significant differences arose between the NH_4Cl treated chloroplasts, which are significantly more photodamaged than any of the other treated or control chloroplasts (z-test, $P < 0.05$). The DAD treated chloroplasts, with and without lincomycin have significantly higher qP_d value at the procedure end (z-test, $P < 0.05$). The results here suggest that NPQ is the most important factor determining photoprotection. Inhibition of NPQ resulted in significantly reduced light tolerance and a greater degree of photoinhibition by the procedure end. Conversely, enhanced NPQ increased the light tolerance of 50% of chloroplasts, and only resulted in 4% of RCII being closed. The addition of lincomycin reduced the tolerance of chloroplasts compared to the WT, suggesting

that D1 protein repair does start during the procedure. In NPQ enhanced conditions, the difference between lincomycin treated chloroplasts and none-treated is reduced. This could be an important research consideration for improving yields crops that have NPQ capacities. This is not surprising as the D1 repair cycle will play less of a prominent role if there are fewer RCII damaged. 45 min light exposure was perhaps too long for some of the chloroplast samples, as Fv/Fm was reduced in some of the follow up experiments, therefore the same principle conditions were applied to whole leaves to be certain that the DUAL-PAM experiment conclusions were correct.

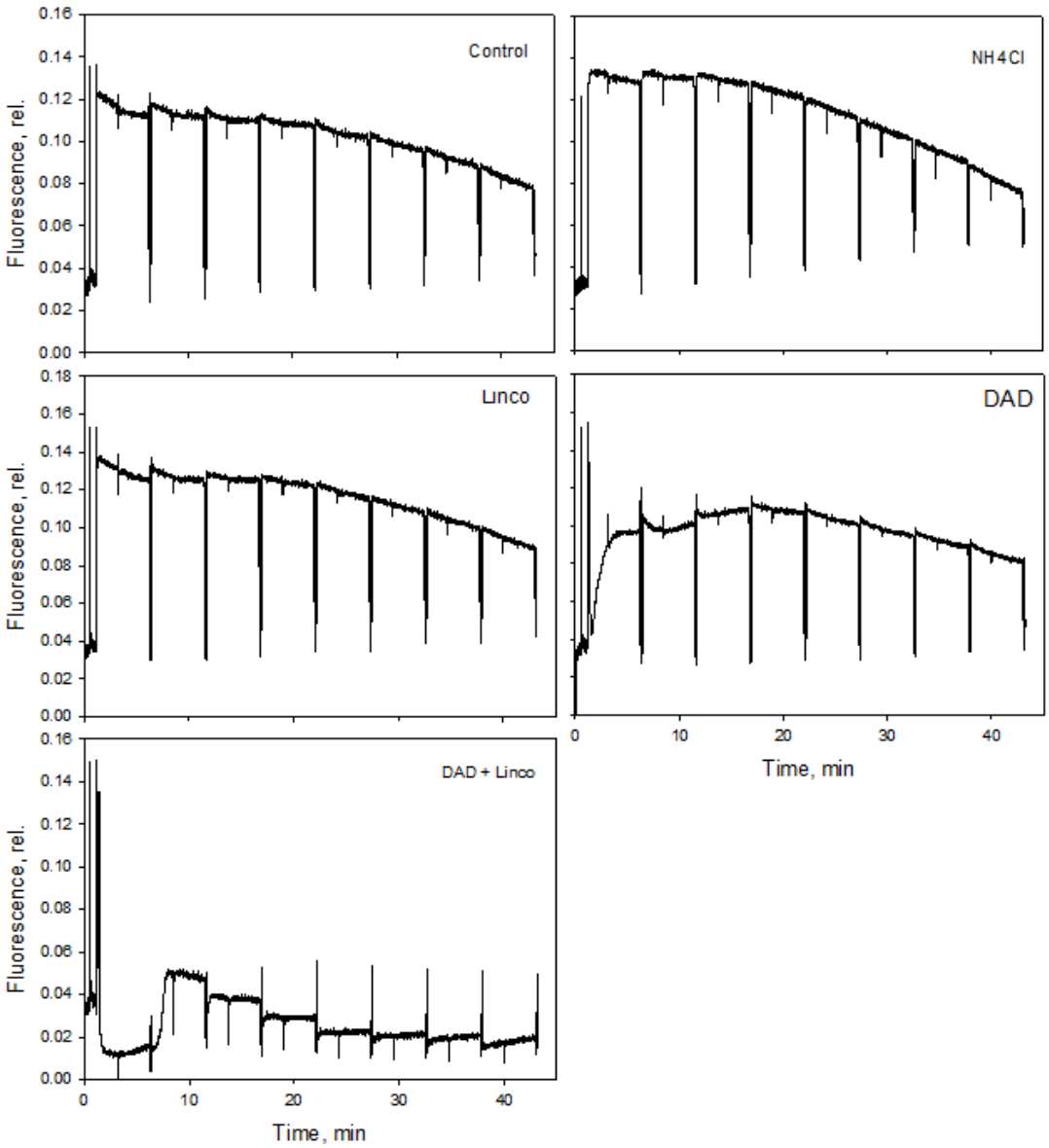

Figure 8.03 Typical chlorophyll fluorescence scheme of induction performed on WT (A) control (B) NH_4Cl (C) lincomycin (D) DAD and (E) DAD + lincomycin treated intact chloroplasts. The eight-step increasing actinic light (AL) routine used in this example 0, 95, 170, 286, 448, 698, 865, 1,076 and 1,667 µmol m^{-2} s^{-1} AL intensities were used.

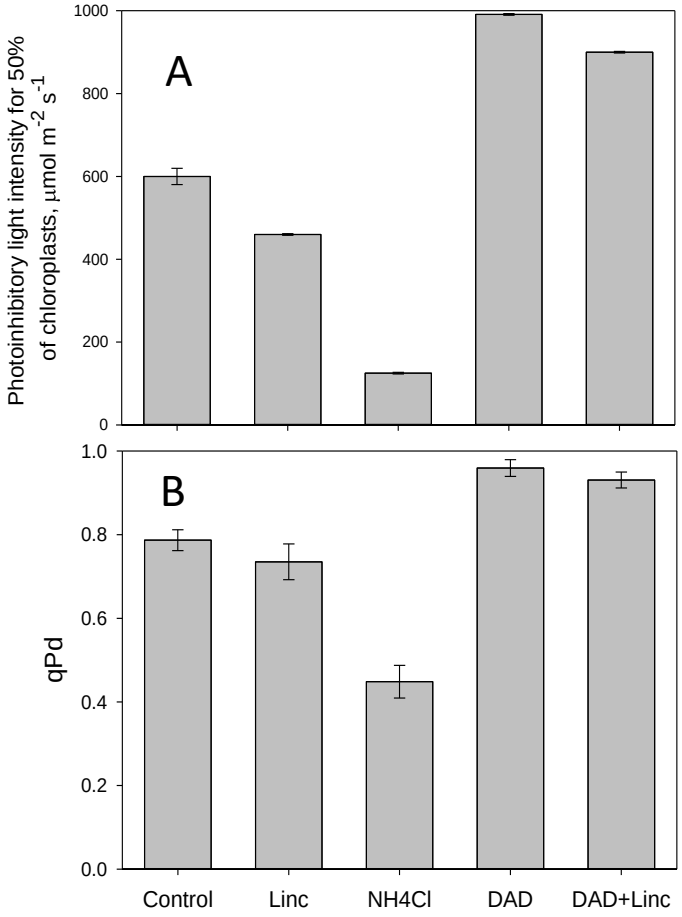

Figure 8.04A The light intensity which caused photoinhibition (qP_d < 0.98) in 50% of chloroplasts. Actinic light intensities used on the DUAL-PAM-100 were: 95, 170, 286, 448, 698, 865, 1076 and 1667 µmol m^{-2} s^{-1}. Different letters correspond to significantly different results (z-test, P < 0.05). B The average qP_d value at the end of the procedure. Error bars represent the SEM (n = 6).

Whole leaves were then subjected to the pNPQ assessment procedure, with the typical 0, 90, 190, 285, 420, 625, 820, 1150, 1500 µmol photons m^{-2} s^{-1} sequence used. Whole leaf infiltration with DAD did not work, either by vacuum infiltration or by soaking cotton wool in solution. Therefore, L17 plants, which have enhanced NPQ compared to WT, were used as the 'NPQ enhanced' subject (Fig 8.05). The L17 leaves and WT leaves were infiltrated with HEPES and sorbitol, so that the control would also be affected by any cell disruption or increased absorption that might occur with infiltration techniques (Vogelmann and Evans, 2002). As was the case with intact chloroplasts, an NPQ enhanced test group was also infiltrated with the D1 repair inhibitor lincomycin. D1 protein repair and NPQ inhibited leaves were ascertained using lincomycin and NH_4Cl infiltrated WT leaves respectively. The results obtained were remarkably similar to the chloroplast infiltration experiments. The light tolerance curves obtained show the same trend, that NPQ-less leaves are most susceptible to photodamage, with 50% of leaves displaying photoinhibition at 50 µmol photons m^{-2} s^{-1}. The next groups to suffer photoinhibition in 50% of leaves is the D1 inhibited WT group at 340 µmol photons m^{-2} s^{-1}, then WT at 400 µmol photons m^{-2} s^{-1}, lincomycin infiltrated L17 leaves at 600 µmol photons m^{-2} s^{-1} with the most tolerant being the NPQ enhanced L17 leaves at 725 µmol photons m^{-2} s^{-1}. The light intensities inducing photoinhibition in 50% of leaves were significantly different between all groups (z-test, $P < 0.05$), which was the same result as the light intensity inducing photoinhibition in 50% of chloroplasts (Fig 8.06A). The degree of photodamage (qP_d) in leaves at the end of the procedure also showed the same pattern as that in chloroplasts (Fig 8.06B). The best protected leaves were L17, and L17 infiltrated with lincomycin. These two groups have significantly higher average qP_d values that the other groups with 0.95 and 0.9 correspondingly (z-test, $P < 0.01$). WT control and lincomycin infiltrated WT leaves were the next best protected with 0.85 and 0.8 qP_d values, which was significantly higher than NH_4Cl infiltrated leaves (z-test, $P < 0.01$). The NPQ-less leaves had an average of 54% damaged RCII, only having 0.46 qP_d by the procedure end. The leaf infiltration experiments match and support the chloroplast infiltration experiments.

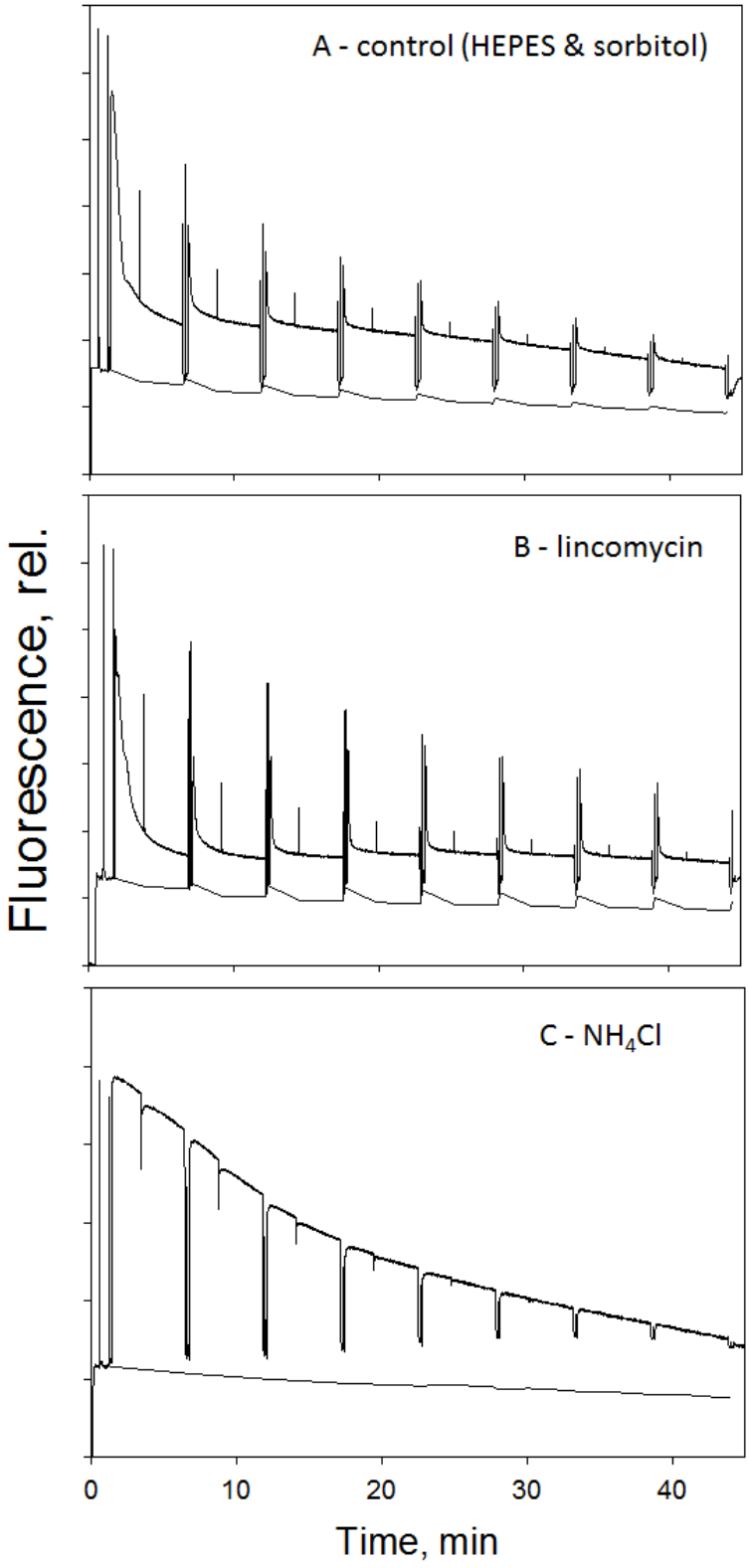

Figure 8.05 Typical chlorophyll fluorescence schemes of induction performed on (A) HEPES and sorbitol (B) lincomycin (C) NH_4Cl infiltrated leaves. The eight-step increasing actinic light (AL) routine used in this example is 0, 90, 190, 280, 420, 625, 820, 1150, 1500 µmol m^{-2} s^{-1} AL.

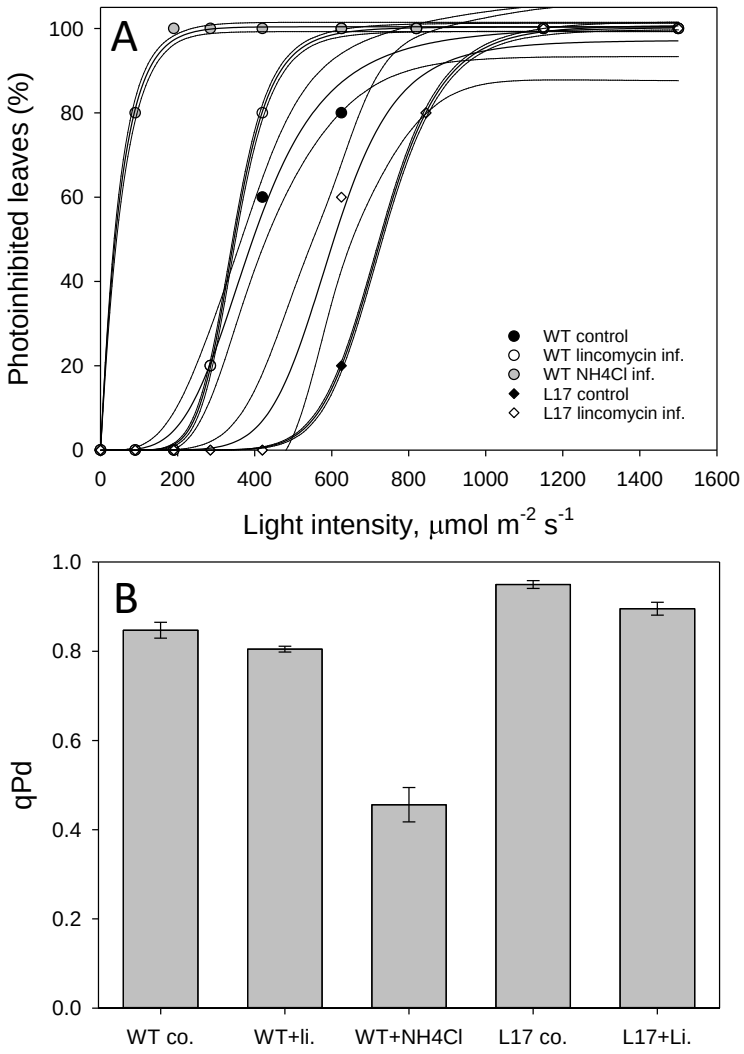

Figure 8.06A Leaf population tolerance calculated from the pNPQ procedure on detached leaves infiltrated with HEPES and sorbitol (WT and L17 control) and either lincomycin or ammonium chloride (NH_4Cl). Regression analysis was performed using with SigmaPlot12.0 (Sigmoidal fit, Hill 3 parameter, f = a*x^b/[c^b+x^b]). B Average qP_d values at the end of the pNPQ procedure. Error bars represent SEM (n = 5). Different letters correspond to significantly different results (z-test, $P < 0.05$).

A documented problem with uncouplers is that they can have undesired effects on the photosynthetic membrane, owing to their aggressive interaction with proteins and lipids. There is a genetic mutant (*Var2*) that has an inhibited D1 repair cycle. Combined with the L17 and WT plants, it seemed worthwhile to check that the conclusions drawn with the chemical-induced inhibition of different processes is the

same as genetically altered inhibition of the same processes. A documented problem with the *Var2* plants is that they have a variegated leaf (Bailey *et al.*, 2002), which gives rise to the name Var, but also that the excitation pressure in these plants is enhanced compared to WT plants, possibly due to RCII changes. Owing to this problem, the WT plants used were a combination of plants grown at 100 and 250 µmol photons m^{-2} s^{-1}, which had the same average 1-qP as the *Var2* plants (Fig 8.08B). Five plants were exposed to the 0, 90, 190, 285, 420, 625, 820, 1150, 1500 µmol photons m^{-2} s^{-1} actinic light procedure, with five more being exposed to 80 and 90% of these values too (Fig 8.07). Light tolerance curves were produced using the data, and these again showed a similar trend to the results obtained in the uncoupler experiments (8.08A). *Var2* plants had a significantly lower light intensity (500 µmol photons m^{-2} s-1) that causes photoinhibition in 50% of leaves, compared to WT and L17 plants (z-test, $P < 0.05$). Furthermore, the NPQ-enhanced plants had a significantly higher tolerated light intensity for 50% of leaves, at 950 µmol photons m^{-2} s^{-1} compared to the 650 µmol photons m^{-2} s^{-1} by WT leaves. This means that the three independent experiments have a correlation between the importance of NPQ and D1 repair in phototolerance. Fig 8.09 illustrates the importance of D1 protein repair and pNPQ in the light tolerance of plants during the pNPQ assessment procedure. Approximately 20% of the light tolerance capacity of control plants is due to the D1 protein repair rate. The importance of this mechanism is reduced in NPQ enhanced conditions. This clearly demonstrates that pNPQ is more important than D1 protein repair during the pNPQ assessment procedure. However, it is apparent that D1 protein repair plays a role. Furthermore, the pNPQ assessment procedure is designed to allow maximum pNPQ to form, without the speed of its formation being an impact. It was therefore important to see whether D1 protein repair was variable, and whether it would play a more significant role when plants were exposed to immediate high light conditions and the velocity of pNPQ formation was a variable.

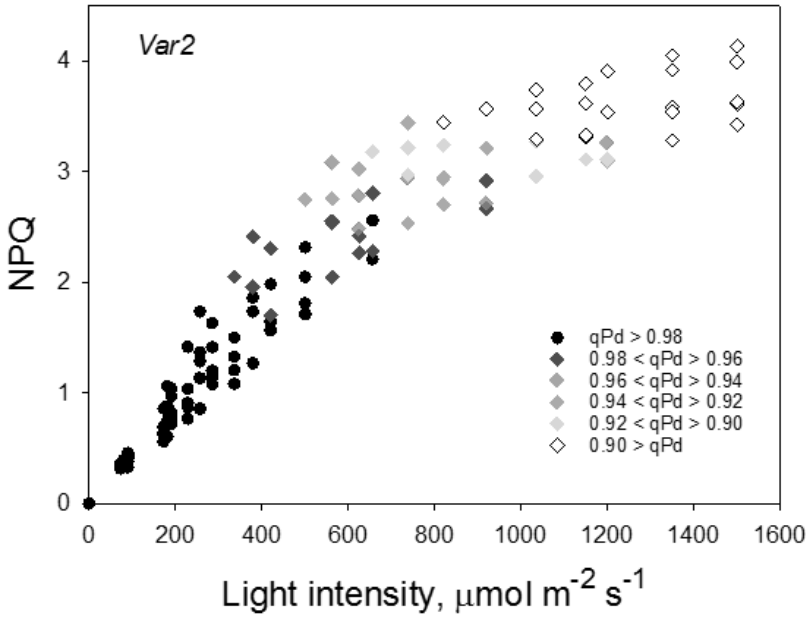

Figure 8.07 Relationship between NPQ, light intensity and qP_d parameters in the *Var2* mutant *Arabidopsis* plants conducted during the pNPQ assessment procedure.

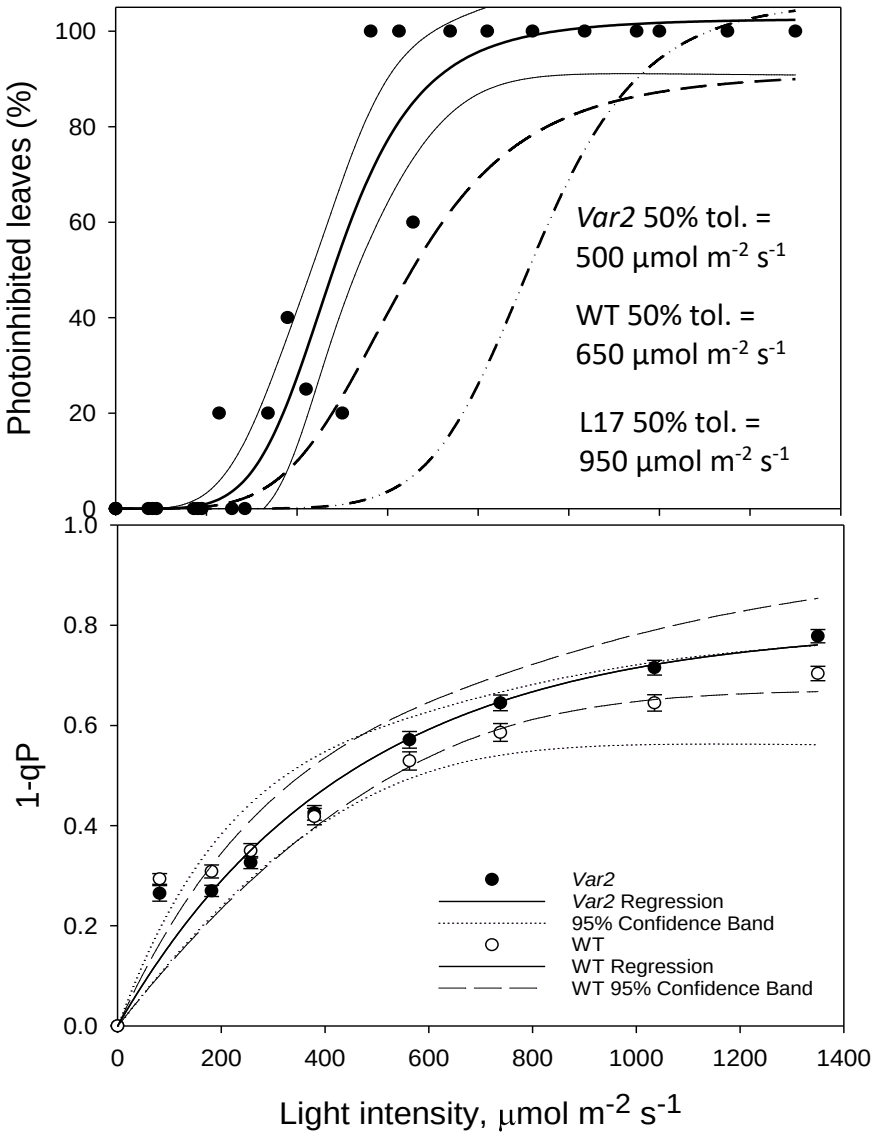

Figure 8.08A Population phototolerance for WT and *Var2* whole intact leaves. Plants were considered photoinhibited when qP_d < 0.98. 10 WT and 5 *Var2* and L17 repeats were performed for each light intensity. Regression analysis was performed with SigmaPlot12.0 (Sigmoidal fit, Hill 3 parameter, f = a*x^b/[c^b+x^b]). B Excitation pressure of whole intact WT and *Var2* leaves measured during the pNPQ assessment procedure. Regression analysis was performed using SigmaPlot12.0 (Exponential Rise to Maximum, Single, 2 parameter, f = a*[1-exp(-b*x)]). Error bars represent SEM (n = 10).

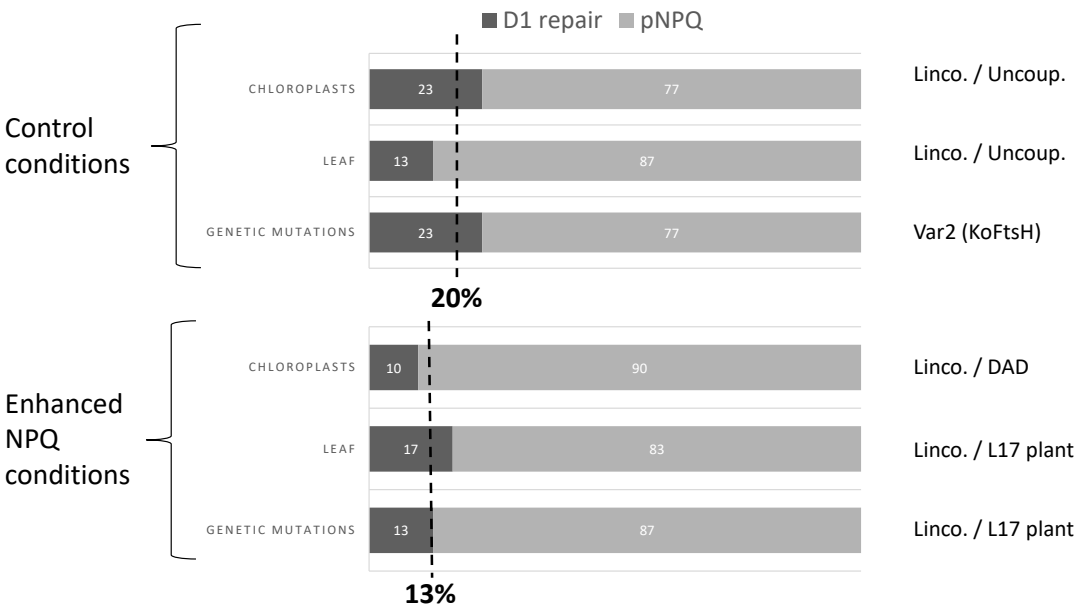

Figure 8.09 Estimated contribution of D1 protein and pNPQ to light tolerance of chloroplasts and leaves in control and enhanced NPQ conditions.

In order to test the importance of D1 protein repair in constant high light conditions, whole attached leaves were illuminated with 2200 µmol photons m^{-2} s^{-1} for up to 12 hours. This was the highest actinic light intensity achievable with a JUNIOR-PAM, and considerably above 1500 µmol photons m^{-2} s^{-1}, a light intensity that some L17 plants could tolerate without photodamage, and therefore a suitable light intensity to induce photodamage in all subject plants here. WT and L17 plants were used for reasons previously explained. *npq4* plants were used here as they have slow forming pNPQ and would therefore be best plant to assess the maximum D1 protein repair contribution. WT plants watered with lincomycin were the D1 protein repair inhibited group. qP_d was measured throughout the course of the 12-hr illumination period by having a 10 s dark period with FR-light illumination to relieve the excitation pressure around PSII. The trends of qP_d decline offer an important insight into the D1 protein repair mechanism (Fig 8.10). All plants types showed a qP_d decline until ~2 hours of illumination, a timeframe consistent with literature for the activation of D1 protein repair (Tyystjarvi *et al.*, 1994; Sacharz, 2015). At this point, two of the plant types showed a recovery of qPd back towards 1.00, indicative of D1 protein repair, whilst the other two had continued decline in qPd but at different rates. Of the two that recovered, L17 plants, which have higher NPQ forming capacities recovered the best. pNPQ serves to reduce the excitation pressure around PSII. It therefore fits that the highest forming pNPQ plant had the greatest rate of D1 protein repair. If the rate of D1 damage is less, due to less excitation pressure, this could mean that even if the rate of D1 protein repair was constant, then the higher NPQ forming plants would recover more quickly. L17 and WT plants average qP_d declined to ~0.61, yet the L17 plants recovered to 0.88, yet the WT to only 0.75 after 12 hours of illumination. *npq4* plants, had an initial decline in qP_d dropping to 0.57, this continued to decline reaching 0.53 ten hours later. The NPQ levels of *npq4* plants was not as low as might be expected, but crucially in the first hour, it was markedly lower than the WT and L17 plants, which caused the deep photoinhibition seen. The average NPQ levels were also lower than the WT in the latter parts of the illumination period which may explain why qP_d never recovered in the *npq4* plants. Lincomycin-treated plants, which had the lowest NPQ capacity here, seemed unable to relieve the excitation pressure caused

by 2200 µmol photons m^{-2} s^{-1}. It is unusual that lincomycin-treated plants had such a low NPQ capacity when it has been demonstrated that weakly coupled antenna have higher quenching capacity than connected antenna (Belgio *et al.*, 2012; Ware *et al.*, 2015). The high light intensity used here may have caused the leaf damage, indeed some photobleaching was evident on the leaves, which is why the experiments were stopped at ~8 hours. Unfortunately, it was not able to conduct further repeats due to a limitation of plant material at the time my laboratory experiments were due to be finished. The remainder of the plants were used to perform Western blots on D1 protein levels, as this would offer an alternative approach to the fluorescence based experiments used so far.

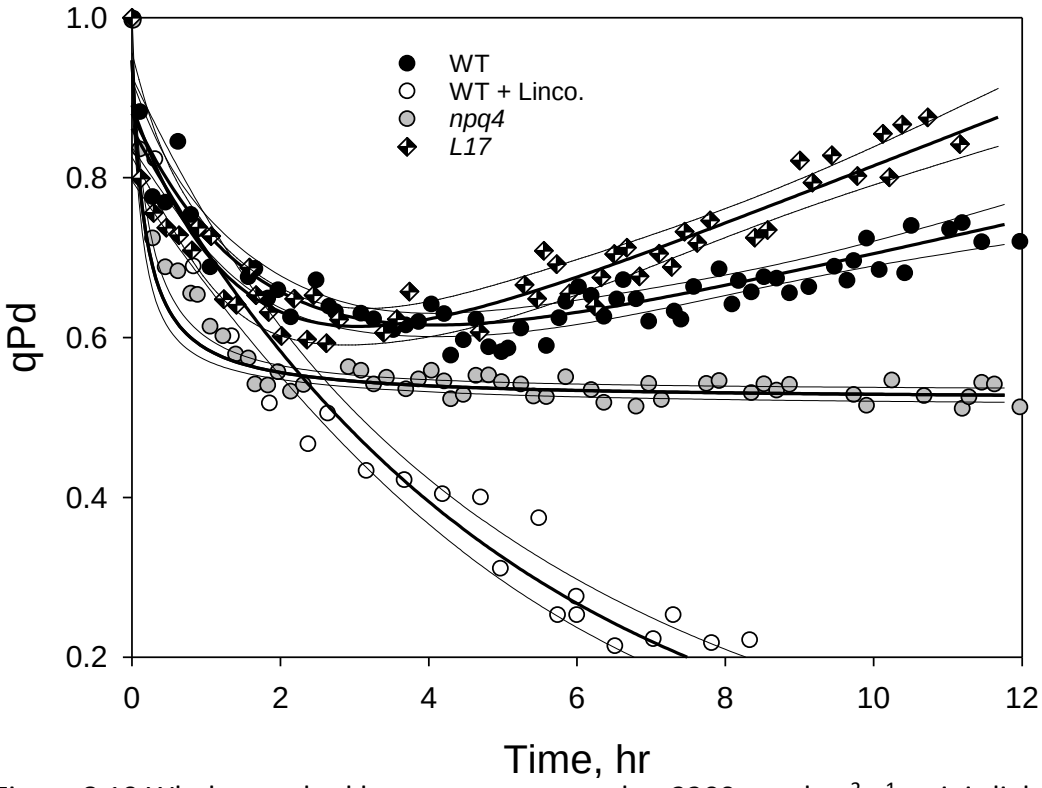

Figure 8.10 Whole attached leaves were exposed to 2200 µmol m^{-2} s^{-1} actinic light for 12 hours using a JUNIOR-PAM (Walz). Saturating pulses were applied every 10 min, after 10 sec of far red light in the dark. Data points are the average of 3 independent plants. Regression analysis was performed using SigmaPlot 12.0 (WT/L17, Exponential Decay, Exponential Linear Combination f = y0+a*exp(-b*x)+c*x; WT + Linco./*npq4*, Exponential Decay, Modified Single, 3 Parameter, f = a*exp[b/(x+c)]).

Three types of plant material were used to measure the amount of protein that had been degraded. Leaves were only exposed for 3 hours as this was well within the timeframe at which photobleaching could occur, but also long enough that lincomycin-treated plants had lower qP_d levels than WT and L17 plants. Leaves were exposed to ~2000 µmol photons m^{-2} s^{-1}, with leaves being immediately frozen in liquid nitrogen afterwards. D1 protein levels relative to WT plants were found to be 78 and 101% in the lincomycin-treated and L17 plants respectively (Fig 8.11). D1 protein concentrations were calculated as a proportion of lhca2, which is a stable protein and unlikely to vary between the different plant types. This offers additional support to the HL fluorescence experiments, that a decline in qP_d reflects RCII closure and D1 protein degradation. The L17 and WT plants which had similar qP_d results, here has similar amount of D1 protein. The lincomycin-treated plants which had the much lower qP_d values, also had less intact D1 protein.

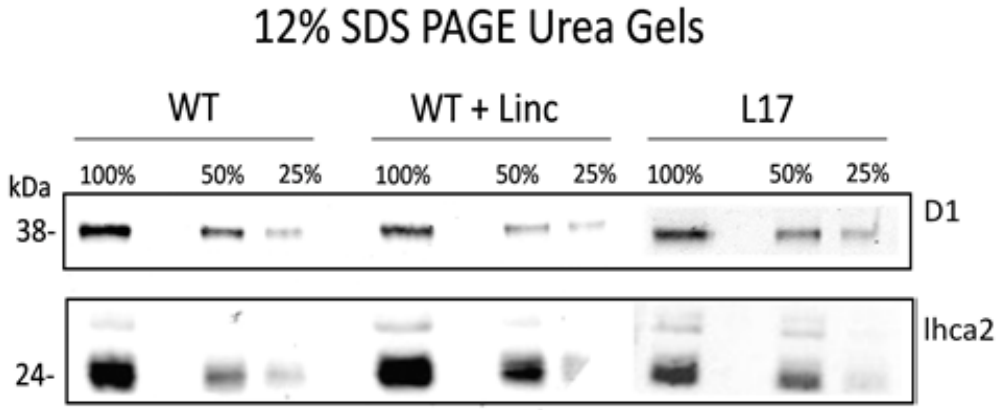

Figure 8.11 Western blot analysis of reaction center D1 and lhca2 antenna proteins. Leaves were exposed to 2000 µmol photons m^{-2} s^{-1} for 3 hr before being immediately frozen in liquid nitrogen. Separation of unstacked thylakoids was carried out on 12% acrylamide gel. 1 µg of chlorophyll per lane was loaded and detection was performed with ImageJ software. See Materials and Methods for antibody and procedure details.

The final point of investigation in D1 protein repair was to ascertain what the rate of repair was dependent on, if anything at all. Firstly, plants with different dynamics of NPQ relaxation were tested to see if the rates of qP_d recovery were different. WT, L17 and *npq4* plants were exposed to 1500 µmol photons m^{-2} s^{-1} until qP_d reached ~0.85. The NPQ levels were significantly different at the time qP_d reached ~0.85 (*t*-test, $P < 0.05$). NPQ declined to ~0.55 two hours after the AL was removed, which demonstrated different NPQ recovery rates (Fig 8.12B). However, qP_d recovery rates were remarkable similar, and were not significantly different at any point during the 2-hr recovery (Fig 8.12A). This suggests that the levels of NPQ do not affect the recovery of closed RCII.

Next, WT plants were exposed to 1500 µmol photons m^{-2} s^{-1} until qP_d reached between 0.4-0.499, 0.5-0.599, 0.6-0.699, 0.7-0.799, 0.8-0.899 or 0.9-0.999 (Fig 8.13). Upon reaching this value, the AL was turned off and qP_d recovery monitored. There is an initial jump in qP_d recovery during the first 30 min after AL removal, before a steadier recovery over the next 90 min. Due to the seemingly dramatic differences during this initial period, the qP_d recovery rates were plotted as a function of time (Fig 8.13). The rates of recovery increase as the extent of photodamage increased. The rates of recovery are significantly less when plants have only 10-20% of damaged RCII, compared with those with 60-30% photodamage (z-test, $P < 0.05$).

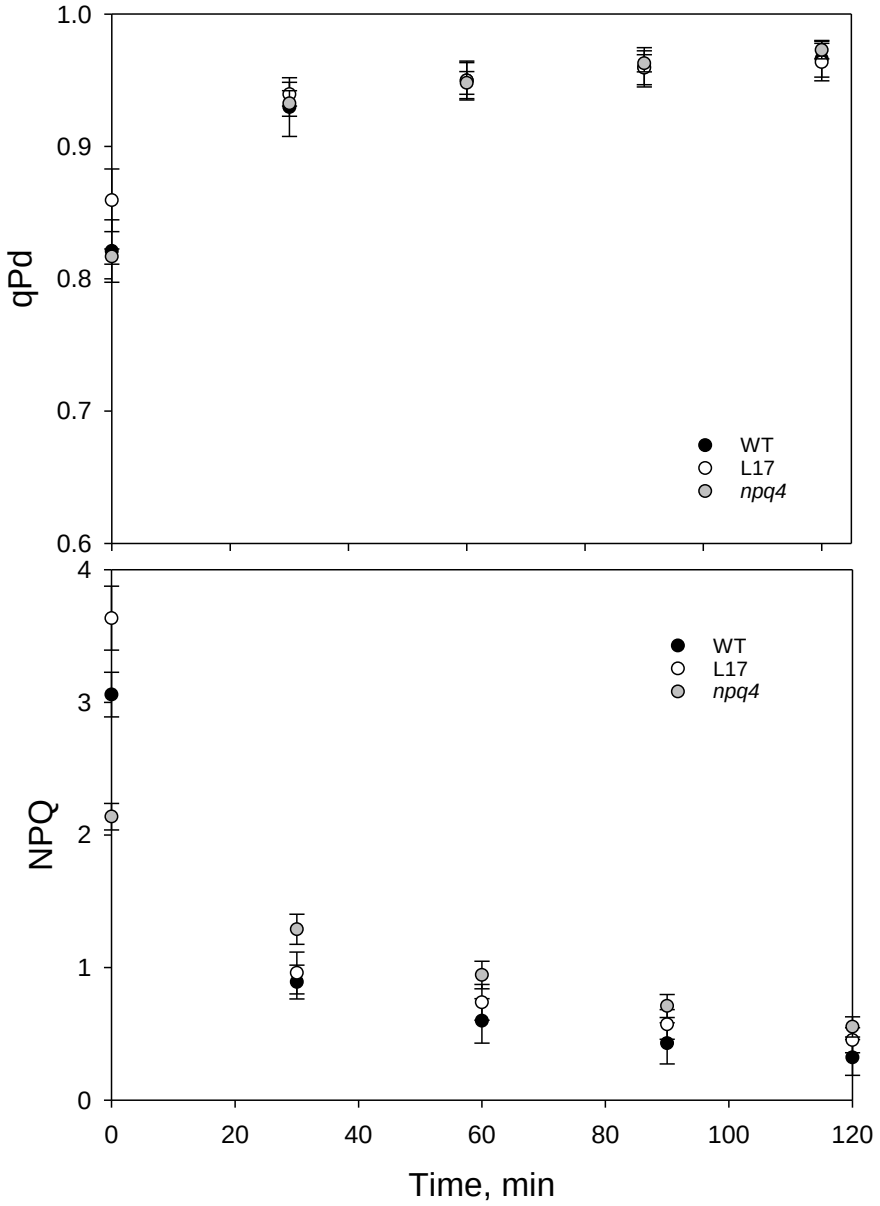

Figure 8.12A Whole attached leaves were exposed to 1500 µmol m^{-2} s^{-1} actinic light (AL) for 5-15 mins using a JUNIOR-PAM (Walz), until qP_d dropped to ~0.85. Saturating pulses were applied every 5 min, after 10 sec of far red light in the dark. During recovery, SP were applied every 30 min for 2 hr. Data points are the average of 3-6 independent plants. Error bars represent SEM (n = 3-6). B SP were applied every 5 min during illumination to measure NPQ. After qP_d reached ~0.85, NPQ values were measured every 30 min in the dark. Error bars represent SEM (n = 3-6).

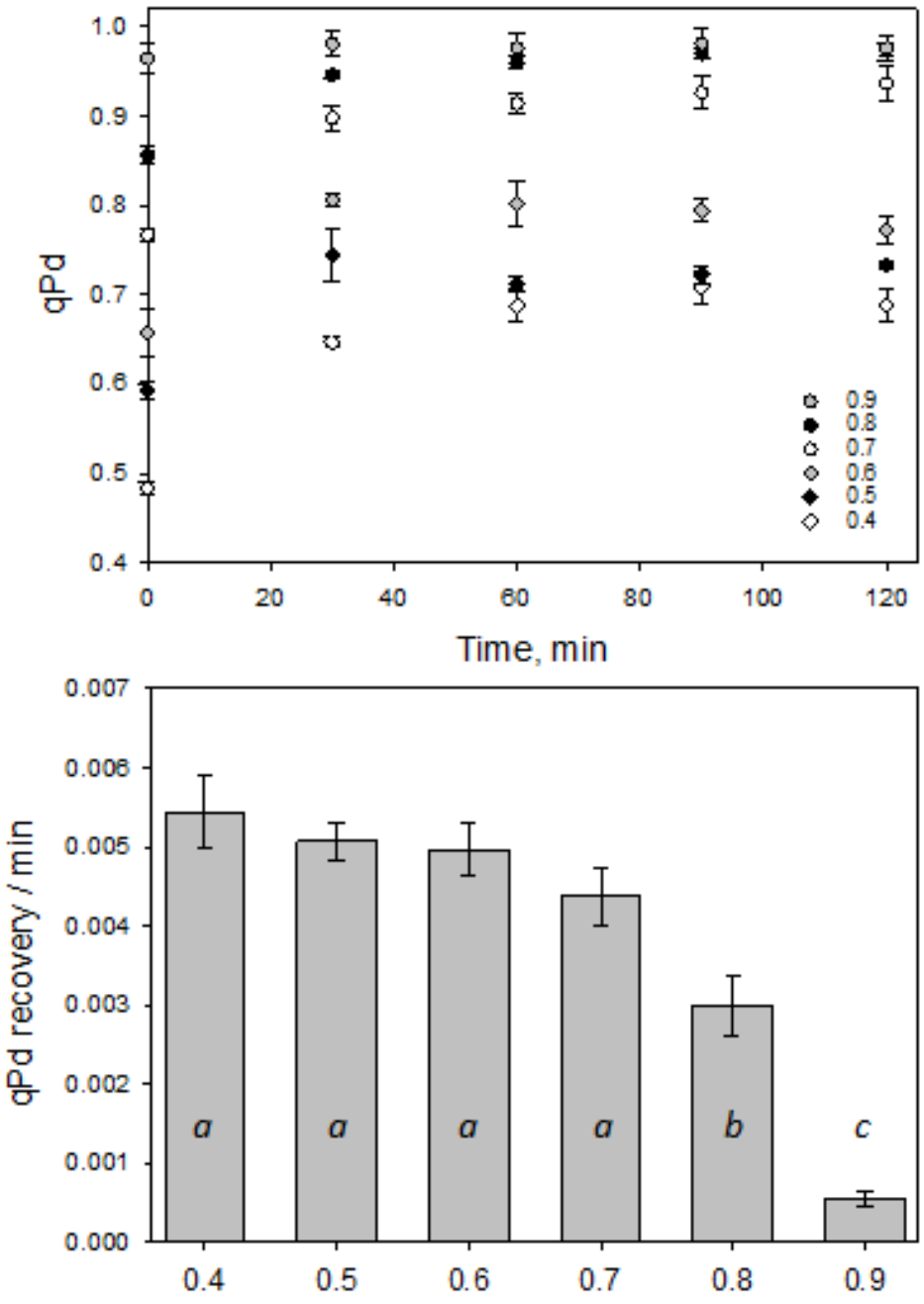

Figure 8.13A 1500 µmol m^{-2} s^{-1} actinic light (AL) was applied to whole intact leaves using JUNIOR-PAM (Walz). Leaves were illuminated until qP_d dropped to 0.4-1, taking between 2-30 min. qP_d recovery was monitored by applying saturating pulses every 30 min in the dark. B The initial rate of recovery in the first 30 min after removal of AL. Different letters correspond to significantly different results (*z*-test, $P < 0.05$). Error bars represent SEM (n = 3).

8.3 Discussion

- Plants with either the NPQ or D1 repair mechanism were isolated by vacuum infiltration on leaves, infiltration performed on chloroplasts or by genetic mutation.
- It was demonstrated that protein repair accounts for approximately 20% of high light tolerance.
- In NPQ enhanced conditions, the dependency on D1 protein repair is reduced to ~13%.
- The rates of D1 protein repair are not dependent on NPQ levels, but rather the amount of photodamage that has been sustained, with lower qPd values predicting faster repair rates.
- qPd values were found to correspond with intact D1 protein levels in the thylakoid membrane, via Western blot analysis.

Chapter IX –

Summary and Future Work

9 Discussion

In this project I established a new pNPQ assessment procedure. This built on the theory established by Ruban and Murchie (2012), which had theoretically validated the use of qP_d as a parameter to measure RCII closure. The establishment included the actinic light intensities, far-red intensity, duration of exposures and total length of the procedure. A .txt program file containing the code for this was written, and the process including the .exe file to extract data detailed in Appendix 1 and Appendix 4. Together this has ensured this is reproducible for any other user wishing to employ the procedure. Whilst developing this, plant growth conditions were optimised, including the stratification of seeds, new soil, higher light intensities for growth, no thinning during growth, and watering plants from below. These techniques combined to produce plants with higher Fv/Fm values (0.80<), notably healthier physical characteristics, and rectified the qP_d rise phenomena. Taken together, this early work helped to ensure maximum ΦPSII's, so that pNPQ and photoinhibition could, as near as is feasibly possible, be the only factors that affect ΦPSII.

Using the pNPQ assessment procedure, it was demonstrated that the fluorescence contribution of PSI should be considered when measuring ΦPSII. The establishment of the procedure allowed for the testing of PSI fluorescence contributions to PSII fluorescence measurements. As proposed by Pfündel *et al.*, (2013), the ΦPSI fluorescence should be considered as this offers more precise information on the ΦPSII. The model of a constant 24% contribution from PSI fluorescence to the Fo level, as proposed by Pfündel *et al.*, (2013) was first tested. However, a constant offset was shown to invalidate ΔFo measurements. Coupled with previous literature findings (Ruban *et al.,* 1991; Richter *et al.,* 1999; Holzwarth *et al.,* 2009; Miloslavina *et al.,* 2011; Ballottari *et al.,* 2014) the constant fluorescence offset seems to be incorrect. Based on literature and experimental findings, which both provide evidence that fluorescence originating from PSI is quenched, a decreasing contribution of PSI fluorescence was tested. This restored the relationship predicted between $Fo'_{act.}$ and $Fo'_{calc.}$, the function of the qP_d parameter (Ruban and

Murchie, 2012; Ruban and Belgio, 2014) and light tolerance curves (Ruban and Belgio, 2014). The results presented here suggest that the fluorescence contribution of PSI is quenchable at high light intensities, furthermore, that a correction for it should be used to accurately calculate Fv/Fm, NPQ and ΦPSII values in chlorophyll *a* fluorescence measurements.

Ontogenesis has been shown to affect the high-light tolerance of plants. The aim of this experiment was to quantify the light tolerance of plants at different ages. It was found that light tolerance is indeed age dependent. Juvenile and senescent phases were the most susceptible to damage, with adult and reproductive phases the most tolerant. Eight-week old plants were found to have the highest tolerance, with 1,385 µmol photons m^{-2} s^{-1} required to cause photoinhibition in 50% of leaves. Interestingly, juvenile and senescent plants have the highest NPQ levels during the actinic light procedure, but they were also the most susceptible to photodamage. Higher NPQ levels at these phases of ontogenesis has been reported previously, but susceptibility to photodamage varies depending on the plant species (Dodd et al. 1998; Manetas et al. 2002; Choinski Jr. et al., 2003; Liu et al. 2009). The novelty of the pNPQ assessment procedure is that we can see the high NPQ in these plants is not protective, and appears to need time to evolve. Besides assessing the pNPQ capacities, the ETR, chlorophyll content, Chl *a*/*b* ratios, anthocyanin levels, Fv/Fm, leaf thickness and ROS accumulation were all tested to see whether they contributed to the age-dependent light tolerance. The patterns of pNPQ capacity, total chlorophyll content and ETR were found to match very closely, suggesting that these three factors are the most important for determining high light tolerance during ontogenesis. The dependency of pNPQ formation on age is also true of leaves of different ages on the same plant. Inner, intermediate and outer leaves were tested on the same plant, and were also found to have the same age-related relationship to light tolerance.

The PsbS protein has previously been stated to be essential for NPQ (Li *et al.*, 2002) but also demonstrated to not be a requirement (Johnson and Ruban, 2011). The aim of this research was to therefore quantify the contribution of PsbS protein to pNPQ, and measure the PsbS-dependent quenching capacity of plants devoid of

RCII. A combination of non-invasive PAM fluorescence experiments, coupled with TCSCP and FFEM experiments, allowed for a detailed description of the dependency and dynamics of NPQ on PsbS to be formed. Fluorescence analysis showed that plants overexpressing PsbS protein (*L17*) have higher NPQ and pNPQ capacities than WT and PsbS knock-out (*npq4*) plants. This led to a higher light intensity required to cause the first signs of photoinhibition in 50% of leaves in the L17 plants compared to the WT and *npq4* plants. The WT however had a higher ΦPSII compared to L17 plants, suggesting that overexpression of PsbS protein compromises the rates of photosynthesis in these plants. This increased pNPQ, and thus deeper quenching is harder to relax, which causes a decreased ΦPSII even after the removal of actinic light (Ruban *et al.*, 2003). Furthermore, varying the PsbS protein concentration affects phototolerance but not the mechanism of NPQ. Ruban and Belgio (2014) and Ware *et al.,* (2014) showed that it is not the type or components of pNPQ that govern photoprotection but the capacity of pNPQ, a result also seen here. Varying the concentration of the PsbS protein affects the dynamics of pNPQ formation. Having no PsbS protein causes NPQ to form more slowly, and increases the amount of photodamage that arises. This is evident under a constant high light procedure, when the rate and amplitude of pNPQ are both determining factors, not just the absolute capacity. The final investigation in this chapter involved the testing of varied PsbS protein concentration on lincomycin-treated membranes. As already mentioned, this model system allows the investigation of NPQ in a system devoid of RCII and crucially *in vivo*. In this system, it was shown that aggregated LHCII alone can cause a 700 nm absorption peak. This adds support for the Horton model that has suggested aggregated LHCII can quench energy of longer wavelengths (Ruban and Horton, 1992). Furthermore, the 729 nm band associated with PSI can be almost completely quenched, suggesting that in highly quenched systems, NPQ is present in PSI. The degree of quenching of the PSI band, and the size of the 700 nm peak, depend on the amount of NPQ formed. PsbS protein concentration affects the kinetics of NPQ formation, so *npq4* thylakoid membranes had to be exposed to high light for considerably longer than WT or *L17* plants. The change in spectra was attributed to changes in LHCII aggregation by FFEM. In *L17* thylakoid membranes, NPQ resulted in three-times more LHCII in any

given 25 nm radius than in the dark-adapted thylakoid membranes. Unfortunately, the FFEM experiment was attempted with *npq4* and WT thylakoids, however, the freeze-fracture machine would not work successfully again. Only fractures that were not clean enough to reliably recognise and count LHCII and RCII were produced. Furthermore, as the results of the publication were invited to be published in a special edition of the journal, therefore it was not possible to profile effects of PsbS protein concentration on LHCII aggregation.

The aim of this chapter was to quantify the contribution of different xanthophylls *in vivo* to pNPQ, using the most accurate fluorescence parameter for determining the onset of photoinhibition, qP_d. WT plants were demonstrated to have the highest phototolerance capacity, ΦPSII and pNPQ capacity. Of the three groups of mutants, plants expressing lutein, violaxanthin and/or zeaxanthin, the ones expressing zeaxanthin has the highest tolerance. The drawback here is that zeaxanthin expressing plants have reduced ΦPSII compared to other genotypes. *lut2* and *viol* plants had the joint highest ΦPSII, with *lut2* plants also having the highest light tolerance capacity. As WT plants, followed by single knock-out mutants, then multiple knock-outs had the highest photoprotective capacities, the structural roles of xanthophylls was also investigated to ascertain whether this was also a factor in light tolerance. Structural changes to LHCII would be expected to manifest in altered Chl *a*/*b*, PSI/PSII and LHCII/PSII ratios (Table 6.01, Table 6.04). Indeed, this proved to be the case, with *zea* plants having significantly smaller antenna sizes than all mutants except for *lute* (z-test, $P < 0.05$). In a complex relationship, the mutants with smaller antenna sizes actually had increased excitation pressure (1-qP) compared to the WT (Fig 6.10B). This is not a novel finding though, as it has been previously reported that plants with physically smaller antennas led to larger build-ups of excitation pressure (Härtel *et al.*, 1996). It does appear though that the antenna domain is altered by the lack of the structural anchor lutein. A future investigation to add to the results obtained here, would be to alter the actinic light intensities applied to generate the same excitation pressure, and measure which mutant can develop the highest pNPQ/NPQ capacities. This would limit the variation in ETR results through the impaired energy transfer pathways from

mutants with altered LHCII. However, pNPQ dissipates excess energy accumulated in the membrane, and thus, changing the AL intensity, would somewhat negate the selection pressure of requiring pNPQ to tolerate high light. At present, it is not possible to alter the individual light intensities on the JUNIOR-PAM, so this would be an experiment for the future when software developments might enable it. The results obtained here suggest that it is not one particular xanthophyll that is the 'true quencher', but rather a range of xanthophylls that are required to quench the photosynthetic membrane. A key reason for this could be the structural changes that occur when the membrane is quenched, which was demonstrated in Chapter 5. Altering the xanthophyll compositions of the antenna proteins appears to affect their aggregation properties, thus partially inhibiting NPQ. This could be due to the removal of neoxanthin in some of the mutants, the key xanthophyll in 'twisting' the LHCII trimeric complexes to bring Chl *a* terminal-emitters into proximity with lutein (Ruban *et al.*, 2005). This has been proposed to be the major dissipative pathway of excess energy in the photosynthetic membrane, and could thus be a reason for the significantly reduced NPQ in mutants compared to WT plants. This is perhaps not a surprise, as over millions of years, the machinery present in higher plants that is responsible for light harvesting and excess energy dissipation, is remarkably similar between species. This suggests that plants have already evolved a successful combination of apparatus, which maximises photoprotection, whilst minimising the reduction in ΦPSII. The key conclusion from this work is that no one xanthophyll seems to offer exceptional photoprotection. Disrupting the cocktail of mutants changes the structure of the photosynthetic membrane, which indicates that structure is key for pNPQ formation, and perhaps changing the stoichiometry of xanthophylls is not going to improve crop efficiency. As was recently the case with the research published by Kromdijk *et al.*, (2016), changing the enzyme regulatory pathway to change xanthophyll expression should be a future avenue of research. The findings here would suggest that increasing zeaxanthin concentrations under low fluctuating light, and increasing lutein concentrations in high light compared to the WT could improve the photoprotective capacities of plants.

Plants acclimated to different light intensities were also investigated to ascertain whether the qP_d rise phenomenon discovered in plants grown under the laboratories previous conditions, was correlated with plant acclimation histories. Indeed, plants grown under high light conditions were the most tolerant to the actinic light procedure. Fv/Fm is significantly reduced in low light acclimated plants, suggesting an increased antenna network (Aro *et al.*, 1993; Wientjes *et al.*, 2013). At low light intensities or in the dark, increased LHCII creates a longer excitation pathway leads to more energy being lost via fluorescence and NPQ, whereas at high light intensities, it causes RCII to become saturated more quickly (Belgio *et al.*, 2014). Lincomycin-treatment exacerbates the increased LHCII:RCII ratio, with treatment resulting in a 150% increase in LHCII compared to control plants. As RCII is limited in size, and can thus only be bound to a limited number of LHCII, the effect of accumulating extra LHCII in the membrane was investigated. In the lincomycin-treated and low light acclimated plants, there is a disparity between the physical and energetic coupling of antenna to RCII. A hypothesis was developed that the discrepancy between the physically and functionally bound LHCII causes the qP_d rise phenomena. Belgio *et al.*, (2012) had demonstrated that the disconnected LHCII in lincomycin-treated systems had higher NPQ capacities that the WT plants. A model was created to visualise the differences between photochemical and non-photochemical quenching in heterogeneous membranes. The formula of Oxborough and Baker (1997; Equation 1.18) was modified to be able to incorporate heterogeneous membranes where disconnected antenna occurs (Equation 7.04). The discrepancy between $Fo'_{calc.}$ and $Fo'_{act.}$ can be rectified using a new formula developed here. This allows the pNPQ assessment procedure to be successfully applied to plants that are acclimated to different light intensities, or plants that are exposed to abiotic stresses to be compared.

Finally, the importance of reaction center repair and pNPQ on high light tolerance was determined. Using several approaches on leaves and chloroplasts, it was determined that pNPQ is more important than reaction center repair during the pNPQ assessment procedure. In plants with control amounts of NPQ, D1 protein repair accounts for approximately 20% of high light tolerance. In NPQ enhanced

conditions, the dependency is reduced to ~13%. Extended runs of extreme high light also support the notion that pNPQ is the most important factor in phototolerance. The rates of D1 protein repair are not dependent on NPQ levels, but rather the amount of photodamage that has been sustained, with lower qP_d values resulting in faster repair rates. This was calculated over a 30-min period after the removal of actinic light, as plants with lower qP_d values would naturally be able to exhibit greater recovery. The repair rates of the D1 protein were ascertained. Measuring qP_d restoration rates and through Western blots, it was discovered that repair rates do not affect pNPQ measurements using the assessment procedure. Indeed, for longer measurements of two hours or more, rates of repair should be considered, as there are even measurable differences in D1 protein quantities using Western blots.

The establishment of the pNPQ assessment procedure outlined here opens an interesting range of future research topics. The quantification of minor antenna protein complexes, the major antenna protein complex, state transitions and chloroplast migration quenching mechanisms could be quantified. Furthermore, the NPQ mechanisms of several different species could be elucidated, such as cyanobacteria, diatoms and mosses. pNPQ assessment could also be employed in the field on cultivated crops, but at present, without the development of a shutter to create the dark periods required for Fo' measurements, this would be difficult. Using the IMAGING-PAM, it has been shown that it can and would be useful to measure pNPQ on whole plant surface areas owing to the heterogeneity of its development. However, I imagine the costs to do this on a large scale would be huge and it may not be feasible.

There are two broad strategies to improve photosynthetic efficiency: increasing the absorption area of plants, and/or increasing the efficiency of absorption and conversion to carbon containing products. The work in this thesis falls entirely into the latter of these. pNPQ will be unlikely to change the absorption area of plants, unless as a secondary effect of an NPQ-related inhibition. It has been shown that altering NPQ dynamics, and therefore increasing photosynthesis efficiency, can significantly affect crop yields. It has been predicted that faster relaxation of NPQ

could increase crops yields by 20-30% (Zhu *et al.*, 2004; Kromdijk *et al.*, 2016). The work by Kromdijk *et al.*, (2016) has shown faster zeaxanthin epoxidation in shade conditions increases tobacco plant yields by 15%. My work has shown that the components of NPQ, PsbS protein and xanthophylls, are required for optimal pNPQ formation. Therefore, despite altering the kinetics of NPQ formation and relaxation, I wonder whether there is much more to elucidate in the NPQ process. The most logical step would appear to be increasing rates of photochemistry, as this would eradicate the need for pNPQ/NPQ and that would surely be the most sensible focus of research. The future of the pNPQ methodology could therefore be to test different species, that have colonised different habitats, to measure the relationships between ΦPSII and pNPQ. The components that contribute to the different pNPQ/ΦPSII relationships can then be investigated with a view to modify more traditional crops to inhabit these environments. This could, for instance, improve photosynthesis and crop productivity by accelerating recovery from photoprotection.

There are of course limitations to any technique, and PAM fluorescence is no exception. Some criticisms of fluorescence are that: light absorption affects ETR and 1-qP measurements and that it cannot be reliably predicted; that leaves and the photosynthetic membrane undergo significant conformational changes during measurements; that an area of ~1-10 mm that is used to predict whole leaf or plant behaviour; and that Fv/Fm and other fluorescence parameters might not provide the results that researchers expect e.g. Fv/Fm to measure plant fitness (Murchie and Lawson, 2013). There are however numerous benefits of using fluorescence to assess plant performance: it shows a greater degree of accuracy than any other technique, particularly using Western blots which have a ±15-20% error; new PAM devices are cheaper than many other pieces of equipment, such as O_2 electrodes; it offers *in situ*, *in vivo* and real-time assessments of plant fitness, NPQ formation and reaction center damage, something that no other technique can; and it can also be employed underwater, in the field and in laboratories, displaying the vast adaptability of it as a technique. Although it does take a while to gain the experience required to interpret results of fluorescence traces, PAM fluorescence can show transitional details of changes in the membrane that are not offered in

other techniques. For instance, Western blots take 1-2 hours to produce any changes in thylakoidal D1 protein quantities, and only provides a snapshot of a particular moment in time. Fluorescence is therefore a highly useful tool, and hopefully given the results found during the course of my PhD, pNPQ and qP_d will be used in the future to contribute to our knowledge of environmental responses in the green lineage.

Chapter X –

References

Adams WW., Zarter CR., Mueh KE., Amiard V., Demmig-Adams B. (2006) Energy dissipation and photoinhibition: a continuum of photoprotection. In *Photoprotection, Photoinhibition, Gene Regulation, and Environment* (eds Demmig-Adams B., Adams WW., Mattoo AK.) 49–64. Springer, Dordrecht.

Ahn TK., Avenson TJ., Ballottari M., Cheng Y-C., Niyogi KK., Bassi R., Fleming GR. (2008) Architecture of a charge-transfer state regulating light harvesting in a plant antenna protein. *Science* 320: 794–797.

Al-Khalili J. (2014) "The Mystery Of Photosynthesis, Let There Be Life, The Secrets Of Quantum Physics - BBC Four". BBC. N.p., 2017. Web. 8 Feb. 2017.

Allen JF., Fornsberg J. (2001) Molecular recognition in thylakoid structure and function. *Trends Plant Sci* 6: 317-326.

Amasino R. (2010) Seasonal and developmental timing of flowering. *Plant J* 61: 1001–1013.

Amunts A., Drory O., Nelson N. (2007) The structure of a plant photosystem I supercomplex at 3.4 Angstrom resolution. *Nature*: 447: 58–63.

Amunts A., Toporik H., Borovikova A., Nelson N. (2010) Model of plant Photosystem I structure determination and improved and biogenesis: membrane transport, structure, function. *J Biol Chem* 285:3478-3486.

Anderson JM., Chow WS., Goodchild DJ. (1988) Thylakoid membrane organisation in sun/shade acclimation. *Aust J Plant Physiol* 15: 11-26

Andersson J., Walters RG., Horton P., Jansson S. (2001) Antisense inhibition of the photosynthetic antenna proteins CP29 and CP26: Implications for the mechanism of protective energy dissipation. *Plant Cell* 13: 1193-1204.

Anwaruzzaman M., Chin BL., Li X-P., Lohr M., Martinez DA., Niyogi KK. (2004) Genomic analysis of mutants affecting xanthophyll biosynthesis and regulation of photosynthetic light harvesting in *Chlamydomonas reinhardtii*. *Photosynth Res* 82: 265-76.

Arnon DI., Allen MB, Whatley FR. (1954) Photosynthesis by isolated chloroplasts. *Nature* 174: 394–396.

Aro E-M., McCaffery S., Anderson JM. (1993a) Photoinhibition and D1 protein degradation in peas acclimated to different growth irradiances. *Plant Physiol* 130: 835-843.

Aro E-M., Virgin I., Andersson B. (1993b) Photoinhibition of Photosystem II. Inactivation, protein damage and turnover. *Biochim Biophys Acta* 1143: 113-134.

Avery GS. (1933) Structure and development of the tobacco leaf. *Am J Bot* 20: 565–592.

Babani F., Lichtenthaler HK. (1996) Light-induced and age-dependent development of chloroplasts in etiolated barley leaves as visualized by determination of photosynthetic pigments, CO2 assimilation rates and different kinds of chlorophyll fluorescence ratios. *J Plant Physiol* 148: 555–566.

Bailey S., Horton P., Walters RG. (2004) Acclimation of *Arabidopsis thaliana* to the light environment: the relationship between photosynthetic function and chloroplast composition. *Planta* 218: 793–802.

Bailey S., Thompson E., Nixon PJ., Horton P., Mullineaux CW., Robinson C., Mann NH. (2002) A critical role for the *Var2* FtsH homologue of Arabidopsis thaliana in the photosystem II repair cycle in vivo. *J Biol Chem* 277: 2006–2011.

Bailey S., Walters RG., Jansson S., Horton P. (2001) Acclimation of *Arabidopsis thaliana* to the light environment: the existence of separate low light and high light responses. *Planta* 213: 794–801.

Baker NR. (2008) Chlorophyll fluorescence: a probe of photosynthesis *in vivo*. *Ann Rev Plant Biol* 59: 89–113.

Ballottari M., Alcocer MJP., D'Andrea C., Viola D., Ahn TK., Petrozza A., Polli D., Fleming GR., Cerullo G., Bassi R (2014) Regulation of photosystem I light harvesting by zeaxanthin. *Proc Natl Acad Sci USA* 111: 2431–2438.

Ballottari M., Dall'Osto L., Morosinotto T., Bassi R. (2007) Contrasting behavior of higher plant photosystem I and II antenna systems during acclimation. *J Biol Chem* 282: 8947–8958.

Barber J. (1995) Molecular basis of the vulnerability of photosystem II to damage by light. *Aust. J. Plant Physiol* 22: 201-208.

Barber J. (2002) Photosystem II: a multisubunit membrane protein that oxidises water. *Curr Opin Struc Biol* 12: 523–530.

Barber J. (2009) Photosynthetic energy conversion: natural and artificial. *Chem Soc Rev* 38: 185-196.

Barker DH., Seaton GGR., Robinson SA. (1997) Internal and external photoprotection in developing leaves of the CAM plant *Cotyledon orbiculata*. *Plant Cell Environ* 20: 617–624.

Barros, T., Royant, A., Standfuss, J., Dreuw, A., Kühlbrandt, W. (2009) Crystal structure of plant light-harvesting complex shows the active, energy-transmitting state. *EMBO J* 28: 298–306.

Bassi R. (1996) Biochemistry and molecular biology of pigment binding proteins. In: *Light as an energy source and information carrier in Plant Physiology* (eds Jennings, Zucchelli, Ghetti, Colobbetti.), Plenum Press. New York 41-63

Bassi R., Dainese P. (1992) A supramolecular light-harvesting complex from chloroplast photosystem-II membranes. *Eur J Biochem* 204: 317-326.

Bassi R., Høyer-Hansen G., Barbato R., Giacometti GM., Simpson DJ. (1987) Chlorophyll-proteins of the photosystem II antenna system. *J Biol Chem* 27: 13333-13341.

Bassi R., Pineau B., Dainese P., Marquardt J. (1993) Carotenoid-binding proteins of photosystem II. *Eur J Biochem* 212: 297–303.

Becker B, Marin B (2009) Streptophyte algae and the origin of embryophytes. *Ann Bot* 103: 999–1004.

Belgio E., Johnson MP., Jurić S., Ruban AV. (2012) Higher plant photosystem II light-harvesting antenna, not the reaction center, determines the excited state lifetime-both the maximum and the nonphotochemically quenched. *Biophys J* 102: 2761–2771.

Belgio, E., Kapitonova, E., Chmeliov, E., Duffy, C.D.P., Ungerer, P., Valkunas, L., Ruban, AV. (2014) Economic photoprotection in Photosystem II that retains a complete light harvesting system with slow energy traps. *Nat Comm* 5, 5433.

Belgio, E., Ungerer, P., Ruban, AV. (2015) Light harvesting superstructures of green plant chloroplasts lacking photosystems. *Plant Cell Environ* 38: 2035-2047.

Bellafiore S., Barneche F., Peltier G., Rochaix J-D. (2005) State transitions and light adaptation require chloroplast thylakoid protein kinase STN7. *Nature* 433: 892–895.

Ben-Shem A., Frolow F., Nelson N. (2003) Crystal structure of plant photosystem I. *Nature* 426: 630–635.

Benson, S., Maheswaran, P., Ware, M.A., Hunter, C.N., Horton, P., Jansson, S., Ruban, AV., Johnson, M.P. (2015) An intact photosystem I light harvesting antenna system is required for complete state transitions in *Arabidopsis*. *Nature Plants* 1: 15176.

Berg JM., Tomoczko JL., Streyr L. (2002) The light reactions of photosynthesis. In: *Biochemistry* (eds Berg JM., Tomoczko JL., Streyr L.) 527-547. Freeman and Company, New York.

Bergantino E., Segalia A., Brunetta A., Teardo E., Rogoni F., Giacometti GM., Szabo I. (2003) Light- and pH-dependent structural changes in the PsbS protein of photosystem II. *Proc. Natl Acad. Sci. USA* 100: 15265–15270.

Berner R. (1997). Paleoclimate - The rise of plants and their effect on weathering and atmospheric CO2. *Science* 276: 544-546.

Bernhardt K., Trissl HW. (1999) Theories for kinetics and yields of fluorescence and photochemistry: how, if at all, can different models of antenna organization be distinguished experimentally? *Biochim Biophys Acta* 1409: 125–142.

Betterle N., Ballottari M., Zorzan S., de Bianchi S., Cazzaniga S., Dall'Osto L., Bassi R. (2009) Light-induced dissociation of an antenna heterooligomer is needed for non-photochemical quenching induction. *J Biol Chem* 284: 15255–15266.

Biswal U., Mohanty P. (1976) Aging induced changes in photosynthetic electron transport of detached barley leaves. *Plant Cell Physiol* 17: 323–331.

Björkman O., Demmig B. (1987) Photon yield of O_2 evolution and chlorophyll fluorescence characteristics at 77 K among vascular plants of diverse origins. *Planta* 170: 489–504.

Björkman O., Demmig-Adams B. (1994) Regulation of photosynthetic light energy capture, conversion, and dissipation in leaves of higher plants. In *Ecophysiology of Photosynthesis* (eds Schulze ED., Caldwell MM.), 17–47. Berlin: Springer-Verlag.

Blankenship RE. (2002) *Molecular Mechanisms of Photosynthesis*. Oxford: Blackwell Science.

Boekema EJ., Hankamer B., Bald D., Kruip J., Nield J., Boonstra AF., Rögner M. (1995) Supramolecular structure of the photosystem II complex from green plants and cyanobacteria. *Proc. Natl Acad. Sci. USA* 92: 175–179.

Boekema EJ., van Breemen JFL., Dekker JP. (1998) Specific association of photosystem II and light-harvesting complex II in partially solubilized photosystem II membranes. *FEBS Lett* 424: 95–99.

Boekema EJ., van Breemen JFL., van Roon H. Dekker JP. (2000) Arrangement of photosystem II supercomplexes in crystalline macrodomains within the thylakoid membrane of green plant chloroplasts. *J Mol Biol* 301: 1123-1133.

Boekema EJ., van Roon H., Calkoen F., Bassi R., Dekker JP. (1999) Multiple types of association of photosystem II and its light-harvesting antenna in partially solubilized photosystem II membranes. *Biochemistry* 38: 2233–2239.

Bondada B., Oosterhuis D. (1998) Decline in photosynthesis as related to alterations in chloroplast ultrastructure of a cotton leaf during ontogeny. *Photosynthetica* 35: 467–471.

Borsani O., Valpuesta V., Botella M. (2001) Evidence for a role of salicylic acid in the oxidative damage generated by NaCl and osmotic stress in *Arabidopsis* seedlings. *Plant Physiol* 126: 1024–1030.

Bouvier, F., D'harlingue Alain., Backhaus RA., Kumagai MH., Camara B. (2000) Identification of neoxanthin synthase as a carotenoid cyclase paralog. *Eur J Bioch*em 267: 6346–6352.

Boyes DC., Zayed AM., Ascenzi R., McCaskill AJ., Hoffman NE., Davis KR., Görlach J. (2001) Growth stage-based phenotypic analysis of *Arabidopsis*: a model for high throughput functional genomics in plants. *Plant Cell* 13: 1499–1510.

Briantais J-M., Vemotte C., Picaud M., Krause GH. (1979) A quantitative study of the slow decline of chlorophyll *a* fluorescence in isolated chloroplasts. *Biochim Biophys Acta* 548: 128-138.

Bricker TM. Frankel LK. (2011) Auxiliary functions of the PsbO, PsbP and PsbQ proteins of higher plant photosystem II: a critical analysis. *J Photochem Photobiol B*: Biol 104: 165-178.

Bricker TM., Roose JL., Fagerlund RD., Frankel LK. Eaton-Rye JJ. (2012), The extrinsic proteins of photosystem II. *Biochim Biophys Acta* 1817: 121-142.

Brooks MD., Sylak-Glassman EJ., Fleming GR., Niyogi KK. (2013) A thioredoxin-like/β-propeller protein maintains the efficiency of light harvesting in *Arabidopsis*. *Proc Natl Acad Sci USA* 110: 2733–2740.

Brugnoli E., Björkman O. (1992) Chloroplast movements in leaves: Influence on chlorophyll fluorescence and measurements of light-induced absorbance changes related to ΔpH and zeaxanthin formation. *Photosynth Res* 32: 23–35.

Bugos RC., Yamamoto HY. (1996) Molecular cloning of violaxanthin de-epoxidase from romaine lettuce and expression in *Escherichia coli*. *Proc Natl Acad Sci USA* 93: 6320-6325.

Butler WL. (1980) Energy transfer between photosystem II units in a connected package model of the photochemical apparatus of photosynthesis (photochemical model). *Proc Natl Acad Sci USA* 77: 4697–4701.

Caffarri S., Broess K., Croce R., van Amerongen H. (2009) Excitation energy transfer and trapping in higher plant photosystem II complexes with different antenna sizes. *Biophys J* 100: 2094–2103.

Caffarri S., Croce R., Breton J., Bassi R. (2001) The major antenna complex of photosystem II has a xanthophyll binding site not involved in light harvesting. *J Biol Chem* 276: 35924–35933.

Caffarri S., Tibiletti T., Jennings RC., Santabarbara S. (2014) A comparison between plant photosystem I and photosystem II architecture and functioning. *Curr Protein Pept Sci* 15: 296–331.

Cakmak I., Horst WJ. (1991) Effect of aluminum on lipid peroxidation, superoxide-dismutase, catalase and peroxidase activities in root-tips of soybean (Glycine max). *Physiologia Plantarum* 83: 463–468.

Cao S., Zhang X., Xu D., Fan X., Mou S., Wang Y., Ye N., Wang W. (2013) A transthylakoid proton gradient and inhibitors induce a non-photochemical fluorescence quenching in unicellular algae *Nannochloropsis* sp. *FEBS Lett* 587: 1310–1315.

Cape J., Bowman M., Kramer D. (2006) Understanding the Cytochrome *bc* complexes by what they don't do. The Q-cycle at 30. *Trends Plant Sci* 11: 45-55.

Carvalho FEL., Ware MA., Ruban AV. (2015) Quantifying the dynamics of light tolerance in *Arabidopsis* plants during ontogenesis. *Plant Cell Environ* 38: 2603-2617.

Catský J., Tichá I. (1979) CO2 compensation concentration in bean leaves: Effect of photon flux density and leaf age. *Biologia Plantarum* 21: 361–364.

Chailakhyan M. (1968) Internal factors of plant flowering. *Ann Rev Plant Physiol* 19: 1–37.

Chazdon RL., Pearcy RW. (1991) The importance of sunflecks for forest understory plants. *BioScience* 41: 760–766.

Choinski JS., Ralph PA., Eamus DA. (2003) Changes in photosynthesis during leaf expansion in *Corymbia gummifera*. Aust J Bot: 51: 111–118.

Chow WS., Melis A., Anderson JM. (1990) Adjustments of photosystem stoichiometry in chloroplasts improve the quantum efficiency of photosynthesis. *Proc Natl Acad Sci USA* 87: 7502–7506.

Croce R., Remelli R., Varotto C., Breton J., Bassi R. (1999a) The neoxanthin binding site of the major light harvesting complex LHCII from higher plants. *FEBS Lett* 456: 1–6.

Croce R., van Amerongen H. (2014) Natural strategies for photosynthetic light harvesting. *Nat Chem Biol* 10: 492-501.

Croce R., Weiss S., Bassi R. (1999b) Carotenoid binding sites of the major light-harvesting complex II of higher plants. *J Biol Chem* 274: 29613–29623.

Cui M., Vogelmann TC., Smith WK. (1991) Chlorophyll and light gradients in sun and shade leaves of *Spinacia oleracea*. *Plant Cell Environ* 14: 493–500.

Dall'Osto L., Cazzaniga S., Wada M., Bassi R. (2014) On the origin of a slowly reversible fluorescence decay component in the *Arabidopsis npq4* mutant. *Phil Trans R Soc B* 369: 1640.

Dall'Osto L., Lico C., Alric J., Giuliano G., Havaux M., Bassi R. (2006) Lutein is needed for efficient chlorophyll triplet quenching in the major LHCII antenna complex of higher plants and effective photoprotection *in vivo* under strong light. *BMC Plant Biol* 6: 32.

Dall'Osto L., Unlu C., Cazzaniga S., Van Amerongen H. (2014) Disturbed excitation energy transfer in Arabidopsis thaliana mutants lacking minor antenna complexes of photosystem II. *Biochim Biophys Acta* 1837: 1981–1988.

Dalrymple B. (2001). The age of the Earth in the twentieth century: a problem (mostly) solved. *Geol Soc London* 190: 205–221.

Darwin CR. (1865) On the movements and habits of climbing plants. *J Linn Soc* 9: 1–118.

Darwin CR. (1881) Movements of plants. *Nature* 23: 409.

Dau H. (1994) Molecular mechanism and quantitative models of variable photosystem II fluorescence. *Photochem Photobiol* 60: 1–23.

De Bianchi S., Betterle N., Kouril R., Cazzaniga S., Boekema E., Bassi R., Dall'Osto L. (2011) *Arabidopsis* mutants deleted in the light-harvesting protein Lhcb4 have a disrupted photosystem II macrostructure and are defective in photoprotection. *Plant Cell* 23: 2659–2679.

De Bianchi S., Dall'Osto L., Tognon G., Morosinotto T., Bassi R. (2008) Minor Antenna Proteins CP24 and CP26 Affect the Interactions between Photosystem II Subunits and the Electron Transport Rate in Grana Membranes of *Arabidopsis*. *Plant Cell* 20: 1012–1028.

De Las Rivas J., Andersson B., Barber J. (1992) Two sites of primary degradation of the D1-protein induced by acceptor or donor side photo-inhibition in photosystem II core complexes. *FEBS Lett* 301: 246-252.

De Las Rivas J., Balsera M., Barber J. (2004) Evolution of oxygenic photosynthesis: genome-wide analysis of the OEC extrinsic proteins. *Trends Plant Sci* 9: 18-25.

De Las Rivas J., Shipton CA., Ponticos M., Barber J. (1993) Acceptor side mechanism of photoinduced proteolysis of the D1 protein in photosystem II reaction centers. *Biochem* 32: 6944-50

Dekker JP., Boekema EJ. (2005). Supramolecular organization of thylakoid membrane proteins in green plants. *Biochim Biophys Acta* 1706: 12–39.

Dell JR., Toivonen PMA. (2003) Use of chlorophyll fluorescence in postharvest quality assessments of fruits and vegetables. In: *Practical Applications of Chlorophyll Fluorescence in Plant Biology*. (eds De Ell JR., Toivonen PMA.) Kluwer Academic Publishers, Dordrecht, The Netherlands.

Demmig B., Winter K., Kruger A., Czygan FC. (1987) Photoinhibition and zeaxanthin formation in intact leaves: a possible role of the xanthophyll cycle in the dissipation of excess light. *Plant Physiol* 84: 218-24.

Demmig-Adams B. (1990) Carotenoids and photoprotection: a role for the xanthophyll zeaxanthin. *Biochim Biophys Acta* 1020: 1-24.

Demmig-Adams B., Adams WW. (1992) Photoprotection and other responses of plants to high light stress. *Ann Rev Plant Physiol Plant Mol Biol* 43: 599–626.

Demmig-Adams B., Cohu CM., Muller O., Adams WW. (2012) Modulation of photosynthetic energy conversion efficiency in nature: from seconds to seasons. *Photosynth Res* 113: 75-88.

Dodd IC., Critchley C., Woodall GS., Stewart GR. (1998) Photoinhibition in differently coloured juvenile leaves of *Syzygium* species. *J Ex Bot* 49: 1437–1445.

Dreuw A., Fleming GR., Head-Gordon M. (2003) Charge-transfer state as a possible signature of a zeaxanthin-chlorophyll dimer in the non-photochemical quenching process in green plants. *J Phys Chem B* 107: 6500-6503.

Duffy CDP., Chmeliov J., Macernis M., Sulskus J., Valkunas L., Ruban AV. (2013) Modelling of fluorescence quenching by lutein in the plant light-harvesting complex LHCII. *J Phys Chem B* 117: 10975-10986.

Duffy CDP., Chmeliov J., Macernis M., Sulskus J., Valkunas L., Ruban AV. (2013) Light-harvesting processes in the dynamic photosynthetic antenna. *J Phys Chem B* 15: 18752-18770.

Engelmann EC., Zucchelli G., Garlaschi FM., Casazza AP., Jennings RC. (2005) The effect of outer antenna complexes on the photochemical trapping rate in barley thylakoid Photosystem II. *Biochim Biophys Acta* 1706: 276–286.

Epron D., Dreyer E., Bréda N. (1992) Photosynthesis of oak trees (*Quercus petraea* (Matt) Liebl.) during drought stress under field conditions: diurnal course of net CO2 assimilation and photochemical efficiency of photosystem II. *Plant Cell Environ* 15: 809–820

Falkowski PG., Katz ME., Knoll AH., Quigg A., Raven JA., Schofield O., Taylor FRJ. (2004) The evolution of modern phytoplankton. *Science* 305:354–360

Farber A., Young AJ., Ruban AV., Horton P., Jahns P. (1997) Dynamics of xanthophyll-cycle activity in different antenna subcomplexes in the photosynthetic membranes of higher plants: the relationship between zeaxanthin conversion and nonphotochemical fluorescence quenching. *Plant Physiol* 115:1609–1618.

Fukuyama K. (2004) Structure and function of plant-type ferredoxins. *Photosynth Res* 81: 289-301.

Edwards D., Davies KL., Axe L. (1992) A vascular conducting strand in the early land plant *Cooksonia*. *Nature* 357: 683-685.

Edwards D., Feehan J. (1980) Records of *Cooksonia*-type sporangia from late Wenlock strata in Ireland. *Nature* 287: 41-42.

Ferreira KN., Iverson TM., Maghlaoui K., Barber J. Iwata S. (2004) Architecture of the photosynthetic oxygen-evolving center. *Science* 303: 1831-1838.

Foyer CH., Shigeoka S. (2011) Understanding oxidative stress and antioxidant functions to enhance photosynthesis. *Plant Physiol* 155: 93–100.

Frank HA., Chynwat V., Desamero RZB., Farhoosh R., Erickson J., Bautista J. (1997) On the photophysics and photochemical properties of carotenoids and their role as light-harvesting pigments in photosynthesis. *Pure Appl Chem* 69: 2117–2124.

Fu QNA., Ehleringer JR. (1989) Heliotropic leaf movements in common beans controlled by air temperature. *Plant Physiol* 91: 1162–1167.

Funk C., Schroder WP., Green BR., Renger G., Andersson B. (1994) The intrinsic 22 kDa protein is a chlorophyll-binding subunit of photosystem II. *FEBS Lett* 342: 261-266.

Funk C., Schroder WP., Napiwotzki A., Tjus SE., Renger SG, Anderson B. (1995) The PSII-S Protein of Higher Plants: A New Type of Pigment-Binding Protein? *Biochemistry* 34: 11133–11141.

Gamon JA., Pearcy RW. (1989) Leaf movement, stress avoidance and photosynthesis in *Vitis californica*. *Oecologia* 79: 475–481

Genty B., Briantais J-M., Baker NR. (1989) The relationship between the quantum yield of photosynthetic electron-transport and quenching of chlorophyll fluorescence. *Biochim Biophys Acta* 990: 87-92.

Germano M., Yakushevska AE., Keegstra W., van Gorkom HJ., Dekker JP., Boekema EJ. (2002) Supramolecular organization of photosystem I and light- harvesting complex I in *Chlamydomonas reinhardtii*. *FEBS Lett* 525: 121–125.

Gerotto C., Franchin C., Arrigoni G., Morosinotto T. (2015) *In vivo* identification of photosystem II light harvesting complexes interacting with photosystem II subunit S. *Plant Physiol* 168: 1747–1761.

Gilmore AM., Hazlett TL., Debrunner PG., Govindjee. (1996) Comparative time-resolved photosystem II chlorophyll *a* fluorescence analyses reveal distinctive differences between photoinhibitory reaction center damage and xanthophyll cycle-dependent energy dissipation. *Photochem Photobiol* 64: 552–563.

Gilmore AM., Matsubara S., Ball MC., Barker DH., Itoh S. (2003) Excitation energy flow at 77 K in the photosynthetic apparatus of overwintering evergreens. *Plant Cell Environ* 26: 1021–1034.

Gilmore AM., Mohanty N., Yamamoto HY. (1994) Epoxidation of zeaxanthin and antheraxanthin reverses nonphotochemical quenching of photo-system-II chlorophyll-*a* fluorescence in the presence of trans-thylakoid delta-pH. *FEBS Lett* 350: 271–274

Giovagnetti V., Ware MA., Ruban, AV. (2015) Assessment of the impact of Photosystem I chlorophyll fluorescence on the pulse-amplitude modulated quenching analysis in leaves of *Arabidopsis thaliana*. *Photosynth Res* 125, 179-189.

Goldberg R., de Paiva G., Yadegari R. (1994) Plant embryogenesis: zygote to seed. *Science* 266: 605–614.

Golden SS., Brusslan J. Haselkorn R. (1986) Expression of a family of psbA genes encoding a photosystem II polypeptide in the cyanobacterium *Anacystis nidulans* R2. *EMBO J* 5: 2789–2798.

Golden SS., Stearns GW. (1988). Nucleotide sequence and transcript analysis of three photosystem II genes from the cyanobacterium *Synechococcus* sp. PCC7942. *EMBO J* 67: 85–96.

Goodenough UW., Staehelin LA. (1971) Structural differentiation of stacked and unstacked chloroplast membranes. Freeze-etch electron microscopy of wild-type and mutant strains of *Chlamidomonas*. *J Cell Biol* 48: 594-619.

Goral TK., Johnson MP., Duffy CD., Brain AP., Ruban AV., Mullineaux CW. (2012). Light-harvesting antenna composition controls the macrostructure and dynamics of thylakoid membranes in *Arabidopsis*. *Plant J* 69: 289–301.

Goss R., Lepetit B. (2014) Biodiversity of NPQ. *J Plant Physiol* 172:13–32.

Greenberg BM., Gaba V., Mattoo AK., Edelman M. (1987). Identification of a primary *in vivo* degradation product of the rapidly turning-over 32 kD protein of photosystem II. *EMBO J* 6: 2865-2869.

Groom QJ., Baker NR. (1992) Analysis of light-induced depressions of photosynthesis in leaves of a wheat crop during the winter. *Plant Physiol* 100: 1217–1223

Guenther A., Karl T., Harley P., Wiedinmyer C., Palmer PI., Geron C. (2006) Estimates of global terrestrial isoprene emissions using MEGAN (Model of Emissions of Gases and Aerosols from Nature). *Atmos Chem Phys* 6: 3181–3210.

Hager A. (1969) Lichtbedingte pH-erniedrigung in einem chloroplasten-kompartiment als ursache der enzymatischen violaxanthin- zeaxanthin umwandlungen; beziehungen zur photosphoslierung. *Planta* 89: 224-243.

Hager A. (1969) Lichtbedingte pH-Erniedrigung in einem Chloroplasten-Kompartiment als Ursache der enzymatischen Violaxanthin-Zeaxanthin-Umwandlung: Beziehung zur Photophosphorylierung. *Planta* 89: 224–243.

Hager A., Holocher K. (1994) Localisation of the xanthophyll cycle enzyme violaxanthin de-epoxidase within the thylakoid lumen and abolition of this mobility by a light dependent pH decrease. *Planta* 192: 581-589.

Hager A., Holocher K. (1994) Localization of the xanthophyll-cycle enzyme violaxanthin de-epoxidase within the thylakoid lumen and abolition of its mobility by a (light-dependent) pH decrease. *Planta* 192:581–589.

Hager A., Perz H. (1970) Veränderung der Lichtabsorption eines Carotenoids im Enzym (De-Epoxidase)-Substrat (Violaxanthin)-Komplex. *Planta* 93:314–322.

Havaux M., Dall'Osto L., Cuiné S., Giuliano G., Bassi R. (2004) The effect of zeaxanthin as the only xanthophyll on the structure and function of the photosynthetic apparatus in *Arabidopsis thaliana. J Biol Chem* 279: 13878–13888.

Havaux M., Straser RJ., Greppin H. (1991) A theoretical and experimental analysis of the qP and qN coefficients of chlorophyll fluorescence quenching and their relation to photochemical and nonphotochemical events. *Photosynth Res* 27: 41–55.

He J., Chee CW., Goh CJ. (1996) 'Photoinhibition' of *Heliconia* under natural tropical conditions: the importance of leaf orientation for light interception and leaf temperature. *Plant Cell Environ* 19: 1238–1248.

Heckman DS., Geiser DM., Eidell BR., Stauffer RL., Kardos NL., Hedges SB. (2001) Molecular evidence for the early colonization of land by fungi and plants. *Science* 293: 1129-1133.

Hideg E., Kós PB., Schreiber U. (2008) Imaging of NPQ and ROS formation in tobacco leaves: heat inactivation of the water-water cycle prevents downregulation of PSII. *Plant Cell* Physiol 49: 1879–1886.

Hill R., Bendall F. (1960) Function of the two cytochrome components in chloroplasts: a working hypothesis. *Nature* 186: 136–137.

Hill R., Bendall F. (1960) Function of two cytochrome components in chloroplasts: a working hypothesis. *Nature* 186: 136–140.

Hogewoning SW., Wientjes E., Douwstra P., Trouwborst G., van Ieperen W., Croce R., Harbinson J. (2012) Photosynthetic quantum yield dynamics: from photosystems to leaves. *Plant Cell* 24: 1921–1935.

Holt NE., Zigmantas D., Valkunas L., Li X-P., Niyogi KK., Flemming GR. (2005) Carotenoid cation formation and the regulation of photosynthetic light harvesting. *Science* 307: 433–436.

Holzwarth AR., Miloslavina Y., Nilkens M., Jahns P. (2009) Identification of two quenching sites active in the regulation of photosynthetic light-harvesting studied by time-resolved fluorescence. *Chem Phys Lett* 483: 262–267.

Hopkinson J. (1964) Studies on the expansion of the leaf surface IV. The carbon and phosphorus economy of a leaf. *J Ex Bot* 15: 125–137.

Hörtensteiner S. (2006) Chlorophyll degradation during senescence. Ann Rev Plant Biol 57: 55–77.

Horton P., Ruban AV. (1992) Regulation of photosystem II. *Photosynth Res* 34: 375-385.

Horton P., Ruban AV. (2004) Molecular design of the photosystem II light harvesting antenna: photosynthesis and photoprotection*. J Ex Bot 5*6:365–373.

Horton P., Ruban AV. Walters RG. (1996) Regulation of light harvesting in green plants (review). *Ann Rev Plant Physiol Plant Mol Biol* 47: 655-684.

Horton P., Ruban AV., Rees D., Pascal A., Noctor GD., Young A. (1991) Control of the light-harvesting function of chloroplast membranes by the proton concentration in the thylakoid lumen: aggregation states of the LHCII complex and the role of zeaxanthin. *FEBS Lett* 292: 1-4.

Horton P., Ruban AV., Wentworth M. (2000) Allosteric regulation of the light harvesting system of photosystem II. Phil Trans R Soc 355: 1361-1370.

Horton P., Wentworth M., Ruban AV. (2005) Control of the light harvesting function of chloroplast membranes: the LHCII-aggregation model for non-photochemical quenching. *FEBS Lett* 579: 4201-4206.

Ivanov AG., Rosso D., Savitch LV., Stachula P., Rosembert M., Oquist G., Hüner NP. (2012) Implications of alternative electron sinks in increased resistance of PSII and

PSI photochemistry to high light stress in cold acclimated *Arabidopsis thaliana*. *Photosynth Res* 113: 191–206.

Jahns P., Holzwarth AR. (2012) The role of the xanthophyll cycle and of lutein in photoprotection of photosystem II. *Biochim Biophys Acta* 1817: 182-193.

Jahns P., Miehe B. (1996) Kinetic correlation of recovery from photoinhibition and zeaxanthin epoxidation. *Planta* 198: 202–210.

Jarillo JA., Gabrys H., Capel J., Alonso JM., Ecker JR., Cashmore AR. (2001) Phototropin-related NPL1 controls chloroplast relocation induced by blue light. *Nature* 410: 952–954.

Johnson MP., Goral TK., Duffy CDP., Brain APR., Mullineaux CW., Ruban AV. (2011) Photoprotective energy dissipation involves the reorganization of photosystem II light harvesting complexes in the grana membranes of spinach chloroplasts. *Plant Cell* 23: 1468-1479.

Johnson MP., Perez-Bueno ML., Zia A., Horton P., Ruban AV. (2009) The zeaxanthin-independent and zeaxanthin-dependent qe components of nonphotochemical quenching involve common conformational changes within the photosystem II antenna in *Arabidopsis*. *Plant Physiol* 149: 1061-1075

Johnson MP., Ruban AV. (2009) Photoprotective energy dissipation in higher plants involves alteration of the excited state energy of the emitting chlorophyll(s) in the light harvesting antenna II (LHCII). *J Biol Chem* 284: 23592–23601.

Johnson MP., Ruban AV. (2010) *Arabidopsis* plants lacking PsbS protein possess photoprotective energy dissipation. *Plant J* 61: 283–289.

Johnson MP., Ruban AV. (2011) Restoration of rapidly reversible photoprotective energy dissipation in the absence of psbs protein by enhanced ΔpH. *J Biol Chem* 286: 19973–19981.

Johnson MP., Zia A., Horton P., Ruban AV. (2010) Effect of xanthophyll composition on the chlorophyll excited state lifetime in plant leaves and isolated LHCII. *Chem Phys* 373: 23-32.

Kaftan D., Brumfeld V., Nevo R., Scherz A., Reich Z. (2002) From chloroplasts to photosystems: in situ scanning force microscopy on intact thylakoid membranes. *EMBO J* 21: 6246–6253.

Kagawa T., Sakai T., Suetsugu N., Oikawa K., Ishiguro S., Kato T., Tabata S., Okada K., Wada M. (2001) *Arabidopsis* NPL1: a phototropin homolog controlling the chloroplast high light avoidance response. *Science* 291: 2138-2141.

Kagawa T., Wada M. (2000) Blue light-induced chloroplast relocation in *Arabidopsis thaliana* as analyzed by microbeam irradiation. *Plant Cell Physiol* 41: 84–93.

Kamiya N., Shen JR. (2003) Crystal structure of oxygen-evolving photosystem II from Thermosynechococcus vulcanus at 3.7-Angstrom resolution. *Proc Natl Acad Sci USA* 100: 98-103.

Kao WY., Forseth IN. (1991) The effects of nitrogen, light and water availability on tropic leaf movements in soybean (Glycine max). *Plant Cell Environ* 14: 287–293.

Kao WY., Forseth IN. (1992) Diurnal leaf movement, chlorophyll fluorescence and carbon assimilation in soybean grown under different nitrogen and water availabilities. *Plant Cell Environ* 15: 703–710.

Kereïche S., Kiss AZ., Kouril R., Boekema E., Horton P. (2010) The PsbS protein controls the macro-organization of photosystem II complexes in the grana membranes of higher plant chloroplasts. *FEBS Lett* 584: 754-764.

Kerstetter R., Poethig R. (1998) The specification of leaf identity during shoot development. *Ann Rev Cell Dev Biol* 14: 373–398.

Kirchhoff H., Hinz HJ., Rösgen J. (2003) Aggregation and fluorescence quenching of chlorophyll *a* of the light-harvesting complex II from spinach *in vitro*. *Biochim Biophys Acta* 1606: 105-116.

Kiss AZ., Ruban AV., Horton P. (2008) The PsbS protein controls the organization of the photosystem II antenna in higher plant thylakoid membranes. *J Biol Chem* 283: 3972–3978.

Klughammer C., Schreiber U. (1994) An improved method, using saturating light pulses, for the determination of photosystem I quantum yield via P700 absorbance changes at 830 nm. *Planta* 192:261–268.

Kok B., Forbush B., Mcgloin M. (1970) Cooperation of charges in photosynthetic O2 evolution - I. A Linear Four Step Mechanism. *Photochem Photobiol* 11: 457-475.

Königer M., Delamaide JA., Marlow ED., Harris GC. (2008) *Arabidopsis thaliana* leaves with altered chloroplast numbers and chloroplast movement exhibit impaired adjustments to both low and high light. *J Ex Bot* 59: 2285-97.

Kouřil R., Dekker JP., Boekema EJ. (2012) Supramolecular organization of photosystem II in green plants. *Biochim Biophys Acta* 1817: 2–12.

Kouril R., Oostergetel GT., Boekema EJ. (2011) Fine structure of granal thylakoid membrane organization using cryo electron tomography. *Biochim Biophys Acta* 1807: 368–374.

Kouřil R., Wientjes E., Bultema J.B., Croce R., Boekema EJ. (2013) Highlight vs. low-light: effect of light acclimation on photosystem II composition and organization in *Arabidopsis thaliana*. *Biochim Biophys Acta* 1827: 411–419.

Kramer DM., Johnson G., Kiirats O., Edwards GE. (2004) New fluorescence parameters for the determination of Q_A redox state and excitation energy fluxes. *Photosynth Res* 79: 209-218.

Krause GH. (1974) Changes in chlorophyll fluorescence in relation to light dependent cation transfer across thylakoid membranes. *Biochim Biophys Acta* 333: 301–313.

Krause GH. (1988) Photoinhibition of photosynthesis. An evaluation of damaging and protective mechanisms. *Physiol Plant* 74: 566–574.

Krause GH., Behrend U. (1986) ΔpH-dependent chlorophyll fluorescence quenching indicating a mechanism of protection against photoinhibition of chloroplasts. *FEBS Lett* 200: 298-302.

Krause GH., Laasch H., Weis E. (1988) Regulation of thermal dissipation of absorbed light energy in chloroplasts indicated by energy-dependent fluorescence quenching. *Plant. Physiol Biochem* 26: 445-452.

Krause GH., Virgo A., Winter K. (1995) High susceptibility to photoinhibition of young leaves of tropical forest trees. *Planta* 197: 583–591.

Krause GH., Weis E. (1991) Chlorophyll fluorescence and photosynthesis: the basics. *Ann Rev Plant Physiol Plant Mol Biol* 42: 313-249.

Krieger A., Moya I., Weis E. (1992) Energy-dependent quenching of chlorophyll *a* fluorescence: effect of pH on stationary fluorescence and picosecond-relaxation kinetics in thylakoid membranes and photosystem II preparations. *Biochim Biophys Acta* 1102: 167–176.

Krieger A., Weis E. (1993) The role of calcium in the pH-dependent control of photosystem II. *Photosynth Res* 37: 117–130.

Külheim C., Ågren J., Jansson S. (2002) Rapid regulation of light harvesting and plant fitness in the field. *Science* 297: 91-93.

Külheim C., Jansson S. (2005) What leads to reduced fitness in non-photochemical quenching mutants? *Physiologia Plantarum*. 125: 202-211.

Kutík J., Kocová M., Holá D., Körnerová M. (2000) The development of chloroplast ultrastructure and hill reaction activity during leaf ontogeny in different maize (*Zea mays* L.) genotypes. *Photosynthetica* 36: 497–507.

Kyle DJ. (1987) The biochemical basis for photoinhibition of photosystem II. In: *Photoinhibition, topics of photosynthesis.* (eds Kyle DJ., Osmond CB., Arntzen CJ.) 197-226. Amsterdam: Elsevier.

Kyle DJ., Ohad I., Arntzen CJ. (1984) Membrane protein damage and repair: selective loss of a quinone protein function in chloroplast membranes. *Proc Natl Acad Sci USA* 81: 4070–4074.

la Porta N., Bertamini M., Nedunchezhian N., Muthuchelian K. (2006) Photosynthetic changes that occur during aging of cypress (*Cupressus sempervirens* L.) needles. *Photosynthetica* 44: 555–560.

Lazár D. (2013) Simulations show that a small part of variable chlorophyll *a* fluorescence originates in photosystem I and contributes to overall fluorescence rise. *J Theor Biol* 335: 249–264.

Lee HY., Hong YN., Chow WS. (2001) Photoinactivation of photosystem II complexes and photoprotection by non-functional neighbours in *Capsicum annuum* L. leaves. *Planta* 212: 332–342.

Leitsch J., Schnettger B., Critchley C., Krause GH. (1994) Two mechanisms of recovery from photoinhibition in vivo: reactivation of photosystem II related and unrelated to D1 protein turnover. *Planta* 194: 15–21.

Leong TY., Anderson JM. (1984a) Adaptation of the thylakoid membranes of pea chloroplasts to light intensities. 1. Study on the distribution of chlorophyll–protein complexes. *Photosynth Res* 5: 105-115.

Leong TY., Anderson JM. (1984b) Adaptation of the thylakoid membranes of pea chloroplasts to light intensities. 2. Regulation of electron transport capacities, electron carriers, coupling factor (CF1) activity and rates of photosynthesis. *Photosynth Res* 5: 117-128.

Li X., Shi M., Hall C., Funk WP., Schröder. (2012) Photosystem II, a growing complex: updates on newly discovered components and low molecular mass proteins *Biochim Biophys Acta* 1817: 13–25.

Li XP., Björkman O., Shih C., Grossman AR., Rosenquist M., Jansson S, Niyogi K.K. (2000) A pigment-binding protein essential for regulation of photosynthetic light harvesting. *Nature* 403: 391–395.

Li XP., Muller-Moule P., Gilmore AM, Niyogi KK. (2002) PsbS-dependent enhancement of feedback de-excitation protects photosystem II from photoinhibition. *Proc Natl Acad Sci USA* 99: 15222–15227.

Li X-P., Phippard A., Pasari J., Niyogi KK. (2002) Structure–function analysis of photosystem II subunit S (PsbS) *in vivo*. *Funct. Plant Biol*. 29: 1131-1139.

Lichtenthaler HK., Buschmann C., Döll M., Fietz HJ., Bach T., Kozel U., Meier D., Rahmsdorf U. (1981) Photosynthetic activity, chloroplast ultrastructure, and leaf characteristics of high-light and low-light plants and of sun and shade leaves. *Photosynth Res* 2: 115-141.

Liu N., Lin Z.-F., van Devender A., Lin GZ., Peng CL., Pan XP. (2009) Spectral reflectance indices and pigment functions during leaf ontogenesis in six subtropical landscape plants. *Plant Growth Reg* 58: 73–84.

Liu Z., Yan H., Wang K., Kuang T., Zhang J., Gui L., An X., Chang W. (2004) Crystal structure of spinach major light-harvesting complex at 2.72 Å resolution. *Nature* 428: 287–292.

Lodish H., Berk A., Zipursky SL., Matsudaira P., Baltimore D., Darnell J. (1995) *Molecular Cell Biology* (ed Freeman WH.) 175. New York: Scientific American Books.

Loll B., Kern J., Saenger W., Zouni A., Biesiadka J. (2005) Towards complete cofactor arrangement in the 3.0 Angstrom resolution structure of Photosystem II. *Nature* 438: 1040-1044.

Lu Y-K., Chen Y-R., Yang C-M. (1995) Influence of Fe- and Mg-deficiency on the thylakoid membranes of a chlorophyll-deficient *ch5* mutant of *Arabidopsis thaliana*. *Bot Bull Acad Sin* 36: 175–179.

Mäenpää P., Andersson B. (1989) Photosystem II heterogeneity and long-term acclimation of light-harvesting. *Z Naturforsch Tiel C* 12: 403–406.

Malkin S., Armond PA., Mooney HA., Fork DC. (1981) Photosystem II photosynthetic unit sizes from fluorescence induction in leaves: correlation to photosynthetic capacity. *Plant Physiol* 67: 570–579.

Manetas Y., Drinia A., Petropoulou Y. (2002) High contents of anthocyanins in young leaves are correlated with low pools of xanthophyll cycle components and low risk of photoinhibition. *Photosynthetica* 40: 349–354.

Matile P., Schellenberg M., Peisker C. (1992) Production and release of a chlorophyll catabolite in isolated senescent chloroplasts. *Planta* 187: 230–235.

Matsubara S., Chow W. (2004) Populations of photoinhibited photosystem II reaction centers characterized by chlorophyll *a* fluorescence lifetime *in vivo*. *Proc Natl Acad Sci USA* 101: 18234–9.

Maxwell K., Johnson GN. (2000) Chlorophyll fluorescence – a practical guide. *J Ex Bot* 345: 659-668.

Melis A. (1999) Photosystem II damage and repair cycle in chloroplasts: what modulates the rate of photodamage *in vivo*? *Trends Plant Sci* 4: 130-135.

Mills J., Barber J. (1975) Energy-dependent cation-induced control of chlorophyll a fluorescence in isolated intact chloroplasts. *Arch Biochem Biophys* 170: 306–314.

Miloslavina Y., de Bianchi S., Dall'Osto L., Bassi R., Holzwarth AR. (2011) Quenching in *Arabidopsis thaliana* mutants lacking monomeric antenna proteins of photosystem II. *J Biol Chem* 286: 36830–36840

Miloslavina Y., Wehner A., Lambrev PH., Wientjes E., Reus M., Garab G., Croce R., Holzwarth AR. (2008) Far-red fluorescence: a direct spectroscopic marker for LHCII oligomer formation in non-photochemical quenching. *FEBS Lett* 582: 3625–3631.

Milthorpe F. (1959) Studies on the expansion of the leaf surface I. The influence of temperature. *J Ex Bot* 10: 233–249.

Moise N., Moya I. (2004) Correlation between lifetime heterogeneity and kinetics heterogeneity during chlorophyll fluorescence induction in leaves: 2. Multi-frequency phase and modulation analysis evidences a loosely connected PSII pigment-protein complex. *Biochim Biophys Acta* 1657:47–60

Monitoring The Earth From Space With Seawifs. *Oceancolor.gsfc.nasa.gov.* N.p., 2017. Web. 10 Feb. 2017.

Müller MG., Lambrev P., Reus M., Wientjes E., Croce R., Holzwarth AR. (2010) Singlet energy dissipation in the photosystem II light-harvesting complex does not involve energy transfer to carotenoids. *Chem Phys* Chem 11: 1289–1296.

Müller P., Li X-P., Niyogi KK. (2001) Non-photochemical quenching. A response to excess light energy. *Plant Physiol* 125: 1558–1566.

Muller-Moule P., Conklin Pl., Niyogi KK., (2002) Ascorbate Deficiency Can Limit Violaxanthin De-Epoxidase Activity *in vivo*. *Plant Physiol* 125: 970-977.

Mullineaux CW., Ruban AV., Horton P. (1994) Prompt heat release associated with ΔpH-dependent quenching in spinach thylakoid membranes. *Biochim Biophys Acta* 1185: 119-123.

Munné-Bosch S., Alegre L. (2002) Plant aging increases oxidative stress in chloroplasts. *Planta* 214: 608–615.

Murata N. (1969) Control of excitation transfer in photosynthesis. I. Light induced change of chlorophyll *a* fluorescence in *Porphyridium cruentum*. *Biochim Biophys Acta* 172: 242–251.

Nadeau J., Sack F. (2002) Control of stomatal distribution on the *Arabidopsis* leaf surface. *Science* 296: 1697–1700.

Nath K., Phee B-K., Jeong S., Lee SY., Tateno Y., Allakhverdiev SI. (2013) Age-dependent changes in the functions and compositions of photosynthetic complexes in the thylakoid membranes of *Arabidopsis thaliana*. *Photosynth Res* 117: 547–556.

Neff M., Chory J. (1998) Genetic interactions between phytochrome A, phytochrome B, and cryptochrome 1 during *Arabidopsis* development. *Plant Physiol* 118: 27–36.

Nelson N. (2009) Plant photosystem I—the most efficient nano-photochemical machine. *J Nanosci Nanotechnol* 9: 1709–1713.

Nelson N. (2011) Photosystems and global effects of oxygenic photosynthesis. *Biochim Biophys Acta* 1807: 856–863.

Neubauer C. (1993) Multiple effects of dithiothreitol on nonphotochemical fluorescence quenching in intact chloroplasts. *Plant Physiol* 103**: 5**75-583.

Neubauer C., Yamamoto HY. (1992) Mehler-peroxidase reaction mediates zeaxanthin formation and zeaxanthin-related fluorescence quenching in intact chloroplasts. *Plant Physiology* 99: 1354-1361.

Nield J., Funk C., Barber J. (2000) Supermolecular structure of photosystem II and location of the PsbS protein. *Phil Trans R Soc B* 355: 1337-1344.

Niklas K. (1998) The influence of gravity and wind on land plant evolution. *Rev Paleobot Palynol* 102: 1-14.

Nilkens M., Kress E., Lambrev P., Miloslavina Y., Müller M., Holzwarth AR., Jahns P. (2010) Identification of a slowly inducible zeaxanthin-dependent component of non-photochemical quenching of chlorophyll fluorescence generated under steady-state conditions in *Arabidopsis*. *Biochim Biophys Acta* 1797: 466-475.

Nilkens M., Kress E., Lambrev PH., Miloslavina Y., Müller M., Holzwarth AR., Jahns P. (2010) Identification of a slowly inducible zeaxanthin-dependent component of non-photochemical quenching of chlorophyll fluorescence generated under steady state conditions in *Arabidopsis*. *Biochim Biophys Acta* 466–475.

Nilsson A., Stys D., Drakenberg T., Spangfort MD., Forsen S., Allen JF. (1997) Phosphorylation controls the three-dimensional structure of plant light harvesting complex II. J Biol Chem 272, 18350−18357.

Nishiyama Y., Allakhverdiev SI., Murata N. (2011) Protein synthesis is the primary target of reactive oxygen species in the photoinhibition of photosystem II. *Physiologia Plantarum* 142: 35–46.

Niyogi KK., Björkman O., Grossman AR. (1997) *Chlamydomonas* xanthophyll cycle mutants identified by video imaging of chlorophyll fluorescence quenching. *Plant Cell* 9: 1369-1380.

Niyogi KK., Grossman AR., Bjorkman O. (1998) *Arabidopsis* Mutants Define a Central Role for the Xanthophyll Cycle in the Regulation of Photosynthetic Energy Conversion. *Plant Cell* 10: 1121-1134.

Niyogi KK., Li X-P., Rosenberg V., Jung H-S. (2005) Is PsbS the site of non-photochemical quenching in photosynthesis? *J Ex Bot* 56: 375–382.

Niyogi KK., Truong TB. (2013) Evolution of flexible non-photochemical quenching mechanisms that regulate light harvesting in oxygenic photosynthesis. *Curr Opin Plant Biol* 16: 307–314.

Noctor G., Rees D., Young A., Horton P. (1991) The relationship between zeaxanthin, energy-dependent quenching of chlorophyll fluorescence, and trans-thylakoid pH gradient in isolated chloroplasts. *Biochim Biophys Acta* 1057: 320-330.

Noctor G., Ruban AV., Horton P. (1993) Modulation of ΔpH-dependent nonphotochemical quenching of chlorophyll fluorescence in spinach chloroplasts. *Biochim Biophys Acta* 1183: 339–344.

Noodén LD. (1988) The phenomenon of senescence and aging. In *Senescence and Aging in Plants* (eds L.D. Noodén & A.C. Leopold) 1–50. Academic Press, San Diego.

O'Reilly EJ., Olaya-Castro A. (2014) Non-classicality of the molecular vibrations assisting exciton energy transfer at room temperature. *Nat Commun* 5:3012.

Ogawa T., Obata F., Shibata K. (1966) The pigment−proteins in spinach chloroplasts. *Biochim Biophys Acta* 112: 223−234

Ögren E., Sjöström M. (1990) Estimation of the effect of photoinhibition on the carbon gain in leaves of a willow canopy. *Planta* 181: 560–567.

Ohad I., Kyle DJ., Arntzen CJ. (1984) Membrane-protein damage and repair - removal and replacement of inactivated 32-kilodalton polypeptides in chloroplast membranes. *J Cell Biol* 99: 481-485.

Oquist G., Brunes L., Hallgren J-E. (1982) Photosynthetic efficiency during ontogenesis of leaves of *Betula pendula*. *Plant Cell Environ* 5: 17–21.

Osmond CB. (1994) What is photoinhibition? Some insights from comparisons of shade and sun plants. In: *Photoinhibition of photosynthesis*. (eds Baker NR., Bowyer JR.) 1-24. Bios Scientific, Lancaster, UK.

Oxborough K., Baker NR. (1997) Resolving chlorophyll *a* fluorescence of photosynthetic efficiency into photochemical components – calculation of qP and Fv'/Fm' without measuring Fo. *Photosynth Res* 54: 135–142.

Pastenes C., Pimentel P., Lillo J. (2004) Leaf movements and photoinhibition in relation to water stress in field-grown beans. *J Exp Bot* 56: 425–433.

Paul MJ., Foyer CH. (2001) Sink regulation of photosynthesis. *J Ex Bot* 52: 1383–1400.

Peers G., Truong TB., Ostendorf E., Busch A., Elrad D., Grossman AR., Hippler M., Niyogi KK. (2009) An ancient light-harvesting protein is critical for the regulation of algal photosynthesis. *Nature* 462: 518–521.

Pessarakli M. (2005) *Handbook of Photosynthesis II*. Taylor and Francis Group. CRC Press, Florida, USA.

Peter G., Thornber J. (1991) Biochemical composition and organization of higher plant photosystem II light-harvesting pigment-proteins. *J Biol Chem* 266: 16745–16754.

Peter GF., Thornber PJ. (1991) Biochemical composition and organization of higher plant photosystem II light-harvesting pigment-proteins. *J Biol Chem* 266: 16745-16754.

Peterson RB., Oja V., Eichelmann H., Bichele I., Dall'Osto L., Laisk A. (2014) Fluorescence F_0 of photosystems II and I in developing C_3 and C_4 leaves, and implications on regulation of excitation balance. *Photosynth Res* 122: 41–56.

Petrou K., Belgio E., Ruban AV. (2014) pH sensitivity of chlorophyll fluorescence quenching is determined by the detergent/protein ratio and the state of LHCII aggregation. *Biochim Biophys Acta* 1837: 1533-1539.

Pfündel EE., Klughammer C., Meister A., Cerovic ZG. (2013) Deriving fluorometer-specific values of relative PSI fluorescence intensity from quenching of F_0 fluorescence in leaves of *Arabidopsis thaliana* and *Zea mays*. *Photosynth Res* 114:189–206.

Pisciotta JM., Zou Y., Baskakov IV. (2010) Light-Dependent Electrogenic Activity of Cyanobacteria *PloS one* 5: e10821.

Porra R., Thompson W., Kriedemann P. (1989) Determination of accurate extinction coefficients and simultaneous equations for assaying chlorophylls *a* and *b* extracted with four different solvents. *Biochim Biophys Acta* 975: 384–394.

Powles SB. (1984) Photoinhibition of photosynthesis induced by visible light. *Ann Rev Plant Physiol* 35: 15-44.

Powles SB. (1984) Photoinhibition of photosynthesis induced by visible light. *Ann Rev Plant Physiol* 35: 15-44.

Qiang Fu. (2003) Radiation (Solar). In *Encyclopedia of atmospheric sciences* (ed Holton JR.) 5: 1859–1863. Amsterdam, Academic Press.

Qin X., Suga M., Kuang T., Shen J-R. (2015) Structural basis for energy transfer pathways in the plant PSI-LHCI supercomplex. *Science* 348: 989–995.

Radochová B., Tichá I. (2008) Excess irradiance causes early symptoms of senescence during leaf expansion in photoautotrophically *in vitro* grown tobacco plants. *Photosynthetica* 46: 471–475.

Raven JA. (1984) Physical correlates of the morphology of early vascular plants. *Bot J Linn Soc* 88: 105–126.

Raven JA. (1994) Physiological analyses of aspects of the functioning of vascular tissue in early land plants. *Bot J Scotl* 47: 49-64.

Raven PH., Johnson GB. (1989) *Biology.* Boston: Times Mirror/Mosby College Publishing.

Rees D., Young A., Noctor G., Britton G., Horton P. (1989) Enhancement of the ΔpH-dependent dissipation of excitation energy in spinach chloroplasts by light-activation: correlation with the synthesis of zeaxanthin. *FEBS Lett* 256: 85-90.

Rhee KH., Morris EP., Barber J., Kuhlbrandt W. (1998) Threedimensional structure of the plant photosystem II reaction centre at 8 A resolution. *Nature* 396: 283-286.

Richter M., Goss R., Wagner B., Holzwarth AR. (1999) Characterization of the fast and slow reversible components of non-photochemical quenching in isolated pea thylakoids by picosecond time-resolved chlorophyll fluorescence analysis. *Biochemistry* 38: 12718–12726.

Rintamäki E., Martinsuo P., Pursiheimo S., Aro E-M. (2000) Cooperative regulation of light-harvesting complex II phosphorylation via the plastoquinol and ferredoxin-thioredoxin system in chloroplasts. *Proc Natl Acad Sci USA* 97:11644–11649.

Ruban A. (2012) *The Photosynthetic Membrane: Molecular Mechanisms and Biophysics of Light Harvesting.* Oxford: Wiley-Blackwell.

Ruban AV (2009) Plants in light. *Commun Integr Biol* 2: 50-55.

Ruban AV. (2015) Evolution under the Sun: optimising light harvesting in photosynthesis. *J Ex Bot* 66: 7-23.

Ruban AV. (2015) Evolution under the sun: optimizing light harvesting in photosynthesis. *J Ex Bot* 66: 7–23.

Ruban AV. Horton P. (1999) The xanthophyll cycle modulates the kinetics of nonphotochemical energy dissipation in isolated light harvesting complexes, intact chloroplasts and leaves. *Plant Physiol* 119: 531-542.

Ruban AV., Belgio E. (2014) The relationship between maximum tolerated light intensity and photoprotective energy dissipation in the photosynthetic antenna: chloroplast gains and losses. *Phil Trans R Soc B* 369: 20130222.

Ruban AV., Berera R., Ilioaia C., van Stokkum IHM., Kennis JTM., Pascal AA., van Grondelle R. (2007) Identification of a mechanism of photoprotective energy dissipation in higher plants. *Nature* 450: 575–578.

Ruban AV., Duffy CDP., Johnson MP. (2011) Natural light harvesting: principles and environmental trends. *Energy Environ Sci* 4: 1643-1650.

Ruban AV., Horton P. (1992) Mechanism of delta pH-dependent dissipation of absorbed excitation energy by photosynthetic membranes. I. Spectroscopic analysis of isolated light harvesting complexes. *Biochim Biophys Acta* 1102: 30-38.

Ruban AV., Horton P. (1994) Spectroscopy of non-photochemical and photochemical quenching of chlorophyll fluorescence in leaves; evidence for a role of the light harvesting complex of photosystem II in the regulation of energy dissipation. *Photosynth Res* 40: 181-190.

Ruban AV., Johnson MP, Duffy CDP. (2012) The photoprotective molecular switch in the photosystem II antenna. *Biochim Biophys Acta* 1817: 167–181.

Ruban AV., Johnson MP. (2009) Dynamics of higher plant photosystem cross-section associated with state transitions. *Photosynth Res*. 99: 173-183.

Ruban AV., Lavaud J., Rousseau B., Guglielmi G., Horton P., Etienne A-L. (2004) The super-excess energy dissipation in diatom algae: comparative analysis with higher plants. *Photosynth Res* 82: 165-175.

Ruban AV., Lee PJ., Wentworth M., Young A.J, Horton P. (1999) Determination of the stoichiometry and strength of binding of xanthophylls to the photosystem II light harvesting complexes. *J Biol Chem* 274: 10458–10465.

Ruban AV., Murchie EH. (2012) Assessing the photoprotective effectiveness of non-photochemical chlorophyll fluorescence quenching: a new approach. *Biochim Biophys Acta* 1817: 977–982.

Ruban AV., Rees D., Noctor GD., Young A., Horton P. (1991) Long-wavelength chlorophyll species are associated with amplification of high-energy-state excitation quenching in higher plants. *Biochim Biophys Acta* 1059: 355–360.

Ruban AV., Solovieva S., Horton P. (2006) Plasticity in the composition of the light harvesting antenna of higher plants preserves structural integrity and biological function. *J Biol Chem* 281: 14981–14990.

Ruban AV., Young A., Horton P. (1993) Induction of nonphotochemical energy dissipation and absorbance changes in leaves; evidence for changes in the state of the light harvesting system of photosystem II *in vivo*. *Plant Physiol* 102: 741–750.

Ruban AV., Young A., Horton P. (1994) Modulation of chlorophyll fluorescence quenching in isolated light harvesting complex of photosystem II. *Biochim Biophys Acta* 1196: 123-127.

Ruban AV., Young AJ., Pascal AA., Horton P. (1994) The effects of illumination on the xanthophyll composition of the photosystem II light harvesting complexes of spinach thylakoid membranes. *Plant Physiol* 104: 227–234.

Sabater B., Martín M. (2013) Chloroplast control of leaf senescence. In *Plastid Development in Leaves During Growth and Senescence, Advances in Photosynthesis and Respiration* (eds Biswal B., Krupinska K., Biswal UC.) 529–550. Springer, Dordrecht.

Sakai T., Kagawa T., Kasahara M., Swartz TE., Christie JM., Briggs WR., Wada M., Okada K. (2001) *Arabidopsis* nph1 and npl1: blue light receptors that mediate both phototropism and chloroplast relocation. *Proc Natl Acad Sci USA* 98: 6969-6974.

Sanderson MJ. (2003) Molecular data from 27 proteins do not support a Precambrian origin of land plants. *Am J Bot* 90: 954-956.

Sapozhnikov DI., Kransovskaya TA., Maevskaya AN. (1957) Change in the interrelationship of the basic carotenoids of the plastids of green leaves under the action of light. *Dokl. Acad. Nauk USSR* 113: 465-467.

Särvikas P., Hakala M., Pätsikkä E., Tyystjärvi T., Tyystjärvi E. (2006) Action spectrum of photoinhibition in leaves of wild type and *npq1-2* and *npq4-1* mutants of *Arabidopsis thaliana*. *Plant Cell Physiol* 47: 391-400.

Schreiber U. (1986) Detection of rapid induction kinetics with a new type of high-frequency modulated chlorophyll fluorometer. *Photosynth Res* 9: 261-272.

Schurr U.,Walter A., Rascher U. (2006) Functional dynamics of plant growth and photosynthesis – from steady-state to dynamics – from homogeneity to heterogeneity. *Plant Cell Environ* 29: 340–352.

Seeman JR., Sharkey TD., Wang J., Osmanod CB. (1987) Environmental effects on photosynthesis, nitrogen-use efficiency, and metabolite pools in leaves of sun and shade plants. *Plant Physiol* 84: 796-802.

Šesták Z., Catský J. (1962) Intensity of photosynthesis and chlorophyll content as related to leaf age in *Nicotiana sanderae* hort. *Biologia Plantarum* 4: 131–140.

Shackel KA., Hall AE. (1979) Reversible leaflet movements in relation to drought adaptation of cowpeas, *Vigna Unguiculata* (L.) Walp. *Aust J Plant Physiol* 6: 265–276.

Shi C., Hu N., Huang H., Gao J., Zhao Y.-J., Gao L-Z. (2012a) An improved chloroplast DNA extraction procedure for whole plastid genome sequencing. *PloS one* 7, e31468.

Shi LX., Hall M., Funk C., Schroder WP. (2012b) Photosystem II, a growing complex: updates on newly discovered components and low molecular mass proteins. *Biochim Biophys Acta -Bioenergetics* 1817: 13-25.

Siefermann D., Yamamoto HY. (1975) Properties of NADPH and oxygen-dependent zeaxanthin epoxidation in isolated chloroplasts: a transmembrane model for the violaxanthin cycle. *Biochem Biophys Res Commun* 62: 456-461.

Siffel P., Santrucek J., Lang M., Braunová Z., Simkova M., Synkova H, Lichtenthaler H.K. (1993) Age dependence of photosynthetic activity, chlorophyll fluorescence parameters and chloroplast ultrastructure in aurea and green forms of *Nicotiana tabacum* Su/su mutant. *Photosynthetica* 29: 81–94.

Staehelin LA. (2003) Chloroplast structure: from chlorophyll granules to supra-molecular architecture of thylakoid membranes. *Photosynth Res* 76: 185-196.

Standfuss J., Terwisscha van Scheltinga AC., Lamborghini M., Kuhlbrandt W. (2005) Mechanisms of photoprotection and nonphotochemical quenching in pea light-harvesting complex at 2.5 Å resolution. *EMBO J* 24: 919-928.

Strebeyko P. (2000) Size and Power of a Chlorophyll *a* molecule. *Photosynthetica* 38: 159- 160.

Sun R., Liu K., Dong L., Wu Y., Paulsen H., Yang C. (2015) Direct energy transfer from the major antenna to the photosystem II core complexes in the absence of minor antennae in liposomes. *Biochim Biophys Acta* 1847: 248–261.

Sylak-Glassman EJ., Malnoë A., De Re E., Brooks MD., Fischer AL., Niyogi KK., Fleming GR. (2014) Distinct roles of the photosystem II protein PsbS and zeaxanthin in the regulation of light harvesting in plants revealed by fluorescence lifetime snapshots. *Proc Natl Acad Sci USA* 111(49): 17498–17503.

Takahashi S., Badger MR. (2011) Photoprotection in plants: a new light on photosystem II damage *Trends Plant Sci* 16: 53–60.

Takahashi S., Badger MR. (2011) Photoprotection in plants: a new light on photosystem II damage. *Trends Plant Sci* 16: 53–60.

Teardo E., de Laureto PP., Bergantino E., Dalla Vecchia F., Rigoni F., Szabo D., Giacometti GM. (2007) Evidences for interaction of PsbS with photosynthetic complexes in maize thylakoids. *Biochim Biophys Acta* 1767: 703-11.

Thiele A., Krause GH., Winter K. (1998) *In situ* study of photoinhibition of photosynthesis and xanthophyll cycle activity in plants growing in natural gaps of the tropical forest. *Aust J Plant Physiol* 25: 189–195.

Thiele A., Schirwitz K., Winter K., Krause GH. (1996) Increased xanthophyll cycle activity and reduced D1 protein inactivation related to photoinhibition in two plant systems acclimated to excess light. *Plant Sci* 115: 237–250.

Thiele A., Winter K., Krause GHG. (1997) Low inactivation of D1 protein of photosystem II in young canopy leaves of *Anacardium excelsum* under high-light stress. *J Plant Physiol* 151: 286–292.

Thordal-Christensen H., Zhang Z., Wei Y., Collinge DB. (1997) Subcellular localization of H2O2 accumulation in papillae and hypersensitive response during the barley-powdery mildew interaction. *Plant J* 11: 1187–1194.

Thornber JP. (1969) Comparison of a chlorophyll *a*−protein complex isolated from a blue−green alga with chlorophyll−protein complexes obtained from green bacteria and higher plants. *Biochim Biophys Acta* 172: 230−241.

Tichá I. (1985) Ontogeny of leaf morphology. In *Photosynthesis During Leaf Development* (ed Sestak Z.)16–50. Academia, Prague.

Tikkanen M., Piippo M., Suorsa M., Sirpio S., Mulo P., Vainonen J., Vener AV., Allahverdiyeva Y., Aro EM. (2006) State transitions revisited – a buffering system for dynamic low light acclimation of *Arabidopsis*. *Plant Mol Biol* 62: 779–793.

Triantaphylidès C., Havaux M. (2009) Singlet oxygen in plants: production, detoxification and signalling. *Trends Plant Sci* 14:219–228.

Trissl HW., Gao Y., Wulf K. (1993) Theoretical fluorescence induction curves derived from coupled differential equations describing the primary photochemistry of photosystem II by an exciton-radical pair equilibrium. *Biophys J* 64:974–988.

Trissl HW., Lavergne J. (1994) Fluorescence induction from photosystem II: analytical equations for the yields of photochemistry and fluorescence derived from analysis of a model including exciton-radical pair equilibrium and restricted energy transfer between photosynthetic units. *Aust J Plant Physiol* 22: 183–193.

Tsuboi H., Wada M. (2011) Chloroplasts can move in any direction to avoid strong light. *J Plant Res* 124: 201–210.

Tsukaya H. (2013) Leaf development. The *Arabidopsis* Book. Am Soc Plant Biol 11: e0163.

Tyystjärvi E., Aro EM. (1996) The rate constant of photoinhibition, measured in lincomycin-treated leaves, is directly proportional to light intensity. *Proc Natl Acad Sci USA* 93:2213–2218.

Umena Y., Kawakami K., Shen J-R., Kamiya N. (2011) Crystal structure of oxygen-evolving photosystem II at a resolution of 1.9 Å. *Nature* 473: 55–60.

Valkunas L., Chmeliov J., Trinkunas G., Duffy CDP., van Grondelle R., Ruban AV. (2011) Excitation migration, quenching, and regulation of photosynthetic light harvesting in photosystem II. *J Phys Chem B* 115: 9252-9260.

Valladares F., Pearcy RW. (1997) Interactions between water stress, sun–shade acclimation, heat tolerance and photoinhibition in the sclerophyll *Heteromeles arbutifolia*. *Plant Cell Environ* 20: 25–36.

van Amerongen H., Croce R. (2013) Light harvesting in photosystem II. *Photosynth Res* 116: 251–263.

van Amerongen H., van Grondelle R. (2001) Understanding the energy transfer function of LHCII, the major light-harvesting complex of green plants. *J Phys Chem B* 105: 604–617.

van Grondelle R., Novoderezhkin VI. (2006) Energy transfer in photosynthesis: experimental insights and quantitative models. *Phys Chem Chem Phys* 8: 793-807.

van Lijsebettens M., Clarke J. (1998) Leaf Development in *Arabidopsis*. *Plant Physiol Biochem* 36: 47–60.

van Oort B., Alberts M., de Bianchi S., Dall'Osto L., Bassi R., Trinkunas G., Croce R., van Amerongen H. (2010) Effect of antenna depletion in Photosystem II on excitation energy transfer in *Arabidopsis thaliana*. *Biophys J* 98: 922-931.

Vass I. (2012) Molecular mechanisms of photodamage in the photosystem II complex. *Biochim Biophys Acta* 1817:209–217.

Vass I., Styring S., Hundal T., Koivuniemi A., Aro E-M., Andersson B. (1992) Reversible and irreversible intermediates during photoinhibition of photosystem II: stable reduced QA species promote chlorophyll triplet formation. *Proc Natl Acad Sci USA* 89: 1408–1412.

Verhoeven AS., Adams WW., Demmig-Adams B. (1996) Close relationship between the state of the xanthophyll cycle pigments and photosystem II efficiency during recovery from winter stress. *Physiol Plant* 96: 567–576.

Vogelmann TC., Evans JR. (2002) Profiles of light absorption and chlorophyll within spinach leaves from chlorophyll fluorescence. *Plant Cell Environ* 25: 1313–1323.

Wagner B., Goss R., Richter M., Wild A., Holzwarth AR. (1996) Picosecond time-resolved study on the nature of high-energy-state quenching in isolated pea thylakoids. Different localization of zeaxanthin dependent and independent mechanisms. *J Photochem Photobiol B* Biol 36: 339–350.

Wahadoszamen M., Berera R., Ara AM., Romero E., van Grondelle R. (2012) Identification of two emitting sites in the dissipative state of the major light harvesting antenna. *Phys Chem Chem Phys* 14: 759–766.

Walter A., Rascher U., Osmond B. (2004) Transitions in photosynthetic parameters of midvein and interveinal regions of leaves and their importance during leaf growth and development. *Plant Biology* 6: 184–191.

Walters RG., Horton P. (1993) Theoretical assessment of alternative mechanisms for non-photochemical quenching of PS II fluorescence in barley leaves. *Photosynth Res* 36: 119–139.

Walters RG., Ruban AV., Horton P. (1995) Higher plant light-harvesting complexes LHCIIa and LHCIIc are bound by dicyclohexylcarbodiimide during inhibition of energy dissipation. *Eur J Bioch*em 226: 1063-1069.

Ware MA., Belgio E., Ruban AV. (2014) Comparison of the protective effectiveness of NPQ in *Arabidopsis* plants deficient in PsbS protein and zeaxanthin. J Exp Bot 66: 1259-1270.

Ware MA., Belgio E., Ruban AV. (2015) Photoprotective capacity of non-photochemical quenching in plants acclimated to different light intensities. *Photosynth Res* 126: 261-274.

Ware MA., Dall'Osto L., Ruban AV. (2016) An *in vivo* quantitative comparison of photoprotection in *Arabidopsis* xanthophyll mutants. *Front Plant Sci* 7: 841.

Ware MA., Giovagnetti V., Belgio E., Ruban AV. (2015) PsbS protein modulates non-photochemical chlorophyll fluorescence quenching in membranes depleted from photosystems. *J Photochem Photobiol B* 152: 301-307.

Wentworth M., Ruban AV. Horton P. (2003) Thermodynamic Investigation into the Mechanism of the Chlorophyll Fluorescence Quenching in Isolated Photosystem II Light Harvesting Complexes. *J Biol Chem* 278: 21845 – 21850.

Wientjes E., van Amerongen H., Croce R. (2013) Quantum yield of charge separation in photosystem II: functional effect of changes in the antenna size upon light acclimation. *J Phys Chemi B* 117: 11200–11208.

Wilk L., Grunwald M., Liao PN., Walla PJ., Kühlbrandt W. (2013) Direct interaction of the major light-harvesting complex II and PsbS in nonphotochemical quenching. *Proc Natl Acad Sci USA* 110: 245452–5456.

Willstätter R., Stoll A. (1913) Untersuchungen über Chlorophyll. Springer, Berlin.

Woo HR., Chung KM., Park JH., Oh SA., Ahn T., Hong SH., Nam HG. (2001) ORE9, an F-Box protein that regulates leaf senescence in *Arabidopsis*. *Plant Cell* 13: 1779–1790.

Wraight CA, Crofts AR. (1970) Energy-dependent quenching of chlorophyll *a* fluorescence in isolated chloroplasts. *Eur J Bioch* 17: 319–327.

Yakushevska AE., Keegstra W., Boekema EJ., Dekker JP., Andersson J., Jansson S., Ruban AV., Horton P. (2003) The structure of photosystem II in *Arabidopsis*: localization of the CP26 and CP29 antenna complexes. *Biochemistry* 42: 608-613.

Yakushevska AE., Ruban AV., Jensen PE., van Roon H., Niyogi K., Horton P., Boekema EJ. (2001) Supermolecular organization of photosystem II and its associated light-harvesting antenna in the wild-type and *npq4* mutant of *Arabidopsis thaliana*. *Proceedings of the 12th International Congress on Photosynthesis*. CSIRO Publishing.

Yamamoto HY. (1979) Biochemistry of the violaxanthin cycle in higher plants. *Pure Appl Chem* 51: 639–648.

Yamamoto HY., Kamite L. (1972) The effects of dithiothreitol on violaxanthin de-epoxidation and absorbance changes in the 500-nm region. *Biochim Biophys Acta* 267: 538–543.

Zeng XQ., Chow WS., Su LJ., Peng XX., Peng CL. (2010) Protective effect of supplemental anthocyanins on *Arabidopsis* leaves under high light. *Physiologia Plantarum* 138: 215–225.

Zhang J., Chen C., Zhang D., Li H., Li P., Ma F. (2014) Reactive oxygen species produced via plasma membrane NADPH oxidase regulate anthocyanin synthesis in apple peel. *Planta* 240: 1023–1035.

Zimmermann P., Heinlein C., Orendi G., Zentgraf U. (2006) Senescence specific regulation of catalases in *Arabidopsis thaliana* (L.) Heynh. *Plant Cell Environ* 29: 1049–1060.

Chapter XI – Appendix

Appendix 1: JUNIOR-PAM - pNPQ Assessment Procedure

```
// initialisation
$SW = 0.6       // satpulse width = 0.6s
$FRI = 8        // far red intensity = 8
$A = 0          // actinic light off
$FOM = 0        // disable Fo' mode
$FRW = 7        // set far red width to 7s


// 1. F0 for 30s;
$FR = 1         // far red on
$M = 1          // measuring light on
delay 30        // wait 30s

// 2. Pulse (600 ms);
$FOFM = 1               // trigger a sat-pulse (FOFM mode)
delay 10
$FR = 1         // far red on

// 3. Fo + far red for 30 s;
delay 30        // wait 30s
$S = 1          // trigger satpulse

// 4. Far red off. Act. Light 90 uM for 5 min with 2/3 min duration pulses;
$FR = 0         // far red off
$AI = 4         // actinic intensity 4
$A = 1          // actinic light on
$FOM = 0        // disable Fo' mode

// the following will repeat the commands inbetween "do" and "until" 1 times
$i = 0          // loopvar = 0
do              // repeat
```

```
        delay 120       // wait 120s
        $S = 1          // trigger sat-pulse
        inc $i          // increase loopvar by 1
until $i = 1    // until loopvar = 1
delay 180       // wait 180s
$FOM = 0        // disable Fo' mode
$A = 0          // actinic light off
$S = 1          // trigger sat-pulse
$FRW = 7        // set far red width to 7s
$FR = 1         // far red on
delay 10        // wait 10s

$i = 0          // loopvar = 0
do              // repeat
$S = 1          // trigger sat-pulse
        wait $S = 0     // make sure that the last sat-pulse is completed
        delay 5// wait 5s
        inc $i          // increase loopvar by 1
until  $i = 1   // until loopvar = 1


// 4. Far red off. Act. Light 190 uM for 5 min with 2/3 min duration pulses;
$FR = 0         // far red off
$AI = 6         // actinic intensity 6
$A = 1          // actinic light on
$FOM = 0        // disable Fo' mode

// the following will repeat the commands inbetween "do" and "until" 1 times
$i = 0          // loopvar = 0
do              // repeat
        delay 120       // wait 120s
        $S = 1          // trigger sat-pulse
```

```
        inc $i          // increase loopvar by 1
until $i = 1    // until loopvar = 1
delay 180       // wait 180s
$FOM = 0        // disable Fo' mode
$A = 0          // actinic light off
$S = 1          // trigger sat-pulse
$FRW = 7        // set far red width to 7s
$FR = 1         // far red on
delay 10        // wait 10s
$i = 0          // loopvar = 0
do              // repeat
$S = 1          // trigger sat-pulse
        wait $S = 0     // make sure that the last sat-pulse is completed
        delay 5// wait 5s
        inc $i          // increase loopvar by 1
until  $i = 1   // until loopvar = 1


// 4. Far red off. Act. Light 285 uM for 5 min with 2/3 min duration pulses;
$FR = 0         // far red off
$AI = 7         // actinic intensity 7
$A = 1          // actinic light on
$FOM = 0        // disable Fo' mode

// the following will repeat the commands inbetween "do" and "until" 1 times
$i = 0          // loopvar = 0
do              // repeat
        delay 120       // wait 120s
        $S = 1          // trigger sat-pulse
        inc $i          // increase loopvar by 1
until $i = 1    // until loopvar = 1
delay 180       // wait 180s
```

```
$FOM = 0        // disable Fo' mode
$A = 0          // actinic light off
$S = 1          // trigger sat-pulse
$FRW = 7        // set far red width to 7s
$FR = 1         // far red on
delay 10        // wait 10s
$i = 0          // loopvar = 0
do              // repeat
$S = 1          // trigger sat-pulse
        wait $S = 0     // make sure that the last sat-pulse is completed
        delay 5// wait 5s
        inc $i          // increase loopvar by 1
until  $i = 1   // until loopvar = 1


// 4. Far red off. Act. Light 420 uM for 5 min with 2/3 min duration pulses;
$FR = 0         // far red off
$AI = 8         // actinic intensity 8
$A = 1          // actinic light on
$FOM = 0        // disable Fo' mode

// the following will repeat the commands inbetween "do" and "until" 1 times
$i = 0          // loopvar = 0
do              // repeat
        delay 120       // wait 120s
        $S = 1          // trigger sat-pulse
        inc $i          // increase loopvar by 1
until $i = 1    // until loopvar = 1
delay 180       // wait 180s
$FOM = 0        // disable Fo' mode
$A = 0          // actinic light off
$S = 1          // trigger sat-pulse
```

```
$FRW = 7        // set far red width to 7s
$FR = 1         // far red on
delay 10        // wait 10s
$i = 0          // loopvar = 0
do              // repeat
$S = 1          // trigger sat-pulse
        wait $S = 0     // make sure that the last sat-pulse is completed
        delay 5// wait 5s
        inc $i          // increase loopvar by 1
until  $i = 1   // until loopvar = 1


// 4. Far red off. Act. Light 625 uM for 5 min with 2/3 min duration pulses;
$FR = 0         // far red off
$AI = 9         // actinic intensity 9
$A = 1          // actinic light on
$FOM = 0        // disable Fo' mode

// the following will repeat the commands inbetween "do" and "until" 1 times
$i = 0          // loopvar = 0
do              // repeat
        delay 120       // wait 120s
        $S = 1          // trigger sat-pulse
        inc $i          // increase loopvar by 1
until $i = 1    // until loopvar = 2
delay 180       // wait 180s
$FOM = 0        // disable Fo' mode
$A = 0          // actinic light off
$S = 1          // trigger sat-pulse
$FRW = 7        // set far red width to 7s
$FR = 1         // far red on
delay 10        // wait 10s
```

```
$i = 0          // loopvar = 0
do              // repeat
$S = 1          // trigger sat-pulse
        wait $S = 0     // make sure that the last sat-pulse is completed
        delay 5// wait 5s
        inc $i          // increase loopvar by 1
until  $i = 1   // until loopvar = 1


// 4. Far red off. Act. Light 820 uM for 5 min with 2/3 min duration pulses;
$FR = 0         // far red off
$AI = 10                // actinic intensity 10
$A = 1          // actinic light on
$FOM = 0        // disable Fo' mode

// the following will repeat the commands inbetween "do" and "until" 1 times
$i = 0          // loopvar = 0
do              // repeat
        delay 120       // wait 120s
        $S = 1          // trigger sat-pulse
        inc $i          // increase loopvar by 1
until $i = 1    // until loopvar = 2
delay 180       // wait 180s
$FOM = 0        // disable Fo' mode
$A = 0          // actinic light off
$S = 1          // trigger sat-pulse
$FRW = 7        // set far red width to 7s
$FR = 1         // far red on
delay 10        // wait 10s
$i = 0          // loopvar = 0
do              // repeat
```

```
$S = 1          // trigger sat-pulse
        wait $S = 0     // make sure that the last sat-pulse is completed
        delay 5// wait 5s
        inc $i          // increase loopvar by 1
until  $i = 1     // until loopvar = 1


// 4. Far red off. Act. Light 1150 uM for 5 min with 2/3 min duration pulses;
$FR = 0         // far red off
$AI = 11                // actinic intensity 11
$A = 1          // actinic light on
$FOM = 0        // disable Fo' mode

// the following will repeat the commands inbetween "do" and "until" 1 times
$i = 0          // loopvar = 0
do              // repeat
        delay 120       // wait 120s
        $S = 1          // trigger sat-pulse
        inc $i          // increase loopvar by 1
until $i = 1      // until loopvar = 2
delay 180       // wait 180s
$FOM = 0        // disable Fo' mode
$A = 0          // actinic light off
$S = 1          // trigger sat-pulse
$FRW = 7        // set far red width to 7s
$FR = 1         // far red on
delay 10        // wait 10s
$i = 0          // loopvar = 0
do              // repeat
$S = 1          // trigger sat-pulse
        wait $S = 0     // make sure that the last sat-pulse is completed
        delay 5// wait 5s
```

```
        inc $i          // increase loopvar by 1
until  $i = 1     // until loopvar = 1


// 4. Far red off. Act. Light 1500 uM for 5 min with 2/3 min duration pulses;
$FR = 0         // far red off
$AI = 12                // actinic intensity 12
$A = 1          // actinic light on
$FOM = 0        // disable Fo' mode

// the following will repeat the commands inbetween "do" and "until" 1 times
$i = 0          // loopvar = 0
do              // repeat
        delay 120       // wait 120s
        $S = 1          // trigger sat-pulse
        inc $i          // increase loopvar by 1
until $i = 1      // until loopvar = 2
delay 180       // wait 180s
$FOM = 0        // disable Fo' mode
$A = 0          // actinic light off
$S = 1          // trigger sat-pulse
$FRW = 7        // set far red width to 7s
$FR = 1         // far red on
delay 10        // wait 10s
$i = 0          // loopvar = 0
do              // repeat
$S = 1          // trigger sat-pulse
        wait $S = 0     // make sure that the last sat-pulse is completed
        delay 5// wait 5s
        inc $i          // increase loopvar by 1
until  $i = 1     // until loopvar = 1
```

```
// deinit
$FR = 0          // far red off
$FOM = 0         // disable Fo' mode
$A = 0           // actinic light off
```

Appendix 2: JUNIOR-PAM - Constant High Light Procedure

```
// initialisation

$SW = 0.6       // satpulse width = 0.6s

$FRI = 8        // far red intensity = 8

$A = 0          // actinic light off

$FOM = 0        // disable Fo' mode

$FRW = 7        // set far red width to 7s


// 1. F0 for 30s;

$FR = 1         // far red on

$M = 1          // measuring light on

delay 30        // wait 30s


// 2. Pulse (600 ms);

$FOFM = 1               // trigger a sat-pulse (FOFM mode)

delay 10

$FR = 1         // far red on


// 3. Fo + far red for 30 s;

delay 30        // wait 30s

$S = 1          // trigger satpulse
```

```
// 4. Far red off. Act. Light 1500 uM for 5 min with 2/3 min duration pulses;
$AI = 12                    // actinic intensity 12
$A = 1          // actinic light on
$FOM = 0        // disable Fo' mode
$FR = 0         // far red off
// the following will repeat the commands inbetween "do" and "until" 1 times
$i = 0          // loopvar = 0
do              // repeat
delay 120       // wait 120s
$S = 1          // trigger sat-pulse
inc $i          // increase loopvar by 1
until $i = 1    // until loopvar = 1
delay 180       // wait 180s
$FOM = 0        // disable Fo' mode
$A = 0          // actinic light off
$S = 1          // trigger sat-pulse
$FRW = 7        // set far red width to 7s
$FR = 1         // far red on
delay 10        // wait 10s
$i = 0          // loopvar = 0
do              // repeat
$S = 1          // trigger sat-pulse
wait $S = 0     // make sure that the last sat-pulse is completed
```

```
delay 5// wait 5s
inc $i              // increase loopvar by 1
until  $i = 1       // until loopvar = 1



// 4. Far red off. Act. Light 1500 uM for 5 min with 2/3 min duration pulses;
$AI = 12                    // actinic intensity 12
$A = 1              // actinic light on
$FOM = 0            // disable Fo' mode
$FR = 0             // far red off
// the following will repeat the commands inbetween "do" and "until" 1 times
$i = 0              // loopvar = 0
do                  // repeat
delay 120           // wait 120s
$S = 1              // trigger sat-pulse
inc $i              // increase loopvar by 1
until $i = 1        // until loopvar = 1
delay 180           // wait 180s
$FOM = 0            // disable Fo' mode
$A = 0              // actinic light off
$S = 1              // trigger sat-pulse
$FRW = 7            // set far red width to 7s
$FR = 1             // far red on
```

```
delay 10          // wait 10s
$i = 0            // loopvar = 0
do                // repeat
$S = 1            // trigger sat-pulse
wait $S = 0       // make sure that the last sat-pulse is completed
delay 5// wait 5s
inc $i            // increase loopvar by 1
until  $i = 1     // until loopvar = 1



// 4. Far red off. Act. Light 1500 uM for 5 min with 2/3 min duration pulses;
$AI = 12                  // actinic intensity 12
$A = 1            // actinic light on
$FOM = 0          // disable Fo' mode
$FR = 0           // far red off
// the following will repeat the commands inbetween "do" and "until" 1 times
$i = 0            // loopvar = 0
do                // repeat
delay 120         // wait 120s
$S = 1            // trigger sat-pulse
inc $i            // increase loopvar by 1
until $i = 1      // until loopvar = 1
delay 180         // wait 180s
```

```
$FOM = 0        // disable Fo' mode
$A = 0          // actinic light off
$S = 1          // trigger sat-pulse
$FRW = 7        // set far red width to 7s
$FR = 1         // far red on
delay 10        // wait 10s
$i = 0          // loopvar = 0
do              // repeat
$S = 1          // trigger sat-pulse
wait $S = 0     // make sure that the last sat-pulse is completed
delay 5// wait 5s
inc $i          // increase loopvar by 1
until  $i = 1   // until loopvar = 1



// 4. Far red off. Act. Light 1500 uM for 5 min with 2/3 min duration pulses;
$AI = 12                // actinic intensity 12
$A = 1          // actinic light on
$FOM = 0        // disable Fo' mode
$FR = 0         // far red off
// the following will repeat the commands inbetween "do" and "until" 1 times
$i = 0          // loopvar = 0
do              // repeat
```

```
delay 120       // wait 120s
$S = 1          // trigger sat-pulse
inc $i          // increase loopvar by 1
until $i = 1    // until loopvar = 1
delay 180       // wait 180s
$FOM = 0        // disable Fo' mode
$A = 0          // actinic light off
$S = 1          // trigger sat-pulse
$FRW = 7        // set far red width to 7s
$FR = 1         // far red on
delay 10        // wait 10s
$i = 0          // loopvar = 0
do              // repeat
$S = 1          // trigger sat-pulse
wait $S = 0     // make sure that the last sat-pulse is completed
delay 5// wait 5s
inc $i          // increase loopvar by 1
until  $i = 1   // until loopvar = 1



// 4. Far red off. Act. Light 1500 uM for 5 min with 2/3 min duration pulses;
$AI = 12                // actinic intensity 12
$A = 1          // actinic light on
```

```
$FOM = 0        // disable Fo' mode
$FR = 0         // far red off
// the following will repeat the commands inbetween "do" and "until" 1 times
$i = 0          // loopvar = 0
do              // repeat
delay 120       // wait 120s
$S = 1          // trigger sat-pulse
inc $i          // increase loopvar by 1
until $i = 1    // until loopvar = 2
delay 180       // wait 180s
$FOM = 0        // disable Fo' mode
$A = 0          // actinic light off
$S = 1          // trigger sat-pulse
$FRW = 7        // set far red width to 7s
$FR = 1         // far red on
delay 10        // wait 10s
$i = 0          // loopvar = 0
do              // repeat
$S = 1          // trigger sat-pulse
wait $S = 0     // make sure that the last sat-pulse is completed
delay 5// wait 5s
inc $i          // increase loopvar by 1
until  $i = 1   // until loopvar = 1
```

```
// 4. Far red off. Act. Light 1500 uM for 5 min with 2/3 min duration pulses;
$AI = 12                    // actinic intensity 12
$A = 1              // actinic light on
$FOM = 0            // disable Fo' mode
$FR = 0             // far red off
// the following will repeat the commands inbetween "do" and "until" 1 times
$i = 0              // loopvar = 0
do                  // repeat
delay 120           // wait 120s
$S = 1              // trigger sat-pulse
inc $i              // increase loopvar by 1
until $i = 1        // until loopvar = 2
delay 180           // wait 180s
$FOM = 0            // disable Fo' mode
$A = 0              // actinic light off
$S = 1              // trigger sat-pulse
$FRW = 7            // set far red width to 7s
$FR = 1             // far red on
delay 10            // wait 10s
$i = 0              // loopvar = 0
do                  // repeat
```

```
$S = 1          // trigger sat-pulse
wait $S = 0     // make sure that the last sat-pulse is completed
delay 5// wait 5s
inc $i          // increase loopvar by 1
until  $i = 1   // until loopvar = 1



// 4. Far red off. Act. Light 1500 uM for 5 min with 2/3 min duration pulses;
$AI = 12                // actinic intensity 12
$A = 1          // actinic light on
$FOM = 0        // disable Fo' mode
$FR = 0         // far red off
// the following will repeat the commands inbetween "do" and "until" 1 times
$i = 0          // loopvar = 0
do              // repeat
delay 120       // wait 120s
$S = 1          // trigger sat-pulse
inc $i          // increase loopvar by 1
until $i = 1    // until loopvar = 2
delay 180       // wait 180s
$FOM = 0        // disable Fo' mode
$A = 0          // actinic light off
$S = 1          // trigger sat-pulse
```

```
$FRW = 7        // set far red width to 7s
$FR = 1         // far red on
delay 10        // wait 10s
$i = 0          // loopvar = 0
do              // repeat
$S = 1          // trigger sat-pulse
wait $S = 0     // make sure that the last sat-pulse is completed
delay 5// wait 5s
inc $i          // increase loopvar by 1
until  $i = 1   // until loopvar = 1



// 4. Far red off. Act. Light 1500 uM for 5 min with 2/3 min duration pulses;
$AI = 12                // actinic intensity 12
$A = 1          // actinic light on
$FOM = 0        // disable Fo' mode
$FR = 0         // far red off
// the following will repeat the commands inbetween "do" and "until" 1 times
$i = 0          // loopvar = 0
do              // repeat
delay 120       // wait 120s
$S = 1          // trigger sat-pulse
inc $i          // increase loopvar by 1
```

```
until $i = 1      // until loopvar = 2
delay 180         // wait 180s
$FOM = 0          // disable Fo' mode
$A = 0            // actinic light off
$S = 1            // trigger sat-pulse
$FRW = 7          // set far red width to 7s
$FR = 1           // far red on
delay 10          // wait 10s
$i = 0            // loopvar = 0
do                // repeat
$S = 1            // trigger sat-pulse
wait $S = 0       // make sure that the last sat-pulse is completed
delay 5           // wait 5s
inc $i            // increase loopvar by 1
until  $i = 1     // until loopvar = 1



// deinit
$FR = 0           // far red off
$FOM = 0          // disable Fo' mode
$A = 0            // actinic light off
```

Appendix 3: JUNIOR-PAM - qT Assessment Procedure

```
// initialisation
$SW = 0.6       // satpulse width = 0.6s
$FRI = 12       // far red intensity = 12
$A = 0          // actinic light off
$FOM = 0        // disable Fo' mode


// 1. F0 for 30s;
$M = 1          // measuring light on
delay 30        // wait 30s


// 2. Pulse (600 ms) for Fv/Fm;
$FOFM = 1               // trigger a sat-pulse (FOFM mode)


// 3. Fo for 30 s for qP;
delay 30        // wait 30s
$S = 1          // trigger satpulse
// 4. Far red and AL on for 5 min;
$AI = 1         // actinic intensity 1
$A = 1          // actinic light off
```

```
$FOM = 0        // disable Fo' mode
$FR = 1         // far red on
delay 300       // wait 300s
$S = 1          // trigger sat-pulse
wait $S = 0     // make sure that the last sat-pulse is completed
delay 30        // wait 30s


// 5. Actinic light for 20 min;
$FOM = 0        // disable Fo' mode
$A = 1          // actinic light on
$AI = 1         // actinic light 25 µmol
$FR = 0         // far red off
delay 1200      // wait 20min
$S = 1          // trigger sat-pulse
wait $S = 0     // make sure that the last sat-pulse is completed
$A = 0          // actinic light off
$FR = 0         // far red off
delay 30        // wait 30s

// 5. Far red + actinic light for 20 min;
$FOM = 0        // disable Fo' mode
$A = 1          // actinic light on
```

```
$AI = 1          // actinic light 25 µmol
$FR = 1          // far red on
delay 1200       // wait 20min
$S = 1           // trigger sat-pulse
wait $S = 0      // make sure that the last sat-pulse is completed
delay 10         // wait 10s


// deinit
$FR = 0          // far red off
$FOM = 0         // disable Fo' mode
$A = 0           // actinic light off
```

Appendix 4: <u>Protocol - installing software and running procedure</u>

1. Download and install the free WinControl-3 software from the Walz website. This will be an exe-file on the right hand side from the link below otherwise proceed to step 2:

http://www.walz.com/products/chl_p700/junior-pam/downloads.html

Also, for an introductory guide to the device's basic functions and the principles of fluorescence please see the following manual:

http://www.walz.com/downloads/manuals/junior-pam/jpm_071206.pdf

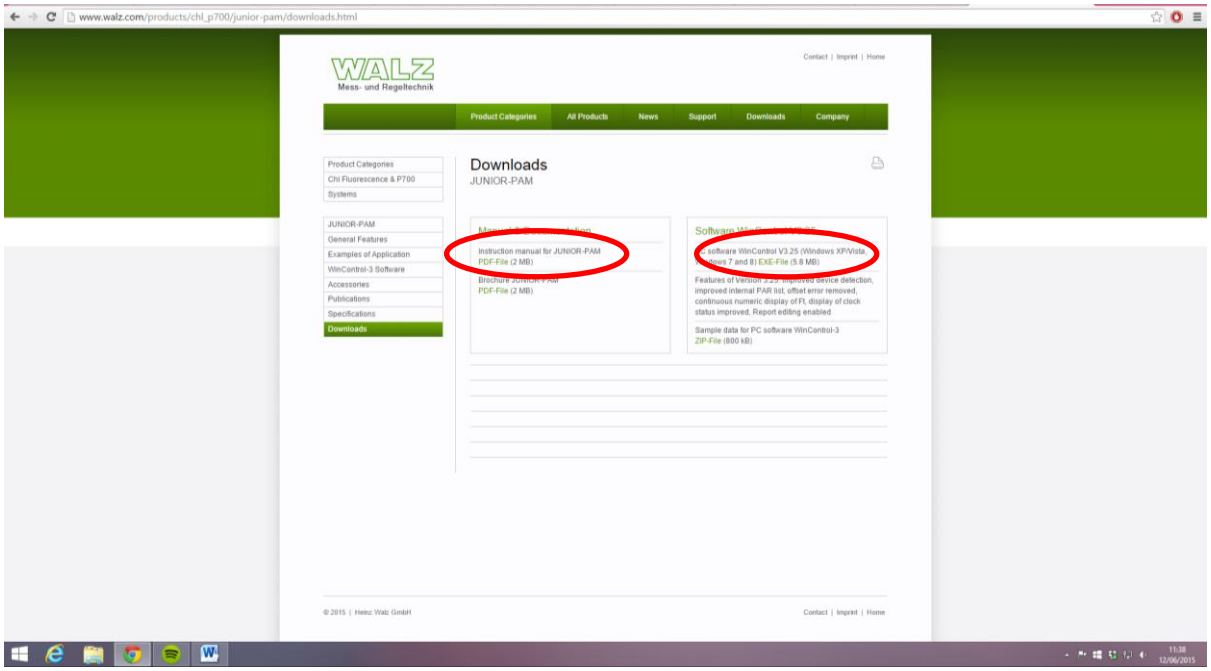

2. Turn on computer device which is compatible with the JUNIOR-PAM and WinControl software.
3. Once the computer has loaded, connect the PAM device to the computer via the USB cable and then double click the WinControl-3 shortcut or open via the program option.
4. Once the software opens, you should view a 'chart' page. This can be seen by the labelled tab in the bottom left of the screen.

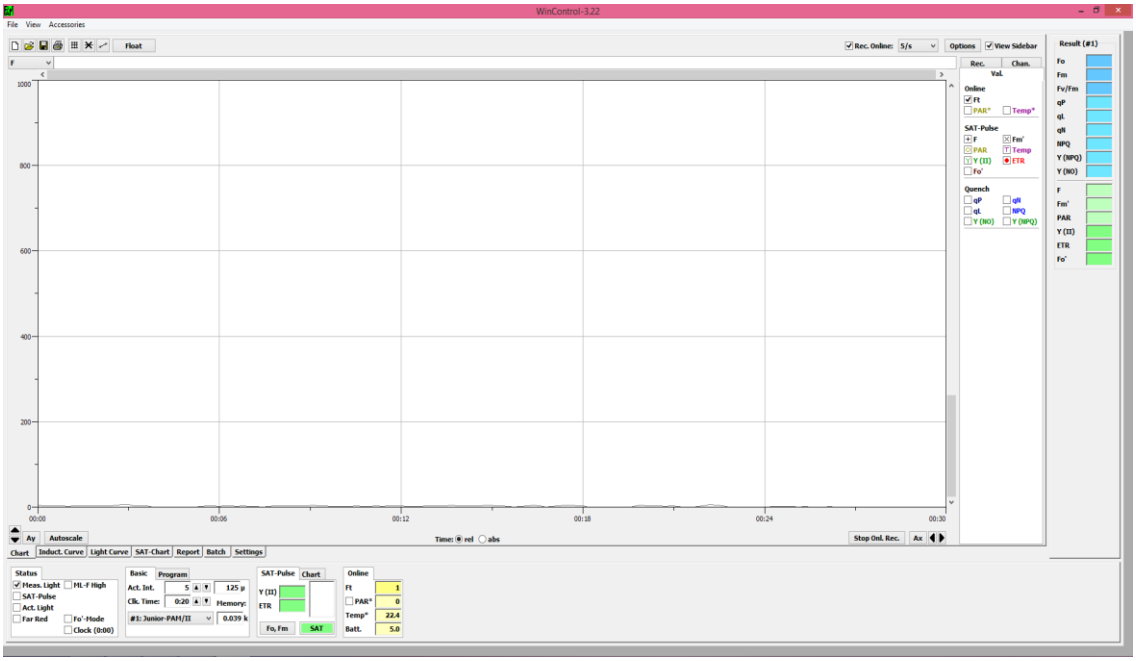

5. Gently insert the 50cm fibre-optic/light guide into the appropriate hole on the fluorimeter, until you feel resistance from the LED within the device. At this point stop pushing, and gently tighten the screw around the fibre (on the fluorimeter) until you feel resistance. Check to make sure that the fibre can no longer be easily removed from the fluorimeter.

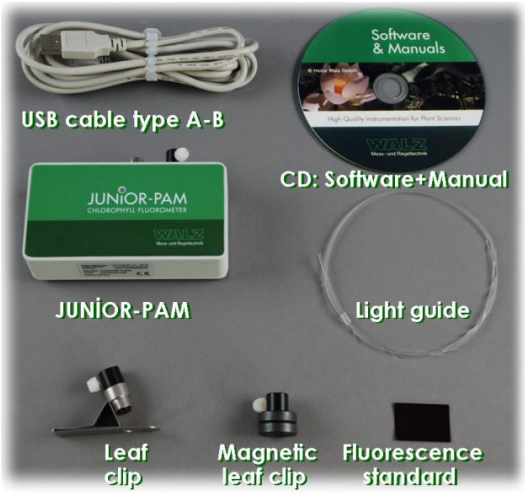

6. Using the control panel in the lower left hand section of the software page, click on… then check the ‘actinic light’ box. The fibre-optic should now be illuminated with blue light.

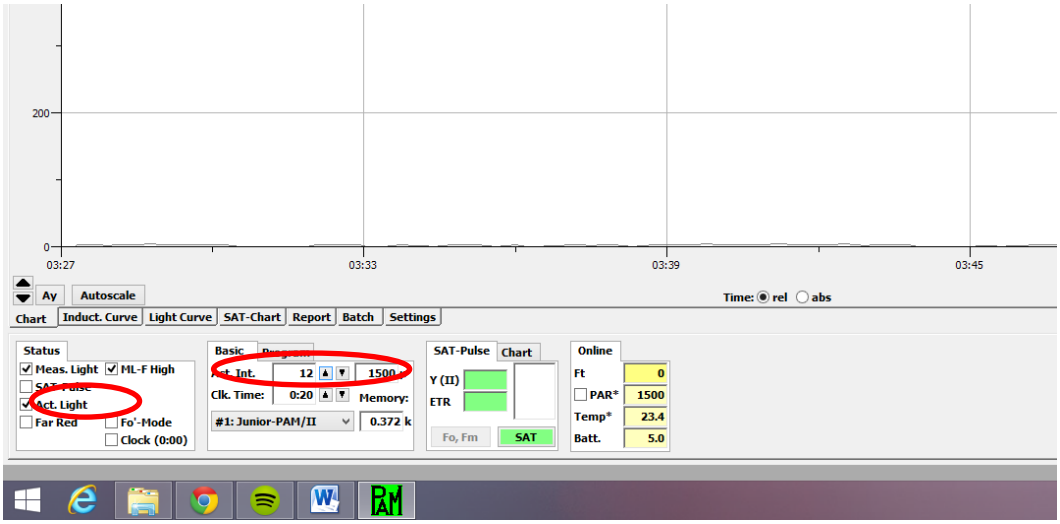

7. Increase the setting to the maximum integer value (12), which should be equivalent to 1500 µmol m^{-2} s^{-1}. This should be confirmed using a light sensor (Walz MQS-B or equivalent). If the reading is less than 1500, or you wish to use a different maximum intensity proceed to 8, however if the settings are fine, please proceed to 11.
8. On the lower centre part of the software page, there will be a tab called settings. Click this, then again on the right there will be a system settings page. Click this again, and confirm ‘OK’ when it recommends that this page is for advanced users.

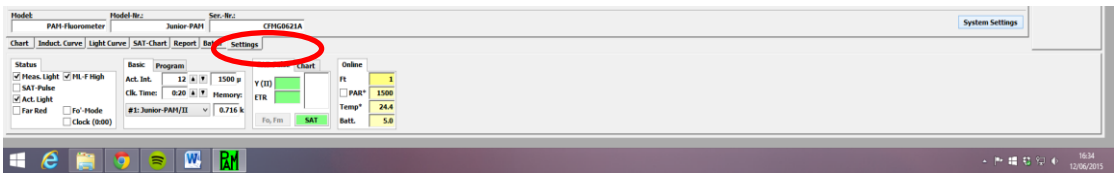

9. In order to ascertain that the emitted actinic light is the same as the predicted light intensity, place the fibre-optic over the light sensor, and using the actinic light toggle options, adjust this until the desired maximum light intensity is reached.

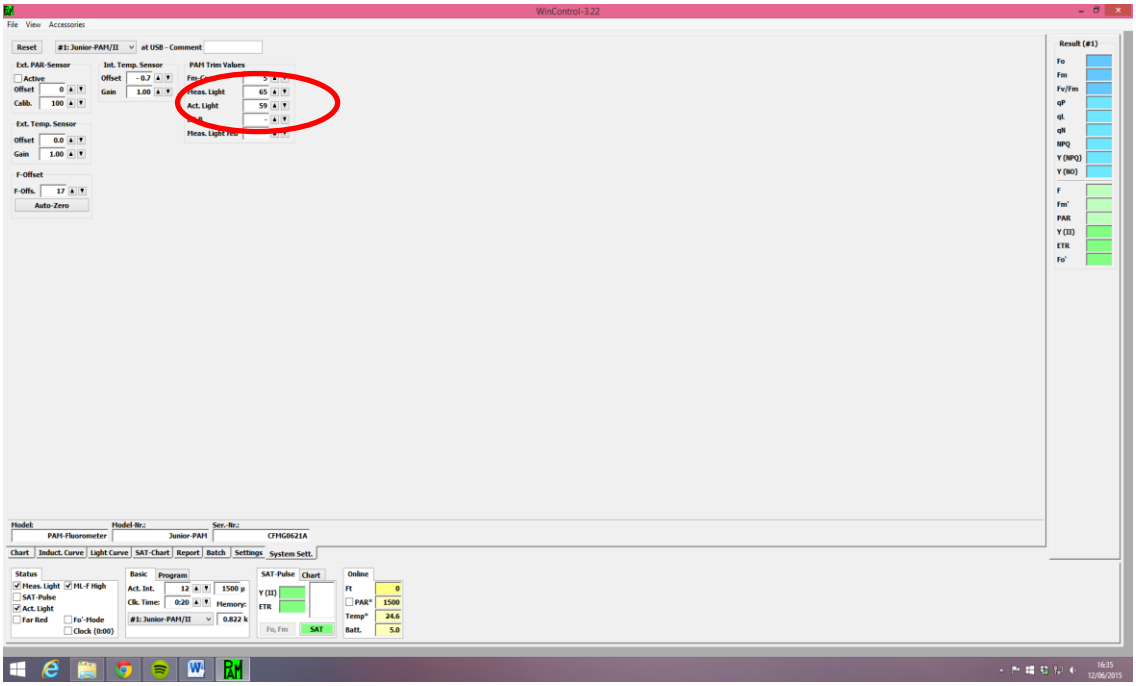

10. Upon finding the desired maximum light intensity, uncheck the ‘actinic light’ box in the bottom left of the screen. The blue light should then have disappeared from the fibre-optic.
11. Go back to the setting page and turn the measuring light intensity down in the top left corner. The frequency should be set to ‘2’, yet the intensity can be set to ‘1’.

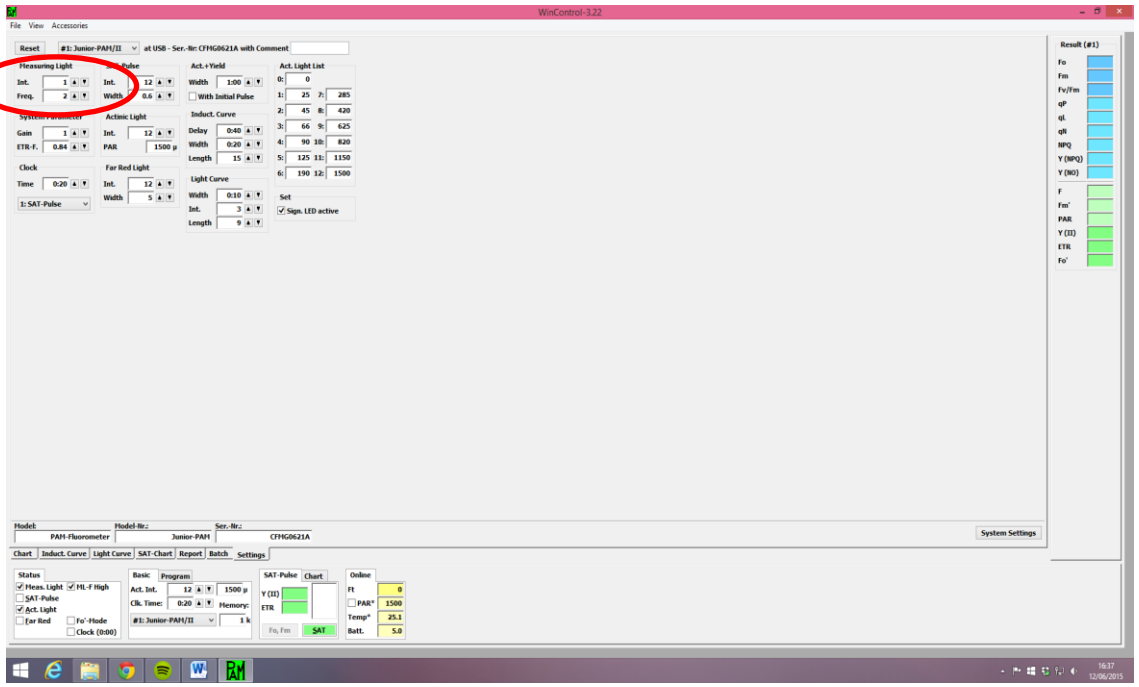

12. Once this is complete, attach the magnetic leaf clip to the end of the fibre-optic, using the fluorescence standard foil as a sandwich between the two magnetic clips.
13. Now uncheck the ‘measuring light’ box in the bottom left of the software screen.
14. Upon doing this, the Ft value displayed in the box in the bottom centre of the software page should be fluctuating about 0. Values in the range of -2 to 2 are acceptable. If this is not the case proceed to 14, otherwise proceed to 17.

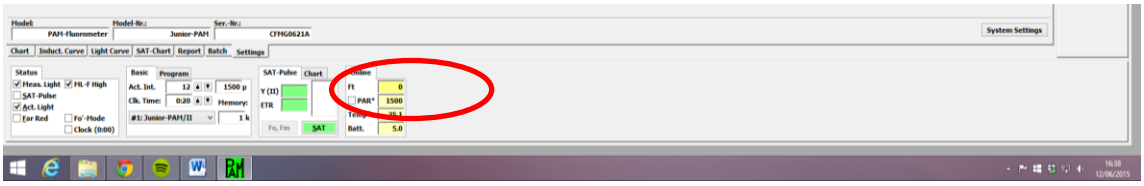

15. Click on the settings tab and advanced system settings. If you have not done this yet you will see a pop-up suggesting this option is for advanced users only, click ok, otherwise the system settings page will load automatically.
16. There is an ‘Auto-Zero’ button on the left hand side of the screen. Click this and the integer in the box will change. Check the Ft value box as before and see if the numbers are fluctuating around 0. If not click the offset button again until 0 is achieved in the Ft value box. In a dark room, the offset value is normally ~6-10 as a guiding reference.

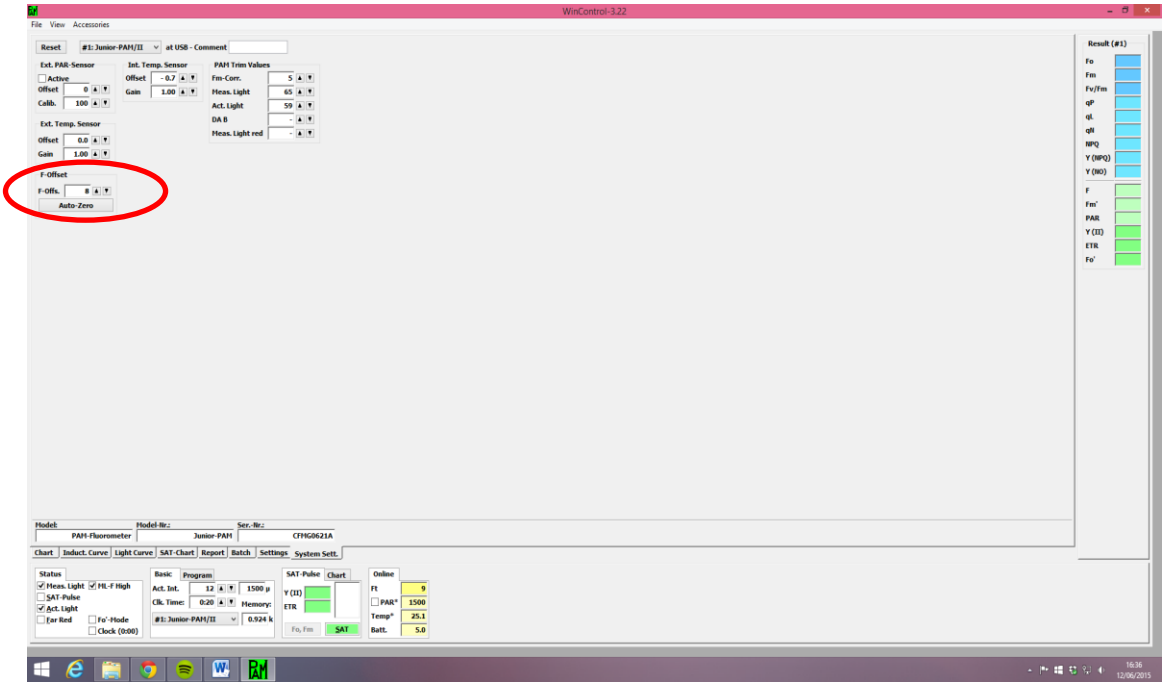

17. So now that the fluorimeter is calibrated, return to the main screen which shows the live fluorescence trace. Click the ‘stop online recording’ button. After this click the ‘clear all data’ icon in the top left corner of the screen. You will be prompted to confirm that this is ok, to which you must click ‘ok’.

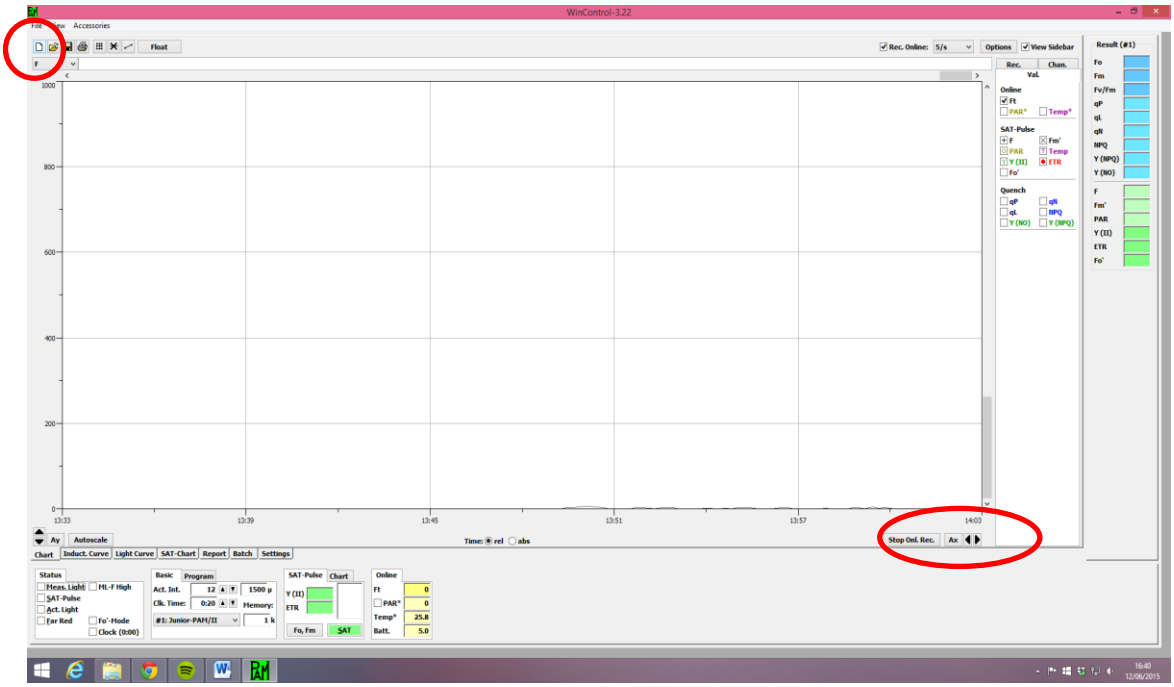

18. Now, proceed to the batch tab in the bottom left part of the screen. Here you can load a pre-programmed batch file. Click the ‘open folder’ icon, then in the bottom right of the new window change the file type to text file, and load the ‘Standard pNPQ procedure’ file. A block of text should now have

appeared in the white space on the batch screen page. You can now click back onto the ‘chart’ tab.

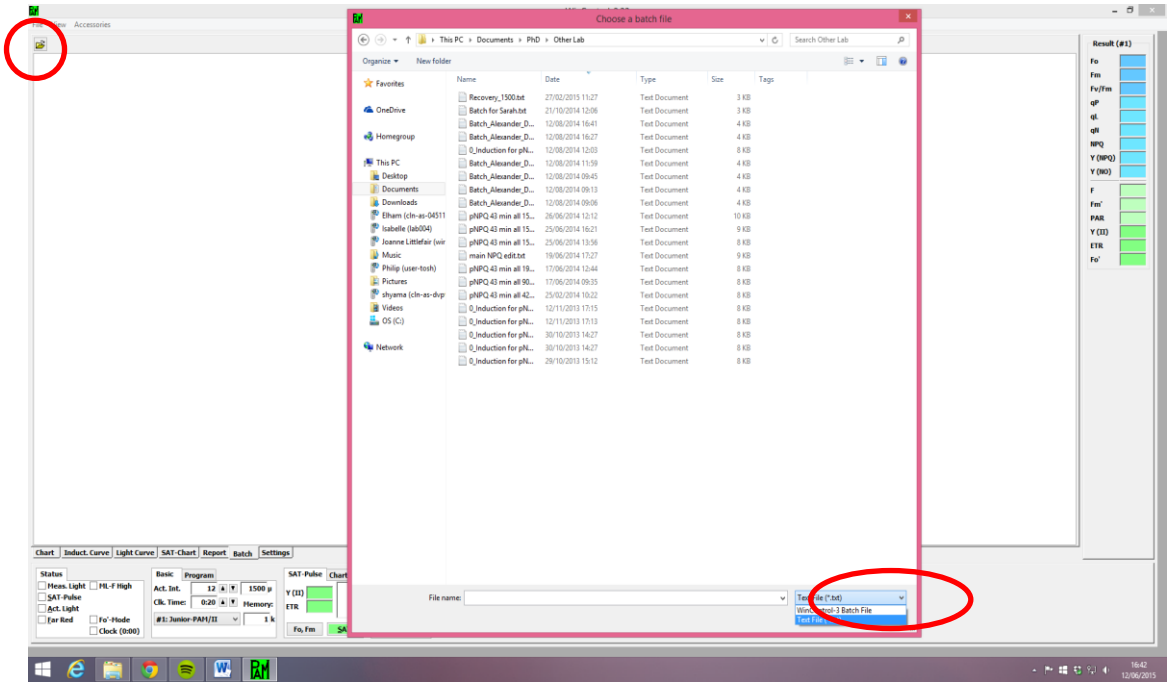

19. Remove the plant to be tested from the dark and attach the magnetic leaf clip. The fibre-optic side should be on the adaxial side of the leaf, the unattached clip on the abaxial. Furthermore, the fluorescence standard should be on the abaxial side, but with the black side touching the leaf. TAKE CARE not to damage the leaf/plant during this procedure.

20. Click on the ‘start online recording’ button.
21. Turn on the measuring light by checking the ‘measuring light’ box. You should now see a fluorescence signal. Depending the plant leaf type, whether it is a mutant or has been subjected to stress treatment, the measuring light intensity should be varied accordingly.

    The measuring light intensity should also be set to the highest value which does not cause photoinhibition of the system, or NPQ to be activated. These can be visualised as a rise or drop in trend of the Ft value. Slight fluctuations around a number are to be expected, you should just be looking for an overall trend. Therefore, start at intensity ‘1’. You can increase the intensity in the settings, system settings tab option.

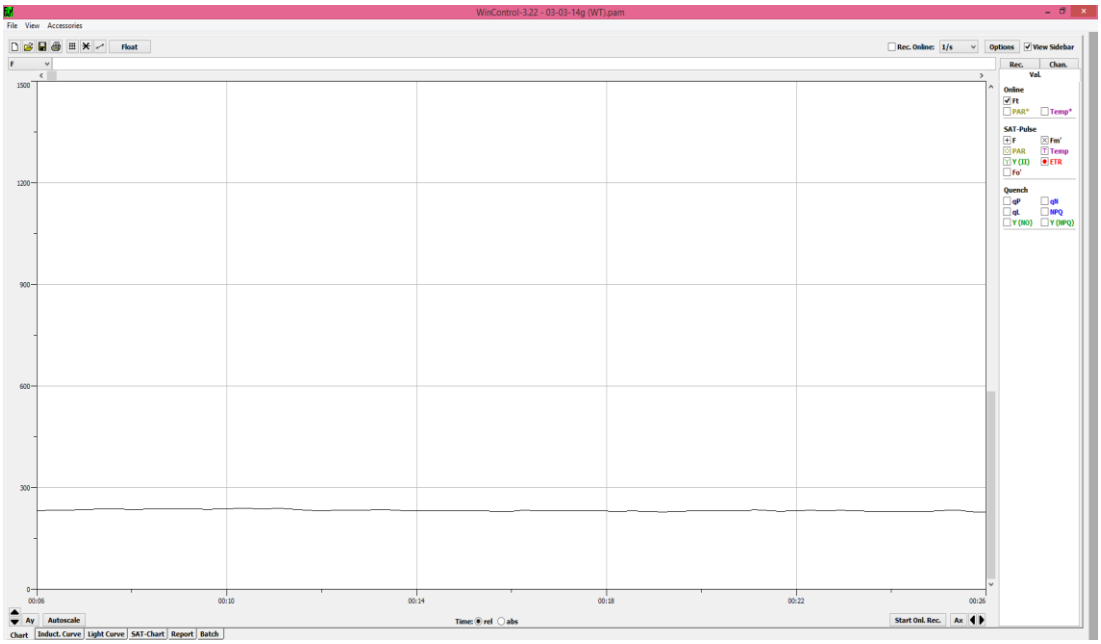

22. Once the correct intensity has been found, the procedure can be started. This is achieved by checking the ‘batch’ box in the bottom left of the screen.

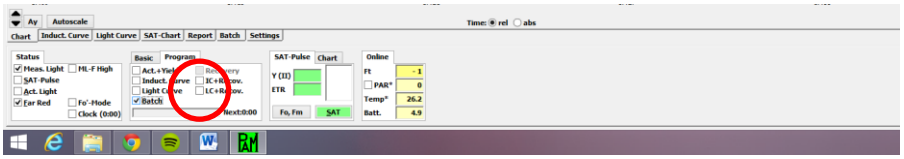

23. The pre-programmed trig-run will now be carried out.
24. After the batch file has finished running, the file can now be saved.
25. Click on the ‘save file’ icon in the top left of the screen and select a directory to save the data file.

Exporting data

1. Open saved file, a copy of the trace will appear as below:

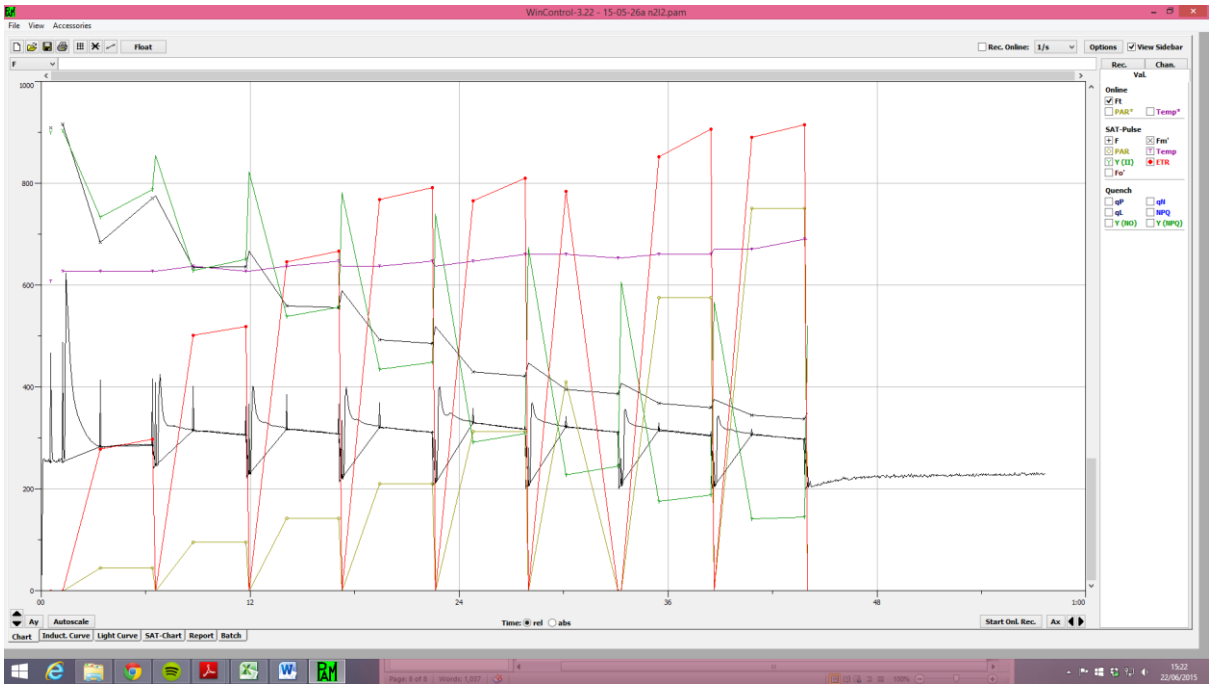

2. Click on the ‘report’ tab in the lower left corner of the page. The select/de-select the boxes on the right hand side so that only: F, PAR, Fo’, Fm’, qP and NPQ are selected.

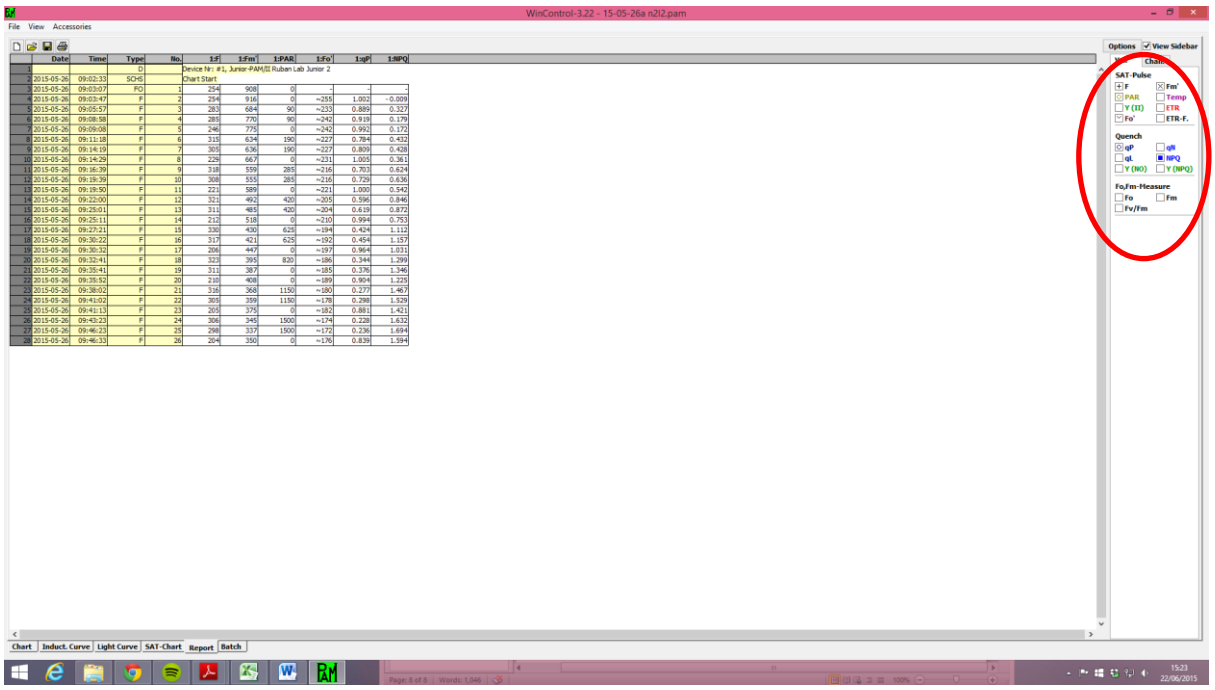

3. Now click ‘options’ in the top right hand corner and ‘export data’.

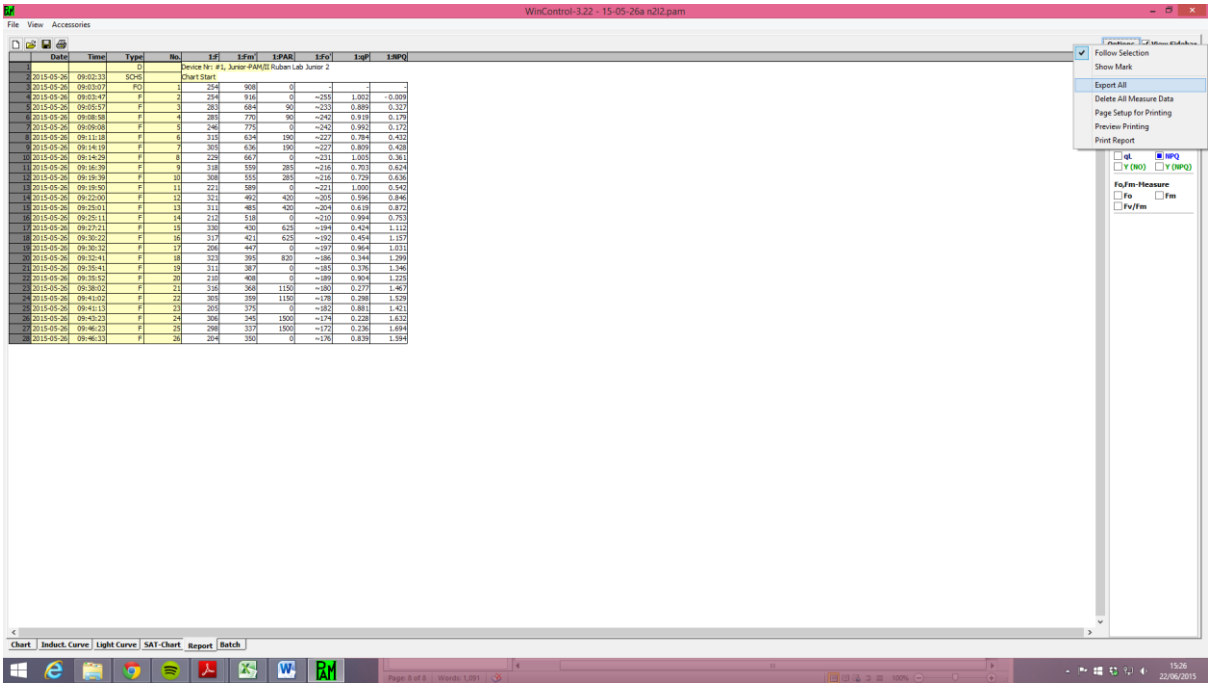

4. Select ‘date time format’ and you will be direct to your directories. From here, choose an appropriate folder to save the file. Name this file ‘input1’.

For any subsequent files, call them ‘input2’, ‘input3’ and so on in consecutive order up to a maximum of 20.

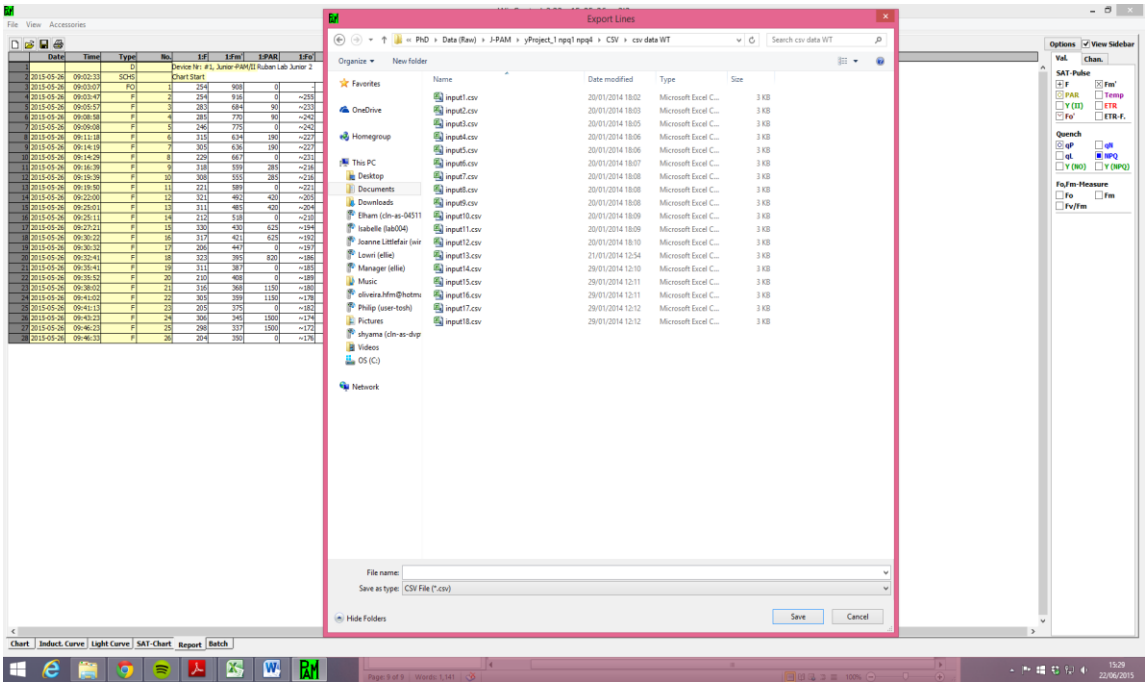

5. After all data files are saved into the folder, paste the ‘pNPQ_File_Proc_2.exe’ file into the folder. Double click on the exe file and wait for the execution to finish. After this, two more text files will appear in the folder.

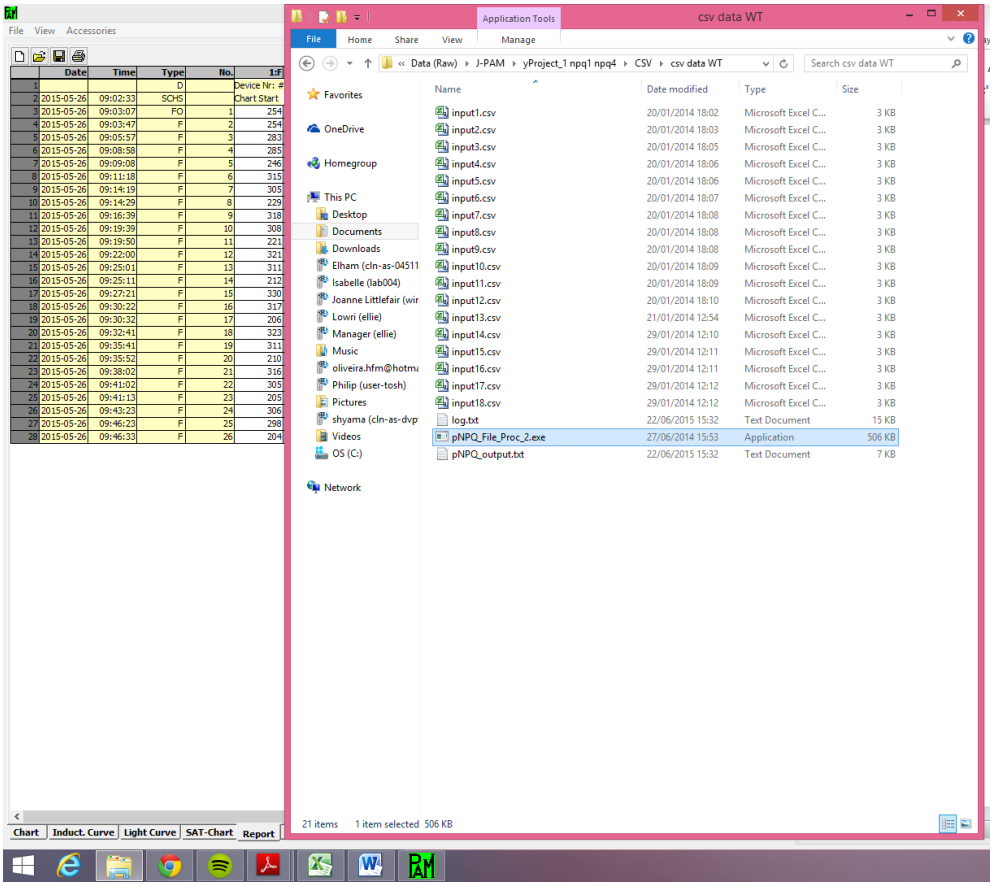

6. Double click on the ‘pNPQ_output.txt’ file and the results will appear in a table format to be copied:

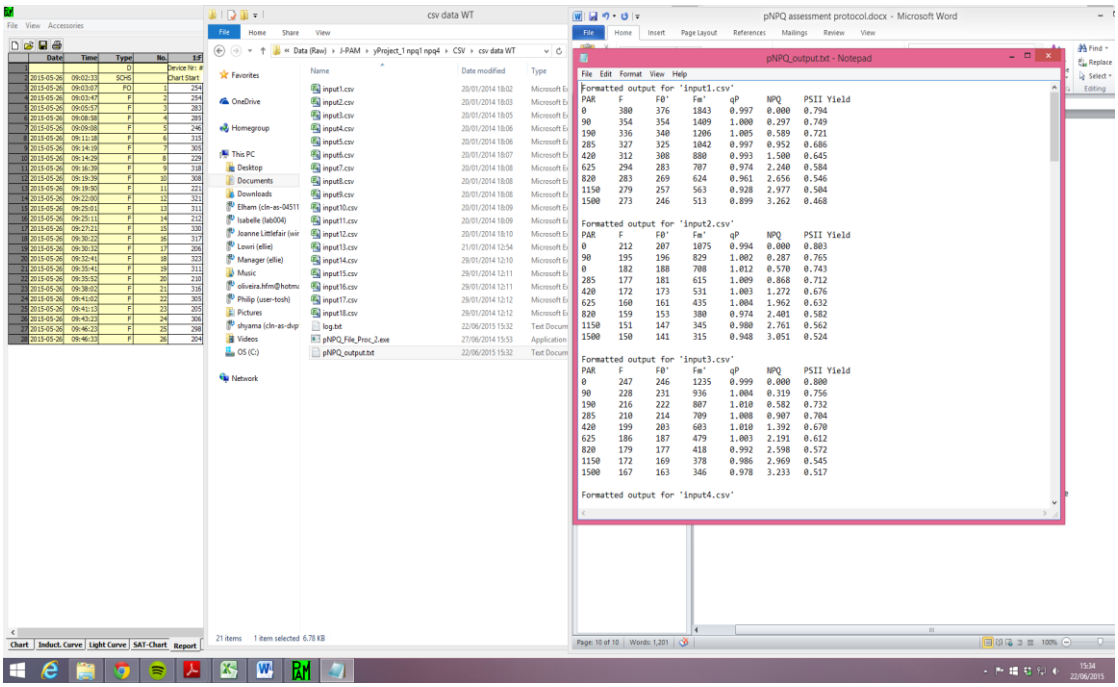

7. If a mistake has been made saving or exporting the files, an error message will appear. In which case, check that files are saved correctly and that the boxes/options are correctly selected:

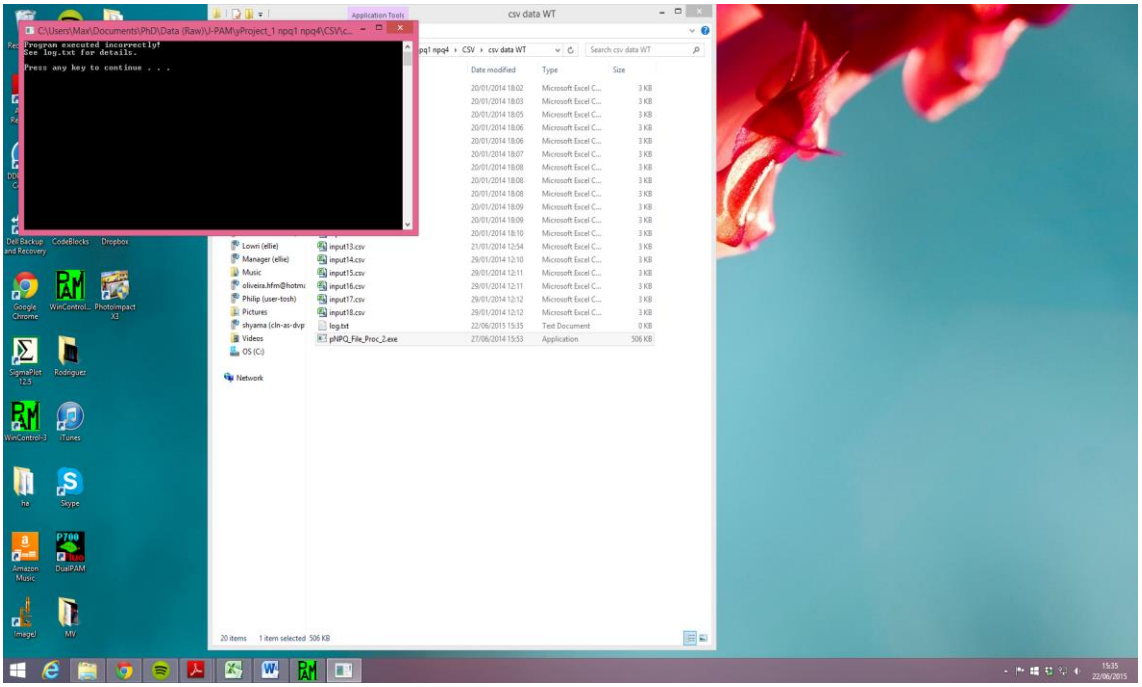

8. Now you can copy and paste the results into excel or another statistical software to analyse your results.